



UNIVERSITÀ DEGLI STUDI DI CAGLIARI  
Facoltà di Scienze Matematiche Fisiche e Naturali  
Dipartimento di Fisica

Ph.D. Thesis FIS/03  
CICLO XXV

THE ELASTIC BEHAVIOR OF  
POLYMER CHAINS: THEORY AND  
SIMULATIONS

FABIO MANCA

May 2013

Relatore: Prof.  
LUCIANO COLOMBO

Co-relatore: Dott.  
STEFANO GIORDANO

Fabio Manca: *The elastic behavior of polymer chains: theory and simulations*, Ph.D. Thesis FIS/03, CICLO XXV, © May 2013

## ABSTRACT

---

This thesis provides a picture on the thermo-elastic behavior of polymer molecules with biological relevance. In particular, this essay deals with the thermo-elasticity of single polymer molecules subjected to uniform stretching (generated by an applied force) or non-uniform stretching (generated by an external field). Analytical expressions and molecular dynamics simulations are elaborated considering some generalizations of the freely-jointed chain (FJC) and the worm-like chain (WLC) models. The analytical theory, based on classical statistical mechanics, allows a rigorous mathematical treatment, while the study of complex systems is covered by means of Monte Carlo simulations.

On the one hand, the uniform stretching of a single polymer, imposed by an external pulling force, is pursued for studying the statistical mechanics of small molecules. When the thermodynamic limit is not satisfied, different boundary conditions (either Helmholtz or Gibbs ensemble) yield different elastic behavior, showing the fascinating intrication native to the thermodynamics of small systems. This complexity is shown to be even more suggestive when investigating bistable molecules of which domains exhibit transitions between two stable states. This scenario leads from cooperative to non-cooperative response of each domain to the external force, depending on the specific statistical ensemble considered. Universal scaling laws are provided, governing the overall elasticity of the polymer systems.

On the other hand, the non-uniform stretching of a single molecule, imposed by an external field, is studied to analyze the average configurational properties of polymers and leads to another very intriguing scenario concerning the behavior of the variances describing the fluctuations of the system. Furthermore, for the WLC model our attention fall in the investigation of the force-extension curve, for which we derive new approximated expressions for a chain immersed into an external field.

## RÉSUMÉ

---

Cette thèse est consacrée à l'étude théorique et numérique du comportement thermo-élastique des polymères d'intérêt biologique. On étudie la thermo-élasticité d'une molécule polymérique soumise soit à une traction uniforme (générée par une force appliquée) soit à une traction non uniforme (générée par un champ extérieur). Des solutions analytiques, ainsi que des simulations de dynamique moléculaire, sont élaborées à partir de deux modèles différents: freely-jointed chain (FJC) et worm-like chain (WLC). La théorie analytique, basée sur la thermodynamique statistique, permet un traitement mathématique rigoureux, tandis que l'étude des systèmes complexes est basée sur des simulations de Monte Carlo.

Dans une première partie, une étude de la traction uniforme d'une macromolécule est proposée afin de comprendre la mécanique statistique qui contrôle le processus d'extension. On constate que, lorsque la limite thermodynamique n'est pas satisfaite, différents comportements élastiques sont observés en changeant les conditions aux limites (ensemble de Helmholtz ou ensemble de Gibbs), montrant ainsi la fascinante intrication de la thermodynamique des petits systèmes (small systems thermodynamics). Cette complexité se révèle encore plus suggestive lorsque on regarde le comportement des molécules bistables dont les domaines présentent des transitions entre deux états stables. Ce scénario est dû à la réponse coopérative ou non-coopérative de la force externe dans chaque domaine, en fonction de l'ensemble statistique considéré. Les lois des échelles universelles régissant l'élasticité globale du système polymère sont fournies.

La seconde partie de la thèse est consacrée à l'étude de la traction non uniforme d'une macromolécule. L'objectif est l'analyse des propriétés configurationnelles moyennes des polymères; cette démarche conduit à l'étude du comportement des variances décrivant les fluctuations du système. En outre, pour le modèle WLC, notre attention s'est portée sur la courbe contrainte-déformation, pour laquelle on obtient de nouvelles expressions pour une chaîne polymérique immergée dans un champ extérieur.

## SOMMARIO

---

La presente tesi concerne lo studio del comportamento termo-elastico di polimeri di interesse biologico. In particolare si studia la termo-elasticità di polimeri a catena singola soggetti a deformazione uniforme (generata da una forza applicata) oppure a deformazione non uniforme (generata da un campo esterno). Si sviluppano simulazioni di dinamica molecolare e si elaborano espressioni analitiche prendendo in considerazione alcune generalizzazioni dei modelli freely-jointed chain (FJC) e worm-like chain (WLC). La teoria, basata sulla meccanica statistica classica, consente un trattamento matematico rigoroso della risposta elastica in strutture semplici e le simulazioni fondate sul metodo Monte Carlo permettono di studiare sistemi più complessi. La deformazione uniforme generata da una singola forza applicata ha permesso di introdurre la meccanica statistica dei piccoli sistemi. In tali condizioni il limite termodinamico non è soddisfatto e diverse condizioni limite (Helmholtz e Gibbs) possono generare differenti risposte elastiche. Tale fenomeno è ancora più rilevante quando si trattano catene polimeriche soggette a trasformazioni configurazionali fra due stati metastabili. In tal caso si osservano risposte cooperative (transizioni simultanee) o non-cooperative (transizioni sequenziali) al variare delle condizioni imposte.

La deformazione non-uniforme di catene polimeriche è studiata al fine di comprendere le proprietà configurazionali medie indotte dal campo applicato. Le varianze sono analizzate per descrivere le fluttuazioni del sistema. Infine, nel caso del modello WLC le curve forza-estensione vengono analizzate e alcune forme analitiche approssimate sono proposte.



## PUBLICATIONS

---

Some ideas and figures have appeared previously in the following publications:

1. F. Manca, S. Giordano, P. L. Palla, R. Zucca, F. Cleri, and L. Colombo, *J. Chem. Phys.* **136**, 154906 (2012). (Ref. [124]).
2. F. Manca, S. Giordano, P. L. Palla, F. Cleri, and L. Colombo, *J. Phys.: Conf. Ser.* **383**, 012016 (2012). (Ref. [209]).
3. F. Manca, S. Giordano, P. L. Palla, F. Cleri, and L. Colombo, *J. Chem. Phys.* **137**, 244907 (2012). (Ref. [210]).
4. F. Manca, S. Giordano, P. L. Palla, F. Cleri, and L. Colombo, *Phys. Rev. E* **87**, 032705 (2013). (Ref. [216]).



# CONTENTS

---

INTRODUCTION	1
<b>I POLYMER CHAINS IN BIOLOGY</b>	<b>5</b>
1 BIO-POLYMERS AND SINGLE MOLECULE EXPERIMENTS	7
1.1 Polymers	7
1.2 Biological polymers	9
1.2.1 Models for bio-polymers	12
1.3 Single molecule stretching experiments	15
1.3.1 Atomic force microscopy (AFM)	17
1.3.2 Force and elasticity measurements	18
1.3.3 Optical tweezers (OTs)	20
1.3.4 Magnetic tweezers (MTs)	21
1.3.5 Flow fields	21
<b>II OUTLINE OF ANALYTICAL AND STATISTICAL MECHANICS</b>	<b>23</b>
2 ANALYTICAL MECHANICS	25
2.1 Constrained systems	26
2.2 Generalized coordinates	27
2.3 Lagrangian approach	29
2.4 The Jacobi integral and the Hamiltonian	31
2.5 Mathematical form of the kinetic energy	32
2.6 The state space and the phase space	34
2.7 Hamiltonian approach	36
3 STATISTICAL MECHANICS	39
3.1 From analytical to statistical mechanics	40
3.2 The Hamiltonian vector field	41
3.3 Liouville's theorem	43
3.4 The ergodic problem	44
3.4.1 Measure-preserving and ergodic system	46
3.4.2 Phase space conservation	47
3.4.3 Birkhoff's ergodic theorem	49
3.5 Microcanonical distribution	49
3.6 Ideal gas phase space volume	52
3.7 Canonical distribution	54

<b>III THEORETICAL AND COMPUTATIONAL APPROACHES</b>	
	59
<b>4 FROM STATISTICAL MECHANICS TO THERMODYNAMICS OF SINGLE POLYMERS</b>	61
4.1 Thermodynamics of polymer chains	63
4.2 Helmholtz ensemble	64
4.3 Gibbs ensemble	70
4.4 Relationship between Helmholtz and Gibbs partition functions	76
4.4.1 Fourier transform theory approach	76
4.4.2 Laplace transform theory approach	78
4.5 Outline of the results	79
<b>5 METROPOLIS MONTE CARLO METHOD</b>	81
5.1 Ensemble average calculations	81
5.2 Simulation method	82
5.2.1 The Metropolis Monte Carlo algorithm	84
5.2.2 Make a trial move	88
5.3 Pseudo random-number generation	89
5.4 A sampling problem: the quasi-ergodicity	91
<b>IV POLYMER CHAINS LOADED BY EXTERNAL FORCES</b>	
	95
<b>6 ELASTICITY OF POLYMERS IN THE GIBBS AND HELMHOLTZ ENSEMBLES</b>	97
6.1 General theoretical framework	99
6.1.1 Polymer with fixed end-to-end distance	99
6.1.2 Polymer under constant load	100
6.2 On the thermodynamic limit	100
6.3 Equivalence of statistical ensembles	103
6.4 Flexible polymer with elastic bonds	107
6.5 Semiflexible polymer with elastic bonds	114
6.6 Outline of the results	119
<b>7 TWO-STATE THEORY OF SINGLE POLYMER STRETCHING</b>	121
7.1 General framework	123
7.2 Theoretical model and calculations	124
7.2.1 Gibbs ensemble: cooperative response	126
7.2.2 Helmholtz ensemble: non-cooperative response	130
7.3 Outline of the results	134

V	POLYMER CHAINS LOADED BY EXTERNAL FIELDS	137
8	EFFECT OF A SEQUENCE OF FORCES ON MONOMERS CHAINS	139
8.1	General theoretical framework	141
8.2	Freely-jointed chain under external field	146
8.2.1	Average values of positions	146
8.2.2	Covariances and variances of positions	152
8.3	Freely-jointed chain with elastic bonds	158
8.4	Worm-like chain under external field	161
8.5	Action of a pulling force not aligned with the external field	167
8.6	Outline of the results	171
	CONCLUSIONS AND PERSPECTIVES	173
VI	APPENDIX	177
A	APPENDIX	179
A.1	Beta Euler function	179
A.2	Fourier integral for functions with spherical symmetry	181
	ACKNOWLEDGMENTS	185
	BIBLIOGRAPHY	187



## INTRODUCTION

---

The recent development of mechanical experiments on single molecules provide a deeper understanding of intermolecular and intramolecular forces, thereby introducing crucial additional information about the thermodynamics and kinetics of several biomolecular processes [1, 2, 3]. Single-molecule experimental methods can be typically based on laser optical tweezers (LOTs) [3], magnetic tweezers (MTs) [4] or atomic force microscope (AFM) [5]. These experimental techniques have been extensively applied to nucleic acids (DNA, RNA and DNA condensation) [6], proteins (protein-protein interaction [7] and protein folding [8]), molecular motors [9] and other long-chain biopolymers [10]. They all provide a valuable insight about the response of polymers to external forces, allowing the detailed investigation of the force-extension relationship for macromolecules. Furthermore, in such experiments the determination of small energies and the detection of large deviations due to Brownian interactions offer a new method for analyzing the basic foundations of statistical mechanics. In particular, the above techniques permit a clearer comprehension of the equilibrium and non-equilibrium thermodynamics of small systems and the experimental verification of fluctuation theorems [11, 12, 13]. These results and successive experimental evidences suggest that the mechanical properties of DNA, and in particular its flexibility [14], have a relevant role in many biological processes [15].

The importance of understanding the force-extension relationship for macromolecules has therefore attracted the attention of physicists and mathematicians, who produced several models and relationships to explain the experimental results. The simplest model of a polymer is known as the *freely-jointed chain* (FJC) model [16, 17, 18], which is appropriate to describe certain biopolymers, including single-stranded DNA (*ssDNA*) and RNA [19]. Another important and well known model is the *worm-like chain* (WLC) [17], which well describes the double-stranded DNA (*dsDNA*). The first famous investigation concerning the stretching

of a chain structure in order to measure its elastic features was performed on the double-stranded DNA: the experimental results appeared in very good agreement with the WLC model [20, 21] while they were only in partial agreement with the FJC model (the latter model typically providing, however, a better fit for single-stranded DNA and RNA [19]). The discrete version of the WLC model has been considered and new interpolation formulas for semiflexible polymers have been introduced [22, 23]. Moreover, efficient techniques for calculating the thermo-mechanical properties of an heterogeneous chain have been developed through the numerical determination of the statistical partition functions under different types of boundary conditions [24]. In spite of the richness of experimental results and the large number of models devoted to explain specific situations, there is often the lacks of a universal theoretical approach able to describe different mechanical behaviours. The philosophy of our approach has been focused on the interest in developing unifying models capturing at the same time different physical pictures.

*the present  
thesis*

In particular, in this thesis we work on the thermo-elasticity of single polymer models of biological relevance. Our approach is twofold, since we adopt both theoretical and numerical techniques considering some generalizations of the FJC and the WLC models. The analytical theory is based on classical statistical mechanics and allows a rigorous mathematical treatment for some systems. On the other hand, the study of more complex systems is covered by means of Metropolis Monte Carlo simulations. The rationale of our approach can be framed within the scheme above defined.

*structure  
of the  
thesis*

The thesis is organized as follows:

PART I provides an overview of the structure of biopolymers and some experimental methods adopted in recent investigations:

- Chapter 1 supplies a brief outline of the main concepts of biopolymers and how these complex structures are modeled for theoretical studies. A discussion on some experimental methods at a single-molecule level is likewise presented.

PART II is addressed to the description of some basic concepts pertaining to analytical and statistical mechanics:

- Chapter 2 deals with analytical mechanics. In order to introduce the statistical mechanics formalism, two reformulations of Newton's mechanics for systems with constraints are presented: the Lagrangian and the Hamiltonian formalisms.
- Chapter 3 deals with statistical mechanics. The outline of classical statistical mechanics is presented, so as to lay the groundwork to introduce the subject of the present thesis: the thermodynamics of single polymer chains. More precisely, the microcanonical and the canonical distributions are briefly discussed.

PART III provides an insight into the thermodynamics of single polymer chains and some applications of the Metropolis Monte Carlo simulation approach:

- Chapter 4 deals with the thermodynamics of a polymer model with a finite number  $N$  of monomers and with an arbitrary potential  $V$  on monomers. For this model, we describe two different approaches that lead to two different ensembles: the Helmholtz and the Gibbs ensembles. The proper partition functions are found and an exact relationship between them is worked out. In particular, it is shown that the Gibbs partition function is the three-dimensional (bilateral or two-sided) Laplace transform of the Helmholtz partition function.
- Chapter 5 is addressed to provide an overview on the Metropolis Monte Carlo method. The reasons that give rise to take profit of the method are discussed, as well as some insidious problems of the approach (i.e., the quasi-ergodicity sampling) are presented.

PART VI provides an insight into the thermodynamics of single polymer chains loaded by external forces and some basic concepts the Metropolis Monte Carlo method are presented:

- Chapter 6 deals with the statistical mechanics of a small polymer chain. We take into consideration the quantitative difference between the thermodynamic behaviour of the Helmholtz or Gibbs ensemble, by investigating the foundations of the statistical mechanics for small systems. While

the analytical approach is useful to obtain the explicit partition function in some specific cases, Metropolis Monte Carlo simulations are crucial to determine the scaling laws controlling the convergence to the thermodynamic limit. In all cases we show that the convergence to the thermodynamic limit upon increasing contour length is described by a suitable power law and a specific scaling exponent, characteristic of each model.

- Chapter 7 provides an insight into the finite-size elasticity of model polymers consisting of domains that can exhibit transitions between two stable states at large applied force. The constant-force (Gibbs) and constant-displacement (Helmholtz) formulations lead to two separated classes of results showing *cooperative* and *non-cooperative* mechanically induced unfolding. We developed a unifying model capturing at the same time the main features of both behaviors, via a unique universal model.

PART V provides some meaningful investigations on the elasticity of single polymer chains immersed in external fields:

- Chapter 8 furnishes a study on the non-uniform stretching of a single, non-branched polymer molecule by an external field (e.g. fluid in uniform motion, or uniform electric field). A universal physical framework that leads to general conclusions on different types of polymers is provided. We derive analytical results both for the freely-jointed chain and the worm-like chain models based on classical statistical mechanics. The average conformation of the polymer and its fluctuation statistics are evaluated by means of Metropolis Monte Carlo.

Part I

POLYMER CHAINS IN BIOLOGY



# BIO-POLYMERS AND SINGLE MOLECULE EXPERIMENTS

---

## Contents

---

1.1	Polymers	7
1.2	Biological polymers	9
1.2.1	Models for bio-polymers	12
1.3	Single molecule stretching experiments	15
1.3.1	Atomic force microscopy (AFM)	17
1.3.2	Force and elasticity measurements	18
1.3.3	Optical tweezers (OTs)	20
1.3.4	Magnetic tweezers (MTs)	21
1.3.5	Flow fields	21

---

The exceptional spectrum of polymeric materials and their properties plays a capital and ubiquitous role in everyday life from those of familiar synthetic plastics to the natural bio-polymers that are fundamental for biological functions. Most of biological macromolecules are composed in large part of polymers, including proteins, nucleic acids and polysaccharides. The investigation on the mechanical properties of bio-polymers plays a crucial role in understanding biological systems. These structures are complex and the comprehension of their behavior is a very fascinating challenge. Experimental methods allow to investigate bio-polymers by means of mechanical stimulus, including forces. All biological motions, from cellular motility to replication and segregation of DNA, are driven by molecular-scale forces. In this Chapter we present an overview on the structure of polymers and some experimental methods adopted at a single-molecule level.

### 1.1 POLYMERS

A polymer is a large molecule (macromolecule) composed of multiple repeating units (monomers) typically connected by *covalent* chemical bonds. A monomer is in general anything that re-



Figure 1.1: **Different types of polymer architectures.** Linear, ring, star-branched and randomly-branched polymers. Taken from: Ref. [16]

peats along the chain. If the macromolecule contains monomers of only one type is called homopolymer [16].



This type of polymer is usually represented as a chain of  $N$  repeating sequences. Macromolecules composed of the same monomers differ from one another for their microstructure, degree of polymerization or architecture [25]. The number  $N$  is also called the *degree of polymerization* and is a very important factor determining manifold conformational properties of polymeric chains [17]. The other two main factors that define the conformational properties of a polymeric chain are the *microstructure*, which is related to the physical arrangement of the monomers along the chain, and the *architecture*, which is the way in which branched monomers lead to a deviation from a simple linear chain. A branched polymer molecule is composed of a main chain with one or different side chains (branches). Types of polymer architecture range from the most simple linear structure to complex branched configurations that can form networks of polymers [26]. Examples of polymer architecture include *linear*, *ring*, *star-branched* and *randomly-branched* polymers (see Fig.1.1) [16].

*degree of  
polymerization*

*oligomers*

If a molecule has less than 20 monomers it is considered to be a small molecule and is called *oligomer*. Frequently polymers contain more than 20 units; linear polymers can contain up to ten billion monomers as for the longest known chromosome.

*heteropolymers*

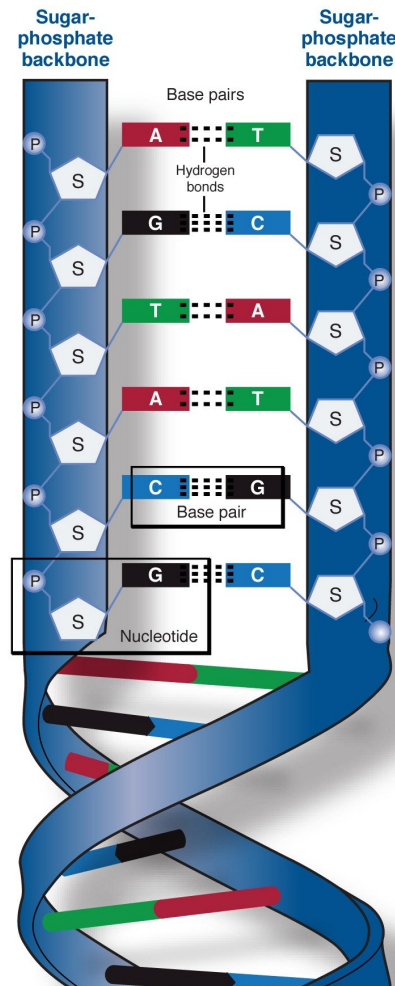
If a macromolecule contains different types of monomers is called *heteropolymer*, which properties depend on microstructure and are subordinated to the sequence of monomers in the chain. When a macromolecule is made by only two different monomers is called *copolymer* [16].

*copolymer*



## 1.2 BIOLOGICAL POLYMERS

Many biological macromolecules are heteropolymers, including proteins, which are made up of different monomeric units [27, 28]. There are four types of biological polymers (bio-polymers) of particular interest in this essay: nucleic acids, ribonucleic acids, proteins and polysaccharides. Deoxyribonucleic acid (DNA), ribonucleic acid (RNA) and proteins are examples of linear heteropolymers. DNA and RNA consist of four types of monomers (nucleotides), while natural proteins are commonly composed by 20 different types of monomers [27, 28, 29]. In Fig.1.2 is shown the simplified structure of a double helix DNA. The three-dimensional framework appears to be slightly richer and more complex, showing a double helix and other substructures. The structural support to the molecule is provided by a *phosphate* backbone. DNA consists of two strands that wind around each other. Each strand has a backbone made of alternating sugar (deoxyribose) and phosphate groups. The two strands are held together by hydrogen bonds between the bases with adenine forming a base pair with thymine and cytosine forming a base pair with guanine. One of the four bases is attached to each sugar: adenine (A), cytosine (C), guanine (G), or thymine (T). These bases make a particular alphabet that is (C, T, A, G) in the case of DNA and (C,



DNA and RNA

Figure 1.2: The structure of the DNA double helix.

Taken from: <http://www.genome.gov/>

One-letter code	Three-letter code	Amino-acid name
A	Ala	Alanine
R	Arg	Arginine
N	Asn	Asparagine
D	Asp	Aspartic acid
C	Cys	Cysteine
Q	Gln	Glutamine
E	Glu	Glutamic acid
G	Gly	Glycine
H	His	Histidine
I	ILe	Isoleucine
L	Leu	Leucine
K	Lys	Lysine
M	Met	Methionine
F	Phe	Phenylalanine
P	Pro	Proline
S	Ser	Serine
T	Thr	Threonine
W	Trp	Tryptophan
Y	Tyr	Tyrosine
V	Val	Valine

Table 1: **Overview of protein sequences.** The abbreviation codes for amino acids (one-letter and three-letter) adopted by the commission on Biochemical Nomenclature of the IUPAC-IUB.

*Taken from: Ref. [28]*

U, A, G) for RNA [6, 25, 27]. The letter U corresponds to a base named uracile.

*proteins*

Proteins are biological macromolecules consisting of one or different chains of amino acids. They perform different functions for biological organisms, including the transport of molecules from one location to another, the catalysis of metabolic reactions, and the replication of DNA. These macromolecules differ from one another principally in their sequence of amino acids. A polymer chain of amino acid residues is called a *polypeptide*. Proteins are made of up to 20 different residues that are indicated with three identifying letters of the corresponding amino acid (See. Tab.1).

		second base in codon						
		T	C	A	G			
T	first base in codon	TTT Phe	TCT Ser	TAT Tyr	TGT Cys	T	third base in codon	
		TTC Phe	TCC Ser	TAC Tyr	TGC Cys			C
		TTA Leu	TCA Ser	TAA stop	TGA stop			A
		TTG Leu	TCG Ser	TAG stop	TGG Trp			G
C	CTT Leu	CCT Pro	CAT His	CGT Arg	T			
	CTC Leu	CCC Pro	CAC His	CGC Arg	C			
	CTA Leu	CCA Pro	CAA Gln	CGA Arg	A			
	CTG Leu	CCG Pro	CAG Gln	CGG Arg	G			
A	ATT Ile	ACT Thr	AAT Asn	AGT Ser	T			
	ATC Ile	ACC Thr	AAC Asn	AGC Ser	C			
	ATA Ile	ACA Thr	AAA Lys	AGA Arg	A			
	ATG Met	ACG Thr	AAG Lys	AGG Arg	G			
G	GTT Val	GCT Ala	GAT Asp	GGT Gly	T			
	GTC Val	GCC Ala	GAC Asp	GGC Gly	C			
	GTA Val	GCA Ala	GAA Glu	GGA Gly	A			
	GTG Val	GCG Ala	GAG Glu	GGG Gly	G			

Figure 1.3: **The genetic code in DNA.** Correspondance between nucleotide sequence of DNA.

Taken from: <http://www.chemguide.co.uk/organicprops/aminoacids/dna4.html>

The base sequences in the DNA strand or in messenger RNA (mRNA) are instructions coded to build chains of protein constituted of amino acids. Even if a protein consists in 20 amino acids, only four different bases make the coded instructions. The set of all rules by which information encoded within genetic material (DNA or mRNA sequences) is translated into proteins (amino acid sequences) by living cells is called the *genetic code* [6].

Biological decoding is accomplished by the ribosome that links amino acids in an order specified by mRNA, using transfer RNA (tRNA) molecules to carry amino acids and to read the mRNA three nucleotides at a time [30]. The genetic code is hugely similar among all organisms, and can be expressed in a simple table with 64 entries (see Fig.1.3).

*codons* A three base sequence in DNA or RNA is called *codon*. In Fig.1.3 it is also shown how the combinations of three bases are used in the coding strand of DNA to code for individual amino acids. The colors underline that most of the amino acids have more than one code. Looking at leucine (Leu): there are six different codons all of which will eventually produce a leucine in the protein chain. Combinations of three bases are used in the coding strand of DNA to code for individual amino acids. Three codons do not have an amino acid written beside them and are known as *stop codons*. They serve as a signal to indicate that the end of the chain has been reached during protein synthesis [6, 27].

*stop  
codons*

Despite some great research evidences, unraveling the origin of the genetic code and translation machinery is an inherently difficult problem [31], and many questions are still awaiting a response. For example, the very complexity of the translation system [32] inevitably suggests that it has been shaped gradually and this implies an evolutionary motivation [30]. This is a great challenge to evolutionists. Moreover, as far as the coding and translation system is concerned, it would seem logical to start with separating the two “origins” - origin of the code, and origin of translation [33, 34]. All these complexities in genetic code investigation drive some scientist to recognize that “biology is frustratingly holistic” [35]. Events at one level can effect and be affected by events at very different levels of scale or time.

*polysaccharides*

Polysaccharides are molecules of *carbohydrate* monomers that are organics compound consisting in atoms of carbon, hydrogen and oxygen. Each carbohydrate monomer is joined together by *glycosidic* bonds. If all the monosaccharide monomers are of the same type, the polysaccharide is called a *homopolysaccharide*. When macromolecules are composed by different type of monosaccharide, they are called *heteropolysaccharides* [27].

### 1.2.1 Models for bio-polymers

To modelize and understand the previous complex structures we describe them as simple chains composed of a sequence of points representing the monomers of the chain and linked by rods representing the bond between monomers (see Fig.1.4) [17, 36].

The bond types for macromolecules can be *covalent* or *ionic* [37]. For the covalent bonds we shall assume a harmonic potential of the form

$$V(x) = (1/2)k(x - b)^2,$$

where  $k$  is a spring constant,  $b$  is the equilibrium bond length and  $x$  is the actual extension of the bond [25]. For certain models, anharmonic potentials are also used based on a finitely extensible non-linear elastic potential (FENE). The FENE potential is harmonic at its minimum but the bonds cannot be stretched beyond a maximum length determined by a certain value of finite extensibility [38].

An important measure describing the physics of a polymer is the *contour length*. If each monomer is joined by a bond with length  $b$ , then the total contour length of the chain is  $L_c = Nb$  [16, 17]. The way in which monomers are connected together is also important: the conformation describes the geometric structure of a polymer. If two monomers are joined by a single bond, then a rotation about that bond is possible. If the two monomers have other monomers or groups attached to them, then configurations in which torsional angle variations are possible. Indeed, angles between monomers are also used for the description of macromolecules.

The simplest model of a polymer regards the molecule as a chain of  $N$  monomers, joined by perfectly flexible bonds with length  $b$  [26, 38]. This model is known as the freely-jointed chain (FJC) model and it corresponds to a random walk where each step has length  $b$  [16, 17, 18]. This model is the most simple one for a single polymer in solution and it is appropriate to describe certain biopolymers, including single-stranded DNA (ssDNA) and RNA [19]. On the contrary, the FJC model is not useful for describing the double-stranded DNA (dsDNA), for which a well description is provided when regarding the polymer as semi-flexible [17, 27]. The semi-flexibility is a property of stiffer polymers with successive segments displaying a sort of *cooperativity* [17]: all pointing in roughly the same direction. The measure of this cooperativity is called *persistence length* that is, roughly speaking,

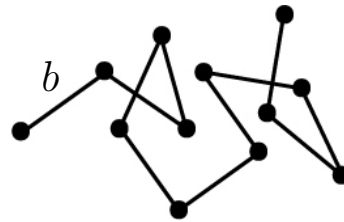


Figure 1.4: A simple polymer model. Each monomer is represented as a bead and each bond as a rigid rod.

*contour  
length*

*Freely  
jointed  
chains*

*Worm  
like  
chains*

the distance along the contour length of the molecule where the molecule keeps a straight direction due to its bending rigidity [1]. More precisely, describing a real polymer chain as a space curve  $\mathbf{r}(s)$  parametrized by a distance  $s$ , it is possible to define  $\mathbf{t}(s)$  as the unit tangent vector to the curve at the position  $s$  (see Fig.1.5). The persistence length is defined by a correlation function that gives the characteristic distance along the contour over which the tangent vectors  $\mathbf{t}(s)$  become uncorrelated:

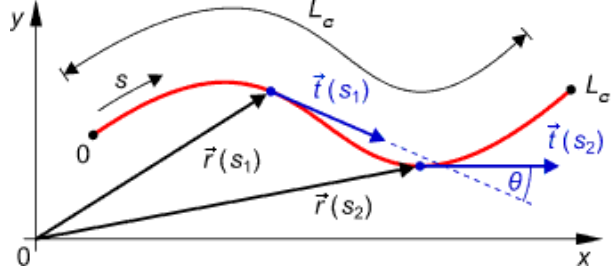


Figure 1.5: **Persistence length.** It measures the length along the chain over which the tangent vectors  $\mathbf{t}(s)$  become decorrelated [16, 26].

$$\langle \mathbf{t}(s) \cdot \mathbf{t}(s') \rangle = e^{-\frac{|s-s'|}{L_p}}, \quad (1.1)$$

where

$$L_p = \frac{\kappa}{k_B T}, \quad (1.2)$$

and  $\kappa$  is the bending stiffness, defined as the Young's modulus of the material times the moment of inertia of a filament cross-section about the axis of rotation. The persistence length is therefore a concept associated with the bending energy of the structure. This characteristic is taken into account by a more physically sound model known as the worm-like chain (WLC) model. While FJC model is flexible only between discrete segments, the WLC model describes elastic properties of semiflexible polymers dealing with rotational-isomeric-states, helicity and stiffness [17]. In particular, the investigation of the stiffness related to a response of a force applied to the macromolecule, has been of central and crucial interest on the past decades biophysical studies [2, 25].

Further, a number of mathematical models have been developed for describing the mechanical response of polymers in different chemical and loading conditions [16, 39, 40]. A technique describing the crossover between these two classes of models, FJC (flexible) and WLC (semiflexible), has been recently introduced [41]. It

has been shown that the alternative between these two regimes depends on the chain bending rigidity and the magnitude of the applied force. Moreover, we remark that models for semiflexible polymer chains can be realized both with continuum and discrete structures. The comparison between these two approaches and their applicability has been largely investigated [42]. A refined technique that has led to important results for the WLC model is based on the path integral formalism (functional integration) [43, 44, 45, 46, 47]. In fact, it has been proved that the calculation of the partition function for a continuous polymer chain exactly corresponds to a Feynmann path integral, as introduced in quantum mechanics [48]. All previous methodologies have been typically developed for analysing homopolymers, but can be also generalised to heteropolymers [49, 50].

Until recently, scientists could only investigate chemical processes on a bulk level. During the past few years, this situation has changed thanks to the development of methods to manipulate single molecules [51, 52, 53, 54]. Forces and stresses that molecules exert on each other are now directly measurable with high precision. These methods are yielding new informations about the forces that hold biomolecules together, revealing fundamental enlightenment concerning how they work and their functions on biological systems.

### 1.3 SINGLE MOLECULE STRETCHING EXPERIMENTS

A key issue in polymer theory concerns the determination of the physical properties of chains starting from the knowledge of the actual chemical architecture and environmental conditions [55, 56]. The response of single molecules provides additional information about thermodynamics and kinetics that is sometimes difficult to obtain in bulk experiments [57, 58]. Actually, measurements taken over single molecules might show a different mechanical behaviour with respect to a measure taken on a single bulk system; this is due to the coupled effects that many molecules have with each other. For example, it has been shown that during the folding process, characterized by the folded and the unfolded state, some proteins transiently visit an intermediate state, which is possible to observe only when regarding a single protein. On the contrary,

the intermediate state is usually masked in bulk measurements where results are averaged over many molecules [59]. One of the most important single-molecule experiment concerns the stretching of a macromolecule in order to measure its elastic features. Modern methods for stretching single molecules provide a valuable insight about the response of polymers to external forces. The interest on single molecules loading encouraged new research and technological developments on related mechanical experiments.

two important  
ways for  
manipulating  
polymer  
chains

external  
forces

Typically, mechanical methods allow the manipulation of a polymer molecule in two ways: the stretching of the chain by the direct action of an external force or by the application of an external field. If we consider homogeneous polymers (with all monomers described by the same effective elastic stiffness), then we obtain a *uniform* strain with the application of an external force and a *non-uniform* strain with an applied field. To exert an external force on a polymer fixed at one end, atomic force microscope (AFM) [5], laser optical tweezers (LOTs) [3] or magnetic tweezers (MTs) [4] can be used. Many experiments have been performed over a wide class of polymers with biological relevance, such as the nucleic acids (DNA, RNA) [6], allowing the stretching of the entire molecule and providing the reading and the mapping of genetic informations along the chain [60, 61]. The first famous investigation was performed on the *dsDNA* and the results appeared in very good agreement with the worm-like chain (WLC) model [20, 21] while they were only in partial agreement with the freely jointed chain (FJC) model (the latter model typically providing, however, a better fit for *ssDNA* and RNA [19]). Furthermore, it has been possible to observe the elastic behaviour of single polymers consisting of domains that exhibit transitions between different stable states [10, 62].

external  
fields

Alternatively, it is possible to manipulate single molecules by an external field. In this case the external field acts on the molecules from a distance or, in other words, without a defined contact point for applying the traction. A non-uniform stretching performed by an external field can be induced either via a hydrodynamic (or electrohydrodynamic) flow field [64, 65, 66] or via an electric (or magnetic) field [67, 68, 69]. The use of an electric field has been adopted for driving the alignment of DNA on a solid surface for applications such as gene mapping and restriction analysis [67]. All such manipulation methods for single molecule experiments

Methods	$F_{\min-\max}$ (N)*	$X_{\min}$ (m)*	Stiffness (Nm <sup>-1</sup> )
Cantilevers	$10^{-11} - 10^{-7}$	$10^{-10}$	0.001 – 100
Photon field	$10^{-13} - 10^{-10}$	$10^{-9}$	$10^{-10} - 10^{-3}$
Magnetic field	$10^{-14} - 10^{-11}$	$10^{-8}$	n.a.
Flow field	$10^{-13} - 10^{-9}$	$10^{-8}$	n.a.

Table 2: **Overview of single-molecule manipulation methods.**

\*These numbers represent only empirical, not absolute limits.

( $F_{\min-\max}$ , force range;  $X_{\min}$ , minimum displacement).

Taken from Ref. [63]

have their capabilities and limitations, which are often very different from one another. In Tab. 2 there are summarized the relevant force ranges, minimum displacement, probe stiffness and other details of each method [63].

### 1.3.1 Atomic force microscopy (AFM)

The atomic force microscopy (AFM) is the simplest single molecules technique in concept. Even if, AFM is born as an imaging tool, it allows as well the manipulation of individual molecules and the measurement of inter- and intramolecular interaction forces with piconewton resolution [70, 71, 72]. This property makes AFM an ideal tool for biological applications [73, 74, 75, 76, 77]. When used for the measurement of inter- and intramolecular interaction forces AFM is also called a molecular force probe (MFP). Two important advantages of the technique resides on the rapidity in sample preparation and on the possibility to conduct measurements of biological samples under physiological conditions [78, 79]. AFM consists of a cantilever with a tip held above a piezoelectric scanning stage. One end of a molecule is sticks to the cantilever tip, while its other end is fixed on the piezoelectric stage. The deflection of the cantilever is measured from the displacement of a low power laser reflected off the cantilever on a position-sensitive detector (PSD) (see Fig. 1.6) [63, 70]. When used for imaging, the AFM cantilever scans the surface of the sample line after line. When used as MFP, a macromolecule is attached to the sample surface and to the AFM cantilever tip.

The piezoelectric stage is retracted along the axial direction, increasing the separation between the cantilever and the sample surface. The force on the molecule is probed by the cantilever deflection, while the extension of the molecule is equal to the separation between the AFM tip and the sample surface. With that, a high-resolution force-extension curves of the single molecule can be detected [70].

*AFM applications*

Atomic force microscopy has been successfully adopted to study mechanical and conformational properties of macromolecules [5], including the unfolding in proteins made of repeating domains [10, 62].

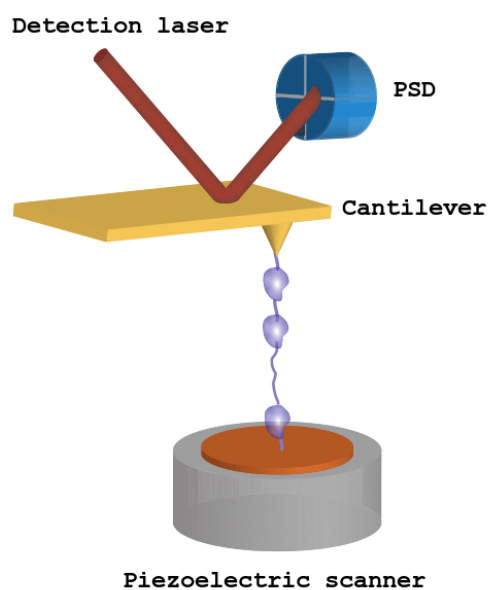


Figure 1.6: **Schematics of atomic force microscopy.**  
Taken from Ref. [70]

### 1.3.2 Force and elasticity measurements

*two types of measures*

While pulling on the macromolecule by an AFM, it is possible to obtain two types of measures: the force response of the molecule and its extension. In fact molecules can be described as springs that generate a restoring force when mechanically stretched. It is important to note that neither force nor extension data are recorded directly but rather through something that can be observed. Force is generally calculated from the bending of a cantilever of known spring constant. The cantilever stiffness depends on the material properties and shape of the cantilever. Typical values for cantilever springs in SME resides on the range  $10 - 10^2$  pN/nm.

*stiffness accuracy*

To obtain precise force data, each cantilever must be properly calibrated before use [70]. The stiffness accuracy depends on the calibration method used and is about  $10 - 20\%$ . The extension data are obtained by measuring the change in displacement be-

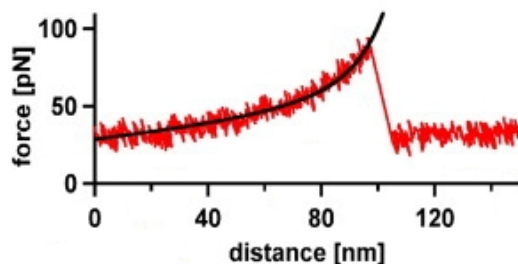


Figure 1.7: **Force-extension curve.** The extension of the molecule until its rupture is appreciable in a force releasing on the cantilever.

tween the ends of the molecule. The accuracy of this data is determined by the quality of the piezoelectric stage. Piezoelectric stages used in SME provide angstrom-level resolution. The force-extension curve (see Fig. 1.7), provides valuable informations on the structure, the folding and unfolding processes and even the chemical activity of the molecule. Measurement of the stretching curve is relatively straightforward. The AFM tip is lowered toward the surface or the sample is lifted toward the cantilever tip by piezoelectric actuators. After the initial contact with the surface, the cantilever is pressed into the surface on which the sample is deposited with a predetermined constant force. The tip is then retracted. Attachment of the sample (RNA, DNA or protein) tethers the cantilever tip to the surface, causing the cantilever to bend toward the surface as the tip is retracted (see Fig. 1.8 ). The value of this force is obtained by the Hooke law [70].

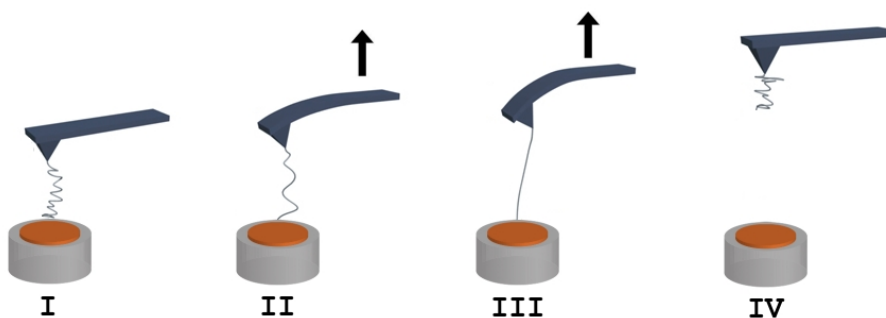


Figure 1.8: **Schematics of a single molecule stretching with AFM.** Initially the molecule is attached to the tip (I), then pulled and its extension is measured (II, III), finally the molecule is released or undergoes a rupture (IV).

### 1.3.3 Optical tweezers (OTs)

A very useful experimental technique are optical tweezers (OTs), also known as optical traps, which can be used to exert forces on dielectric particles ranging in size from nanometers to micrometers. The technique consists in focusing a laser to a diffraction limited spot creating an optical trap. One end of a molecule is tethered to a certain surface, the other end is attached to a bead that is trapped in a laser beam causing the extension of the molecule (see Fig.1.9). The particles near the focus experiences a restoring force within the range 0.1 – 100 pN directed toward the focus [36, 80, 81].

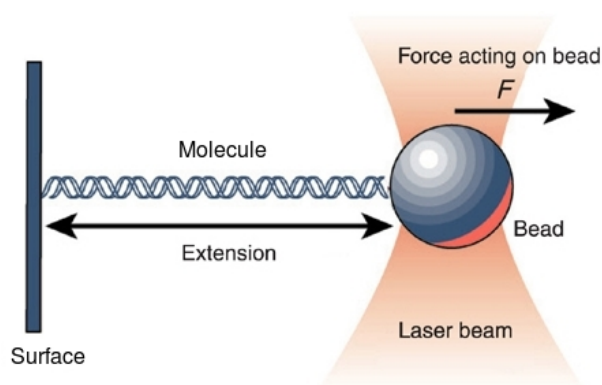


Figure 1.9: **Schematics of an optical tweezers experiment.**

Taken from: <http://jolifukyu.tokai-sc.jaea.go.jp>

The optical field polarizes the dielectric particle and the interaction with the gradient force near the focus results in a force directed along the gradient. There is also a scattering force along the beam propagation direction, which results in a shift of the equilibrium trapping position nearby the focus [70]. For small displacements ( $\sim 150$  nm) of the trapped object from its equilibrium position, the force is linearly proportional to the displacement and the optical trap can be well approximated as a linear spring. The spring constant depends on how tightly the laser is focused, the laser power and the polarizability of the trapped object. Once again, from the knowledge of the spring constant, the

value of the force is obtained by the Hooke law. A great advantage of optical tweezers is the accuracy of the force resolution, which usually is in the order of 0.1 pN [1]. This value is about 10 times more accurate than in AFM, because the stiffness of the trap is at least 100 times less than the one of a cantilever. Therefore the force resolution makes optical tweezers an ideal tool to investigate the behavior of biomolecules [82, 83, 84, 85].

*OTs  
applications*

#### 1.3.4 *Magnetic tweezers (MTs)*

Magnetic tweezers (MTs) are most straightforward to implement then the two previous techniques (AFM, OTs). The method consists on generating a magnetic trap by a pair of permanent magnets placed above the sample [86]. In such manner the concept is similar to that of optical tweezers: a (magnetic) particle in an external magnetic field experiences a force proportional to the gradient of the square of the magnetic field. One end of a molecule is tethered to a certain surface, the other end is attached to a bead, which is trapped in a magnetic field generated by magnets. (see Fig.1.10). Magnetic tweezers are capable of exerting forces of maximum 1 nN (for the case of the electromagnetic tweezers). They can be used to manipulate, and in particular, to rotate magnetic particles ranging from 0.5 to 5  $\mu\text{m}$  [70]. The typical force range that can be measured with this technique is  $10^{-2} - 10$  pN, which is highly sensitive to the typical size of the magnetic bead. The low stiffness of the magnetic trapping potential makes magnetic tweezers ideally to the study of nucleic acid enzymes [69, 87, 88, 89]. For their properties, magnetic fields have been also used to apply torsional stress to individual DNA molecules [68, 69].

*MTs  
applications*

#### 1.3.5 *Flow fields*

Flow fields are a particular case of external fields. They exert forces on each monomer of the molecule (tethered at one end) through the transfer of momentum from the fluid to the monomer. In a *laminar flow*, considering a liquid with viscosity  $\eta$  and velocity  $v$ , the drag force of the liquid in motion can be calculated using the Stokes law. The law is valid for forces up to  $\sim 10$  nN considering the flow as not turbulent. One experimental advantage

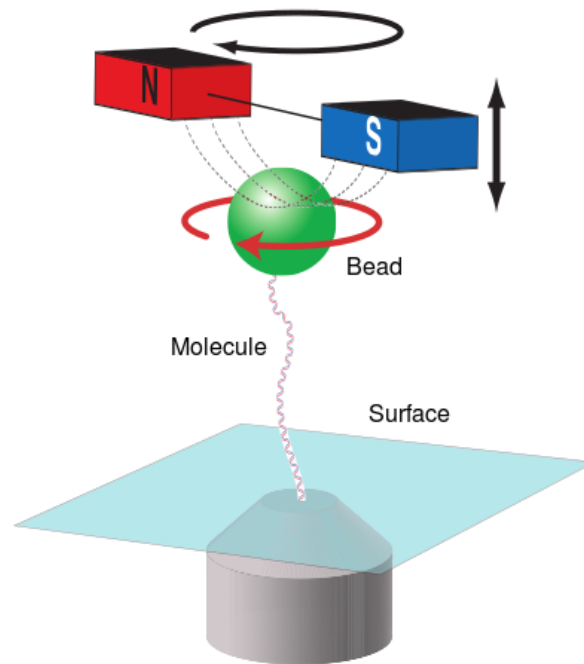


Figure 1.10: **Schematics of a magnetic tweezers experiment.**

*Taken from Ref. [70]*

of using flow fields is that the liquid surrounding the tethered molecule can be easily replaced. This is an important feature for many single-molecules studies of enzymes, which require varying buffer conditions [63].

*flow fields  
applications*

The flow field technique was extensively applied in single-molecule study of DNA elasticity [20] as well as to characterize the rheological properties of individual DNA molecules [90, 91, 92].

Part II

OUTLINE OF ANALYTICAL AND  
STATISTICAL MECHANICS



**Contents**

---

2.1	Constrained systems	26
2.2	Generalized coordinates	27
2.3	Lagrangian approach	29
2.4	The Jacobi integral and the Hamiltonian	31
2.5	Mathematical form of the kinetic energy	32
2.6	The state space and the phase space	34
2.7	Hamiltonian approach	36

---

This Chapter provides a description of some basic concepts pertaining to analytical mechanics that allow a consecutive introduction to the statistical mechanics formalism. Two reformulations of Newton's mechanics for systems with constraints are presented: the Lagrangian and the Hamiltonian formalisms.

There are many circumstances in mechanics whereby the motion of bodies is constrained in some way. In each case, there are forces acting on the constrained bodies and these forces are such as to guarantee the respect of the constraints.

In the Newtonian approach a mechanical system is treated by introducing variables representing the unknown forces, and solving the system of equations for forces and accelerations. As a matter of fact, this is not the unique procedure possible to follow, neither the best one in certain situations. For complicated systems the direct application of Newton's laws might become extremely complex. The reason lies on the fact that the equations are vectorial and forces and accelerations turn out difficult to be determined. This complication is even magnified when considering forces for maintaining constraints on the motion of particles [93].

There exist two reformulations of Newton's mechanics that offer two different ways for solving the problem of motion: the Lagrangian and the Hamiltonian formalisms. The first one is associ-

ated with configuration space, eventually extended by time, while the latter is related to the concept of phase space.

## 2.1 CONSTRAINED SYSTEMS

Let us consider a system composed of  $N$  particles defined in space by the vectors  $\mathbf{x}_1, \mathbf{x}_2, \dots, \mathbf{x}_N$  with  $3N$  independent variables and subjected to  $p$  constraints depending on the positions and the time. The general constraint can be expressed as:

$$f_1(\mathbf{x}_1, \mathbf{x}_2, \dots, \mathbf{x}_N, t) = 0. \quad (2.1)$$

Considering all the  $p$  constraints we can write the following system

$$\begin{cases} f_1(\mathbf{x}_1, \mathbf{x}_2, \dots, \mathbf{x}_N, t) = 0 \\ f_2(\mathbf{x}_1, \mathbf{x}_2, \dots, \mathbf{x}_N, t) = 0 \\ \vdots \\ f_p(\mathbf{x}_1, \mathbf{x}_2, \dots, \mathbf{x}_N, t) = 0, \end{cases} \quad (2.2)$$

*degrees of freedom*

for which we have  $n = 3N - p$  *degrees of freedom* (the number of degrees of freedom is equal to the number of coordinates that are used to specify the configuration of the system minus the number of independent equations of constraint [93]). In other words, one can say that solving a system with  $n$  degrees of freedom and  $N$  particles implies the existence of  $3N - n$  scalar constraint equations on those position variables.

*holonomic and non-holonomic constraints*

Constraints such as the one showed in Eq.(2.1) that are expressible only as a function of coordinates and time, and does not depend on velocities are defined *holonomic*. On the contrary, constraints depending also on velocities, such as:

$$f(\mathbf{x}_1, \mathbf{x}_2, \dots, \mathbf{x}_N, \mathbf{v}_1, \mathbf{v}_2, \dots, \mathbf{v}_N, t) = 0. \quad (2.3)$$

are called *nonintegrable* or *nonholonomic*.

Moreover, if the equations of constraints do not contain the time as an explicit variable, the mechanical system is called *scleronomous* and its constraints are called *scleronomic* constraints; otherwise the system is called *rheonomous* and its constraints are called *rheonomic constraints* [94].

## 2.2 GENERALIZED COORDINATES

In general, the configuration of a system can be expressed in terms of various sets of coordinates. This means that for the analysis of a mechanical system, different coordinate systems are possible. In fact, there is an infinite number of possible choices.

Considering the system in Eq.(2.2) we saw that, at any instant, the values of these coordinates could be expressed as a set of  $3N$  numbers. In other respects, expressing the positions of the particles in terms of spherical coordinates requires as well a set of  $3N$  numbers. The process of obtaining one set of numbers to express the configuration of the same system from the other is known as a *coordinate transformation*. There are some instances where the mathematical analysis of a dynamical system is simplified by choosing a set of independent generalized coordinates. Any set of number that serve to specify the configuration of a system is an example of *generalized coordinate*. This term can refer to any of the commonly used coordinate systems, but it can also refer to any of other sets of parameters that serve to specify the configuration of a system [93]. A system can be fully described by the *scalar generalized coordinates*,  $q_1, q_2, \dots, q_n$ , and the time  $t$ , if and only if all the  $q$ 's are *independent coordinates*. Considering Eq.(2.1), the transformation from old coordinates to generalized coordinates can be represented as follows

*coordinate  
transformation  
independent  
generalized  
coordinates*

$$\mathbf{x}_i = \mathbf{x}_i(q_1(t), q_2(t), \dots, q_n(t), t), \quad (2.4)$$

which we indicate from now on as

$$\mathbf{x}_i = \mathbf{x}_i(\mathbf{q}, t) \quad (2.5)$$

to simplify the notation.

Important enough, we notice that this is a relationship between different descriptions of the same point in configuration space, and the functions  $\mathbf{x}_i$  are independent of the motion of any particle. We are assuming that the  $\mathbf{x}_i$  and the  $q_k$  are each a complete set of coordinates for the space, so the  $q$ 's are also functions of the  $\mathbf{x}_i$  and  $t$ :

$$q_k = q_k(\mathbf{x}_1, \dots, \mathbf{x}_N, t). \quad (2.6)$$

For a more generic discussion, if we have to deal with nonholonomic constraints, hence considering Eq.(2.3), the equivalent coordinate transformation would be:

$$\begin{aligned} \mathbf{x}_i &= \mathbf{x}_i(q_1(t), q_2(t), \dots, q_n(t), p_1(t), p_2(t), \dots, p_n(t), t) \quad (2.7) \\ &= \mathbf{x}_i(\mathbf{q}, \mathbf{p}, t), \end{aligned}$$

where we have also included the possibility of using a coordinate system that changes with time  $t$ . We remand to Section 2.6 for a more detailed discussion on the meaning of the  $\mathbf{p}$  coordinates.

Let us, for the moment, stay on the transformation in Eq.(2.4); adopting the chain rule on this equation, we can write the total time derivative

$$\dot{\mathbf{x}}_i = \frac{d\mathbf{x}_i}{dt} = \frac{\partial \mathbf{x}_i}{\partial q_k} \dot{q}_k + \frac{\partial \mathbf{x}_i}{\partial t} \quad \forall k = 1, \dots, n \quad (2.8)$$

where we used the *Einstein convention* in which repeated indexes are summed over, that is

$$a_k b_k \equiv \sum_{k=1}^N a_k b_k. \quad (2.9)$$

From now on, we will use such a convention for generalized coordinates, whereas for the  $i$  particles we will explicit indicate the summation.

To be a good coordinate system, we should be able to invert the relationship so that

$$q_k = q_k(\mathbf{x}_i, t), \quad (2.10)$$

which we can do as long as we have

$$\det \left( \frac{\partial \mathbf{x}_i}{\partial q_k} \right) \neq 0, \quad (2.11)$$

since it is implied a linear transformation. Using the chain rule on Eq.(2.10), we get

$$\dot{q}_k = \frac{dq_k}{dt} = \frac{\partial q_k}{\partial \mathbf{x}_i} \dot{\mathbf{x}}_i + \frac{\partial q_k}{\partial t}. \quad (2.12)$$

## 2.3 LAGRANGIAN APPROACH

Let us consider a particle identified by the vector  $\mathbf{x}_i$  moving in a surface with a velocity  $\mathbf{v}_i$ . In this condition, the surface applies a certain force  $\Phi_i$  to the particle. If the surface is quiet (i.e. the constraint is scleronomic), we have

$$\sum_{i=1}^N \Phi_i \cdot \mathbf{v}_i = 0 \quad \forall \mathbf{v}_i. \quad (2.13)$$

From Newton's law we can write the total force as the contribution of the forces external to the system  $\mathbf{F}_i$  and the forces of constraint  $\Phi_i$  obtaining

$$\mathbf{F}^{\text{TOT}} = \sum_{i=1}^N m_i \mathbf{a}_i = \sum_{i=1}^N \mathbf{F}_i + \Phi_i. \quad (2.14)$$

If the surface is moving in time (rethonomic constraint) we must consider two admissible sets of velocities of the particles. So doing, the difference between these admissible velocities (the so-called virtual velocity) is tangent to the constraint (i.e. to the differential manifold representing the system). Therefore, Eq.(2.13) becomes

$$\sum_{i=1}^N \Phi_i \cdot (\mathbf{v}_i^{(1)} - \mathbf{v}_i^{(2)}) = 0 \quad \forall \mathbf{v}_i^{(1)}, \mathbf{v}_i^{(2)}. \quad (2.15)$$

From this, by using Eq.(2.8), we obtain

$$\sum_{i=1}^N \Phi_i \cdot (\mathbf{v}_i^{(1)} - \mathbf{v}_i^{(2)}) = \sum_{i=1}^N \Phi_i \cdot \frac{\partial \mathbf{x}_i}{\partial q_k} (\dot{q}_k^{(1)} - \dot{q}_k^{(2)}) = 0 \quad \forall k = 1, \dots, n \quad (2.16)$$

and, since the  $q_k$ 's are independent and arbitrary, we have that

$$\sum_{i=1}^N \Phi_i \cdot \frac{\partial \mathbf{x}_i}{\partial q_k} = 0 \quad \forall k = 1, \dots, n. \quad (2.17)$$

Using Eq.(2.14) one finally gets

$$\sum_{i=1}^N (\mathbf{F}_i - m_i \mathbf{a}_i) \cdot \frac{\partial \mathbf{x}_i}{\partial q_k} = 0 \quad \forall k = 1, \dots, n \quad (2.18)$$

*d'Alembert's principle*

which is called *d'Alembert's principle*. It is possible to demonstrate [93, 94, 95] that the last equation becomes

$$\frac{d}{dt} \left( \frac{\partial K}{\partial \dot{q}_k} \right) - \frac{\partial K}{\partial q_k} = \sum_i \mathbf{F}_i \cdot \frac{\partial \mathbf{x}_i}{\partial q_k} \quad \forall k = 1, \dots, n \quad (2.19)$$

where  $K$  is the total kinetic energy

$$K = \sum_{i=1}^N \frac{1}{2} m_i \mathbf{v}_i \cdot \mathbf{v}_i. \quad (2.20)$$

If the forces are conservatives, hence they are derivables from a scalar potential function

$$V = V(\mathbf{x}_1, \dots, \mathbf{x}_N), \quad (2.21)$$

and we can write

$$\mathbf{F}_i = -\nabla_i V = -\frac{\partial V}{\partial \mathbf{x}_i}, \quad (2.22)$$

where the  $\mathbf{x}_i$ 's are defined in Eq.(2.4). From that, it is possible to write the generalized forces  $Q_k$  as

$$Q_k = \sum_i (-\nabla_i V) \cdot \frac{\partial \mathbf{x}_i}{\partial q_k} = -\sum_i \left( \frac{\partial V}{\partial \mathbf{x}_i} \right) \cdot \frac{\partial \mathbf{x}_i}{\partial q_k} = -\frac{\partial V}{\partial q_k} - \frac{d}{dt} \left( \frac{\partial V}{\partial \dot{q}_k} \right), \quad (2.23)$$

where the last term in the right-hand side of Eq.(2.23) is zero. Therefore, for the generalized forces we have

$$\sum_i (-\nabla_i V) \cdot \frac{\partial \mathbf{x}_i}{\partial q_k} = -\frac{\partial V}{\partial q_k}. \quad (2.24)$$

Combining Eqs.(2.19) and (2.24) we get

$$\frac{d}{dt} \left( \frac{\partial (K - V)}{\partial \dot{q}_k} \right) - \frac{\partial (K - V)}{\partial q_k} = 0, \quad (2.25)$$

*the Lagrangian*

and, defining the new function *Lagrangian*  $L$  as

$$L = K - V, \quad (2.26)$$

we finally obtain

$$\frac{d}{dt} \left( \frac{\partial L}{\partial \dot{q}_k} \right) - \frac{\partial L}{\partial q_k} = 0, \quad (2.27)$$

which define a set of equations, known as the *Lagrange's equations* or, from variational calculus, the *Euler-Lagrange equations*.

The set up of the equations of motion via the Lagrangian formulation (i.e. by means of Eq.(2.27)) allow to solve them in a very convenient way. Indeed, while the original form of the Newton's law imposes to deal with many vectors (forces and accelerations), the Lagrangian formulation allows to work only with two scalar functions: the kinetic energy  $K$  and the potential energy function  $V$ . A standard method is then easily provided to solve the problem of motion of a mechanical system. It is only necessary to write down  $K$  and  $V$  in generalized coordinates, from which it is easily to find the Lagrangian as  $L = K - V$ . Finally, substituting  $L$  in the Lagrange's equations, one get the equations of motion.

*advantages of  
the Lagrangian  
approach*

#### 2.4 THE JACOBI INTEGRAL AND THE HAMILTONIAN

We want now give thought to the Lagrangian along the path of the motion. To do that, let us consider the general form of the Lagrangian, which depends on the  $q$ 's, the  $\dot{q}$ 's and the time, namely  $L = L(q(t), \dot{q}(t), t)$ . As we are interested on the time variation of the Lagrangian, we need to study its total time derivative. Considering Eq.(2.27) we have,

$$\frac{dL}{dt} = \frac{d}{dt} L(q(t), \dot{q}(t), t) = \frac{\partial L}{\partial q_k} \dot{q}_k + \frac{\partial L}{\partial \dot{q}_k} \ddot{q}_k + \frac{\partial L}{\partial t}, \quad (2.28)$$

where we can write the second term in the right-hand side via the following total time derivative

$$\frac{d}{dt} \left( \frac{\partial L}{\partial \dot{q}_k} \dot{q}_k \right) = \frac{d}{dt} \left( \frac{\partial L}{\partial \dot{q}_k} \right) \dot{q}_k + \frac{\partial L}{\partial \dot{q}_k} \ddot{q}_k, \quad (2.29)$$

thus getting

$$\frac{dL}{dt} = \frac{d}{dt} \left( \frac{\partial L}{\partial \dot{q}_k} \dot{q}_k \right) + \frac{\partial L}{\partial t} - \left[ \frac{d}{dt} \left( \frac{\partial L}{\partial \dot{q}_k} \right) - \frac{\partial L}{\partial q_k} \right] \dot{q}_k, \quad (2.30)$$

which becomes

$$\frac{dL}{dt} = \frac{d}{dt} \left( \frac{\partial L}{\partial \dot{q}_k} \dot{q}_k \right) + \frac{\partial L}{\partial t} \quad (2.31)$$

because, from Eq.(2.27), the last term in squared brackets turns out to be zero. Rewriting the last equation we get

$$\frac{\partial L}{\partial t} = \frac{d}{dt} \left( L - \frac{\partial L}{\partial \dot{q}_k} \dot{q}_k \right), \quad (2.32)$$

and introducing a new function

$$H = H(\mathbf{q}, \dot{\mathbf{q}}) = \frac{\partial L}{\partial \dot{q}_k} \dot{q}_k - L, \quad (2.33)$$

we finally gets

$$\frac{dH}{dt} = -\frac{\partial L}{\partial t}. \quad (2.34)$$

*the  
Hamiltonian*

The new function in Eq.(2.33) is called *Hamiltonian* of the system.

If the Lagrangian does not depend on time (e.g. when the system is scleronomous), we expect a conservation law. In fact we have

$$\frac{\partial L}{\partial t} = 0 \quad \Rightarrow \quad \frac{dH}{dt} = 0 \quad (2.35)$$

*the Jacobi  
integral*

that is

$$J \equiv \frac{\partial L}{\partial \dot{q}_k} \dot{q}_k - L = \text{constant}, \quad (2.36)$$

where the quantity  $J$  is a constant of motion and it is called the *Jacobi integral* of the system. Moreover, if the system is scleronomous we find

$$H = K + V. \quad (2.37)$$

Note that, strictly speaking, the name *Hamiltonian* for  $H$  is reserved for the function  $H = H(\mathbf{q}, \mathbf{p}, t)$  on extended *phase space* rather than the function with arguments  $H(\mathbf{q}, \dot{\mathbf{q}}, t)$  as we previously defined (for scleronomous systems) in Eq.(2.21).

## 2.5 MATHEMATICAL FORM OF THE KINETIC ENERGY

We previously discussed that for systems that admit the Lagrangian formulation, equations of motion are easily found by

starting to write  $T$  and  $V$  in generalized coordinates. The transformation of  $T$ , from Cartesian coordinates to generalized coordinates, is obtained by using the transformation equation Eq.(2.4) and finding the velocities from it. From Eq.(2.8), we have the velocities in generalized coordinates, following

$$\mathbf{v}_i = \frac{\partial \mathbf{x}_i}{\partial q_k} \dot{q}_k + \frac{\partial \mathbf{x}_i}{\partial t}. \quad (2.38)$$

The kinetic energy  $T$  is then writable as

$$\begin{aligned} T &= \frac{1}{2} \sum_{i=1}^N \frac{1}{2} m_i \mathbf{v}_i \cdot \mathbf{v}_i \\ &= \frac{1}{2} \sum_{i=1}^N m_i \left( \frac{\partial \mathbf{x}_i}{\partial q_k} \dot{q}_k + \frac{\partial \mathbf{x}_i}{\partial t} \right) \cdot \left( \frac{\partial \mathbf{x}_i}{\partial q_h} \dot{q}_h + \frac{\partial \mathbf{x}_i}{\partial t} \right). \end{aligned} \quad (2.39)$$

Carrying out the expansion, the expression becomes

$$\begin{aligned} T &= \frac{1}{2} \sum_i m_i \frac{\partial \mathbf{x}_i}{\partial q_k} \cdot \frac{\partial \mathbf{x}_i}{\partial q_h} \dot{q}_k \dot{q}_h + \sum_i m_i \frac{\partial \mathbf{x}_i}{\partial q_k} \cdot \frac{\partial \mathbf{x}_i}{\partial t} \dot{q}_k \\ &+ \frac{1}{2} \sum_i m_i \frac{\partial \mathbf{x}_i}{\partial t} \cdot \frac{\partial \mathbf{x}_i}{\partial t}, \end{aligned} \quad (2.40)$$

and respectively defining three new term  $a_0$ ,  $a_k$ ,  $a_{kh}$ , as

$$a_0 = \frac{1}{2} \sum_i m_i \frac{\partial \mathbf{x}_i}{\partial t} \cdot \frac{\partial \mathbf{x}_i}{\partial t}, \quad (2.41)$$

$$a_k = \sum_i m_i \frac{\partial \mathbf{x}_i}{\partial t} \cdot \frac{\partial \mathbf{x}_i}{\partial q_k}, \quad (2.42)$$

$$a_{kh} = \sum_i m_i \frac{\partial \mathbf{x}_i}{\partial q_k} \cdot \frac{\partial \mathbf{x}_i}{\partial q_h}, \quad (2.43)$$

we finally get

$$T = \frac{1}{2} a_{kh} \dot{q}_k \dot{q}_h + a_k \dot{q}_k + a_0, \quad (2.44)$$

*mathematical  
form of the  
kinetic energy*

which is called *mathematical form of the kinetic energy*.

Therefore, the kinetic energy of a system can be written as the sum

of three homogeneous term: one independent of the generalized velocities, one linear and one term that is quadratic in them.

Using the mathematical form of  $T$ , we define the *mathematical form of the Lagrangian* as:

$$\begin{aligned} L &= K - V \\ &= \frac{1}{2} a_{kh} \dot{q}_k \dot{q}_h + a_k \dot{q}_k + a_0 - V. \end{aligned} \quad (2.45)$$

*mathematical  
form of the  
Hamiltonian*

From Eq.(2.33) we find

$$\begin{aligned} H &= \frac{\partial}{\partial \dot{q}_k} \left[ \frac{1}{2} a_{sh} \dot{q}_s \dot{q}_h + a_s \dot{q}_s + a_0 - V \right] \dot{q}_k - L \\ &= \left[ \frac{1}{2} a_{sh} (\delta_{sk} \dot{q}_h + \delta_{hk} \dot{q}_s) + \delta_{sk} a_s \right] \dot{q}_k - L \\ &= \frac{1}{2} a_{kh} \dot{q}_h \dot{q}_k + \frac{1}{2} a_{sk} \dot{q}_s \dot{q}_k + a_k \dot{q}_k - L \\ &= \frac{1}{2} a_{kh} \dot{q}_h \dot{q}_k + V - a_0, \end{aligned} \quad (2.46)$$

that is known as *mathematical form of the Hamiltonian*.

If the system is scleronomous

$$a_{kh} \neq 0 \quad a_k = 0 \quad a_0 = 0, \quad (2.47)$$

then

$$T = \frac{1}{2} a_{kh} \dot{q}_k \dot{q}_h, \quad (2.48)$$

and we get again

$$H = K + V. \quad (2.49)$$

## 2.6 THE STATE SPACE AND THE PHASE SPACE

We previously discussed the advantages obtained passing from the Newtonian to the Lagrangian approach: Lagrange's equations are obtained by a derivation from a scalar function (the Lagrangian  $L$ ) and they have the same structure independently of the coordinates choice. From the Lagrangian we derived another scalar function, the Hamiltonian  $H$ , as a function of  $q$ 's,  $\dot{q}$ 's and the time  $t$ , therefore a function defined in the space of ( $q$ 's,  $\dot{q}$ 's) called the *configuration space*. There exists a convenient way to

*configuration  
space*

write Lagrange's equations that allow us to obtain a system of  $2n$  equations of the first order instead of a system of  $n$  second-order equations. Even if this can appear only another way to write Lagrange's equations, we will see that it is a mandatory rewriting for the foundation of *statistical mechanics*. In fact, using the Hamiltonian formalism the compatibility between probability and dynamics (which is one of the central problems of statistical mechanics) can be formulated in a very easy way by means of the Liouville's theorem.

Let us consider a system with  $n$  degrees of freedom, and a space of possible configurations  $\mathcal{C}$  in which it is fixed a system of local coordinates  $\mathbf{q} = (q_1, \dots, q_n)$ . For such a system, it is possible to rewrite the Lagrange's equations (see Eq.(2.27)) in a *normal form*, obtaining

$$\ddot{\mathbf{q}} = f(\mathbf{q}, \dot{\mathbf{q}}, t), \quad \mathbf{q} \in \mathfrak{R}^n. \quad (2.50)$$

From this, it appears clear that Lagrange's equations form a system of  $n$  second-order equations. We want to show that it is convenient to think the Lagrange's equations as a system of first order equations in a space with a double ( $2n$ ) number of variables. The reason lies in the fact that, for a second order equation as Eq.(2.50), each solution is identified by the pair  $(\mathbf{q}_0, \dot{\mathbf{q}}_0)$  of initial positions and velocities. Therefore, it is spontaneous to evaluate, instead of the space of configurations  $\mathcal{C}$ , another space in which the pairs  $(\mathbf{q}, \dot{\mathbf{q}})$  are thought to be independent from one another. This space is called the *state space*. In this way, it is possible to study the evolution in time of the state space points, namely the pairs positions  $\mathbf{q} = \mathbf{q}(t)$  and velocities  $\dot{\mathbf{q}} = \dot{\mathbf{q}}(t)$ . From this discussion, becomes natural the definition of an another space: instead of the velocities defined as  $\dot{\mathbf{q}}(t)$ , are introduced the auxiliary variables  $\mathbf{p} = (p_1, \dots, p_n)$  which are called *momentum conjugate* to the coordinates  $\mathbf{q} = (q_1, \dots, q_n)$  or *canonical momentum*. They are defined as

*the state space*

*canonical momentum*

$$p_k = \frac{\partial L}{\partial \dot{q}_k}(\mathbf{q}, \dot{\mathbf{q}}, t). \quad (2.51)$$

Their utility comes clear rewriting the Lagrange's equation Eq.(2.27) using the canonical momentum in Eq.(2.51). In fact, from

$$\frac{d}{dt} \left( \frac{\partial L}{\partial \dot{q}_k} \right) - \frac{\partial L}{\partial q_k} = \dot{p}_k - \frac{\partial L}{\partial q_k} = 0 \quad (2.52)$$

one obtain the Lagrange's equations in the following form

$$\dot{p}_k = \frac{\partial L}{\partial q_k}(\mathbf{q}, \dot{\mathbf{q}}, t), \quad (2.53)$$

which is a set of equations of the first order in *normal form*.

*the phase  
space*

Consequently we can now introduce the new space mentioned before, instead of the state space  $(\mathbf{q}, \dot{\mathbf{q}})$ , the so called *phase space*  $(\mathbf{q}, \mathbf{p})$ , where we indicate

$$\mathbf{x} = (x_1, x_2, \dots, x_{2n}) = (q_1, q_2, \dots, q_n, p_1, p_2, \dots, p_n) \quad (2.54)$$

as the generalized coordinates, briefly

$$\mathbf{x} \equiv (\mathbf{q}, \mathbf{p}) \in \mathfrak{R}^{2n}. \quad (2.55)$$

It is possible to show that one can write the whole system in normal form, namely in the form

$$\dot{\mathbf{x}} = \mathbf{V}(\mathbf{x}), \quad (2.56)$$

where  $\mathbf{V}(\mathbf{x})$  is an appropriate vector field  $\in \mathfrak{R}^{2n}$ .

We wish now invert Eq.(2.51) respect to  $\dot{q}_i$ , in order to obtain

$$\dot{q}_k = \dot{q}_k(\mathbf{q}, \mathbf{p}, t). \quad (2.57)$$

*inversion  
of the  
coordinates*

Actually, the possibility of inversion between  $\dot{q}_i$  and  $p_i$  is always possible for all natural mechanical systems, where the Lagrangian is  $L = K - V$  with a potential energy independent of  $\dot{q}_i$ . In general, considering the case of generic Lagrangian functions, (i.e., not necessary of the type  $L = K - V$ ), the condition that the Hessian is not-zero, namely

$$\det \left( \frac{\partial^2 L}{\partial \dot{q}_i \partial \dot{q}_k} \right) \neq 0, \quad (2.58)$$

which guarantees that Eq.(2.51) can be always inverted to furnishes the  $\dot{q}_i$  as a function of  $p_i$  (i.e., considering the  $q_i$ 's and  $t$  as parameters).

## 2.7 HAMILTONIAN APPROACH

As a matter of fact, if the Hessian is not zero (i.e., the condition in Eq.(2.58) is verified) and recalling equation Eq.(2.33), we can now define the proper Hamiltonian as

$$H = H(\mathbf{q}, \mathbf{p}, t) = [p_k \cdot \dot{q}_k - L(\mathbf{q}, \dot{\mathbf{q}}, t)]_{\dot{q}_k = \dot{q}_k(\mathbf{q}, \mathbf{p}, t)}, \quad (2.59)$$

where Eq.(2.57) has been considered, namely the function  $\dot{q}_k$  has been obtained by means of inversion of

$$p_k = \frac{\partial L}{\partial \dot{q}_k}. \quad (2.60)$$

From the previous results we have

$$\dot{q}_k = \frac{\partial H}{\partial p_k}, \quad \frac{\partial L}{\partial q_k} = -\frac{\partial H}{\partial q_k}. \quad (2.61)$$

In conclusion, it is possible to show that, considering a non-degenerate Lagrangian (i.e., the condition in Eq.(2.58) is verified), the Lagrange's equations

*Hamilton's equations*

$$\frac{d}{dt} \frac{\partial L}{\partial \dot{q}_k} = \frac{\partial L}{\partial q_k} \quad (2.62)$$

are equivalent to the Hamilton equations

$$\begin{cases} \dot{q}_k = \frac{\partial H}{\partial p_k} \\ \dot{p}_k = -\frac{\partial H}{\partial q_k}, \end{cases} \quad (2.63)$$

which form a system of  $2n$  differential equations of the first order. Indeed, from the Hamiltonian

$$H = p_h \dot{q}_h(\mathbf{q}, \mathbf{p}, t) - L(\mathbf{q}, \mathbf{p}, t) \quad (2.64)$$

we have for the  $\dot{q}_k$ 's

$$\frac{\partial H}{\partial p_k} = \dot{q}_k(\mathbf{p}, \mathbf{q}, t) + p_h \frac{\partial \dot{q}_h}{\partial p_k} - \frac{\partial L}{\partial p_k}, \quad (2.65)$$

whereas the Lagrangian is defined as

$$L = L(\mathbf{q}, \dot{\mathbf{q}}, t) = L(\mathbf{q}, \dot{\mathbf{q}}(\mathbf{q}, \mathbf{p}, t), t), \quad (2.66)$$

then

$$\frac{\partial L}{\partial p_k} = \frac{\partial L}{\partial \dot{q}_h} \frac{\partial \dot{q}_h}{\partial p_k}, \quad (2.67)$$

and we have,

$$\begin{aligned} \frac{\partial H}{\partial p_k} &= \dot{q}_k + p_h \frac{\partial \dot{q}_h}{\partial p_k} - \frac{\partial L}{\partial \dot{q}_h} \frac{\partial \dot{q}_h}{\partial p_k} \\ &= \dot{q}_k + \left( p_h - \frac{\partial L}{\partial \dot{q}_h} \right) \frac{\partial \dot{q}_h}{\partial p_k} \\ &= \dot{q}_k. \end{aligned} \quad (2.68)$$

The second relation in Eq.(2.63), is obtained from

$$\begin{aligned}\frac{\partial H}{\partial q_k} &= p_h \frac{\partial \dot{q}_h}{\partial q_k} - \frac{\partial L}{\partial q_k} \\ &= p_h \frac{\partial \dot{q}_h}{\partial q_k} - \dot{p}_k - \frac{\partial L}{\partial \dot{q}_h} \frac{\partial \dot{q}_h}{\partial q_k} \\ &= -\dot{p}_k.\end{aligned}\tag{2.69}$$

---

**Contents**


---

3.1	From analytical to statistical mechanics	40
3.2	The Hamiltonian vector field	41
3.3	Liouville's theorem	43
3.4	The ergodic problem	44
3.4.1	Measure-preserving and ergodic system	46
3.4.2	Phase space conservation	47
3.4.3	Birkhoff's ergodic theorem	49
3.5	Microcanonical distribution	49
3.6	Ideal gas phase space volume	52
3.7	Canonical distribution	54

---

So far, it has been considered the notion of *state of a system* in relation to its dynamics (*microscopic state*) and we discussed how the equations of motion can be solved with the formalism of analytical mechanics. As a matter of fact, statistical mechanics is composed of two formalisms, one is analytical mechanics while the other is statistics. As previously showed, the problem of analytical mechanics can be solved by means of Lagrange's equations (if considering the space state), or better for some cases, via the Hamilton's equations (if considering the phase space). The dynamics of the motion is a deterministic problem that is solved by knowing the initial conditions  $(\mathbf{q}_0, \dot{\mathbf{q}}_0)$  for the Lagrangian approach, or  $(\mathbf{q}_0, \mathbf{p}_0)$  for the Hamiltonian one. However, for systems composed of a huge number of particles (e.g., a gas), the microscopic state is not accessible and, consequently, a deterministic knowing of the initial conditions is not achievable. For such systems it is only possible to carry out a weaker concept of the state. In thermodynamics the simplification of this concept is extraordinary hard and, as known, the system is not described by using the  $n \sim 10^{23}$  degrees of freedom, whereas by imaging the state

as something empirically accessible and sometimes described by variables as the temperature and the volume (*macroscopic state*), or by basic field variables in the study of the thermodynamics of fluids such as the velocity of the fluid.

Statistical mechanics, operates as a bridge between the two different concepts of state, microscopic and macroscopic. On the one hand, it is assumed that a microscopic state is assigned and a certain Hamiltonian defines its dynamics, therefore the system is characterized by a deterministic dynamics. On the other hand, it is contemplated the assumption that the informations contained in the microscopic state are not accessible and are redundant. This leads to a new definition of state: the *statistical state*, which is called *ensemble* [96]. Supposing a lack of information in the initial state of the system, it is assigned a priori probability on the initial data. This probability should be well defined so that the two elements analytical mechanics and statistics will be consistently connected.

### 3.1 FROM ANALYTICAL TO STATISTICAL MECHANICS

Hamilton's equations of motion (see Eq.(2.63)) lay the groundwork to the transition from the analytical to the statistical mechanics. In fact, with the introduction of the conjugate momentum pertaining to the Hamiltonian formulation, it is possible to show that, independently of the choice of the  $q$ 's, the equations of motion satisfy the normal system form in Eq.(2.56), and the canonical coordinates act as they were orthogonal Cartesian coordinates.

Considering an arbitrary Lebesgue-measurable domain  $D_t = D(t)$ , it is possible to associate with it a measure that we indicate as  $dV = \text{vol}(D_t)$ . This measure represents the volume element of the considered region of the phase space, and it is defined considering the canonical coordinates  $(\mathbf{q}, \mathbf{p})$  as they were orthogonal Cartesian coordinates, hence

$$dV = dq_1 \dots dq_n dp_1 \dots dp_n; \quad (3.1)$$

independently of the choice of the  $q$ 's coordinates. The concept of measure is discussed in more details in Section 3.4.1.

Having defined the unit volume of the phase space, we can now deal with the problem of the definition of a priori probability on the initial data. This problem is known to be trivial if the possible

*advantages  
of the  
Hamiltonian  
formulation*

*volume  
of the  
phase space*

data set  $N$  is finite, whereas to be much more complex if it is not [97]. In the latter case, ( $N \rightarrow \infty$ ), as the space is a continuum, it is necessary to assign an initial probability density  $\rho_0(\mathbf{x})$  in the phase space with the properties

$$\rho_0(\mathbf{x}) \geq 0, \quad \int \rho_0(\mathbf{x}) dV = 1, \quad (3.2)$$

and the problem is now to find a corresponding probability density  $\rho(\mathbf{x}, t)$  at a certain time  $t$  evolved from the initial one  $\rho_0(\mathbf{x})$ . From that, the probability that a representative point of the system would be in an arbitrary domain of the phase space  $D_0 \subset \Gamma$  is

$$\Pr(\mathbf{x} \in D_0) = \int_{D_0} \rho_0(\mathbf{x}) dV, \quad (3.3)$$

where  $\Gamma$  is called *Gamma space*, which is the phase space of the global system, and the element of volume  $dV$  is defined in Eq.(3.1).

From Eq.(3.3), for a generic observable of interest  $f$ , which is a function of the dynamics variables  $\mathbf{x}$  and  $\mathbf{p}$ , it is then possible to define its mean value as the weighted mean  $\langle f \rangle_{\rho(t)}$  on all possible states of the system as

$$\langle f \rangle_{\rho(t)} = \int f(\mathbf{x}) \rho(\mathbf{x}, t) dV. \quad (3.4)$$

In this case, a physical state is a set of identical systems, called *ensemble*, which differs for the initial conditions and that evolves independently from the others states. Thus, the system evolves in time accordingly to a density probability  $\rho(\mathbf{x}, t)$  that connects the initial state to the state of the system at a certain time  $t$ .

*concept of ensemble*

### 3.2 THE HAMILTONIAN VECTOR FIELD

We previously discussed how in the Hamiltonian formulation the canonical coordinates act as they were orthogonal Cartesian coordinates. Actually, the utility of the canonical coordinates lies in the fact that the corresponding equations of motions, i.e. the Hamilton's equations, have a particular symmetric structure. As a matter of fact, we already discussed that the Hamiltonian formulation represents a system of differential equation in normal form (see Eq.(2.56)), namely

$$\dot{\mathbf{x}} = \mathbf{V}(\mathbf{x}), \quad (3.5)$$

and we already stated that  $\mathbf{V}(\mathbf{x})$  is an appropriate vector field  $\in \mathfrak{R}^{2n}$ , but without specifying anything else. Actually the vector field  $\mathbf{V}(\mathbf{x})$  is called *Hamiltonian vector field* and is constructed in a suitable way, which turns out in some important properties of the Hamiltonian and of the Hamiltonian vector field. In fact, the vector field is constructed as following:

$$\mathbf{V}_H(\mathbf{x}) = \mathbb{E} \nabla H(\mathbf{x}), \quad (3.6)$$

where  $\mathbb{E}$  is the *symplectic matrix* [98]

$$\mathbb{E} = \begin{pmatrix} 0_n & \mathbb{I}_n \\ -\mathbb{I}_n & 0_n \end{pmatrix} \quad (3.7)$$

and the gradient

$$\nabla H(\mathbf{x}) = \left( \frac{\partial H}{\partial q_k}, \frac{\partial H}{\partial p_k} \right) \quad (3.8)$$

is defined as a simple extension of the equivalent definitions for the Cartesian space  $\mathbb{R}^3$ .

We finally have

$$\mathbf{V}_H(\mathbf{x}) = \left( \frac{\partial H}{\partial p_k}, -\frac{\partial H}{\partial q_k} \right). \quad (3.9)$$

*orthogonality*

The reason of this particular vector field definition lies in the fact that, in this way,  $\mathbf{V}_H(\mathbf{x})$  is orthogonal to the gradient of the Hamiltonian. This is straightforwardly proved by means of a direct calculation; namely using Eq.(3.6) and Eq.(3.9) we have

$$\begin{aligned} \mathbf{V}_H(\mathbf{x}) \cdot \nabla H &= \left( \frac{\partial H}{\partial p_k}, -\frac{\partial H}{\partial q_k} \right) \cdot \left( \frac{\partial H}{\partial q_h}, \frac{\partial H}{\partial p_h} \right) \\ &= \frac{\partial H}{\partial p_k} \frac{\partial H}{\partial q_k} - \frac{\partial H}{\partial q_k} \frac{\partial H}{\partial p_k} \\ &= 0, \end{aligned} \quad (3.10)$$

where it has been used the Schwarz's theorem for the commutation of the partial derivatives.

*solenoidality*

Furthermore, from Eq.(3.6) turns out that, as a consequence of its particular structure, the Hamiltonian vector field is *solenoidal*:

$$\begin{aligned} \nabla \cdot \mathbf{V}_H(\mathbf{x}) &= \left( \frac{\partial}{\partial q_k}, \frac{\partial}{\partial p_k} \right) \cdot \left( \frac{\partial H}{\partial p_h}, -\frac{\partial H}{\partial q_h} \right) \\ &= \frac{\partial^2 H}{\partial q_k \partial p_k} - \frac{\partial^2 H}{\partial p_k \partial q_k} \\ &= 0. \end{aligned} \quad (3.11)$$

Summarizing, the *gradient* of the Hamiltonian and the *divergence* of the Hamiltonian vector field in the *phase space* have been defined as an extension of the familiar definitions for the ordinary space  $\mathfrak{R}^3$ , referred to orthogonal Cartesian coordinates. This is far from obvious because, even in the *ordinary space*  $\mathfrak{R}^3$ , when using polar or spherical coordinates, the gradient and the divergence have expressions completely different with respect to the case in which Cartesian coordinates are considered. The same consideration is true concerning the property of solenoidality of the Hamiltonian vector field.

### 3.3 LIOUVILLE'S THEOREM

Let now consider a generic velocity field  $\mathbf{V} = \mathbf{V}(\mathbf{q}, \mathbf{p})$  in the phase space and the ensemble measure of a region  $V_0$  of the phase space at the initial time instant  $t = 0$ . During the evolution of the system, also the ensemble evolves in time and this results in the change of the probability density  $\rho_0$  and the region of volume  $V_0$  they occupy. In other words, we are considering the problem of how a corresponding probability density  $\rho(\mathbf{x}, t)$  evolves from a initial density  $\rho_0(\mathbf{x})$ . The function  $\rho(\mathbf{x}, t)$  must satisfy the continuity equation,

$$\int_{V_0} \frac{\partial \rho}{\partial t} dV + \int_{\partial V_0} \mathbf{V} \rho \cdot \boldsymbol{\Sigma} = 0 \quad \forall V_0, \quad (3.12)$$

being  $\boldsymbol{\Sigma}$  a closed surface element and  $\partial V_0$  its boundary. From Stoke's theorem we can write:

$$\int_{\partial V_0} \mathbf{V} \rho \cdot \boldsymbol{\Sigma} = \int_{V_0} \nabla \cdot (\mathbf{V} \rho) dV. \quad (3.13)$$

Writing Eq.(3.12) in local form, we have

$$\frac{\partial \rho}{\partial t} + \nabla \cdot (\mathbf{V} \rho) = 0, \quad (3.14)$$

which is known as the *Liouville's equation*. Considering a Hamiltonian vector field  $\mathbf{V} = \mathbf{V}_H(\mathbf{x})$ , we rewrite Eq.(3.12) as

$$\frac{\partial \rho}{\partial t} + \nabla \cdot (\mathbf{V}_H \rho) = 0, \quad (3.15)$$

and, recalling Eqs.(3.9) and (3.11), we can write

$$\begin{aligned} \frac{\partial \rho}{\partial t} + \nabla \cdot (\mathbf{V}_H \rho) &= \frac{\partial \rho}{\partial t} + (\nabla \cdot \mathbf{V}_H) \rho + \mathbf{V}_H \cdot (\nabla \rho) \\ &= \frac{\partial \rho}{\partial t} + \left( \frac{\partial H}{\partial p_k}, -\frac{\partial H}{\partial q_k} \right) \cdot \left( \frac{\partial \rho}{\partial q_k}, \frac{\partial \rho}{\partial p_k} \right) \\ &= \frac{\partial \rho}{\partial t} + \frac{\partial H}{\partial p_k} \frac{\partial \rho}{\partial q_k} - \frac{\partial H}{\partial q_k} \frac{\partial \rho}{\partial p_k}, \end{aligned} \quad (3.16)$$

then, from Eq.(3.15), we get

$$\frac{\partial \rho}{\partial t} + \{\rho, H\} = 0, \quad (3.17)$$

where we used the Poisson brackets notation. We note now that

$$\begin{aligned} \frac{d\rho}{dt} &= \frac{\partial \rho}{\partial q_k} \dot{q}_k + \frac{\partial \rho}{\partial p_k} \dot{p}_k + \frac{\partial \rho}{\partial t} \\ &= \frac{\partial \rho}{\partial q_k} \frac{\partial H}{\partial p_k} - \frac{\partial \rho}{\partial p_k} \frac{\partial H}{\partial q_k} + \frac{\partial \rho}{\partial t}, \end{aligned} \quad (3.18)$$

where we recalled the Hamilton's equations (see Eq.(2.63)). From Eqs.(3.17) and (3.18) we get

*Liouville's  
theorem*

$$\frac{d\rho}{dt} \equiv \frac{d}{dt} \rho(\mathbf{q}(t), \mathbf{p}(t), t) = 0. \quad (3.19)$$

This means that for Hamiltonian systems the continuity equation becomes the following equation, known as the *Liouville's theorem*, and the phase space probability distribution function  $\rho$  is a constant of the motion. In other words, it is possible to think the points of the phase space as they were the constituent of an incompressible fluid.

Moreover, from Eq.(3.15) follows that we have finally fixed the problem to find a corresponding probability density  $\rho(\mathbf{x}, t)$  evolved from the initial one  $\rho_0(\mathbf{x})$ .

### 3.4 THE ERGODIC PROBLEM

In this Section, a concise discussion of the ergodic problem is exposed. An initial recall of the essential theoretical setup is mandatory, hence presented, for introducing the *ergodic hypothesis*, which is a crucial mainstay of statistical mechanics.

Nowadays, the ergodic theory is a quite general branch of mathematics that studies *dynamical systems* with an invariant measure and related problems, however its initial development was motivated by problems of statistical physics. A central concern of ergodic theory is the behavior of a dynamical system when it is allowed to run for a long time. One of the most important result concerning this point is the *Poincaré recurrence theorem*, which states that almost all points in any subset of the phase space eventually revisit the set [97, 99]. Some specific ergodic theorems provide more precise informations under certain conditions. One of them is the *Birkhoff's ergodic theorem* (discussed in Section 3.4.3), which claims that the time average of a function along the trajectories exists almost everywhere and is related to the space average. At its simplest form, a dynamical system is a function  $T$  defined on a set  $\Omega$ . As the original motivation of the ergodic problems was classical mechanics, the set  $\Omega$  considered was the set of all possible states of given dynamical system. This set is what we previously mentioned as configuration space or phase space (depending on what kind of formalism we are dealing with). From that,

$$T : \Omega \rightarrow \Omega \quad (3.20)$$

is the law of motion which prescribes that if the system is at state  $\mathbf{x}$  now, then it will evolve to state  $T(\mathbf{x})$  after one unit of time. The aim of the theory is to describe the behavior of  $T^n(\mathbf{x})$  as  $n \rightarrow \infty$  with  $n \in \mathbb{Z}$ , and this understanding is related to understanding the behavior of the system at the far future.

Considering a box containing a gas made of  $N$  identical molecules, classical mechanics says that knowing the initial generalized positions  $\mathbf{q}$  and momenta  $\mathbf{p}$ , it is possible to determine the positions and momenta of each molecule at time  $t$  by solving Hamilton's equations (see Eq.(2.63)), namely where we call  $(\mathbf{q}, \mathbf{p}) := (q_1, \dots, q_N; p_1, \dots, p_N)$  the state of the system. Let  $\Omega$  denote the collection of all possible states, then

$$T_t : (\mathbf{q}, \mathbf{p}) \mapsto (\mathbf{q}(t), \mathbf{p}(t)) \quad (3.21)$$

denotes the map which gives solution of Eq.(2.63) with the initial condition  $(\mathbf{q}(0), \mathbf{p}(0))$ . The Ergodic Hypothesis, states that for certain invariant measures  $\mu$ , many functions  $f : \Omega \rightarrow \mathfrak{R}$ , and many states  $\mathbf{x} = (\mathbf{q}, \mathbf{p})$ , the time average of  $f$  exists and equals the space average of  $f$ .

In order to present a more detailed and accessible discussion of the ergodic hypothesis, we recall some mathematical setup in the following.

### 3.4.1 Measure-preserving and ergodic system

Let consider a system composed by the triplet  $(\Omega, \mathcal{A}, \mu)$  where:

- $\Omega \subset \mathfrak{R}^n$  is a set of points  $x_i \in \mathfrak{R}$ , sometime called *the space*.
- $\mathcal{A}$  is an element of the  $\sigma$ -algebra on  $\Omega$ , namely a collection of subsets of  $\Omega$ , which contains the empty set, and which is closed under complements and countable unions. The elements of  $\mathcal{A}$  are called *measurable sets*.
- $\mu : \mathcal{A} \subset \Omega \rightarrow \mathfrak{R}$  a *measure* on  $\Omega$  such that

$$\mu(A \subset \Omega) = \int_{A \subset \Omega \subset \mathfrak{R}^n} g(\mathbf{x}) d\mathbf{x} = \int_{A \subset \Omega \subset \mathfrak{R}^n} d\mu \quad (3.22)$$

$$\mu(\Omega) = 1, \quad (3.23)$$

consequently

$$\mu(\Omega) = \int_{\Omega} d\mu = 1. \quad (3.24)$$

Let also be  $T$  a function  $T : \Omega \rightarrow \Omega$  called *transformation* on  $\Omega$  where its inverse is applied to a given set

$$T^{-1}(A) = \{\mathbf{x} \in \Omega : T(\mathbf{x}) \in A\}. \quad (3.25)$$

*measure-preservity*

The transformation  $T$  is said to be *measure-preserving* with respect to  $\mu$  (or viceversa) if

$$\mu(T^{-1}(A)) = \mu(A) \quad (3.26)$$

*ergodicity*

is verified and, it is said to be *ergodic* if

$$T^{-1}(A) = A \Leftrightarrow \{\mu(\emptyset) = 0 \text{ or } \mu(A) = 1\} \quad (3.27)$$

is verified.

A system  $(\Omega, \mathcal{A}, \mu, T)$  for which both the previous properties are valid is called an *ergodic dynamical system*.

From a *probabilistic point of view*, a measure preserving transformation on a *probability space* is a *probability preserving transformation*. Much of the power and usefulness of ergodic theory is due

to the following probabilistic interpretation of the abstract set up discussed above.

Suppose  $(X, A, \mu, T)$  is a probability preserving transformation. We can think of:

- $\Omega$  as of a *sample space*, namely the collection of all possible states  $x$  of a random system [100],
- $A$  as the *collection of all measurable events* [97, 100],
- $\mu$  is the *probability law*:  $\Pr[x \in E] := \mu(E)$ ,
- measurable functions  $f : \Omega \rightarrow \mathfrak{R}$  are *random variables*  $f(x)$ ,
- the sequence  $\Omega_n := f \cdot T^n (n \geq 1)$  is a *stochastic process* [97, 100].

### 3.4.2 Phase space conservation

Considering a dynamical system

$$\dot{x} = f(x, t), \tag{3.28}$$

*the phase flux*

where  $x_0 \in R^n$  is the initial state and  $x(x_0, t) \in R^n$  is the state of the system at time  $t$ , we introduce the *phase flux*  $\Phi^t$ , which is the evolution at time  $t$  of the initial data  $x_0$ , namely

$$x = \Phi(x_0, t) = \Phi^t. \tag{3.29}$$

Considering a subset  $x \in P_0 \subset \mathfrak{R}^n$  we can define the measure

$$\text{mis}P_0 = \int_{P_0} dx \tag{3.30}$$

of the initial subset  $x_0 \in P_0 \subset \mathfrak{R}^n$  and the measure of the evolved subset  $x \in P_t \subset \mathfrak{R}^n$

$$\text{mis}P_t = \int_{P_t} dx. \tag{3.31}$$

We are now interested on studying how  $\text{mis}P_0$  is related to  $\text{mis}P_t$ . To do this, let us consider the evolution in time of  $\text{mis}P_t$ ,  $\frac{d}{dt} \int_{P_t} dx$ . We get

$$\frac{d}{dt} \int_{P_t} dx = \frac{d}{dt} \int_{P_0} \mathbb{J}(t) dx = \int_{P_0} \frac{d}{dt} \mathbb{J}(t) dx, \tag{3.32}$$

where  $\mathbb{J}(t)$  denoted the Jacobian matrix

$$\mathbb{J}(t) = \det \left( \frac{\partial x}{\partial x_0} \right). \tag{3.33}$$

Then, we can now study the total derivative in time

$$\frac{d}{dt}\mathbb{J}(t) = \frac{d}{dt} \left[ \det \left( \frac{\partial \Phi^t}{\partial \mathbf{x}_0} \right) \right]. \quad (3.34)$$

Remembering that for a generic matrix  $\mathbb{A}(t)$ , its derivative in time is given by

$$\frac{d}{dt}\mathbb{A}(t) = \det \mathbb{A}(t) \operatorname{tr} \left( \mathbb{A}(t)^{-1} \frac{d\mathbb{A}(t)}{dt} \right), \quad (3.35)$$

where  $\operatorname{tr}(\mathbb{M})$  denotes the trace of the generic matrix  $\mathbb{M}$ .

From this we get

$$\begin{aligned} \frac{d}{dt}\mathbb{J}(t) &= \mathbb{J}(t) \operatorname{tr} \left[ \left( \frac{\partial \Phi^t}{\partial \mathbf{x}_0} \right)^{-1} \frac{d}{dt} \left( \frac{\partial \Phi^t}{\partial \mathbf{x}_0} \right) \right] \\ &= \mathbb{J}(t) \operatorname{tr} \left[ \left( \frac{\partial \Phi^t}{\partial \mathbf{x}_0} \right)^{-1} \frac{\partial}{\partial \mathbf{x}_0} \left( \frac{\partial \Phi^t}{\partial t} \right) \right] \\ &= \mathbb{J}(t) \operatorname{tr} \left[ \left( \frac{\partial \Phi^t}{\partial \mathbf{x}_0} \right)^{-1} \frac{\partial}{\partial \mathbf{x}_0} f(\Phi^t, t) \right] \\ &= \mathbb{J}(t) \operatorname{tr} \left[ \left( \frac{\partial \Phi^t}{\partial \mathbf{x}_0} \right)^{-1} \left( \frac{\partial f}{\partial \mathbf{x}} \right)_{\Phi^t} \frac{\partial \Phi^t}{\partial \mathbf{x}_0} \right] \\ &= \mathbb{J}(t) \operatorname{tr} \left[ \frac{\partial f}{\partial \mathbf{x}} \right] \\ &= \mathbb{J}(t) \nabla \cdot \mathbf{f}. \end{aligned} \quad (3.36)$$

Then, we finally get

$$\frac{d}{dt} \int_{P_t} d\mathbf{x} = \int_{P_0} \mathbb{J}(t) \nabla \cdot \mathbf{f} d\mathbf{x}_0 = \int_{P_t} \nabla \cdot \mathbf{f} d\mathbf{x}, \quad (3.37)$$

which is a general results with several applications.

*phase space  
conservation*

For Hamiltonian systems, we get the particular result

$$\frac{d}{dt} \int_{P_t} d\mathbf{x} = 0 \quad (3.38)$$

because, as previously discussed, the Hamiltonian vector field is solenoidal. From Eq.(3.38) we have that

$$\int_{P_0} d\mathbf{x} = \int_{P_t} d\mathbf{x}, \quad (3.39)$$

which means that the volume of every domain  $P$  of the phase space is a constant of the motion. Eq.(3.39) is a result of crucial importance known as the *phase space conservation* law. In other words, we have that

$$J(t) = 1 \quad \forall t. \tag{3.40}$$

### 3.4.3 Birkhoff's ergodic theorem

Let consider a measure  $\mu$  on  $\Omega$  and a dynamical system with a flux  $\Phi^t$ , then for every integrable function  $f(x)$  (in the sense of Lebesgue), it is possible to define almost everywhere (for almost all  $x_0$  [100]) along the trajectories two averages.

The first is the *space average* (or *ensemble average*) of  $f$ , which is *ensemble average*

$$\langle f \rangle = \int_{\Omega} g(x)f(x) dx, \tag{3.41}$$

being  $g(x)$  the density function on the relevant region of phase space, while the second is the *time average* *time average*

$$\bar{f}(x_0) = \lim_{t \rightarrow \infty} \frac{1}{t} \int_0^t f[\Phi(x_0, t)] dt. \tag{3.42}$$

Furthermore, if  $f$  is measure-preserving and ergodic holds almost everywhere that

$$\bar{f}(x_0) = \langle f \rangle, \tag{3.43}$$

which states that for an ergodic transformation the time average equals the space average almost everywhere.

This theorem is one of the existing theorem related to the study of the *ergodic hypothesis*. This hypothesis says that, over long periods of time, the time spent by a particle in some region of the phase space of microstates with the same energy is proportional to the volume of this region. As a matter of fact, this is a quite sophisticate and delicate topic, suffice to states that, under fairly general conditions, a proof of the ergodic hypothesis is still absent for most of real mechanical systems [101]. *the ergodic hypothesis*

## 3.5 MICROCANONICAL DISTRIBUTION

We discussed how, for mechanical systems, the Liouville theorem states that the measure  $\mu$  is invariant. This means that, con-

sidering Eq.(3.41), the density function  $g(\mathbf{x})$  is constant. Moreover, if the system is ergodic, it is possible to use space averages instead of measuring time averages as an instrument does. In particular, if

$$g(\mathbf{x}) = 1 \quad \forall \mathbf{x}, \quad (3.44)$$

the phase space measure  $\mu$  is equivalent to the Lebesgue measure. In this conditions, the general statistical distribution is called the *microcanonical distribution* and the corresponding ensemble is called the *microcanonical ensemble*. In other words, we are considering the important assumption for which all the accessible microstates are equally probable.

Let us consider a Hamiltonian system in a  $6N$ -dimensional phase space, where the probability densities evolve as solutions of the Liouville's equation Eq.(3.19). If this system is scleronomous and isolated, the total energy  $E$  remains constant, hence the motion of the  $N$ -particle will be confined to a  $(6N - 1)$  dimensional surface given by

$$H(\mathbf{q}, \mathbf{p}, t) = E \quad \forall t, \quad (3.45)$$

and we denote the surface as  $\Gamma(E)$ . As we previously discussed, we have not access to the detailed dynamics of the system, but we can instead study averages over the surface  $\Gamma(E)$  (a generic domain) of the phase space. This averages are a special case of ensemble averages. We will see in Chapter 5 how this is similarly done in Metropolis Monte Carlo method that simulates ensemble averages rather than time averages.

Considering the probability density  $\rho(\mathbf{q}, \mathbf{p})$  in the phase space, we can write

$$\Pr\{\mathbf{Q} < \mathbf{q} < \mathbf{Q} + d\mathbf{Q}, \quad \mathbf{P} < \mathbf{p} < \mathbf{P} + d\mathbf{P}\} = \rho(\mathbf{Q}, \mathbf{P})d\mathbf{Q}d\mathbf{P}$$

then, the probability that a point of the system is located in an arbitrary domain of the phase space is

$$\Pr\{(\mathbf{Q}, \mathbf{P}) \in A \subset \mathfrak{R}^{2n}\} = \int_A \rho(\mathbf{q}, \mathbf{p})d\mathbf{q}d\mathbf{p}. \quad (3.46)$$

Instead of working with the constant energy surface  $\Gamma(E)$  we assume that all the states are equally probable in  $(E, E + \Delta E)$ . This means that all  $(\mathbf{q}, \mathbf{p})$  are contained into the domain

$$E < H(\mathbf{q}, \mathbf{p}) < E + \Delta E \quad (3.47)$$

occur with equal probability in the ensemble [102, 103, 104, 99]. In other words, we can take into a consideration the energy between a range  $E, E + \Delta E$  and, in this domain the probability density function is defined as

$$\rho(\mathbf{q}, \mathbf{p}) = \begin{cases} \text{const if: } & E < H(\mathbf{q}, \mathbf{p}) < E + \Delta E \\ 0 & \text{elsewhere.} \end{cases} \quad (3.48)$$

In the special case in which we are considering a closed classical system of energy  $E$ , we have that the probability density function is defined as

*microcanonical ensemble*

$$\rho_{\Delta E}(\mathbf{q}, \mathbf{p}) = \gamma r_{\Delta E}(H(\mathbf{q}, \mathbf{p}) - E), \quad (3.49)$$

where  $\gamma$  is an oportune constant and  $r_{\Delta E}(x)$  is the generic window function

$$r_{\Delta E}(x) = \begin{cases} \frac{1}{\Delta E} & \text{if } x \in (0, \Delta E) \\ 0 & \text{elsewhere,} \end{cases} \quad (3.50)$$

for which we have

$$\int_{-\infty}^{\infty} r_{\Delta E}(x) dx = \int_0^{\infty} r_{\Delta E}(x) dx = 1, \quad (3.51)$$

and therefore

$$\lim_{\Delta E \rightarrow 0} r_{\Delta E}(x) = \delta(x). \quad (3.52)$$

The ensemble corresponding to Eq.(3.49) is called *microcanonical ensemble*.

From the normalization properties (see Eq.(3.2)) of the probability density function

$$\int \rho(\mathbf{q}, \mathbf{p}) d\mathbf{q} d\mathbf{p} = 1, \quad (3.53)$$

we have

$$\gamma \int r_{\Delta E}(H(\mathbf{q}, \mathbf{p}) - E) d\mathbf{q} d\mathbf{p} = 1, \quad (3.54)$$

from which we can find the value of the normalization constant

$$\gamma = \frac{1}{\Delta E \int_{\{(\mathbf{q}, \mathbf{p}): E < H(\mathbf{q}, \mathbf{p}) < E + \Delta E\}} d\mathbf{q} d\mathbf{p}}, \quad (3.55)$$

*microcanonical  
distribution  
with finite  
 $\Delta E$*

and finally the explicit form of the probability density function

$$\rho_{\Delta E}(\mathbf{q}, \mathbf{p}) = \frac{r_{\Delta E}(H(\mathbf{q}, \mathbf{p}) - E)\Delta E}{\int_{\{H < E + \Delta E\}} d\mathbf{q}d\mathbf{p} - \int_{\{H < E\}} d\mathbf{q}d\mathbf{p}} \quad (3.56)$$

which is called *microcanonical distribution* with a finite  $\Delta E$ .

If we consider the surface between  $E$  and  $E + \Delta E$  with a tolerance  $\Delta E \rightarrow 0$ , then we define the phase space volume as

$$\Omega(E) = \int_{H(\mathbf{q}, \mathbf{p}) < E} d\mathbf{q}d\mathbf{p}, \quad (3.57)$$

and looking for the limit  $\Delta E \rightarrow 0$  of

$$\rho_{\Delta E}(\mathbf{q}, \mathbf{p}) = \frac{\Delta E}{\Omega(E + \Delta E) - \Omega(E)} r_{\Delta E}(H(\mathbf{q}, \mathbf{p}) - E), \quad (3.58)$$

namely

$$\rho(\mathbf{q}, \mathbf{p}) = \lim_{\Delta E \rightarrow 0} \rho_{\Delta E}(\mathbf{q}, \mathbf{p}) \quad (3.59)$$

$$= \lim_{\Delta E \rightarrow 0} \frac{\Delta E}{\Omega(E + \Delta E) - \Omega(E)} r_{\Delta E}(H(\mathbf{q}, \mathbf{p}) - E), \quad (3.60)$$

*microcanonical  
distribution  
with  $\Delta E \rightarrow 0$*

we finally get

$$\rho(\mathbf{q}, \mathbf{p}) = \frac{1}{\frac{d\Omega(E)}{dE}} \delta(H(\mathbf{q}, \mathbf{p}) - E), \quad (3.61)$$

which is known as the *microcanonical distribution* for  $\Delta E \rightarrow 0$ .

### 3.6 IDEAL GAS PHASE SPACE VOLUME

Let us consider a monoatomic the ideal gas composed of  $N$  non-interacting point particles, then the potential energy  $U(\mathbf{q}, \mathbf{p}) = 0$  by definition and the system has  $n = 3N$  degrees of freedom. Consequently the Hamiltonian  $H(\mathbf{q}, \mathbf{p})$  is

$$H(\mathbf{p}) = K(\mathbf{p}) = \sum_{i=1}^N \frac{m_i}{2} \mathbf{p}_i \cdot \mathbf{p}_i, \quad (3.62)$$

and recalling Eq.(3.45) we get

$$E = \sum_{k=1}^{n=3N} \frac{p_k^2}{2m}, \quad (3.63)$$

which defines the surface of a  $3N$  dimensional sphere of radius  $R = \sqrt{2m\bar{E}}$ . From Eq.(3.57), we can write

$$\Omega(E) = \int_{H(\mathbf{q},\mathbf{p}) < E} d\mathbf{q}d\mathbf{p} = \int_{\sum_{k=1}^{n=3N} p_k^2 < 2mE} d\mathbf{q}d\mathbf{p} = V_n(R)V^N, \quad (3.64)$$

where  $V_n(R)$  is the volume of a 3D sphere with ray  $R$  in a  $n$ -dimensional space defined as

$$V_n(R) = \frac{\pi^{n/2}}{\Gamma(\frac{n}{2} + 1)} R^n, \quad (3.65)$$

and the Gamma function  $\Gamma(n)$  is an extension of the factorial function with its argument shifted down by 1, valid for real and complex numbers. That is, if  $n$  is a positive integer, the Gamma function is defined

*the Gamma function*

$$\Gamma(n) = (n - 1)!. \quad (3.66)$$

From Eq.(3.64) and Eq.(3.65) we get

$$\Omega(E) = \frac{\pi^{n/2}}{\Gamma(\frac{n}{2} + 1)} (2mE)^{\frac{n}{2}} V^N, \quad (3.67)$$

and studying the total derivative with respect to the energy  $E$  we get from the last equation Eq.(3.67)

$$\frac{d\Omega(E)}{dE} = \frac{\pi^{n/2}}{\Gamma(\frac{n}{2} + 1)} (2m)^{\frac{n}{2}} \frac{n}{2} E^{\frac{n}{2}-1} V^N. \quad (3.68)$$

If we consider true that for the microcanonical distribution is valid the energy equipartition theorem, then from Eqs. (3.61), (3.63) and Eq.(3.68), we get the kinetic energy

$$\langle K \rangle = \frac{1}{2} n \frac{\Omega(E)}{\Omega'(E)}, \quad (3.69)$$

and remembering that if we have a general function  $f(\mathbf{q}, \mathbf{p})$  we can get the average of it by Eq.(3.4), namely

$$\langle f(\mathbf{q}, \mathbf{p}) \rangle = \int f(\mathbf{q}, \mathbf{p}) \rho(\mathbf{q}, \mathbf{p}) d\mathbf{q}d\mathbf{p}, \quad (3.70)$$

it is possible to define the temperature  $T$  as

$$T = \frac{1}{k_B} \frac{\Omega(E)}{\Omega'(E)}, \quad (3.71)$$

and from Eq.(3.69) and Eq.(3.71) we can write

$$\langle K \rangle = \frac{1}{2}nk_B T. \quad (3.72)$$

Finally, we get for an ideal gas

$$\frac{\Omega(E)}{\Omega'(E)} = \frac{E^{\frac{n}{2}}}{\frac{n}{2}E^{\frac{n}{2}-1}} = \frac{2}{n}E = k_B T, \quad (3.73)$$

and the total energy

$$E = \frac{n}{2}k_B T = \frac{3}{2}Nk_B T. \quad (3.74)$$

### 3.7 CANONICAL DISTRIBUTION

We want now study a system composed by a heat bath with a constant temperature  $T$  and another system that is much more smaller than the first one. The two systems are free to exchange energy and are isolated from the rest of the universe, so that the total particle numbers and volume of each system are constant. Under these assumptions the total energy of the system will be constant (weak interaction). If we indicate with  $\rho_1(\mathbf{q}_1, \mathbf{p}_1)$  the distribution of the small system and with  $\rho_2(\mathbf{q}_2, \mathbf{p}_2)$  the distribution of the eath bath we can write the total distribution of the system as  $\rho(\mathbf{q}_1, \mathbf{p}_1, \mathbf{q}_2, \mathbf{p}_2)$ .

Remembering that in probability theory if  $x$  and  $y$  are two random variables, we can define the probability density function  $\rho(x, y)$  as

$$\Pr\{X < x < X + dX, Y < y < Y + dY\} = \rho(X, Y)dXdY \quad (3.75)$$

so that

$$\Pr\{(x, y) \in A \subset \mathfrak{R}^2\} = \int_A \rho(x, y) dx dy, \quad (3.76)$$

we can write

$$\begin{aligned} \Pr\{X < x < X + dX\} &= \int_1 \rho(X) dX & (3.77) \\ &= \Pr\{X < x < X + dX, -\infty < y < \infty\} \\ &= \int_x^{x+dX} \int_{-\infty}^{\infty} \rho(x, y) dy dx \\ &= \int_{-\infty}^{\infty} \rho(x, y) dy dX, \end{aligned}$$

from which, referring to our two systems, we get

$$\rho(\mathbf{q}_1, \mathbf{p}_1) = \int \rho(\mathbf{q}_1, \mathbf{q}_2, \mathbf{p}_1, \mathbf{p}_2) d\mathbf{q}_2 d\mathbf{p}_2, \quad (3.78)$$

and recalling Eq.(3.60) we have

$$\begin{aligned} \rho_1(\mathbf{q}_1, \mathbf{p}_1) &= \lim_{\Delta E \rightarrow 0} \int \frac{\Delta E}{\Omega(E + \Delta E) - \Omega(E)} \\ &\times r_{\Delta E}(H(\mathbf{q}, \mathbf{p}) - E) d\mathbf{q}_2 d\mathbf{p}_2. \end{aligned} \quad (3.79)$$

In the hypothesis of weak interaction, we can write

$$H(\mathbf{q}_1, \mathbf{q}_2, \mathbf{p}_1, \mathbf{p}_2) = H_1(\mathbf{q}_1, \mathbf{p}_1) + H_2(\mathbf{q}_2, \mathbf{p}_2), \quad (3.80)$$

where  $H_1(\mathbf{q}_1, \mathbf{p}_1)$  and  $H_2(\mathbf{q}_2, \mathbf{p}_2)$  are the energies of the two systems. We chose a tolerance  $\Delta E$  so that the statistical weights  $\Omega(E_1 + \Delta E_1)$ ,  $\Omega(E_2 + \Delta E_2)$  are proportional to  $\Delta E$

$$\begin{aligned} \rho_1(\mathbf{q}_1, \mathbf{p}_1) &= \lim_{\Delta E \rightarrow 0} \frac{\Delta E}{\Omega(E + \Delta E) - \Omega(E)} \\ &\times \int r_{\Delta E}(H_1(\mathbf{q}_1, \mathbf{p}_1) + H_2(\mathbf{q}_2, \mathbf{p}_2) - E) d\mathbf{q}_2 d\mathbf{p}_2 \\ &= \lim_{\Delta E \rightarrow 0} \int \frac{\Delta E}{\Omega(E + \Delta E) - \Omega(E)} \\ &\times \int_{E < H_1 + H_2 < E + \Delta E}^{E - H_1 < H_2 < E - H_1 + \Delta E} \frac{1}{\Delta E} d\mathbf{q}_2 d\mathbf{p}_2 \\ &= \lim_{\Delta E \rightarrow 0} \int \frac{\Delta E}{\Omega(E + \Delta E) - \Omega(E)} \\ &\times \frac{\Omega_2(E - H_1 + \Delta E) - \Omega_2(E - H_1)}{\Delta E}, \end{aligned} \quad (3.81)$$

and when  $\Delta E \rightarrow 0$ , we get

$$\rho_1(\mathbf{q}_1, \mathbf{p}_1) = \frac{\Omega_2'(E - H_1(\mathbf{q}_1, \mathbf{p}_1))}{\Omega'(E)}. \quad (3.82)$$

Assuming now that the heat bath is an ideal gas (whit n big), we write

$$\begin{aligned}
 \rho_1(\mathbf{q}_1, \mathbf{p}_1) &= \frac{\Omega'_2(E - H_1(\mathbf{q}_1, \mathbf{p}_1))}{\Omega'(E)} & (3.83) \\
 &= \frac{\Omega'_2(E) \Omega'_2(E - H_1(\mathbf{q}_1, \mathbf{p}_1))}{\Omega(E)' \Omega'_2(E)} \\
 &= \gamma \frac{[E - H_1(\mathbf{q}_1, \mathbf{p}_1)]^{\frac{n}{2}-1}}{E^{\frac{n}{2}-1}} \\
 &= \gamma \left[ 1 - \frac{H_1(\mathbf{q}_1, \mathbf{p}_1)}{E} \right]^{\frac{n}{2}-1} \\
 &= \gamma \left[ 1 - \frac{H_1(\mathbf{q}_1, \mathbf{p}_1)}{\frac{n}{2}k_B T} \right]^{\frac{n}{2}-1}.
 \end{aligned}$$

Considering the limit  $n \rightarrow \infty$ , then

$$\frac{n}{2} - 1 \approx \frac{n}{2} \quad (3.84)$$

and denoting the last as

$$x = \frac{n}{2}, \quad (3.85)$$

we can write

$$\lim_{x \rightarrow \infty} \gamma \left[ 1 - \frac{H_1(\mathbf{q}_1, \mathbf{p}_1)}{\frac{n}{2}k_B T} \right]^{\frac{n}{2}-1} = \gamma \lim_{x \rightarrow \infty} \left[ 1 - \frac{1}{x} \frac{H_1(\mathbf{q}_1, \mathbf{p}_1)}{k_B T} \right]^x, \quad (3.86)$$

where  $E$  is the total energy of the ideal gas in Eq.(3.74). Remembering that

$$\lim_{n \rightarrow \infty} \left( 1 + \frac{1}{n} \right)^n = e, \quad (3.87)$$

with the change of variables

$$y = -\frac{xk_B T}{H_1(\mathbf{q}_1, \mathbf{p}_1)}, \quad (3.88)$$

*the Gibbs ensemble*

and gathering the constant terms in  $Z$ , one work out

$$\begin{aligned}
 \rho_1(\mathbf{q}_1, \mathbf{p}_1) &= \frac{1}{Z} \lim_{y \rightarrow \infty} \left( 1 + \frac{1}{y} \right)^{-\frac{yH_1(\mathbf{q}_1, \mathbf{p}_1)}{k_B T}} & (3.89) \\
 &= \frac{1}{Z} e^{-\frac{H_1(\mathbf{q}_1, \mathbf{p}_1)}{k_B T}},
 \end{aligned}$$

which represents the so called *Gibbs ensemble*.

We can rewrite the last equation introducing the notation

$$\beta = \frac{1}{k_B T} \quad (3.90)$$

as

$$\rho_1(\mathbf{q}_1, \mathbf{p}_1) = \frac{1}{Z} e^{-\beta H_1(\mathbf{q}_1, \mathbf{p}_1)}, \quad (3.91)$$

which is called the *canonical distribution*. While in the microcanonical distribution the energy  $E$  is specified and the temperature  $T$  is a derived quantity, in the canonical ensemble the temperature of the system is kept fixed and the energy fluctuates above its mean values.

The constant term  $Z$  is actually

$$Z = \int e^{-\beta H_1(\mathbf{q}_1, \mathbf{p}_1)} d\mathbf{q}_1 d\mathbf{p}_1, \quad (3.92)$$

having the role of a normalizing term and it is called the *canonical partition function*.

*the canonical  
distribution*

*the partition  
function*



Part III

THEORETICAL AND COMPUTATIONAL  
APPROACHES



## FROM STATISTICAL MECHANICS TO THERMODYNAMICS OF SINGLE POLYMERS

---

### Contents

---

4.1	Thermodynamics of polymer chains	63
4.2	Helmholtz ensemble	64
4.3	Gibbs ensemble	70
4.4	Relationship between Helmholtz and Gibbs partition functions	76
4.4.1	Fourier transform theory approach	76
4.4.2	Laplace transform theory approach	78
4.5	Outline of the results	79

---

So far, we discussed how polymer molecules are recurrent in biological systems. Their understanding in term of elasticity and mechanical behavior is of crucial importance for natural sciences (see Chapter 1). Mechanical experiments on polymers provided a crucial elucidation about the molecular behaviour of several biomolecular processes. In particular, the behaviour of single polymer chains has been studied and single molecules techniques developed over the years include mechanical and optical methods [1, 2, 3]. We already introduced the simplest model of a single polymer, the *Freely-jointed chains* (FJC) model, which describes the molecule as a chain of  $N$  monomers, joined by perfectly flexible bonds with length  $b$  [26, 38]. Even if, FJC is the most simple model for a single polymer, it is appropriate to describe certain biopolymers, including single-stranded DNA (ssDNA) and RNA [19]. On the other hand, this model is not useful for describing other kind of biopolymers, for which a well description is provided by the *Worm-like chains* (WLC) model [17, 27].

Usually, FJC and WLC models describe the polymer with some assumptions, this is the reason why we can refer to them with the generic term *ideal chains*. Two main assumptions are typically considered in the analytical developments of the standard FJC

and WLC models: (a) inextensibility, expressed as a fixed bond length between two adjacent monomers, and (b) the number of monomers constituting the chain is supposed very high. The first assumption is used even in the case of large applied forces, although it has been shown that the polymer may enter a regime where the elasticity of the molecular and chemical bonds becomes important. This phenomenon has been experimentally observed for DNA [105], polyelectrolytes [106] and F-actin [107]. Typical corrections aimed at describing bond elasticity have been introduced through additional spring-like terms [108]. The second assumption is related to the concept of thermodynamics limit ( $N \rightarrow \infty$ ). We will discuss in Chapter 6 the consequences of both assumptions and what happens when they are not longer valid.

As a first theoretical analysis, in this Chapter, we deal with the thermodynamics of a polymer model that maintains generality on both the two assumptions. To do this, we consider a polymer chain with a finite number  $N$  of monomers and with an arbitrary potential  $V$  on monomers without the hypothesis of the interaction pairing. The advantage to consider such a model is that, when desired, we can specify a particular bond potential and eventually study the system for an infinite number of monomers ( $N \rightarrow \infty$ ). The specification of a particular bond potential allow us to consider different kind of elasticity contribution of the chemical bonds, depending on the considered systems and loading regimes. A typical choice is to assume the bond potential harmonic, which leads to the well-known bead-spring chain models. On the one hand much work has been performed using Hookean springs [109], even if these models are sometimes insufficient in describing polymer behavior elasticity. On the other hand it is well known that finite-extensibility plays an important role in determining the rheological properties of polymers [110, 111]. In certain cases, we can also specify the spring stiffness approaching to infinite, in order to turn our model in the classical FJC or WLC models that assumes a fixed bond length between monomers.

The advantage to consider a finite number  $N$  of monomers, lies on the fact that we are interested on investigate the thermodynamics of the system out of the thermodynamic limit, with the possibility on the same ground, to study our systems in the thermodynamic limit when requested.

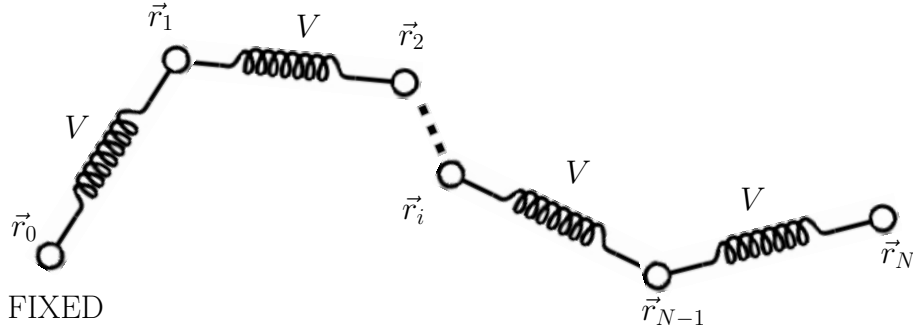


Figure 4.1: Polymer chain model. The monomer  $\mathbf{r}_0$  is clamped while the other monomers are free to fluctuate.

Two different approaches, which lead to two different ensembles, are described: the Helmholtz and the Gibbs ensembles. We determine the proper partition functions and we derive an exact relationship between them. In particular, we find that the Gibbs partition function is the three-dimensional (bilateral or two-sided) Laplace transform of the Helmholtz partition function.

#### 4.1 THERMODYNAMICS OF POLYMER CHAINS

Let us consider a chain of monomers in a long molecule, each monomer representing a group of atoms or molecules along the polymer backbone. The classical dynamics of monomers is described by the set of positions  $\mathbf{r}_i$  ( $i = 1, \dots, N$ ) and momenta  $\mathbf{p}_i$  ( $i = 1, \dots, N$ ). We assume that one terminal monomer is fixed at position  $\mathbf{r}_0 \equiv (0, 0, 0)$  and that monomers interact through an arbitrary potential (see Fig. 4.1). The dynamics of the system is described by the Hamiltonian

*our polymer model*

$$h_0(\mathbf{r}_1, \dots, \mathbf{r}_N, \mathbf{p}_1, \dots, \mathbf{p}_N) = \sum_{i=1}^N \frac{\mathbf{p}_i \cdot \mathbf{p}_i}{2m} + V(\vec{\mathbf{r}}_1, \dots, \vec{\mathbf{r}}_N). \quad (4.1)$$

Moreover, we consider this system in contact with a thermal bath characterized by a temperature  $T$ . It means that, at thermal equilibrium, its statistical properties are described by the density probability in the phase space, hence by the canonical distribution, previously discussed in Eq.(3.90), namely

*polymer immersed in a thermal bath*

$$\rho(\mathbf{q}, \mathbf{p}) = \frac{1}{Z} e^{-\frac{h_0(\mathbf{q}, \mathbf{p})}{k_B T}}, \quad (4.2)$$

*main  
goal*

where we have introduced the canonical variables  $\mathbf{q} = (\mathbf{r}_1, \dots, \mathbf{r}_N)$  and  $\mathbf{p} = (\mathbf{p}_1, \dots, \mathbf{p}_N)$ , the Boltzmann constant  $k_B$  and the partition function  $Z$ . The convergence of thermal equilibrium to the canonical distribution is proved in Chapter 3: all the consequences will be demonstrated in detail. The main goal of this Chapter is to obtain the macroscopic (or mesoscopic) thermodynamics of the system starting from the above canonical distribution. To this aim we follow two dual approaches that are equivalent in the limit of a large system (thermodynamic limit) hence for systems with  $N \rightarrow \infty$ .

*similitude  
with an  
ideal gas*

In the first approach we suppose to fix the position  $\mathbf{r}_N$  of the last component of the chain and we define  $\mathbf{r} \equiv \mathbf{r}_N$  as a macroscopic (or deterministic) variable. This case is similar to that of an ideal gas into a given volume  $V$ . In the second approach we suppose to apply a given force  $\mathbf{f}$  to the last particle and we consider  $\mathbf{f}$  as a macroscopic variable. This case is similar to that of a gas constrained with a certain pressure  $P$ .

#### 4.2 HELMHOLTZ ENSEMBLE

*reduced  
Hamiltonian*

By setting a given end-to-end distance, positions  $\mathbf{r}_0$ ,  $\mathbf{r}_N$  and momenta  $\mathbf{p}_0$ ,  $\mathbf{p}_N$  are fixed (see Fig.4.2), and we can use the following reduced Hamiltonian

$$h(\mathbf{q}, \mathbf{p}, \mathbf{r}) = h_0(\mathbf{r}_1, \dots, \mathbf{r}_{N-1}, \mathbf{r}_N = \mathbf{r}, \mathbf{p}_1, \dots, \mathbf{p}_{N-1}, \mathbf{p}_N = 0).$$

*Helmholtz  
partition  
function*

where, in this case the microscopic variables are defined as  $\mathbf{q} = (\mathbf{r}_1, \dots, \mathbf{r}_{N-1})$  and  $\mathbf{p} = (\mathbf{p}_1, \dots, \mathbf{p}_{N-1})$ , in terms of which the system partition function is written

$$Z_{\mathbf{r}}(\mathbf{r}, T) = \int_{\Gamma_{N-1}} e^{-\frac{h(\mathbf{q}, \mathbf{p}, \mathbf{r})}{k_B T}} d\mathbf{q} d\mathbf{p}, \quad (4.3)$$

*force  
exerted on  
the system*

where  $\Gamma_{N-1} = \mathfrak{R}^{6(N-1)}$ . The force exerted on  $\mathbf{r} \equiv \mathbf{r}_N$  by the others components of the chain is  $-\frac{\partial h}{\partial \mathbf{r}_N}$  by definition of interaction potential energy. Its mean (or average) value defines the macroscopic force and the constitutive equation of the chain. The force exerted on the system (from outside) is:

$$\mathbf{f} = \left\langle \frac{\partial h(\mathbf{q}, \mathbf{p}, \mathbf{r})}{\partial \mathbf{r}_N} \right\rangle = \int_{\Gamma} \frac{\partial h(\mathbf{q}, \mathbf{p}, \mathbf{r})}{\partial \mathbf{r}} \rho(\mathbf{q}, \mathbf{p}, \mathbf{r}) d\mathbf{q} d\mathbf{p} \quad (4.4)$$

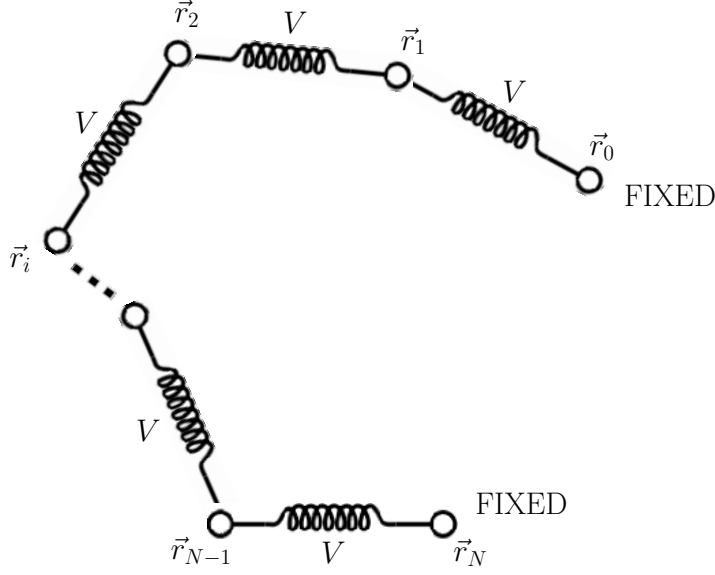


Figure 4.2: A polymer chain under the Helmholtz boundary conditions: monomers  $\mathbf{r}_0$  and  $\mathbf{r}_N$  are clamped.

or equivalently

$$f(\mathbf{r}, T) = \frac{\int_{\Gamma} \frac{\partial h(\mathbf{q}, \mathbf{p}, \mathbf{r})}{\partial \mathbf{r}} e^{-\frac{h(\mathbf{q}, \mathbf{p}, \mathbf{r})}{k_B T}} d\mathbf{q} d\mathbf{p}}{\int_{\Gamma} e^{-\frac{h(\mathbf{q}, \mathbf{p}, \mathbf{r})}{k_B T}} d\mathbf{q} d\mathbf{p}}. \quad (4.5)$$

Actually, the concept of macroscopic force, here introduced for the specific case of the position of the monomer  $\mathbf{r}_N$ , is much more general and is often referred to the concept of the *Landau free energy*. As a matter of fact, keeping fixed a general set of monomers (in this case  $\mathbf{r}_0, \mathbf{r}_N$  are fixed), the average force over all the configurations of all the remaining  $n$  monomers acting on the  $i$ -th monomer ( $\mathbf{r}_1, \dots, \mathbf{r}_{N-1}$  in this case) at any fixed configuration is given by:

$$-\Delta_i U^n = \frac{\int e^{-\beta V} (-\Delta_i V) d\mathbf{q}_1 \dots d\mathbf{q}_{N-1}}{\int e^{-\beta V} d\mathbf{q}_1 \dots d\mathbf{q}_{N-1}}, \quad (4.6)$$

where  $i = 1, \dots, N$ ,  $\beta = 1/k_B T$ , the  $\Delta_i U^n$  is the average force and therefore  $U^n$  is the so-called *potential of the mean force* or the *Landau free energy* [99, 112, 113].

We also remark that the constitutive equation Eq.(4.5) can be directly obtained from the partition function  $Z_r$  in Eq.(4.3). We work out:

$$\frac{\partial Z_r}{\partial \mathbf{r}} = \int_{\Gamma} e^{-\frac{h(\mathbf{q}, \mathbf{p}, \mathbf{r})}{k_B T}} \left( -\frac{1}{k_B T} \right) \frac{\partial h(\mathbf{q}, \mathbf{p}, \mathbf{r})}{\partial \mathbf{r}} d\mathbf{q} d\mathbf{p}. \quad (4.7)$$

*Helmholtz  
constitutive  
equation*

By combining Eqs.(4.5) and (4.7) we find:

$$f(\mathbf{r}, T) = -k_B T \frac{1}{Z_r} \frac{\partial Z_r}{\partial \mathbf{r}} = -k_B T \frac{\partial}{\partial \mathbf{r}} \log(Z_r). \quad (4.8)$$

In addition to the constitutive equation, the statistical mechanics also furnishes the macroscopic thermodynamics as follows. We consider the average value of the Hamiltonian as the internal energy of the system, namely

$$\begin{aligned} U &= \langle h(\mathbf{q}, \mathbf{p}, \mathbf{r}) \rangle \\ &= \int_{\Gamma} h(\mathbf{q}, \mathbf{p}, \mathbf{r}) \rho(\mathbf{q}, \mathbf{p}, \mathbf{r}, T) d\mathbf{q} d\mathbf{p} \\ &= \frac{\int_{\Gamma} h(\mathbf{q}, \mathbf{p}, \mathbf{r}) e^{-\frac{h(\mathbf{q}, \mathbf{p}, \mathbf{r})}{k_B T}} d\mathbf{q} d\mathbf{p}}{\int_{\Gamma} e^{-\frac{h(\mathbf{q}, \mathbf{p}, \mathbf{r})}{k_B T}} d\mathbf{q} d\mathbf{p}}. \end{aligned} \quad (4.9)$$

*very slow  
motion  
assumption*

In order to introduce the thermodynamics we must consider a transformation of the system. It means that the end-position  $\mathbf{r} = \mathbf{r}(t)$  can vary in time and also the temperature  $T = T(t)$  is a dynamical variable. In general, these assumptions lead to the out-of-equilibrium statistical mechanics. However, we assume a very slow motion of  $\mathbf{r}$  and  $T$  and, therefore, we may say that the system evolves through a quasi-static transformation. This kind of transformation passes through a sequence of equilibrium states and thus the dynamical probability density in the phase space is simply given by

$$\rho(\mathbf{q}, \mathbf{p}, \mathbf{r}(t), T(t)) = \frac{1}{Z_r} e^{-\frac{h(\mathbf{q}, \mathbf{p}, \mathbf{r}(t))}{k_B T}}, \quad (4.10)$$

where  $Z_r$  is given by Eq.(4.3), with  $\mathbf{r} = \mathbf{r}(t)$  and  $T = T(t)$ . As long as we are considering a very slow motion of  $\mathbf{r}$  and  $T$ , the transformations of the system pass through a sequence of equilibrium states: in these hypothesis it is significant looking for the variation

in time of the internal energy  $U$ . Starting from Eq.(4.9), the time dependence is only in the variables  $\mathbf{r}$  and  $T$ . We have

$$\begin{aligned}\frac{dU}{dt} &= \int_{\Gamma} \frac{d}{dt} [h(\mathbf{q}, \mathbf{p}, \mathbf{r}(t)) \rho(\mathbf{q}, \mathbf{p}, \mathbf{r}(t), T(t))] d\mathbf{q} d\mathbf{p} \\ &= \int_{\Gamma} \frac{dh(\mathbf{q}, \mathbf{p}, \mathbf{r}(t))}{dt} \rho(\mathbf{q}, \mathbf{p}, \mathbf{r}(t), T(t)) d\mathbf{q} d\mathbf{p} \\ &+ \int_{\Gamma} h(\mathbf{q}, \mathbf{p}, \mathbf{r}(t)) \frac{d\rho(\mathbf{q}, \mathbf{p}, \mathbf{r}(t), T(t))}{dt} d\mathbf{q} d\mathbf{p}.\end{aligned}\quad (4.11)$$

Now we are able to identify two integrals: the first one represents the work made on the system, while the second one is the heat entering the system. Denoting with the letter  $A$  the first integral, and with the letter  $B$  the second one, we can write

$$\begin{aligned}A &= \int_{\Gamma} \frac{dh(\mathbf{q}, \mathbf{p}, \mathbf{r}(t))}{d\mathbf{r}} \frac{d\mathbf{r}(t)}{dt} \rho(\mathbf{q}, \mathbf{p}, \mathbf{r}(t), T(t)) d\mathbf{q} d\mathbf{p} \\ &= \frac{d\mathbf{r}(t)}{dt} \int_{\Gamma} \frac{dh(\mathbf{q}, \mathbf{p}, \mathbf{r}(t))}{d\mathbf{r}} \rho(\mathbf{q}, \mathbf{p}, \mathbf{r}(t), T(t)) d\mathbf{q} d\mathbf{p} \\ &= \mathbf{f} \cdot \frac{d\mathbf{r}(t)}{dt},\end{aligned}\quad (4.12)$$

having considered Eq.(4.4) or Eq.(4.5). The product force-velocity is the power, i.e. the work  $W$  made for unit of time. It means that we can write

$$A = \frac{dW}{dt}.\quad (4.13)$$

Let us denote for simplicity of notation,  $h = h(\mathbf{q}, \mathbf{p}, \mathbf{r}(t))$  and  $\rho = \rho(\mathbf{q}, \mathbf{p}, \mathbf{r}(t))$ , then for the second integral  $B$ , we elaborate the Gibbs distribution as

$$\rho = \frac{e^{-\frac{h}{k_B T}}}{\int_{\Gamma} e^{\frac{h}{k_B T}} d\mathbf{q} d\mathbf{p}} = e^{\frac{F-h}{k_B T}},\quad (4.14)$$

where  $F$  is called Helmholtz free energy and it is linked to the partition function by the relation

$$\frac{1}{Z_r} = e^{\frac{F}{k_B T}}\quad (4.15)$$

equivalently we have

$$F = -k_B T \log Z_r.\quad (4.16)$$

For brevity, let us indicate the exponential argument in Eq.(4.15) as

$$\eta = \frac{F - h}{k_B T} \quad (4.17)$$

and therefore we get

$$\rho = e^\eta. \quad (4.18)$$

The integral B assumes the form

$$\begin{aligned} B &= \int_{\Gamma} h \frac{d\rho}{dt} d\mathbf{q} d\mathbf{p} \\ &= \int_{\Gamma} h \frac{de^\eta}{dt} d\mathbf{q} d\mathbf{p} \\ &= \int_{\Gamma} h e^\eta \dot{\eta} d\mathbf{q} d\mathbf{p}. \end{aligned} \quad (4.19)$$

Since  $\int_{\Gamma} \rho d\mathbf{q} d\mathbf{p} = 1$  we have

$$\int_{\Gamma} e^\eta d\mathbf{q} d\mathbf{p} = 1 \quad (4.20)$$

and we obtain

$$\frac{d}{dt} \int_{\Gamma} e^\eta d\mathbf{q} d\mathbf{p} = \int_{\Gamma} e^\eta \dot{\eta} d\mathbf{q} d\mathbf{p} = 0. \quad (4.21)$$

Again, since F does not depend on  $\mathbf{p}$  and  $\mathbf{q}$ , we have

$$\int_{\Gamma} F e^\eta \dot{\eta} d\mathbf{q} d\mathbf{p} = 0, \quad (4.22)$$

and we can write

$$B = \int_{\Gamma} (h - F) e^\eta \dot{\eta} d\mathbf{q} d\mathbf{p}. \quad (4.23)$$

and recalling Eq.(4.17) we have that  $h - F = -k_B T \eta$ , then we finally obtain

$$B = - \int_{\Gamma} k_B T \eta \dot{\eta} e^\eta d\mathbf{q} d\mathbf{p}. \quad (4.24)$$

To better understand the meaning of the previous integral we may calculate  $\langle \eta \rangle$ , namely

$$\langle \eta \rangle = \int_{\Gamma} \eta \rho d\mathbf{q} d\mathbf{p} = \int_{\Gamma} \eta e^\eta d\mathbf{q} d\mathbf{p} \quad (4.25)$$

and the variation in time of the average value of  $\eta$  as

$$\frac{d\langle\eta\rangle}{dt} = \int_{\Gamma} \dot{\eta} e^{\eta} d\mathbf{q}d\mathbf{p} + \int_{\Gamma} \eta e^{\eta} \dot{\eta} d\mathbf{q}d\mathbf{p}. \quad (4.26)$$

The first term is zero because of Eq.(4.21) and we obtain

$$B = -k_B T \frac{d}{dt} \langle\eta\rangle, \quad (4.27)$$

where  $B$  can be interpreted as the heat given to the system for unit of time. We obtain

$$B = \frac{dQ}{dt} = T \frac{dS}{dt}, \quad (4.28)$$

where we have introduced the *entropy*

$$S = -k_B \langle \log \rho \rangle = -k_B \int_{\Gamma} \rho \log(\rho) d\mathbf{q}d\mathbf{p}. \quad (4.29)$$

In conclusion, we obtained the first and the second principles starting from the Gibbs distribution. We can we easily get the thermodynamic energy balance in the form

$$\frac{dU}{dt} = \frac{dW}{dt} + \frac{dQ}{dt}, \quad (4.30)$$

where the first term represents the work done by the external force

$$\frac{dW}{dt} = \mathbf{f} \cdot \frac{d\mathbf{r}}{dt} \quad (4.31)$$

and the second one represents the heat entering the system

$$\frac{dQ}{dt} = T \frac{dS}{dt}. \quad (4.32)$$

From the relation  $h - F = -k_B T \eta$  we perform the average and we obtain

$$U - F = TS \quad (4.33)$$

from which we have that the *Helmholtz free energy*  $F$  is given by

$$F = U - TS. \quad (4.34)$$

*Helmholtz  
free energy*

This is the standard definition in classical thermodynamics. Furthermore, from Eq.(4.8) and Eq.(4.15), we have that

$$\mathbf{f} = -k_B T \frac{\partial}{\partial \mathbf{r}} \log Z_r = \frac{\partial F(\mathbf{r}, T)}{\partial \mathbf{r}}, \quad (4.35)$$

which is a simple form of the constitutive equation.

Several thermodynamics relations follows from the scheme above. From Eq.(4.30) we can write

$$dU = \mathbf{f} \cdot d\mathbf{r} + TdS. \quad (4.36)$$

and, if  $U = U(\mathbf{r}, S)$ , we get

$$\mathbf{f} = \frac{\partial U}{\partial \mathbf{r}} \quad \text{and} \quad T = \frac{\partial U}{\partial S}. \quad (4.37)$$

Moreover, from Eq.(4.34), we work out

$$\begin{aligned} dF &= dU - TdS - SdT \\ &= \mathbf{f} \cdot d\mathbf{r} + TdS - TdS - SdT \\ &= \mathbf{f} \cdot d\mathbf{r} - SdT. \end{aligned} \quad (4.38)$$

from which, if  $F = F(\mathbf{r}, T)$ , we get

$$\mathbf{f} = \frac{\partial F}{\partial \mathbf{r}} \quad \text{and} \quad S = -\frac{\partial F}{\partial T}. \quad (4.39)$$

The classical thermodynamics of a gas or a fluid is obtained by substituting  $\mathbf{r}$  and  $\mathbf{f}$  with the volume  $V$  and pressure  $P$ , respectively.

### 4.3 GIBBS ENSEMBLE

We suppose now to consider a given applied force  $\mathbf{f}$  to the particle placed at  $\mathbf{r}_N$  (see Fig.4.3). This force can be introduced by means of an addition potential energy  $-\mathbf{f} \cdot \mathbf{r}_N$  so that  $\frac{\partial}{\partial \mathbf{r}_N}(-\mathbf{f} \cdot \mathbf{r}_N) = \mathbf{f}$  as requested; therefore the system is described by the following *augmented Hamiltonian*

*augmented  
Hamiltonian*

$$\tilde{h}(\mathbf{q}, \mathbf{p}, \mathbf{f}) = h(\mathbf{r}_1, \dots, \mathbf{r}_N, \mathbf{p}_1, \dots, \mathbf{p}_N) - \mathbf{f} \cdot \mathbf{r}_N \quad (4.40)$$

where the quantities  $\mathbf{q} = \mathbf{r}_1, \dots, \mathbf{r}_N$  and  $\mathbf{p} = \mathbf{p}_1, \dots, \mathbf{p}_N$  are the microscopic variables while  $\mathbf{f}$  assumes the role of the macroscopic

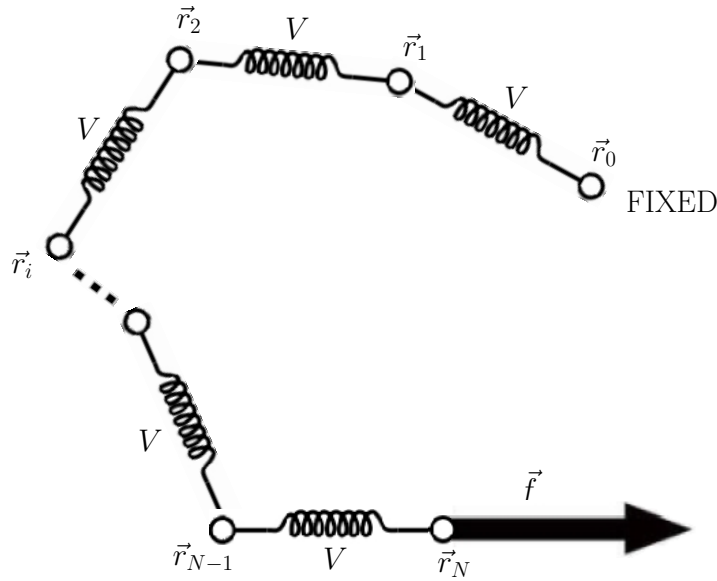


Figure 4.3: A polymer chain under the Gibbs boundary conditions: while the monomer  $r_0$  is clamped, the one at  $r_N$  is subject to a constant traction  $f$ .

variable. It is important to notice that, imaging to rigidly translate in space the molecule of  $\mathbf{r}_X$ , such that  $\mathbf{r}_0 \rightarrow \mathbf{r}_0 + \mathbf{r}_X$  and  $\mathbf{r}_N \rightarrow \mathbf{r}_N + \mathbf{r}_X$ , the  $h$  term is unchanged while the term  $\mathbf{f} \cdot \mathbf{r}_N$  goes into  $\mathbf{f} \cdot (\mathbf{r}_N + \mathbf{r}_X)$ . Actually, while the  $h$  term clearly appears unchanged, the last term appears to make the augmented Hamiltonian  $\tilde{h}$  position dependent. However, as the force applied is a constant of the motion, also the scalar product is constant and all the other results that comes out are valid and independent of the position of the last monomer. The ensemble partition function is now given by

*Gibbs  
partition  
function*

$$Z_f = Z(f, T) = \int_{\Gamma} e^{-\frac{\tilde{h}(\mathbf{q}, \mathbf{p}, f)}{k_B T}} d\mathbf{q}d\mathbf{p}, \tag{4.41}$$

and the corresponding Gibbs distribution is

$$\rho(\mathbf{q}, \mathbf{p}, f, T) = \frac{1}{Z_f} e^{-\frac{\tilde{h}(\mathbf{q}, \mathbf{p}, f)}{k_B T}}. \tag{4.42}$$

As before, we may determine the constitutive equation of the system: to this aim we observe that  $\frac{\partial \tilde{h}}{\partial f} = -r_N$ , and therefore we cal-

culate the average position of the head of the chain as  $\mathbf{r} = \langle \mathbf{r}_N \rangle$  or more explicitly

$$\mathbf{r} = - \left\langle \frac{\partial \tilde{h}}{\partial \mathbf{f}} \right\rangle = - \int_{\Gamma} \frac{\partial \tilde{h}}{\partial \mathbf{f}} \rho d\mathbf{q} d\mathbf{p}, \quad (4.43)$$

which is the counterpart of Eq.(4.5). By using Eqs.(4.41) and (4.42) in Eq.(4.43), we obtain

$$\mathbf{r}(\mathbf{f}, T) = - \frac{\int_{\Gamma} \frac{\tilde{h}(\mathbf{q}, \mathbf{p}, \mathbf{f})}{\partial \mathbf{f}} e^{-\frac{\tilde{h}(\mathbf{q}, \mathbf{p}, \mathbf{f})}{k_B T}} d\mathbf{q} d\mathbf{p}}{\int_{\Gamma} e^{-\frac{\tilde{h}(\mathbf{q}, \mathbf{p}, \mathbf{f})}{k_B T}}}, \quad (4.44)$$

which is the counterpart of Eq.(4.8). This constitutive equation can also be expressed by means of the partition function  $Z_f$ . In fact, by differentiating Eq.(4.41) with respect to  $\mathbf{f}$ , we get

$$\frac{\partial Z_f}{\partial \mathbf{f}} = \int_{\Gamma} \frac{\tilde{h}(\mathbf{q}, \mathbf{p}, \mathbf{f})}{\partial \mathbf{f}} \left( -\frac{1}{k_B T} \right) e^{-\frac{\tilde{h}(\mathbf{q}, \mathbf{p}, \mathbf{f})}{k_B T}} d\mathbf{q} d\mathbf{p} \quad (4.45)$$

and therefore

$$\mathbf{r}(\mathbf{f}, T) = k_B T \frac{1}{Z_f} \frac{\partial Z_f}{\partial \mathbf{f}} = k_B T \frac{\partial}{\partial \mathbf{f}} \log(Z_f). \quad (4.46)$$

*Gibbs  
constitutive  
equation*

Now, we can introduce the macroscopic thermodynamics by identifying the average value of the augmented Hamiltonian with the enthalpy of the system. We can write

$$\begin{aligned} h &= \langle \tilde{h}(\mathbf{q}, \mathbf{p}, \mathbf{f}) \rangle \\ &= \int_{\Gamma} \tilde{h}(\mathbf{q}, \mathbf{p}, \mathbf{f}) \rho(\mathbf{q}, \mathbf{p}, \mathbf{f}, T) d\mathbf{q} d\mathbf{p} \\ &= \frac{\int_{\Gamma} \tilde{h}(\mathbf{q}, \mathbf{p}, \mathbf{f}) e^{-\frac{\tilde{h}(\mathbf{q}, \mathbf{p}, \mathbf{f})}{k_B T}} d\mathbf{q} d\mathbf{p}}{\int_{\Gamma} e^{-\frac{\tilde{h}(\mathbf{q}, \mathbf{p}, \mathbf{f})}{k_B T}} d\mathbf{q} d\mathbf{p}}. \end{aligned} \quad (4.47)$$

As previously, we suppose that  $\mathbf{f} = \mathbf{f}(t)$  and  $T = T(t)$  in order to introduce a quasi-static transformation and we develop the time derivative of the enthalpy, namely

$$\begin{aligned} \frac{dh}{dt} &= \int_{\Gamma} \frac{d}{dt} [\tilde{h}(\mathbf{q}, \mathbf{p}, \mathbf{f}) \rho(\mathbf{q}, \mathbf{p}, \mathbf{f}, T)] d\mathbf{q} d\mathbf{p} \\ &= \int_{\Gamma} \frac{\tilde{h}(\mathbf{q}, \mathbf{p}, \mathbf{f})}{dt} \rho(\mathbf{q}, \mathbf{p}, \mathbf{f}, T) d\mathbf{q} d\mathbf{p} \\ &+ \int_{\Gamma} \tilde{h}(\mathbf{q}, \mathbf{p}, \mathbf{f}) \frac{d\rho(\mathbf{q}, \mathbf{p}, \mathbf{f}, T)}{dt} d\mathbf{q} d\mathbf{p}, \end{aligned} \quad (4.48)$$

where the first term is

$$\begin{aligned}
 A &= \int_{\Gamma} \frac{\partial \tilde{h}(\mathbf{q}, \mathbf{p}, f)}{\partial f} \frac{df}{dt} \rho(\mathbf{q}, \mathbf{p}, f, T) d\mathbf{q} d\mathbf{p} \\
 &= \frac{df}{dt} \int_{\Gamma} \frac{\partial \tilde{h}(\mathbf{q}, \mathbf{p}, f)}{\partial f} \rho(\mathbf{q}, \mathbf{p}, f, T) d\mathbf{q} d\mathbf{p} \\
 &= -\frac{df}{dt} \cdot \mathbf{r}.
 \end{aligned} \tag{4.49}$$

The second term can be developed by introducing a new form of the Gibbs distribution

$$\rho(\mathbf{q}, \mathbf{p}, f, T) = \frac{1}{Z_f} e^{-\frac{\tilde{h}}{k_B T}} = e^{\frac{G - \tilde{h}}{k_B T}}. \tag{4.50}$$

Here we have used the relations

$$\frac{1}{Z_f} = e^{\frac{G}{k_B T}} \quad \text{or} \quad G = -k_B T \log(Z_f). \tag{4.51}$$

where  $G$  is the *Gibbs free energy*.

For brevity, let us indicate

$$\phi = \frac{G - \tilde{h}}{k_B T}. \tag{4.52}$$

We now develop the calculation of  $B$  starting from Eq.(4.19). The integral  $B$  assumes the present form

$$B = \int_{\Gamma} \tilde{h} \frac{d}{dt} e^{\phi} d\mathbf{q} d\mathbf{p} = \int_{\Gamma} \tilde{h} \dot{\phi} e^{\phi} d\mathbf{q} d\mathbf{p}. \tag{4.53}$$

Since

$$\int_{\Gamma} e^{\phi} d\mathbf{q} d\mathbf{p} = 1 \tag{4.54}$$

we obtain

$$\frac{d}{dt} \int_{\Gamma} e^{\phi} d\mathbf{q} d\mathbf{p} = \int_{\Gamma} e^{\phi} \dot{\phi} d\mathbf{q} d\mathbf{p} = 0 \tag{4.55}$$

and since  $G$  is independent on  $\mathbf{q}$  and  $\mathbf{p}$ , we can write

$$\int_{\Gamma} G e^{\phi} \dot{\phi} d\mathbf{q} d\mathbf{p} = 0. \tag{4.56}$$

We can write B (see Eq.(4.53)) also as

$$B = \int_{\Gamma} (\tilde{h} - G) \dot{\phi} e^{\phi} d\mathbf{q} d\mathbf{p} = - \int_{\Gamma} k_B T \phi \dot{\phi} e^{\phi} d\mathbf{q} d\mathbf{p}. \quad (4.57)$$

The average value of  $\phi$  is given by

$$\langle \phi \rangle = \int_{\Gamma} \phi e^{\phi} d\mathbf{q} d\mathbf{p} \quad (4.58)$$

and its time derivative is

$$\frac{d\langle \phi \rangle}{dt} = \int_{\Gamma} [\dot{\phi} e^{\phi} + \phi \dot{\phi} e^{\phi}] d\mathbf{q} d\mathbf{p} = \int_{\Gamma} \phi \dot{\phi} e^{\phi} d\mathbf{q} d\mathbf{p}. \quad (4.59)$$

From Eqs.(4.57) and (4.59) we obtain that

$$B = -k_B T \frac{d}{dt} \langle \phi \rangle \quad (4.60)$$

or equivalently

$$B = T \frac{dS}{dt} = \frac{dQ}{dt}, \quad (4.61)$$

where we have introduced the *entropy*

$$S = -k_B \langle \log(\rho) \rangle = -k_B \int_{\Gamma} \rho \log(\rho) d\mathbf{q} d\mathbf{p}. \quad (4.62)$$

It is important to remark that Eq.(4.62) is not identical to Eq.(4.29) since the probability density  $\rho$  in the latter developed case corresponds to the Gibbs ensemble. We will discuss after that, only when the thermodynamic limit of a large system is satisfied, the two approaches yield the same results. The time derivative of the enthalpy has been obtained in the form

$$\frac{dh}{dt} = -\frac{d\mathbf{f}}{dt} \cdot \mathbf{r} + T \frac{dS}{dt}. \quad (4.63)$$

Since in the thermodynamic limit we have the equivalence of the ensembles, we can also consider Eq.(4.36), namely

$$\frac{dU}{dt} = \mathbf{f} \cdot \frac{d\mathbf{r}}{dt} + T \frac{dS}{dt} \quad (4.64)$$

and we obtain by subtraction

$$\frac{dh}{dt} - \frac{dU}{dt} = -\frac{d\mathbf{f}}{dt} \cdot \mathbf{r} - \mathbf{f} \cdot \frac{d\mathbf{r}}{dt} = -\frac{d}{dt} (\mathbf{f} \cdot \mathbf{r}) \quad (4.65)$$

or equivalently:

$$h = U - \mathbf{f} \cdot \mathbf{r}, \quad (4.66)$$

which is the standard definition of enthalpy in thermodynamics. Within the Gibbs ensemble, from the definition of  $\phi$  in Eq.(4.59), we can write

$$G - \hat{h} = k_B T \phi \quad (4.67)$$

and performing the average we obtain

$$G = h - TS, \quad (4.68) \quad \text{Gibbs free energy}$$

which is the *standard definition of Gibbs free energy*. Moreover, from Eqs.(4.46) and (4.51) we have

$$\mathbf{r} = k_B T \frac{\partial}{\partial \mathbf{f}} \log(Z_f) = -\frac{\partial G(\mathbf{f}, T)}{\partial \mathbf{f}}. \quad (4.69)$$

Some thermodynamic relations from enthalpy and Gibbs free energy follow. From Eq.(4.63) we have that

$$dh = -\mathbf{r} \cdot d\mathbf{f} + TdS \quad (4.70)$$

and, if  $h = h(\mathbf{f}, S)$  we obtain

$$\mathbf{r} = -\frac{\partial h}{\partial \mathbf{f}}, \quad T = \frac{\partial h}{\partial S}. \quad (4.71)$$

From Eq.(4.68) we have

$$\begin{aligned} dG &= dh - TdS - SdT \\ &= -\mathbf{r} \cdot d\mathbf{f} + TdS - TdS - SdT \\ &= -\mathbf{r} \cdot d\mathbf{f} - SdT, \end{aligned} \quad (4.72)$$

from which, if  $G = G(\mathbf{f}, T)$ , we can write

$$\mathbf{r} = -\frac{\partial G}{\partial \mathbf{f}}, \quad S = -\frac{\partial G}{\partial T}. \quad (4.73)$$

As previously discussed, the classical thermodynamics for gas and liquids can be obtained by substituting  $\mathbf{r}, \mathbf{f}$  with  $V, P$ .

#### 4.4 RELATIONSHIP BETWEEN HELMHOLTZ AND GIBBS PARTITION FUNCTIONS

By taking into consideration Eqs.(4.3) and (4.41), as well as the known integral

$$\int_{\mathfrak{R}^3} \exp \left\{ -\frac{1}{k_B T} \frac{\mathbf{p} \cdot \mathbf{p}}{2m} \right\} d\mathbf{p} = (2\pi m k_B T)^{3/2}, \quad (4.74)$$

*Z<sub>f</sub> and Z<sub>r</sub>  
relationship*

the exact relationship between  $Z_f$  and  $Z_r$  can be obtained as

$$Z_f(\mathbf{f}, T) = (2\pi m k_B T)^{\frac{3}{2}} \int_{\mathfrak{R}^3} Z_r(\mathbf{r}, T) e^{\frac{\mathbf{f} \cdot \mathbf{r}}{k_B T}} d\mathbf{r}, \quad (4.75)$$

showing that the Gibbs partition function is the three-dimensional (bilateral or two-sided) Laplace transform of the Helmholtz partition function (except for a non relevant multiplicative constant). Now, it is important to obtain the inverse relation giving the Helmholtz partition function in terms of the Gibbs one. For this purposes, we can adopt two different ways: one by means of the Fourier Transform, the other, using the Laplace transform.

##### 4.4.1 Fourier transform theory approach

It is useful to invert the previous integral relation. From equation (4.75), we introduce the imaginary argument  $\mathbf{f} = -i\mathbf{g}$ , so that

$$Z_f(-i\mathbf{g}, T) = (2\pi m k_B T)^{\frac{3}{2}} \int_{\mathfrak{R}^3} Z_r(\mathbf{r}, T) e^{-i\frac{\mathbf{g} \cdot \mathbf{r}}{k_B T}} d\mathbf{r}. \quad (4.76)$$

Now we have obtained a Fourier transformation between  $Z_f(-i\mathbf{g}, T)$  and  $Z_r(\mathbf{r}, T)$ . Therefore we can write

$$\frac{Z_f(-i\mathbf{g}, T)}{(2\pi m k_B T)^{\frac{3}{2}}} = \int_{\mathfrak{R}^3} Z_r(\mathbf{r}, T) e^{-i\frac{\mathbf{g} \cdot \mathbf{r}}{k_B T}} d\mathbf{r}. \quad (4.77)$$

The Fourier transform follows the rules

$$\begin{cases} F(\boldsymbol{\omega}) = \int_{\mathfrak{R}^3} f(\mathbf{r}) e^{-i\boldsymbol{\omega} \cdot \mathbf{r}} & (3D - FT) \\ f(\mathbf{r}) = \frac{1}{(2\pi)^3} \int_{\mathfrak{R}^3} F(\boldsymbol{\omega}) e^{i\boldsymbol{\omega} \cdot \mathbf{r}} & (3D - IFT). \end{cases} \quad (4.78)$$

Defining  $\mathbf{r} = \mathbf{g}/k_B T$  and performing the change of variable  $\mathbf{g} = k_B T \boldsymbol{\omega}$  with  $\boldsymbol{\omega} \in \mathfrak{R}^3$ , we can write

$$\frac{Z_f(-ik_B T \boldsymbol{\omega}, T)}{(2\pi m k_B T)^{\frac{3}{2}}} = \int_{\mathfrak{R}^3} Z_r(\mathbf{r}, T) e^{-i\boldsymbol{\omega} \cdot \mathbf{r}} d\mathbf{r}. \quad (4.79)$$

In the right-hand side we recognize a standard Fourier transform and the inverse relation is obtained as

$$Z_r(\mathbf{r}, T) = \frac{1}{(2\pi)^3} \int_{\mathfrak{R}^3} \frac{Z_f(-ik_B T \boldsymbol{\omega}, T)}{(2\pi m k_B T)^{\frac{3}{2}}} e^{i\boldsymbol{\omega} \cdot \mathbf{r}} d\boldsymbol{\omega}. \quad (4.80)$$

By the change of variable  $\boldsymbol{\phi} = -k_B T \boldsymbol{\omega}$  we obtain the relation  $d\boldsymbol{\phi} = (k_B T)^3 d\boldsymbol{\omega}$  and, therefore, we get

$$Z_r(\mathbf{r}, T) = \frac{1}{(2\pi)^3} \int_{\mathfrak{R}^3} \frac{Z_f(i\boldsymbol{\phi}, T)}{(2\pi m k_B T)^{\frac{3}{2}}} e^{i\frac{\boldsymbol{\phi} \cdot \mathbf{r}}{k_B T}} \frac{d\boldsymbol{\phi}}{(k_B T)^3}. \quad (4.81)$$

Since

$$\begin{aligned} (2\pi)^3 (2\pi m k_B T)^{\frac{3}{2}} (k_B T)^3 &= \left[ 2\pi k_B T \sqrt{2\pi m k_B T} \right]^3 \\ &= \left[ (2\pi k_B T)^{\frac{3}{2}} \sqrt{m} \right]^3 \\ &= (2\pi k_B T)^{\frac{9}{2}} m^{\frac{3}{2}}, \end{aligned} \quad (4.82)$$

we finally get

$$Z_r(\mathbf{r}, T) = \frac{1}{(2\pi k_B T)^{9/2} m^{3/2}} \int_{\mathfrak{R}^3} Z_f(i\boldsymbol{\phi}, T) e^{-i\frac{\boldsymbol{\phi} \cdot \mathbf{r}}{k_B T}} d\boldsymbol{\phi}, \quad (4.83)$$

which states that, in order to derive the Helmholtz partition function, one must use the analytic continuation of the Gibbs partition function over the imaginary argument.

Eqs.(4.75) and (4.83) allow to obtain each partition function with an integral over  $\mathfrak{R}^3$ , which is much easier than the original integral over the whole phase space. So, when one of the two partition functions is determined, the other can be simply obtained analytically or numerically, depending on the complexity of the system. Moreover, the relationship between the two partition functions is very important for enlightening the meaning of the thermodynamic limit, as described in Chapter 6.

#### 4.4.2 Laplace transform theory approach

As a matter of fact, one can obtain the last relation in Eq.(4.83) also by means of the Laplace transform theory. Referring to Eq.(4.75), and performing the change of variable  $f = -k_B T \mathbf{S}$ , where  $\mathbf{S}$  is the vector Laplace variable, we can write

$$Z_f(-k_B T \mathbf{S}, T) = (2\pi m k_B T)^{\frac{3}{2}} \int_{\mathfrak{R}^3} Z_r(\mathbf{r}, T) e^{-\mathbf{S} \cdot \mathbf{r}} d\mathbf{r}, \quad (4.84)$$

or equivalently

$$\frac{Z_f(-k_B T \mathbf{S}, T)}{(2\pi m k_B T)^{\frac{3}{2}}} = \int_{\mathfrak{R}^3} Z_r(\mathbf{r}, T) e^{-\mathbf{S} \cdot \mathbf{r}} d\mathbf{r}. \quad (4.85)$$

Recalling the Laplace transform property

$$\begin{cases} F(S) = \int_{-\infty}^{+\infty} f(t) e^{-St} dt & \text{(LT)} \\ f(t) = \frac{1}{2\pi i} \int_{\gamma-i\infty}^{\gamma+i\infty} F(S) e^{St} dS & \text{(ILT)}, \end{cases} \quad (4.86)$$

and those in three dimensions

$$\begin{cases} F(\mathbf{S}) = \int_{\mathfrak{R}^3} f(\mathbf{r}) e^{-\mathbf{S} \cdot \mathbf{r}} d\mathbf{r} & \text{(3D - LT)} \\ f(\mathbf{r}) = \frac{1}{(2\pi i)^3} \int_{i\mathfrak{R}^3} F(\mathbf{S}) e^{\mathbf{S} \cdot \mathbf{r}} d\mathbf{S} & \text{(3D - ILT)}, \end{cases} \quad (4.87)$$

we can write

$$Z_r(\mathbf{r}, T) = \frac{1}{(2\pi i)^3} \int_{i\mathfrak{R}^3} \frac{Z_f(-k_B T \mathbf{S}, T)}{(2\pi m k_B T)^{\frac{3}{2}}} e^{\mathbf{S} \cdot \mathbf{r}} d\mathbf{S}. \quad (4.88)$$

From this, with a change of variable  $\mathbf{S}$  to  $\mathbf{r}$ , namely

$$\mathbf{S} = -i \frac{\boldsymbol{\Phi}}{k_B T}, \quad d\mathbf{S} = \left( -\frac{i}{k_B T} \right)^3 d\boldsymbol{\Phi}, \quad (4.89)$$

we obtain again Eq.(4.83),

$$Z_r(\mathbf{r}, T) = \frac{1}{(2\pi k_B T)^{9/2} m^{3/2}} \int_{\mathfrak{R}^3} \frac{Z_f(i\boldsymbol{\Phi}, T)}{e}^{-i \frac{\boldsymbol{\Phi} \cdot \mathbf{r}}{k_B T}} d\boldsymbol{\Phi}. \quad (4.90)$$

The present results can be further simplified when the applied force is taken to be collinear with the end-to-end vector distance. We suppose that the Helmholtz partition function exhibits the spherical symmetry, leading to the scalar relation  $Z_r(\mathbf{r}, T) = Z_r(r, T)$ . In other words,  $Z_r$  depends on  $r$  only through its modulus  $r$ . In this case the Gibbs partition function shows such a spherical symmetry as well:  $Z_f(\mathbf{f}, T) = Z_f(f, T)$ . Conversely, a similar constraint is, in turn, obtained for the Helmholtz function if spherical symmetry is assumed for the Gibbs function. It can be proved that  $Z_r$  and  $Z_f$  fulfill the following relationships

*spherical  
symmetry*

$$Z_f(f, T) = \alpha \int_0^\infty Z_r(r, T) \frac{\beta r}{f} \sinh \frac{fr}{k_B T} dr, \quad (4.91)$$

and

$$Z_r(r, T) = \alpha \int_0^\infty Z_f(i\eta, T) \frac{\eta}{\beta r} \sin \frac{\eta r}{k_B T} d\eta, \quad (4.92)$$

where  $\alpha = \left(\frac{2}{\pi k_B T}\right)^{1/2}$  and  $\beta = \frac{(2\pi m k_B T)^3}{m^{3/2}}$ . We observe that Eqs.(4.91) and (4.92) are the counterparts of Eqs.(4.75) and (4.83) for a model with spherical symmetry.

#### 4.5 OUTLINE OF THE RESULTS

Here we introduced general extensions of the two most known models of a single polymer, the FJC and WLC. While both models describe the polymer with the assumptions of inextensibility (fixed bond length), we introduced the typical corrections aimed at describing bond elasticity through additional spring-like terms [105, 106, 107, 109, 110, 111]. Considering a polymer chain with a finite number  $N$  of monomers and with an arbitrary potential  $V$  on monomers, we described two different ensembles: the Helmholtz and the Gibbs ensembles. Some examples in literature testify the interest on investigate the differences on the elasticity of a polymer chains subjected to different ensembles, showing a different behavior when out of the thermodynamic limits. Simple models describing internal barriers to bond rotation [114], single ideal Gaussian chain [115] and DNA stretching [116] as been considered. Often, the elasticity of the polymers is investigated by means of computer simulations [117, 118, 119, 120, 121], or is described

by some theoretical interpolation formulas [21, 22, 23], but there are a restricted case of results presenting closed analytical forms [43, 122, 123]. Considering a polymer subjected to both ensembles, we determine the proper partition functions and we derive an exact relationship between them. Moreover, we found also a closed form that allows to analytically switch from one ensemble to another, by means of a simple bilateral Laplace transform of the partition functions. Such a theoretical framework, allows a suitable investigation of the convergence to the thermodynamic limit for small systems (see Chapter 6) and the interpretation of some experimental results (see Chapters 7 and 8), taking advantage from the exactly theoretical formulas developed.

## METROPOLIS MONTE CARLO METHOD

---

In Chapter 4, we reported our theoretical approach that is grounded on the statistical mechanics formalism. This means that we must handle with ensemble averages. Our aim is now to motivate the reasons we need to use a computational method, in particular, a Monte Carlo (MC) method.

### 5.1 ENSEMBLE AVERAGE CALCULATIONS

We remember that, considering a general function  $f(\mathbf{q}, \mathbf{p})$ , we can get the average of it by the calculation of the integral

$$\langle f(\mathbf{q}, \mathbf{p}) \rangle = \int f(\mathbf{q}, \mathbf{p}) \rho(\mathbf{q}, \mathbf{p}) d\mathbf{q} d\mathbf{p}, \quad (5.1)$$

where the quantity  $\rho(\mathbf{q}, \mathbf{p})$  is a normalized probability density function that depends on two generic variables  $\mathbf{p}$  and  $\mathbf{q}$ .

We need a method that allows us to solve integrals like Eq.(5.1). If  $f(\mathbf{q}, \mathbf{p})$  is a function whose average is of thermodynamic importance, such a method will allow us to find its average. Actually, it is important to remember that Monte Carlo methods are used as well in several fields of science to solve many different problems such as numerical integration and generation of samples from a probability distribution, as briefly discussed in Section 5.2.

To be specific, let us remember the probability density function previously considered for a polymer chain

$$\rho(\mathbf{q}, \mathbf{p}) = \frac{1}{Z} e^{-\frac{H(\mathbf{q}, \mathbf{p})}{k_B T}}, \quad (5.2)$$

and the partition function associated

$$Z = \int_{\Gamma} e^{-\frac{H(\mathbf{q}, \mathbf{p})}{k_B T}} d\mathbf{q} d\mathbf{p}, \quad (5.3)$$

where  $H$  is the Hamiltonian of the system, which expresses the total energy of the system as a function of positions  $\mathbf{q}$  and momenta  $\mathbf{p}$  of the monomers composing the chain. We know that,

being the Hamiltonian  $H = K + V$ , ( $K$  is the kinetic energy and  $V$  the potential energy), it is possible to separate the kinetic part of the partition function from the potential one [124], thus allowing us to perform the calculation of the average function separately for momenta and positions (this is possible only if we use orthogonal coordinates). As  $K$  is a quadratic function of the momenta, the integration over the moments can be carried out analytically, hence is not difficult to calculate in close form the average function  $\langle f(\mathbf{p}) \rangle$ . On the contrary, the complication is related to the calculation of the average function depending on the positions  $\langle f(\mathbf{q}) \rangle$ . Only in few circumstances it is possible to calculate analytically the multidimensional integral over the particles; in all other cases numerical techniques are mandatory [125, 126].

*numerical  
techniques are  
mandatory*

## 5.2 SIMULATION METHOD

Having clarified that we must deal with a numerical problem, we now have to specify the reasons that lead us to use a Monte Carlo method.

*what  
numerical  
method?*

There are many ways to perform ensemble average calculations, as for instance using Simpson's rule or other basic quadrature methods [127, 128]. In any manner, such a methods would request computation of huge magnitude, making them almost useless. Moreover, even if possible, the result that would be obtained would have been subjected to a large statistical error [125].

*Monte  
Carlo  
methods*

One of the most adopted and convenient way to numerically compute integrals is by means of Monte Carlo methods. As numerical methods work, also Monte Carlo is efficient only for some problems (sometimes intractable in other ways) in which all other numerical methods are less efficient. This happens for examples for problems of numerical integration in  $d$  dimensions. Comparing Monte Carlo integration with the Simpson's rule, the error in Simpson's rule with  $n$  nodal points behaves asymptotically as  $d/n^4$  for smooth integrands. In low dimension ( $d < 8$ ) this is much better than Monte Carlo integration, but in high dimension ( $d > 8$ ) it is much worse [129]. This is the reason because Monte Carlo is used for performing high-dimensional integrals and a general domain of its application are systems with many degrees of freedom (far from the perturbative regime). Such systems are part of

the ones of greatest interest in statistical mechanics, and some of them are largely investigated by means of molecular simulations [127, 129, 130].

As a matter of fact, there are two most widely used methods of molecular simulation: one is Monte Carlo and the other is *molecular dynamics* (MD). The two procedures have typically the same system setup, ranging from the representation of molecules regarded as collections of atom-centered interaction sites, to the potential energy terms, and the implementation of periodic boundary conditions. The principal differences are in the modes of sampling the configuration space available to the system [125, 126]. These differences, and the fact that in this work we are investigating the statistical mechanics of equilibrium, lead us to consider a Monte Carlo method instead of molecular dynamics. In fact Monte Carlo methods are well suited to investigations of equilibrium situations [131]; this is due to two important characteristics of Monte Carlo approaches. On the one hand, the temperature is controllable [125, 126], and this allows investigation of phase transitions such as melting, in a simple way. Oppositely, in molecular dynamics there is no simple way of assigning a temperature to the system in advance. Instead, the temperature is calculated from the kinetic energy of the particles. On the other hand, unlike molecular dynamics simulations, Monte Carlo simulations are free from the restrictions of solving Newton's equations of motion. This freedom allows for cleverness in the proposal of moves that generate trial configurations within the statistical mechanics ensemble of choice. In addition, Monte Carlo methods are generally easily parallelizable with some techniques being ideal for use with large CPU clusters. Sometimes no effort is required to separate the problem into a number of parallel tasks and the problem is said to be an *embarrassingly parallel* problem [132].

The incontestable importance of the Monte Carlo and molecular dynamics methods is however in contrast with the investigations of their efficiencies comparison, which is nowadays still lacking. Conformational equilibrations of a box of liquid hexane molecules showed Monte Carlo runs to be 1.6 – 3.8 times faster than those of molecular dynamics [133]. Another investigation on folding simulations of small polypeptides showed that, while both Monte Carlo and molecular dynamics methods successfully gave the same expected results, they do so at different speed: Monte Carlo was

*Monte Carlo  
or  
Molecular  
Dynamics?*

found to be 2 – 2.5 times faster than molecular dynamics [134]. Of course, this efficiency is highly dependent on the level of performance of the individual Monte Carlo and molecular dynamics programs [135].

*Monte Carlo methods are appropriate*

For all the previous reasons Monte Carlo methods are the most convenient way to investigate systems with many degrees of freedom in thermal equilibrium. Although, we must remark that Monte Carlo techniques are used in several fields of science and they can be referred to many different things. As stated in the excellent review by Robert Q. Topper et al., the one and only thing that all Monte Carlo methods have in common is that they all use random numbers to help calculate something [136]. It is hence necessary to specify what we mean by referring to Monte Carlo methods. We refer here, to the utilization of random-walk processes for the purpose of drawing samples from a desired probability function. Such a rationale is called the Metropolis Monte Carlo (MMC) algorithm, and it was originally developed by Metropolis et al. in 1953 as the Monte Carlo importance sampling-algorithm [137].

*Metropolis Monte Carlo*

### 5.2.1 *The Metropolis Monte Carlo algorithm*

*why Metropolis algorithm?*

The importance of this algorithm lies on the way in which it draws samples: rather than simply picking them at random, it generates configurations distributed according to a specified probability distribution function, which is usually the actual probability function of the physical system of interest. More precisely, the simple Monte Carlo algorithm generates random configurations according to a uniform distribution, assigning them a weight equal to the Boltzmann factor. In practice, this simple approach is not feasible because uniform random sampling yields many configurations which have a very small Boltzmann factor: such configurations make a very little contribution to the ensemble average. Actually, a very large number of configurations would provide the correct calculation, but this is prohibitively in many practical problems. The limitations of uniform random sampling is then avoided with the Metropolis sampling that generates random configurations according with the Boltzmann distribution and counts each of them equally. Hence, the Metropolis solution generates configurations that make a large contribution to the ensemble average;

this means that the sampling biases the generation of configurations towards those that make the most significant contribution to the ensemble average.

The Metropolis Monte Carlo algorithm is a particular type of an important sampling procedure, and it differs from the various existent algorithms for the sampling scheme; other sampling techniques are used as well [96, 138]. In any manner, for statistical mechanics, the Metropolis method (grounded on the corresponding algorithm) is certainly the most used one [136].

The MMC algorithm generates successive configurations of the considered system creating a particular random walk: a Markov chain [139, 140]. This walk is made in order to asymptotically (i.e., in the limit that the number of configurations becomes large) generate a distribution of configurations corresponding to the requested probability distribution function.

Defining the transition probability as  $K(q_o \rightarrow q_n)$  to go from the old configuration  $q_o$  to the new one  $q_n$ , the probability of moving to the new configuration is

$$P(q_o \rightarrow q_n) = K(q_o \rightarrow q_n)\rho(q_o). \quad (5.4)$$

This means that, in equilibrium, the average number of accepted moves to any other state is exactly as it is for moving in the reverse direction [125, 126, 136]. It is convenient to impose that in equilibrium the average number of accepted moves from  $q_o$  to any  $q_n$  is balanced by the number of reverse moves. This is a much stronger condition known as the *detailed balance condition*:

$$K(q_o \rightarrow q_n)\rho(q_o) = K(q_n \rightarrow q_o)\rho(q_n). \quad (5.5)$$

*detailed  
balance  
condition*

Many possible forms of the transition matrix satisfy this equation [125, 136]. Considering Eq.(5.5) and summing over all states  $q_n$ , we get

$$\sum_n K(q_n \rightarrow q_o)\rho(q_n) = \sum_n K(q_o \rightarrow q_n)\rho(q_o) = \rho(q_o) \sum_n K(q_o \rightarrow q_n), \quad (5.6)$$

and recalling that, being  $K$  a stochastic matrix, its rows add to one

$$\sum_n K(q_o \rightarrow q_n) = 1, \quad (5.7)$$

we get

$$\sum_n K(q_n \rightarrow q_o) \rho(q_n) = \rho(q_o). \quad (5.8)$$

This means that  $\rho(q_o)$  is an eigenvector of the stochastic matrix with eigenvalue unity, and because of the properties of  $K$ , the other eigenvalues are  $\leq 1$  [125, 136]. Now, imaging to start the Markov process by any given distribution  $\rho^{(1)}$ , (for the standard MMC, starting from a configuration the initial distribution is a Dirac delta function), it is possible to express it as a convex linear combination of the eigenvector of the stochastic matrix. Applying this stochastic matrix to the initial distribution an infinite number of times, namely:

$$\rho = \lim_{\tau \rightarrow \infty} \rho^{(1)} K^\tau, \quad (5.9)$$

the limiting distribution must satisfy the eigenvalue equation Eq.(5.8), with eigenvalues equal to 1. This proves that Metropolis Monte Carlo is independent of the initial distribution.

If we denote the probability of accepting a trial move from  $q_o$  to  $q_n$  as the acceptance probability  $\text{acc}(q_o \rightarrow q_n)$ , we have

$$K(q_o \rightarrow q_n) = \alpha(q_o \rightarrow q_n) \text{acc}(q_o \rightarrow q_n), \quad (5.10)$$

where  $\alpha$  is the transition matrix that determines the probability of performing a trial move from  $q_o$  to  $q_n$ . The possibility of choosing  $\alpha$  with great flexibility, is one of the power of Monte Carlo methods [136].

From Eqs.(5.5) and (5.10), we obtain the ratio of acceptance probabilities

$$\frac{\text{acc}(q_o \rightarrow q_n)}{\text{acc}(q_n \rightarrow q_o)} = \frac{\rho(q_n) \alpha(q_n \rightarrow q_o)}{\rho(q_o) \alpha(q_o \rightarrow q_n)}, \quad (5.11)$$

which is major or equal to zero. If  $\alpha$  is chosen to be a symmetric matrix,  $\alpha(q_o \rightarrow q_n) = \alpha(q_n \rightarrow q_o)$  (as in the original Metropolis scheme [137]), and considering Eq.(5.11), it follows that

$$\frac{\text{acc}(q_o \rightarrow q_n)}{\text{acc}(q_n \rightarrow q_o)} = \frac{\rho(q_n)}{\rho(q_o)} = \exp\{-\beta[V(q_n) - V(q_o)]\}, \quad (5.12)$$

where  $\beta = 1/k_B T$ . According with Eq.(5.12), with the obvious condition that  $\text{acc}(q_o \rightarrow q_n) < 1$ , a trial move should be accepted with a probability

$$\text{acc}(q_o \rightarrow q_n) = \min\{1, \exp\{-\beta[V(q_n) - V(q_o)]\}\}. \quad (5.13)$$

To conclude, we have to explain how we can decide whether a trial move is to be accepted or rejected. In order to do that, it is needed the generation of a random number  $rand$  from a uniform distribution in the interval  $[\xi \in (0, 1)]$ .

*random  
numbers  
generation*

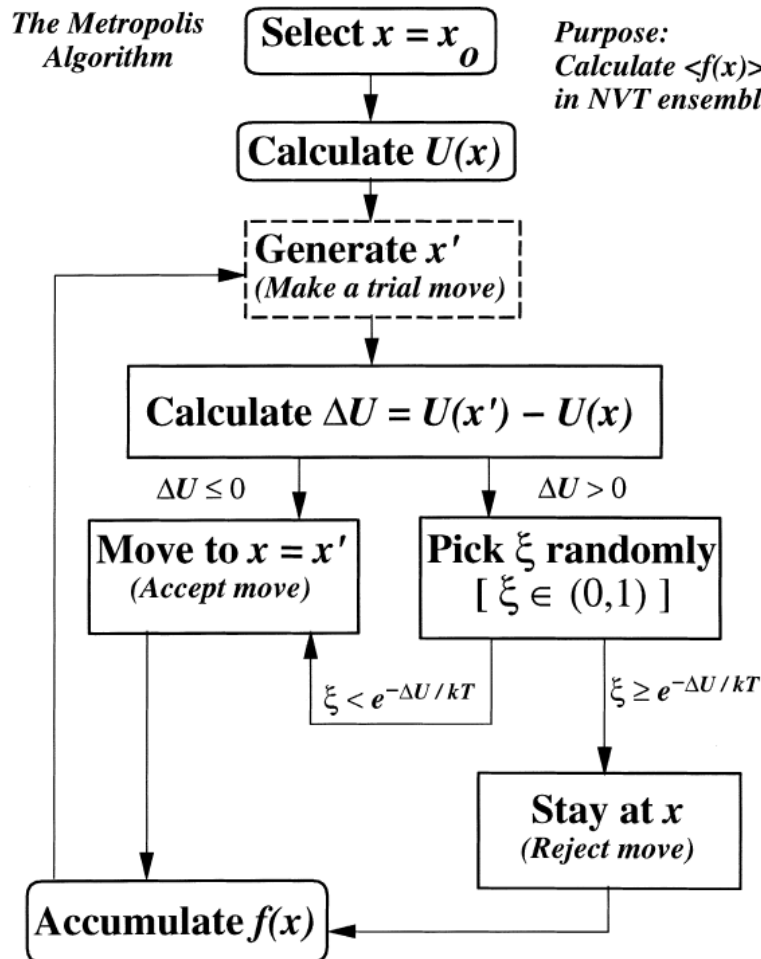


Figure 5.1: Flowchart of the MMC algorithm for sampling in the canonical ensemble. Once an initial configuration has been generated, a trial move is made to generate a new trial configuration according to a move strategy rule.  $U \equiv V$  indicates the potential energy. Taken from: [136]

We will accept the trial move if  $\xi < \text{acc}(q_0 \rightarrow q_n)$ , and we will reject it oppositely. Finally, as remarked by Topper et al., for MMC calculations it is often convenient to work in Cartesian coordinates

*accept  
a trial  
move*

[136]. For this reason, they presented a flowchart of the Metropolis Monte Carlo algorithm in Cartesian coordinates (see Fig. 5.1).

*initial  
state of  
the system*

The initial state of the system (a polymer chain in our case) is defined by a set of randomly chosen positions for the particles (monomers). Then we have to choose a single particle of the system. The fact we choose a single particle is in accordance with the original MMC procedure (single-particle moves) [137]. However, depending on the system, single-particle moves alone are inefficient [136]. The choice of the particle to be moved can be randomly done or in sequence, at the discretion of the programmer. Once we have selected a particle  $\mathbf{x} = \mathbf{x}_o$ , we calculate the total energy  $V(\mathbf{x}_o)$ . Then we give the particle a random displacement, namely the new position will be

*choose a  
particle*

$$\mathbf{x}_n = \mathbf{x}_o + \delta\mathbf{x}, \quad (5.14)$$

*energy  
calculation*

which is a *trial move*. We then calculate the associated energy  $V(\mathbf{x}_n)$ . In the canonical ensemble, if  $\Delta V = V(\mathbf{x}_n) - V(\mathbf{x}_o) \leq 0$ , the trial configuration will be accepted. The probability of move acceptance is

$$\text{acc}(\mathbf{x}_o \rightarrow \mathbf{x}_n) = \min\{1, \exp\{-\beta[V(\mathbf{x}_n) - V(\mathbf{x}_o)]\}\}. \quad (5.15)$$

On the contrary, if  $\Delta V > 0$ , the trial move will not directly be refused, but it may still be conditionally accepted by comparing  $\exp(-\beta\Delta V)$  with a random number  $[\xi \in (0, 1)]$  (Boltzmann test). If  $\xi \leq \exp(-\beta\Delta V)$  the trial move will be accepted, otherwise rejected. This procedure is repeated until equilibration [126, 141, 142]. Once equilibration is reached, any properties of interest must be accumulated. In both cases, accepted or rejected move, the configuration must be included in the average, otherwise the potential energies will not be distributed according to the Boltzmann probability density function [125, 126, 136].

### 5.2.2 Make a trial move

As we can see, a *trial move* generates a new trial configuration starting from a selected particle, according to a precise rule called *move strategy* [136]. There are different ways to perform a trial move, but the simple move strategy, originally proposed by Metropolis et al. [137], is still the most used method. It consists

to preselect a maximum stepsize  $X$ , and to randomly moves each particle (monomer) within a cube of length  $|X|$ , centered on the particle original position.

The displacement extent,  $\delta x = \xi X$ , (where  $\xi$  is a random number  $\in (0, 1)$ ) of the position vectors, governs the magnitude of the trial move and the overall efficiency of the configurational space sampling. However, adopting a too small  $\delta x$  most of the trial moves are accepted but the configurational space is explored too slowly, while a too large  $\delta x$  leads to a high rejection frequency, resulting in little movements through the configurational space. Therefore, one must analyzed several runs in order to optimize its value [125, 126]. For this reason one generally chooses  $\delta x$  so that it ensures an acceptance of the moves (*acceptance ratio*) between 30% and 70%. A common and reasonable choice is to maintain the *acceptance ratio* near 50% [125, 126].

*displacement  
extent*

*acceptance  
ratio*

There are other different ways to impose the  $\delta x$  parameter. One of this is the so called *dynamical adjustment*. In this case,  $\delta x$  is adjusted during the simulation so that about half of trial moves are rejected. This adjustment is normally handled automatically [126]. However, one should be very cautious using this. In fact, the *dynamical adjustment* can lead to serious problems, such as the violation of the detailed balance, as excellently discussed by M. A. Milleret et al. in Ref. [143].

### 5.3 PSEUDO RANDOM-NUMBER GENERATION

Because the Metropolis Monte Carlo method is based on random sampling, one should be careful about the choice of the random generator algorithm. As a matter of fact, some applications require orders of  $10^{15}$  (or more) random numbers [144]; this means they need a high-quality random-number generator in order to obtain reliable results. Firstly, it is important to clarify what we mean when referring to random-number generators: actually they do not produce random numbers. Instead, they utilize a deterministic technique that initializes a pseudo-random sequence of numbers starting from an integer called *seed*. Hence, given the same initial seed, a function for generating random number will produce exactly the same sequence of numbers. These sequences

look like real random numbers only in the case of high-quality generators [136].

Another important consideration for any random-number generator is its period: as the complexity of Monte Carlo studies increase, the period size of the generated sequences must be accurately evaluated. Indeed, even if a long period is not a guarantee of quality in random number generating, short periods can be problematic and they should be avoided. The minimal standard generator of Park and Miller [145] has a period of  $2^{31} - 1$ . Nowadays, this period is not sufficient for the majority of Monte Carlo studies [146]. The problem of random number generators with a small period, lies in the inability to visit all points in the sample space.

*linear  
congruential  
algorithm*

One of the oldest standard algorithm for generating pseudo-random numbers is the *linear congruential generator* (LCG) that is based on the standard *linear congruential algorithm*, developed by D. H. Lehmer [147]. In the LCG, each single number determines its successor with a simple linear function followed by a modular reduction [144]. LCG is very fast and requires minimal memory, but at the same time should not be used for applications where high-quality randomness is critical [144, 148]. For example, it is not suitable for Monte Carlo simulations because of the serial correlation between successive values of the sequence [136].

*Mersenne  
Twister  
algorithm*

When higher quality random numbers are needed, there are better options. For instance, the *Mersenne Twister algorithm*, is a typical choice that, moreover, has been optimized for use with Monte Carlo simulations in a large number of different fields including biochemical problems, cellular biology and computational finance [149, 150, 151]. Its name derives from the fact that the period length is chosen to be a Mersenne prime. This algorithm provides a vastly longer period than the linear congruential one and a variate uniformity [152], as well as it furnishes a very long period:  $2^{19937} - 1$  (many orders of magnitude larger than the estimated number of particles in the observable universe) [152]. Further, the algorithm allows the generation of 623-dimensionally equidistributed uniform points, and it passes numerous tests for statistical randomness, including the Diehard tests [152]. For our investigations, we adopted a pseudo-random generator based on Mersenne Twister algorithm.

## 5.4 A SAMPLING PROBLEM: THE QUASI-ERGODICITY

Even if the Metropolis Monte Carlo method is very powerful and it allows to solve many complex phenomena, there are critical circumstances where the scheme must be modified. In some cases this modification will improve the sampling efficiency; in other more critical cases, a modification is needed to avoid incorrect results. The treatment of all the possible problems one can have when dealing with Monte Carlo methods is out of the scope of the present discussion. At the same time, one of these is of our interest as we have to handle with: the quasi-ergodicity problem [136, 153, 154].

*quasi-ergodicity  
problem*

We remark that, in statistical mechanics, the ergodic hypothesis is fundamental [57, 96, 153, 155] (see Section 3.4.3). Consequently in Monte Carlo computations of thermodynamic properties, it is mandatory that the sampling is ergodic [154, 155]. Thus far, we already stated that a random walk should be ergodic. In this context, when speaking of *ergodic random walk*, we refer to a random walk that can eventually reach every possible state starting from every possible initial state. The quasi-ergodicity or meta-stability problem, is typical for systems having two or more wells (or meta stable states) in the potential energy surface separated by high barriers (see Fig. 5.2).

*ergodic  
random  
walk*

In this case the system must overcome high-energy barriers to reach other regions of phase space, and the sampling is confined in some wells. This problem appears even in the simplest double well problem, when the two wells are separated by a large barrier [156]. This kind of unsuitable sampling is indicated as *quasi-ergodic sampling* [157, 158]. Moreover, when a system is quasi-ergodic, it often appears to be ergodic, hence making the problem particularly difficult to be detected. This complication is not unique to Monte Carlo simulations since it appears as well in molecular dynamics methods [159]. In general, we might not know the potential energy surface of our system, nor the locations of its minima or its depths, as well as for those of the barriers. Looking at Fig. 5.2, there are some possible cases easy to imagine happening in a simulation where the system has the depicted potential surface. If we imagine the initiated configuration of our system in the highest energy well, it is simple to figure out that, at low temperatures a finite Monte Carlo walk may never leave this well. Unfortunately,

*multiple  
well  
potentials*

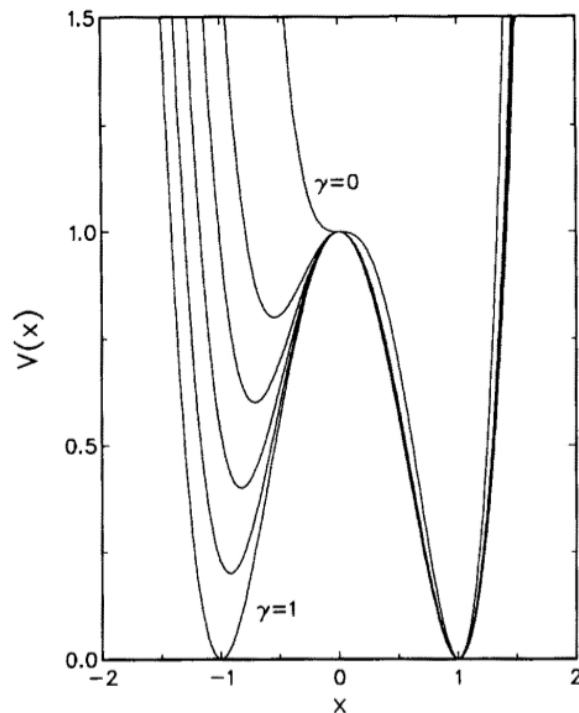


Figure 5.2: Asymmetric one-dimensional double-well potential  $V(x)$ ;  $\gamma$  is the depth of the variable well. Taken from: [156]

thermodynamic properties of such a walk would appear reasonable, even if, the computed thermodynamic properties would reflect the contribution only of the well the simulation started from, hence producing incorrect results. On the contrary, for higher temperatures, a finite Monte Carlo walk may visit both wells, hopping between them at a certain frequency. However, this frequency, might be not properly weighted, thereby still producing incorrect results. In the case where the system must overcome high-energy barriers, the problem would be hypothetically fixed by augmenting the length of a simulation in order to obtain enough statistical samples of all the phase space regions. Nevertheless, in practical applications, this may be extremely long when not totally impractical. An approach that works for simple problem (as the one dimensional we are here considering), is to extend the original Metropolis scheme. One of the simplest adjust consists, for example, in considering more than one maximum displacement [136]. While in the original scheme one considers just a single maximum displacement, we can introduce for this case a second stepsize. As long as, the first would be used for most moves, with a size chosen in or-

*how to  
fix the  
problem?*

der to have an acceptance-ratio equal of 50%, the second one must be chosen to have a length equal to the distance that separates the two minima. In this case, we will use this magnified stepsize just for a portion of the moves. With this expedition, the barrier between the wells would be overcome even at low temperatures. This criterion is called *mag-walking* and it satisfies the detailed balance [156]. This would be, for us, sufficient to handle with a Monte Carlo simulation in which we have a mono-dimensional energy surface with two asymmetric wells as the one in Fig. 5.2. However, in general, mag-walking is sufficient only in simple cases, but is impractical for other important applications. In fact, in general, considering potential with a high number of wells, one should introduce the same number of stepsizes and knows all of them in term of its minima and depths. More sophisticated methods have been proposed to overcome quasi-ergodicity problem from Monte Carlo methods, as umbrella sampling method [153, 160], which is used to reconstruct the Landau free energy when it is known (or hypothesised) a suitable collective variable (direction of metastability). Others solutions are the generalized simulated annealing method to locate the global minimum [161, 162]. Tempering method is used to find the absolute minimum over the configuration space, J-walking and parallel tempering (or replica exchange method) address sampling problems by using information about the underlying potential surface obtained from a high-temperature [163, 164], and histogram methods [165].



Part IV

POLYMER CHAINS LOADED BY  
EXTERNAL FORCES



## ELASTICITY OF POLYMERS IN THE GIBBS AND HELMHOLTZ ENSEMBLES

---

### Contents

---

6.1	General theoretical framework	99
6.1.1	Polymer with fixed end-to-end distance	99
6.1.2	Polymer under constant load	100
6.2	On the thermodynamic limit	100
6.3	Equivalence of statistical ensembles	103
6.4	Flexible polymer with elastic bonds	107
6.5	Semiflexible polymer with elastic bonds	114
6.6	Outline of the results	119

---

As previously discussed, the analytical developments of the FJC and WLC models work under some assumptions. From one hand, we argued that the polymer is modeled as a chain of beads connected by rigid bonds. On the other hand, the FJC and WLC models work under the assumption of the finite, but large enough, contour length. In other words, the contour length  $L_c$  (see Section 1.2.1) is supposed very large. The first assumption should not be adopted if we consider a large applied force as explained in Chapter 4. The second assumption is related to the concept of thermodynamic limit. In fact, the standard rules of equilibrium thermodynamics may not apply to experiments on individual, short-length polymer molecules. In such a case the results may depend on the boundary conditions imposed for stretching the polymer, namely: a fixed end-to-end distance, pertinent to the Helmholtz ensemble of statistical mechanics, or a fixed force applied at one or both ends, rather representing a realization of the Gibbs ensemble. The differences between the two conditions should vanish in the thermodynamic limit ( $N \rightarrow \infty$ ), when the polymer contour length  $L_c$  is much larger than its persistence length  $L_p$  (or to the individual bond length, for completely flexible chains). This phenomenon has been studied and observed for simple models describing internal

barriers to bond rotation [114], for the single ideal Gaussian chain [115] and for DNA stretching [116].

It is important to observe that from the experimental point of view both assumptions, inextensibility and attainment of thermodynamic limit, are often not fulfilled for many practical reasons (e.g. too large applied forces and force-rates, different configurations of the experimental devices, actual procedures for force and distance measurements, and so on). Therefore, in this Chapter we study the effects of the superposition of the two aspects, by considering the mechanical stretching response of extensible polymer chains of arbitrary length. Of course, the above two assumptions are completely independent and, therefore, one can consider all their possible combinations: short chains without extensibility (leading to the FJC or WLC for short chains), extensible long chains at the thermodynamic limit, or short chains with extensibility.

In particular, we take into consideration the quantitative difference between the thermodynamic behaviour within either the Helmholtz or Gibbs ensemble, by investigating the foundations of the statistical mechanics for small systems. This will be done by taking into account flexible (or semiflexible) and extensible polymer chain models of biological interest. It will be showed that in the cases in which the thermodynamic limit is not satisfied, different macroscopic boundary conditions, corresponding to different statistical mechanics ensembles, yield different force-displacement curves. We adopt both analytical and Metropolis Monte Carlo simulations: while the analytical approach is useful to obtain the explicit partition function in some specific cases, MMC simulations are crucial to determine the scaling laws controlling the convergence to the thermodynamic limit.

To this aim, we recall the thermodynamics of a polymer chain with an arbitrary bond potential in the two different approaches, respectively the Helmholtz and the Gibbs ensembles (see Chapter 4). Then, we recall as well the exact relationship between the partition functions pertinent to the different ensembles. From the latter relationship, we then formally prove the existence of the thermodynamic limit for long chains. Furthermore, we evaluate the difference between the two ensembles for FJC and WLC models with extensible bonds. To this aim we develop Metropolis Monte Carlo simulations performing the typical experiment in which the elas-

ticity of single polymer is probed with an AFM tip and we quantitatively evaluate the stretching response differences between the Helmholtz and Gibbs ensembles. In all cases we show that the convergence to the thermodynamic limit upon increasing contour length is described by a suitable power law and a specific scaling exponent, characteristic of each model.

## 6.1 GENERAL THEORETICAL FRAMEWORK

Let us recall the chain of monomers discussed in Section 4.1. We remember that, assuming that one terminal monomer is fixed at position  $\mathbf{r}_0 \equiv (0, 0, 0)$  and that monomers interact through an arbitrary potential, the dynamics of the system is described by the Hamiltonian in Eq.(4.1), namely

$$h_0(\mathbf{r}_1, \dots, \mathbf{r}_N, \mathbf{p}_1, \dots, \mathbf{p}_N) = \sum_{i=1}^N \frac{\mathbf{p}_i \cdot \mathbf{p}_i}{2m} + V(\mathbf{r}_1, \dots, \mathbf{r}_N). \quad (6.1)$$

where  $\mathbf{r}_i$  ( $i = 1, \dots, N$ ) are the set of positions and  $\mathbf{p}_i$  ( $i = 1, \dots, N$ ) are the momenta. Considering the system in thermal equilibrium with a reservoir at temperature  $T$ , its statistical properties are described by the canonical ensemble distribution in Eq.(4.2), namely

$$\rho(\mathbf{q}, \mathbf{p}) = \frac{1}{Z} e^{-\frac{h_0(\mathbf{q}, \mathbf{p})}{k_B T}}. \quad (6.2)$$

### 6.1.1 Polymer with fixed end-to-end distance

By fixing positions  $\mathbf{r}_0$  and  $\mathbf{r}_N$ , we can use the reduced Hamiltonian in Eq.(4.3), in terms of which the system partition function is written as

$$Z_r(\mathbf{r}, T) = \int_{\Gamma_{N-1}} e^{-\frac{h(\mathbf{q}, \mathbf{p}, \mathbf{r})}{k_B T}} d\mathbf{q} d\mathbf{p} \quad \text{with } \Gamma_{N-1} = \mathfrak{R}^{6(N-1)}, \quad (6.3)$$

where the microscopic variables are defined as  $\mathbf{q} = (\mathbf{r}_1, \dots, \mathbf{r}_{N-1})$  and  $\mathbf{p} = (\mathbf{p}_1, \dots, \mathbf{p}_{N-1})$ . The net force exerted on the monomer at position can be used to define the mechanical constitutive equation of the chain, providing Eq.(4.8), which is

$$\mathbf{f}(\mathbf{r}, T) = -k_B T \frac{\partial}{\partial \mathbf{r}} \log Z_r = \frac{\partial F(\mathbf{r}, T)}{\partial \mathbf{r}}, \quad (6.4)$$

*Helmholtz  
or isometric  
ensemble*

where  $F(\mathbf{r}, T) = -k_B T \log Z_r$  is the Helmholtz free energy.

### 6.1.2 Polymer under constant load

On the other hand, assuming that a given force  $\mathbf{f}$  is applied to the terminal monomer at  $\mathbf{r}_N$ , while the end-to-end distance is free to fluctuate, we have that the system is described by the augmented Hamiltonian in Eq.(4.40), in terms of which the system partition function is written as

$$Z_f(\mathbf{f}, T) = \int_{\Gamma_N} e^{-\frac{\tilde{h}(\mathbf{q}, \mathbf{p}, \mathbf{f})}{k_B T}} d\mathbf{q} d\mathbf{p} \quad \text{with } \Gamma_N = \mathfrak{R}^{6N}, \quad (6.5)$$

where  $\mathbf{q} = (\mathbf{r}_1, \dots, \mathbf{r}_N)$  and  $\mathbf{p} = (\mathbf{p}_1, \dots, \mathbf{p}_N)$  are the microscopic variables and  $\mathbf{f}$  acts as a macroscopic variable. Calculating the mean position of the last monomer of the chain through the average value  $\mathbf{r} = \langle \mathbf{r}_N \rangle$  we get Eq.(4.46), which is the constitutive equation in terms of the partition function  $Z_f$ , namely

$$\mathbf{r}(\mathbf{f}, T) = k_B T \frac{\partial}{\partial \mathbf{f}} \log Z_f = -\frac{\partial G(\mathbf{f}, T)}{\partial \mathbf{f}}, \quad (6.6)$$

where  $G(\mathbf{f}, T) = -k_B T \log Z_f$  is the Gibbs free energy.

## 6.2 ON THE THERMODYNAMIC LIMIT

At this point, our previous discussion on the two ensembles, ended with the perspective that it is possible to prove that both the Helmholtz and Gibbs ensembles provide the same constitutive equation for large systems ( $N \rightarrow \infty$ ). We want to prove it in the following.

The two expressions given in Eqs.(6.4) and (6.6), namely

$$\mathbf{f} = \frac{\partial F}{\partial \mathbf{r}}(\mathbf{r}, T), \quad \mathbf{r} = -\frac{\partial G}{\partial \mathbf{f}}(\mathbf{f}, T), \quad (6.7)$$

would represent, in fact, the same constitutive equation if the first relation coincides with the inverse function of the second one and vice-versa. In other words, our statement above is proved as long as it is shown that the Helmholtz and the Gibbs energy functions are related by a Legendre transformation

$$G = F - \mathbf{f} \cdot \mathbf{r} \quad (6.8)$$

*Gibbs or  
isotensional  
ensemble*

*Legendre  
transformation*

as discussed elsewhere [57].

This happens if  $F$  and  $G$  are the Legendre transform of the other function. In other words

$$\mathbf{f} = \frac{\partial F}{\partial \mathbf{f}} \quad \text{is equivalent to} \quad \mathbf{r} = -\frac{\partial G}{\partial \mathbf{f}}, \quad (6.9)$$

if and only if Eq.(6.8) is verified.

In fact, defining  $\mathbf{r} = \Phi(\mathbf{f})$  and  $\mathbf{f} = \Phi^{-1}(\mathbf{r})$ , we obtain

$$\begin{aligned} \frac{\partial G}{\partial \mathbf{f}} &= \frac{\partial F(\Phi(\mathbf{f}), T)}{\partial \mathbf{f}} - \frac{\partial}{\partial \mathbf{f}}(\mathbf{f} \cdot \Phi(\mathbf{f})) \\ &= \frac{\partial F}{\partial \mathbf{r}} \cdot \frac{\partial \Phi}{\partial \mathbf{f}} - \Phi(\mathbf{f}) - \mathbf{f} \cdot \frac{\partial \Phi}{\partial \mathbf{f}} \\ &= \mathbf{f} \cdot \frac{\partial \Phi}{\partial \mathbf{f}} - \mathbf{f} \cdot \frac{\partial \Phi}{\partial \mathbf{f}} - \mathbf{r} = -\mathbf{r}. \end{aligned} \quad (6.10)$$

On the other hand, we can write

$$\begin{aligned} \frac{\partial F}{\partial \mathbf{r}} &= \frac{\partial G(\Phi^{-1}(\mathbf{r}), T)}{\partial \mathbf{r}} + \frac{\partial}{\partial \mathbf{r}}(\mathbf{r} \cdot \Phi^{-1}(\mathbf{r})) \\ &= \frac{\partial G}{\partial \mathbf{f}} \cdot \frac{\partial \Phi^{-1}}{\partial \mathbf{r}} - \Phi^{-1}(\mathbf{r}) + \mathbf{r} \cdot \frac{\partial \Phi^{-1}(\mathbf{r})}{\partial \mathbf{r}} \\ &= -\mathbf{r} \cdot \frac{\partial \Phi^{-1}(\mathbf{r})}{\partial \mathbf{r}} + \mathbf{r} \cdot \frac{\partial \Phi^{-1}(\mathbf{r})}{\partial \mathbf{r}} + \mathbf{f} = \mathbf{f}. \end{aligned} \quad (6.11)$$

While Eq.(6.8) is the Legendre transform of  $F$ , the following

$$F = G + \mathbf{f} \cdot \mathbf{r} \quad (6.12)$$

is the Legendre transform of  $G$ .

We have to show that  $F$  and  $G$  are reciprocally Legendre transform under the thermodynamic limit.

To do this we observe the relations among the free energy and the partition function

$$\frac{1}{Z_r} = e^{\frac{F}{k_B T}} \quad \text{and} \quad \frac{1}{Z_f} = e^{\frac{G}{k_B T}}, \quad (6.13)$$

which are derived from Eq.(4.15) and (4.51). In the previous section we obtained a relation between  $Z_r$  and  $Z_f$  in the form

$$Z_f(\mathbf{f}, T) = (2\pi m k_B T)^{\frac{3}{2}} \int_{\mathfrak{R}^3} Z_r(\mathbf{r}, T) e^{\frac{\mathbf{f} \cdot \mathbf{r}}{k_B T}} d\mathbf{r}$$

*F and G relationship under thermodynamic limit*

and therefore, we may look for the relation between  $F$  and  $G$ . By inserting Eqs.(6.4) and (6.6) in Eq.(4.75) we obtain

$$e^{-\frac{G(\mathbf{f}, T)}{k_B T}} = (2\pi m k_B T)^{\frac{3}{2}} \int_{\mathfrak{R}^3} e^{-\frac{F(\mathbf{r}', T)}{k_B T}} e^{\frac{\mathbf{f} \cdot \mathbf{r}'}{k_B T}} d\mathbf{r}', \quad (6.14)$$

expansion  
of  $F(\mathbf{r}, T)$

which is an exact relation between  $F$  and  $G$ , always satisfied (i.e. valid for any  $N$ ). Now, expanding  $F(\mathbf{r}, T)$  up to the second order in  $\mathbf{r}$  we get

$$F|_{\mathbf{r}'} \simeq F|_{\mathbf{r}} + \frac{\partial F}{\partial \mathbf{r}}(\mathbf{r}' - \mathbf{r}) + \frac{1}{2}(\mathbf{r}' - \mathbf{r}) \cdot \frac{\partial^2 F}{\partial \mathbf{r}^2}(\mathbf{r}' - \mathbf{r}), \quad (6.15)$$

where we did not consider the third order term and higher since, for large  $N$ , their effects are negligible with respect to the leading terms (first and second order). This is a typical approximation adopted and justified within the Laplace method useful for obtaining the asymptotic behavior of integrals (e.g. used for proving the standard Stirling approximation for the factorial function, largely used in several statistical mechanics evaluations) [166]. With the expansion in Eq.(6.15), and substituting

$$\mathbf{f} = \frac{\partial F}{\partial \mathbf{r}}(\mathbf{r}, T) \quad \text{and the inverse} \quad \mathbf{r} = \mathbf{r}(\mathbf{f}) \quad (6.16)$$

we get

$$\begin{aligned} e^{-\frac{G(\mathbf{f}, T)}{k_B T}} &= (2\pi m k_B T)^{\frac{3}{2}} \\ &\times \int_{\mathfrak{R}^3} \exp \left[ -\frac{F(\cdot, T)}{k_B T} - \frac{\mathbf{f} \cdot \mathbf{r}'}{k_B T} + \frac{\mathbf{f} \cdot \mathbf{r}}{k_B T} \right] \\ &\times \exp \left[ -\frac{1}{2k_B T}(\mathbf{r}' - \mathbf{r}) \frac{\partial^2 F}{\partial \mathbf{r}^2}(\mathbf{r}' - \mathbf{r}) + \frac{\mathbf{f} \cdot \mathbf{r}'}{k_B T} \right] d\mathbf{r}', \end{aligned} \quad (6.17)$$

which we can better rewrite as

$$\begin{aligned} e^{-\frac{G(\mathbf{f}, T)}{k_B T}} &= e^{-\frac{F - \mathbf{f} \cdot \mathbf{r}}{k_B T}} \\ &\times (2\pi m k_B T)^{\frac{3}{2}} \int_{\mathfrak{R}^3} \exp \left[ -\frac{1}{2k_B T}(\mathbf{r}' - \mathbf{r}) \frac{\partial^2 F}{\partial \mathbf{r}^2}(\mathbf{r}' - \mathbf{r}) \right] d\mathbf{r}'. \end{aligned} \quad (6.18)$$

Indicating with  $\Gamma$  the multiplicative term on the right and side of Eq.(6.18), namely

$$\Gamma = (2\pi m k_B T)^{\frac{3}{2}} \int_{\mathfrak{R}^3} e^{-\frac{1}{2k_B T}(\mathbf{r}' - \mathbf{r}) \frac{\partial^2 F}{\partial \mathbf{r}^2}(\mathbf{r}' - \mathbf{r})} d\mathbf{r}', \quad (6.19)$$

and taking the logarithm, we can write

$$-\frac{G(\mathbf{f}, T)}{k_B T} = -\frac{\mathbf{F} - \mathbf{f} \cdot \mathbf{r}}{k_B T} + \log \Gamma,$$

and we finally obtain

$$G = \mathbf{F} \cdot \mathbf{r} - k_B T \log \Gamma. \quad (6.20)$$

The quantities  $G$ ,  $\mathbf{F}$ ,  $\Gamma$  and  $\mathbf{f} \cdot \mathbf{r}$  assume an extensive character (i.e. they are proportional to  $N$ ) and, therefore, the logarithmic term in Eq.(6.20) becomes negligible for large systems. Thus, for  $N \rightarrow \infty$ , the Legendre transformation is fulfilled.

In the following we will quantitatively address the convergence to the thermodynamic limit by comparing the Helmholtz and Gibbs ensembles for increasing values of  $N$ , and we will evaluate their differences for small systems (i.e. for short length polymer chains).

### 6.3 EQUIVALENCE OF STATISTICAL ENSEMBLES

We previously discussed that two different statistical ensembles can be considered for extending a single polymer chain. One is the Gibbs (or isotensional) ensemble characterized by a deterministic force applied to the free end of the chain (the other being fixed in a given reference frame), and the other is the Helmholtz (or isometric) ensemble obtained with both the ends of the polymers tethered at two different points of the space. Shortly, the Helmholtz and Gibbs ensemble for a single polymer chain under stretch yield different force extension relations when  $N$  is small. The reason lies on the fact that the degrees of freedom of the single molecule is small. This fact has been proven for different models elsewhere [43, 122, 123]. Moreover, the ensemble equivalence for flexible polymers has been addressed theoretically [43, 115, 116, 117, 167, 168, 169, 170] and by means of computer simulations [117, 118, 119, 120, 121]. However, there is not an overall consensus on this topic. There are some authors that find agreement between averages determined by different ensembles in the thermodynamic limit, [43, 116, 117, 122, 169] while others emphasize deviations [115, 119, 120, 121, 167] even in the thermodynamic limit.

ensemble  
inequivalence

Ensemble inequivalence is typically demonstrated by comparing force-extension relations [115, 117, 121]. From the one hand this seems a natural choice, since such relations the one measured in experiments, however, it is preferable to consider conjugated partition functions and the corresponding thermodynamic potentials as pointed out in Ref. [171, 172]. In Section 6.2 we rigorously proved that when the thermodynamic limit is satisfied (the number of monomers approaches infinity) these ensembles are equivalent from the thermodynamic point of view: it means that the constitutive equations (vector force-extension relations) assume the same mathematical form in both isotensional and isometric conditions. Equivalently, the Helmholtz and Gibbs free energies are linked by a Legendre transform. This general result is coherent with some “forms of inequivalence” observed and they are not in conflict.

ensemble  
equivalence

In order to clearly explain these points we rewrite our results in two different statements hereafter referred to as Property A and Property B. The results of Section 6.2 can be formalized as follows.

**Property A:** *we consider a polymer system with  $N$  monomers described by  $F(\mathbf{r}) = -k_B T \log Z_r(\mathbf{r}, T)$  with Helmholtz isometric conditions ( $\mathbf{r}$  constant) and by  $G(\mathbf{f}) = -k_B T \log Z_f(\mathbf{f}, T)$  with Gibbs isotensional conditions ( $\mathbf{f}$  constant). See the definitions of the partition functions  $Z_r$  and  $Z_f$  in Eqs.(6.3) and (6.5). The corresponding constitutive equations valid for any value of  $N$  are*

$$\langle \mathbf{f} \rangle = \frac{\partial F(\mathbf{r})}{\partial \mathbf{r}} \triangleq \phi(\mathbf{r}) \quad (\text{Helmholtz}), \quad (6.21)$$

$$\langle \mathbf{r} \rangle = -\frac{\partial G(\mathbf{f})}{\partial \mathbf{f}} \triangleq \psi(\mathbf{f}) \quad (\text{Gibbs}). \quad (6.22)$$

Moreover, in the thermodynamic limit (i.e.  $N \rightarrow \infty$ ):

- (i) we have that  $\phi = \psi^{-1}$  or, equivalently,  $\psi = \phi^{-1}$  (where  $\phi$  and  $\psi$  are vector functions mapping  $\mathfrak{R}^3$  in  $\mathfrak{R}^3$ );
- (ii) the following Legendre transforms are valid:

$$G(\phi(\mathbf{r})) = F(\mathbf{r}) - \phi(\mathbf{r}) \cdot \mathbf{r}, \quad (6.23)$$

$$F(\psi(\mathbf{f})) = G(\mathbf{f}) + \mathbf{f} \cdot \psi(\mathbf{f}). \quad (6.24)$$

While the second point (ii) it has been verified through Eq. (6.20), the equivalence between (i) and (ii) is a standard result in the

theory of Legendre transforms [119, 173]. A formal and unequivocally proof of Property A for Gaussian polymers and for chains of rigid rods can be found in Ref. [171], which is a recent work of great importance to clarify this subject. We want to stress an important point: we proved the equivalence for  $N \rightarrow \infty$  between  $\langle \mathbf{f} \rangle = \phi(\mathbf{r})$  and  $\langle \mathbf{r} \rangle = \psi(\mathbf{f})$  (i.e.  $\phi = \psi^{-1}$  for  $N \rightarrow \infty$ ). Conversely, it is possible that other average values may exhibit different behaviors; hence our conclusions are valid only for previous quantities.

Moreover, we remark that the Property A does not state that the density probability is the same for the Helmholtz and the Gibbs ensembles: rather, we proved that the mathematical form of the constitutive equations Eqs. (6.21) and (6.22) are identical in the thermodynamic limit. Consequently some “form of inequivalence”, investigated elsewhere are correct and not conflicting with Property A [115, 167]. We observe that the constitutive laws given in Eqs.(6.21) and (6.22) map different quantities:  $\langle \mathbf{f} \rangle$  and  $\mathbf{r}$  for the Helmholtz ensemble and  $\langle \mathbf{r} \rangle$  and  $\mathbf{f}$  for the Gibbs one. For example, in Fig. 6.4 (see the next Section 6.4) we plot on the same graph  $|\mathbf{r}|$  versus  $|\langle \mathbf{f} \rangle|$  for the Helmholtz results and  $|\langle \mathbf{r} \rangle|$  versus  $|\mathbf{f}|$  for the Gibbs ones (we adopted scalar dimensionless variable for convenience). For  $N \rightarrow \infty$  the two ensembles converged to the same curve, because of the Property A. We also underline that numerical results are further confirmed by the fact that the expression of the asymptotic ( $N$  large) force-extension curve was analytically determined (see Eqs.(6.35) and (6.36)).

Furthermore, we observe that different comparisons, based on different average values [115, 167], can be useful and show some “inequivalences”: they can be summarized as follows.

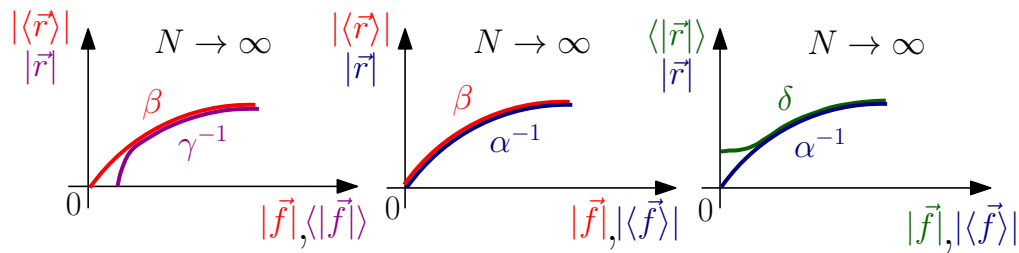


Figure 6.1: Schematic representation of the relationships among the functions defined in Property B. The central panel corresponds to Fig. 6.4. The right panel corresponds to Fig.4 or 5 of Ref.[121].

**Property B:** *for spherically symmetric systems we can consider these force-extension responses*

$$|\langle \mathbf{f} \rangle| = \alpha(|\mathbf{r}|) \quad (6.25)$$

$$\langle |\mathbf{f}| \rangle = \gamma(|\mathbf{r}|) \quad (6.26)$$

*for the Helmholtz case and the following relations*

$$|\langle \mathbf{r} \rangle| = \beta(|\mathbf{f}|) \quad (6.27)$$

$$\langle |\mathbf{r}| \rangle = \delta(|\mathbf{f}|) \quad (6.28)$$

*for the Gibbs one. The functions  $\alpha$  and  $\beta$  are the scalar counterparts of  $\phi$  and  $\psi$  defined in Property A. Hence, we have  $\beta = \alpha^{-1}$  (or  $\alpha = \beta^{-1}$ ) in the thermodynamic limit. On the contrary, one can prove that  $\gamma^{-1} \neq \beta$ ,  $\alpha^{-1} \neq \delta$  and  $\gamma^{-1} \neq \delta$  for any polymer length  $N$  and, therefore, also for systems in the thermodynamic limit.*

It is easy to verify that  $\gamma(0) > 0$  and  $\delta(0) > 0$  for any value of  $N$  by writing the expressions of the average values with the pertinent canonical probability densities. Since it is always true that  $\alpha(0) = 0$  and  $\beta(0) = 0$ , it is not difficult to prove the Property B. The different behavior between  $\gamma$  and  $\beta$  or between  $\alpha^{-1}$  and  $\delta$  is not related to the length of the polymer but rather to the transformation of random variables introduced to determine the average value of the modulus (2-norm) of the vectors  $\mathbf{r}$  and  $\mathbf{g}$  (see Eqs.(6.26) and (6.28)). In Fig.1 one can find three plots explaining the relations among the above functions. We observe that the differences between the curves  $\gamma^{-1}$  and  $\beta$  (or  $\alpha^{-1}$  and  $\delta$ ) are observable in the regime of small forces or extensions, as predicted in Refs. [115, 167]. Indeed, the function  $\delta$  has been analytically studied in the Gaussian approximation and the results have been confirmed in Ref. [121] through molecular dynamics simulations (also with quite small  $N$ ). The dual function  $\gamma$  is less tractable from the analytical point of view (because describes the Helmholtz case) but it could be numerically investigated, e.g. with Monte Carlo techniques or molecular dynamics simulations.

## 6.4 FLEXIBLE POLYMER WITH ELASTIC BONDS

In Eq.(6.1), we considered a polymer chain with an arbitrary potential  $V(\mathbf{r}_1, \dots, \mathbf{r}_N)$ . We want now to specify this potential considering a model in which each bond is represented by a harmonic spring with finite extension, while no potential is acting on bending or torsional degrees of freedom.

*harmonic  
potential*

Each spring is defined

by the potential energy

$$V(x) = \frac{1}{2}k(x - l)^2$$

for  $x \in (l - \Delta, l + \Sigma)$

where  $k$  is the spring

constant,  $l$  is the equilibrium

bond length and

$x$  is the actual extension

of the bond. As it

can be seen in Fig. 6.2,

the potential is set to

infinity for  $x \notin (l - \Delta, l + \Sigma)$

in order to impose

a limited extension

of the spring both for

expansion and compression.

This assumption is

consistent with what dis-

cussed in Ref.[174], where it is shown that a strong force may induce

structural transitions or even the breaking of the polymer

under tension: two phenomena that we want to avoid in this first

analysis. For this reason, we limit the model to the regime of harmonic

bond potentials.

We start with the Gibbs ensemble and we consider the augmented

Hamiltonian

$$\begin{aligned} & \tilde{h}(\mathbf{r}_1, \dots, \mathbf{r}_N, \mathbf{p}_1, \dots, \mathbf{p}_N, \mathbf{f}) \\ &= \sum_{i=1}^N \frac{\mathbf{p}_i \cdot \mathbf{p}_i}{2m} + \frac{1}{2}k \sum_{i=0}^{N-1} (\|\mathbf{r}_{i+1} - \mathbf{r}_i\| - l)^2 - \mathbf{f} \cdot \mathbf{r}_N. \end{aligned} \quad (6.29)$$

*limited  
spring  
extensions*

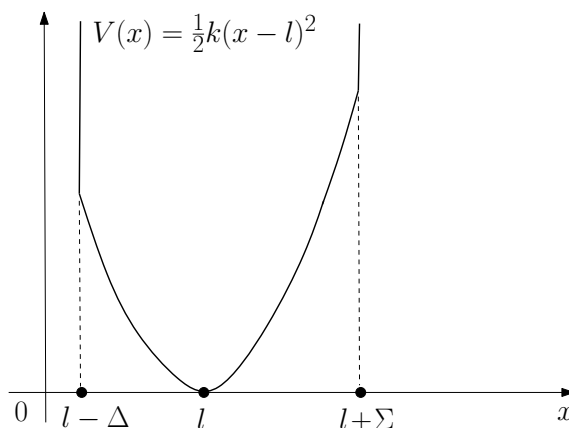


Figure 6.2: Potential energy function for the stretching of a single bond in the polymer chain.

*augmented  
Hamiltonian  
for a chain with  
elastic bonds*

In this case the determination of the spherically-symmetric partition function can be made in closed form. First of all, we separate the kinetic part of the partition function and we adopt the change

of variables  $\xi_{i+1} = \mathbf{r}_{i+1} - \mathbf{r}_i$  ( $i = 0, \dots, N-1$ ). Further, by representing the vector  $\xi_i$  in spherical coordinates, we get

$$Z_f(f, T) = \left( \sqrt{2\pi m k_B T} \right)^{3N} \left( \frac{4\pi k_B T}{f} \right)^N \quad (6.30)$$

$$\times \left[ \int_{l-\Delta}^{l+\Sigma} \exp \left\{ -\frac{k}{2k_B T} (\xi - l)^2 \right\} \sinh \left( \frac{f\xi}{k_B T} \right) \xi d\xi \right]^N.$$

The calculation can be explicitly carried out by making use of the known integral

$$I(\alpha, \beta, x_0, a, b) = \int_a^b x e^{-\alpha(x-x_0)^2} e^{\beta x} dx \quad (6.31)$$

$$= e^{\beta x_0} e^{\frac{\beta^2}{4\alpha}} \left\{ \frac{1}{2\alpha} \left( e^{-\mathcal{A}^2} - e^{-\mathcal{B}^2} \right) \right.$$

$$\left. + \sqrt{\frac{\pi}{\alpha}} \frac{\beta + 2\alpha x_0}{4\alpha} [\operatorname{erf}(\mathcal{B}) - \operatorname{erf}(\mathcal{A})] \right\},$$

where

$$\mathcal{A} = \sqrt{\alpha} \left( a - x_0 - \frac{\beta}{2\alpha} \right), \quad \mathcal{B} = \sqrt{\alpha} \left( b - x_0 - \frac{\beta}{2\alpha} \right), \quad (6.32)$$

and the function  $\operatorname{erf}(z)$  is defined as[175]

$$\operatorname{erf}(z) = \frac{2}{\sqrt{\pi}} \int_0^z e^{-t^2} dt. \quad (6.33)$$

From Eq.(7.13) we can further define the following auxiliary function

$$\Pi(\alpha, \beta, x, a, b) = I(\alpha, \beta, x, a, b) - I(\alpha, -\beta, x, a, b). \quad (6.34)$$

*Gibbs  
partition  
function*

The calculation leads to the exact expression of the Gibbs partition function in the form

$$Z_f(f, T) = \left( \sqrt{2\pi m k_B T} \right)^{3N} \left( \frac{2\pi k_B T}{f} \right)^N \quad (6.35)$$

$$\times \left[ \Pi \left( \frac{k}{2k_B T}, \frac{f}{k_B T}, l, l-\Delta, l+\Sigma \right) \right]^N.$$

*Gibbs  
constitutive  
equation*

This partition function directly provides the (scalar) constitutive equation  $r = r(f)$  as

$$r = k_B T \frac{\partial \log Z_f(f, T)}{\partial f}. \quad (6.36)$$

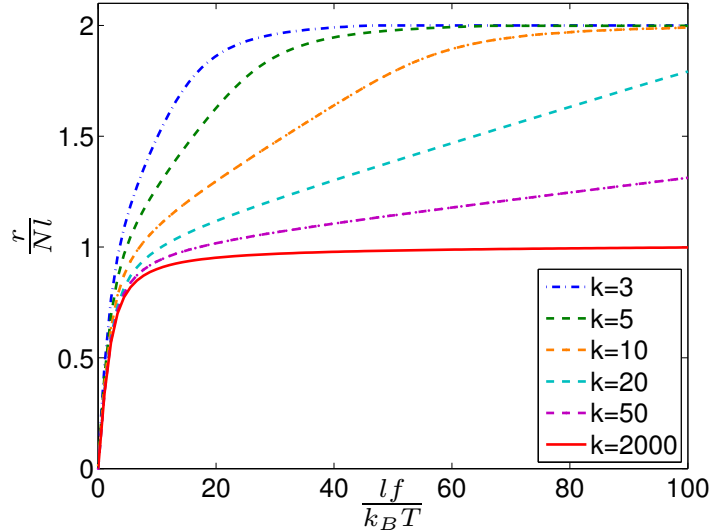


Figure 6.3: Constitutive relation provided by Eq.(6.36) for a flexible polymer with elastic bonds described by the potential reported in Fig. 6.2. The elongation  $r$  and the traction  $f$  are reported, respectively, in the vertical and horizontal axis in dimensionless units (see text). Different relations in the Gibbs ensemble are reported, corresponding to a spring constant varying in the range  $3 \leq k \leq 2000$  (units of  $4 \cdot 10^{-3}$  N/m).

It is interesting to observe that, as expected, in the limit of  $k \rightarrow \infty$  the partition function of the FJC model is recovered

$$Z_f(f, T) = \text{const.} \times \left( \frac{\sinh(\frac{lf}{k_B T})}{\frac{lf}{k_B T}} \right)^N, \quad (6.37)$$

and the constitutive equation  $r = Nl\mathcal{L}(\frac{lf}{k_B T})$  is found, where  $\mathcal{L}(x) = \coth x - 1/x$  is the Langevin function [16, 57].

In Fig. 6.3 we plot the constitutive equations (at constant temperature  $T = 293\text{K}$ ) obtained by applying Eqs.(6.35) and (6.36). We adopted the parameters  $l = 2.5\text{nm}$  (typically used for DNA [22, 23]), placing the walls at  $l - \Delta = 0$  and  $\Sigma + l = 5\text{nm}$ . The plot represents elongation versus traction curves for different values of the spring constant  $k = 3, 5, 10, 20, 50, 2000$  in units of  $k_B T / (\text{nm})^2 = 4 \cdot 10^{-3}$  N/m. While the smallest value of the stretching modulus describes a very soft chain, the largest one actually mimics a FJC. Three different regimes can be detected in Fig. 6.3: the first one, corresponding to a very small applied force, is the entropic region characterized by a linear relation  $r = Nl^2 f / (3k_B T)$ , as it is well known from classical polymer theory [16, 57]; by in-

creasing the applied load, the chain experiences an elastic region characterized by a slope proportional to  $k$ ; finally, the saturation is reached when the bond extension approaches the energy barrier at  $l + \Sigma$ . The length of the polymer chain in the configuration of largest extension ( $f \rightarrow \infty$ ) is  $N(l + \Sigma)$ . It is important to remark that each curve is independent of  $N$ , since the partition function given in Eq.(6.35) is an exact power with exponent  $N$ .

*Helmholtz  
constitutive  
equation*

For the Helmholtz ensemble we use instead Eq.(4.92) combined with the analytic continuation of Eq.(6.35) with  $f = i\eta$ . From this equation we obtain the scalar constitutive equation  $f = f(r)$  (see Eq.(6.4))

$$f = -k_B T \frac{\partial \log Z_r(r, T)}{\partial r}, \quad (6.38)$$

representing the elastic behaviour in the Helmholtz ensemble that depends on the number of monomers  $N$ . We expect a family of curves approaching the Gibbs solution for large  $N$  (thermodynamic limit).

While the numerical implementation of Eq.(6.36) is straightforward, the Helmholtz case (see Eq.(6.38)) is more difficult to handle because of some numerical instabilities and it can be used in a limited range of cases. Therefore, we exploited a Monte Carlo approach that can bypass such problems and can be also adopted for studying more complex chains, such as the WLC model.

*Monte Carlo  
approach  
and results*

The Monte Carlo approach simulates the stretching of the polymer under a force provided by a cantilever (mimicking, for instance, the loading by an atomic force microscope) with a proper adjustable elastic stiffness. In the limit of a soft cantilever the generalized ensemble of the coupled molecule/cantilever system reduces to the Gibbs ensemble for the isolated molecule subjected to a constant force. On the other hand, for a stiff cantilever we obtain the Helmholtz ensemble for the isolated molecule held at a fixed extension by the fluctuating force [168]. This simulation protocol has been already used to prove the existence of transitions from the flexible to the rigid phase for the WLC model under the Helmholtz ensemble [123, 176]. Simulations were performed by using a rather conventional implementation of the Metropolis version of the Monte Carlo algorithm [177]. The initial state of the chain is defined by a set of randomly chosen positions for the monomers. The displacement extent  $\delta r_i$  of the positions vectors

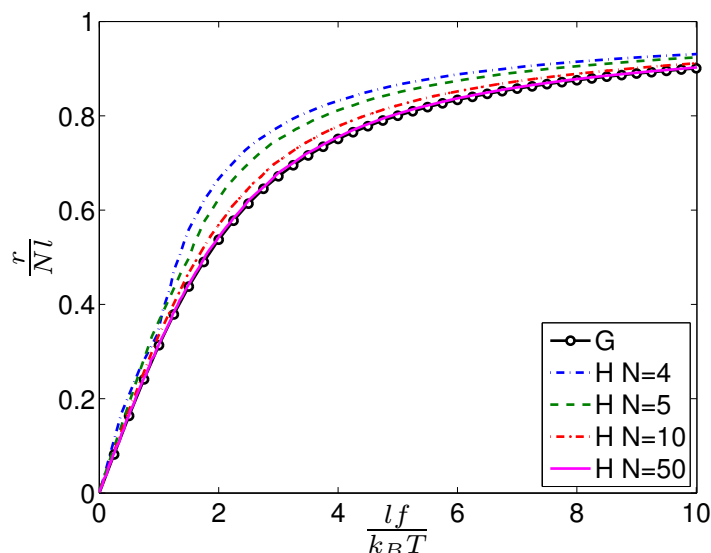


Figure 6.4: Constitutive relation provided by Monte Carlo simulations for a FJC model, both under Helmholtz (H) and Gibbs (G) boundary conditions. The elongation  $r$  and the traction  $f$  are reported, respectively, on the vertical and horizontal axis in dimensionless units (see text). The Helmholtz constitutive relation is reported for different polymer lengths, given by the number  $N$  of monomers in the chain.

governs the magnitude of the trial move and the overall efficiency of the configurational space sampling. However, while a larger  $\delta r_i$  could speed up the search for the minimum, a too large  $\delta r_i$  leads to a high rejection frequency. Therefore, we analyzed several runs in order to optimize its value [125, 126]. We avoided the dynamical adjustment of this parameter since this approach can violate the detailed balance [143].

In Fig. 6.4 we report our Monte Carlo results for the FJC model in both statistical mechanics ensembles. While we observe a single curve for the Gibbs ensemble (since the Langevin function derived from Eq.(6.37) is independent of  $N$ ), we get different elastic response curves for the Helmholtz ensemble with polymer length  $N = 4, 5, 10$  and  $50$ . It is interesting to note that the Helmholtz curves approach the Gibbs one for large  $N$ , as expected for the convergence to the thermodynamic limit. Fig. 6.4 shows that differences between the two ensembles are considerable for short chains.

In order to better characterize the convergence toward the thermodynamic limit, we investigate the ratio between the elongation  $r_H(N) = r/(Nl)$  calculated in the Helmholtz ensemble and the

*FJC  
inextensible  
bonds*

*convergence  
toward the  
thermodynamic  
limit*

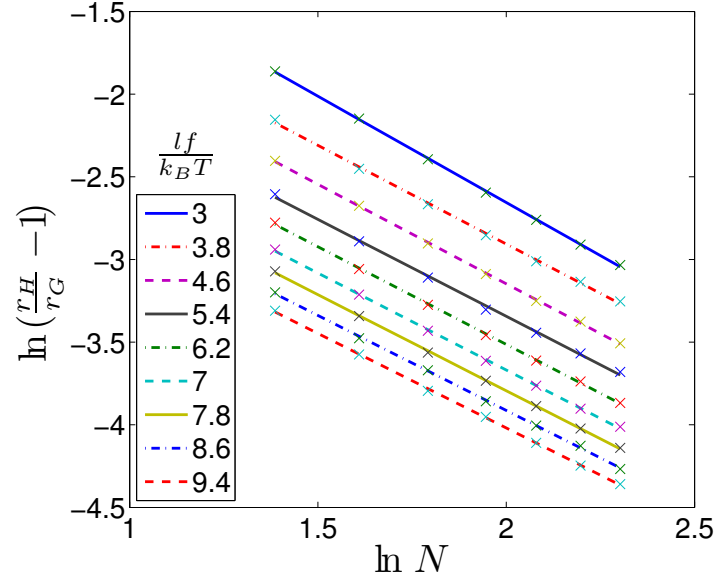


Figure 6.5: Comparison between the elongations  $r_H$  and  $r_G$  for the pure FJC model. The elongations are calculated, respectively in the Helmholtz and Gibbs ensembles as a function of the polymer lengths (given by the number  $N$  of monomers in the chain). All sets of data are nicely fitted by Eq. (6.39) with the same scaling exponent  $\alpha = 1.15 \pm 0.05$ .

elongation  $r_G = r/(Nl)$  for the Gibbs ensemble corresponding to the same number of monomers. Fig. 6.5 proves that Monte Carlo simulations are nicely fitted by the power law

$$\frac{r_H(N)}{r_G} = 1 + \frac{a}{N^{\alpha'}} \quad (6.39)$$

where  $a$  and  $\alpha$  are fitting parameters. Each curve corresponds to a different value of the normalized force  $fl/(k_B T)$ . All data sets were interpolated by linear regression and they provided the same scaling exponent  $\alpha = 1.15 \pm 0.05$ . Therefore, we argue that the convergence to the thermodynamic limit of the FJC model is quantitatively controlled by a unique scaling exponent.

*FJC  
extensible  
bonds*

Further, we are interested in understanding whether this value depends on the specific microscopic model of polymer adopted for the Monte Carlo simulations. To this aim we set a lower value for the elastic constant of the spring between the monomers. In particular, we selected the value  $k = 10k_B T/(nm)^2$  already used in Fig. 6.3. The Monte Carlo simulation results for both the Helmholtz and Gibbs ensemble are shown in Fig. 6.6. As before, we find a single curve for the Gibbs ensemble and a family of curves for the Helmholtz ensemble (corresponding to  $N = 4, 5, 10$

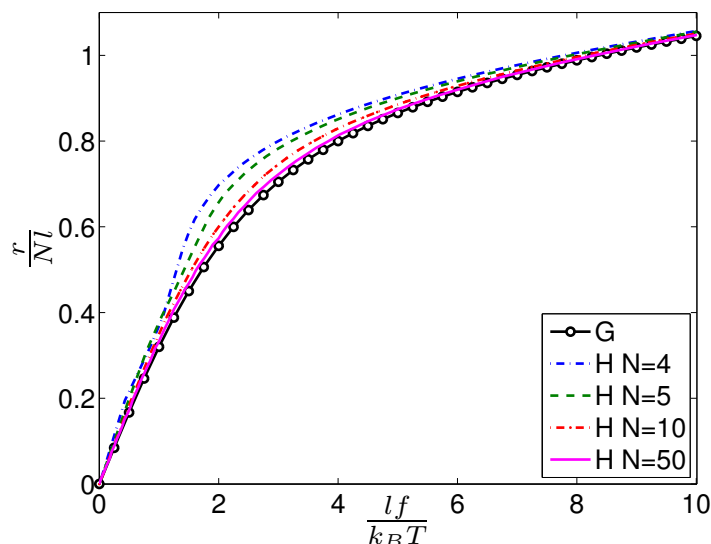


Figure 6.6: Constitutive relation provided by Monte Carlo simulations for a FJC model with elastic bonds between the monomers, both under Helmholtz (H) and Gibbs (G) boundary conditions. The elongation  $r$  and the traction  $f$  are reported, respectively, on the vertical and horizontal axis in dimensionless units (see text). The Helmholtz constitutive relation is reported for different polymer lengths, given by the number  $N$  of monomers in the chain.

and 50, from the top to the bottom). We checked and confirmed the agreement between Eq.(6.38) and the Monte Carlo results also for the Helmholtz ensemble. Once again, the curves in Fig. 6.6 can be used to address the thermodynamic limit issue, as shown in Fig. 6.7. We observe that the linear regression leads now to the scaling exponent  $\alpha = 0.80 \pm 0.05$  for any value of the normalized force  $fl/(k_B T)$ . This result suggests that different polymer models, e.g. rigid versus elastic in this case, have different scaling exponents or, in other words, that they progress differently to reach the thermodynamic limit.

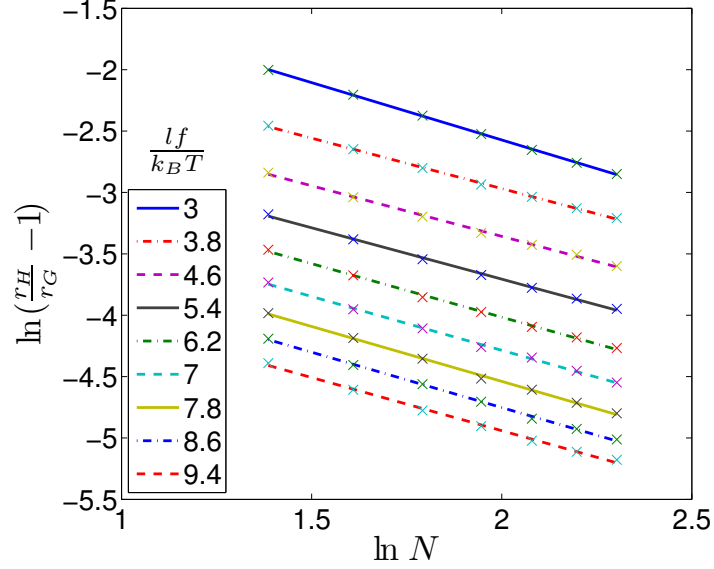


Figure 6.7: Comparison between the elongations  $r_H$  and  $r_G$  for the FJC model with elastic bonds between the monomers. The elongations are calculated, respectively in the Helmholtz and Gibbs ensembles as a function of the polymer length (given by the number  $N$  of monomers in the chain). All sets of data are nicely fitted by Eq. (6.39) with the same scaling exponent  $\alpha = 0.80 \pm 0.05$ .

## 6.5 SEMIFLEXIBLE POLYMER WITH ELASTIC BONDS

In order to make the model polymer more physically sound, we now extend our formal device to a semiflexible chain that incorporates elastic bonds into a discrete version of the WLC model. The augmented Hamiltonian for the Gibbs ensemble is

$$\begin{aligned} \tilde{h}(\mathbf{r}_1, \dots, \mathbf{r}_N, \mathbf{p}_1, \dots, \mathbf{p}_N, \mathbf{f}) &= \sum_{i=1}^N \frac{\mathbf{p}_i \cdot \mathbf{p}_i}{2m} - \mathbf{f} \cdot \mathbf{r}_N \\ &+ \frac{1}{2}\kappa \sum_{i=1}^{N-1} (\mathbf{t}_{i+1} - \mathbf{t}_i)^2 + \frac{1}{2}k \sum_{i=0}^{N-1} (\|\mathbf{r}_{i+1} - \mathbf{r}_i\| - l)^2, \end{aligned} \quad (6.40)$$

where  $\kappa$  is the bending modulus,  $k$  is the stretching modulus and  $\mathbf{t}_i = (\mathbf{r}_{i+1} - \mathbf{r}_i)/\|\mathbf{r}_{i+1} - \mathbf{r}_i\|$  is the unit vector collinear with the  $i$ -th

bond. The corresponding reduced Hamiltonian for the Helmholtz ensemble is given by

$$\begin{aligned} h(\mathbf{r}_1, \dots, \mathbf{r}_{N-1}, \mathbf{p}_1, \dots, \mathbf{p}_{N-1}, \mathbf{r}) &= \sum_{i=1}^{N-1} \frac{\mathbf{p}_i \cdot \mathbf{p}_i}{2m} \\ &+ \frac{1}{2}\kappa \sum_{i=1}^{N-1} (\mathbf{t}_{i+1} - \mathbf{t}_i)^2 + \frac{1}{2}\kappa \sum_{i=0}^{N-1} (\|\mathbf{r}_{i+1} - \mathbf{r}_i\| - l)^2, \end{aligned} \quad (6.41)$$

where the position of the last monomer  $\mathbf{r}_N$  corresponds to the end-to-end vector  $\mathbf{r}$ . As well known, it is not possible to determine the partition functions in closed form for ensembles described by Eqs.(6.40) and (6.41) [21]. Therefore, we take full profit from our Monte Carlo approach and we critically address some approximated solutions. In particular, by considering an inextensible WLC model, the Hamiltonian function in the Gibbs ensemble is given by

*WLC  
inextensible  
bonds*

$$\tilde{h} = \sum_{i=1}^N \frac{\mathbf{p}_i \cdot \mathbf{p}_i}{2m} - \mathbf{f} \cdot \mathbf{r}_N + \frac{1}{2}\kappa \sum_{i=1}^{N-1} (\mathbf{t}_{i+1} - \mathbf{t}_i)^2, \quad (6.42)$$

while in the Helmholtz ensemble it is

$$h = \sum_{i=1}^{N-1} \frac{\mathbf{p}_i \cdot \mathbf{p}_i}{2m} + \frac{1}{2}\kappa \sum_{i=1}^{N-1} (\mathbf{t}_{i+1} - \mathbf{t}_i)^2. \quad (6.43)$$

We remark that we have set the spring constant  $\kappa$  to such a very large value that the bond length remains fixed at the value  $l$ . The constitutive equations are now expected to depend on the number of monomers  $N$  in any ensemble since, for the WLC model, both partition functions given in Eqs.(6.3) and (6.5) cannot be written as an exact power with exponent  $N$ . In Fig. 6.8 we report the Monte Carlo results for the inextensible WLC model: while the Helmholtz family of curves converges from the top to the bottom, upon increasing the polymer length, the Gibbs curves follow the opposite trend. We remark once more the convergence to a central common curve, representing the behavior of the system when the thermodynamic limit is reached. The example summarized in Fig. 6.8 corresponds to the value  $\kappa = 10k_B T$  for the bending modulus at  $T = 293\text{K}$ . This value is comparable to that of polymer chains of biological interest (for example for DNA  $\kappa = 15k_B T$  [21, 22, 23]).

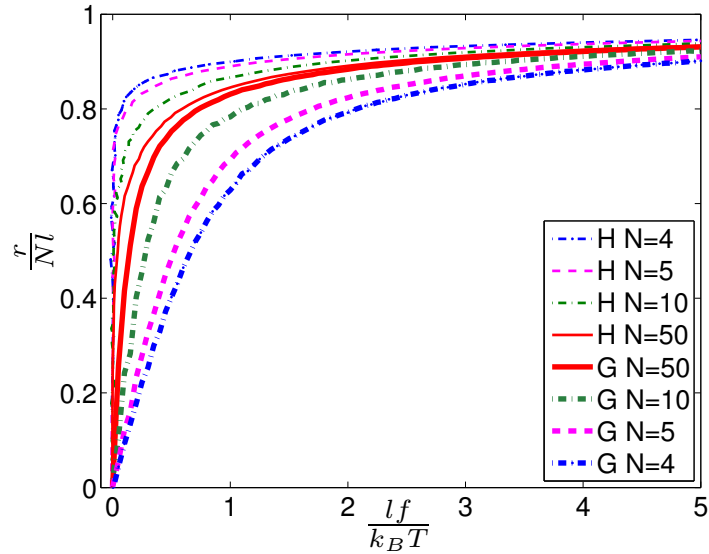


Figure 6.8: Constitutive relation provided by Monte Carlo simulations for the pure WLC model, both under Helmholtz (H) and Gibbs (G) boundary conditions. The elongation  $r$  and the traction  $f$  are reported, respectively, on the vertical and horizontal axis in dimensionless units (see text). The Helmholtz constitutive relation is reported for different polymer lengths, given by the number  $N$  of monomers in the chain.

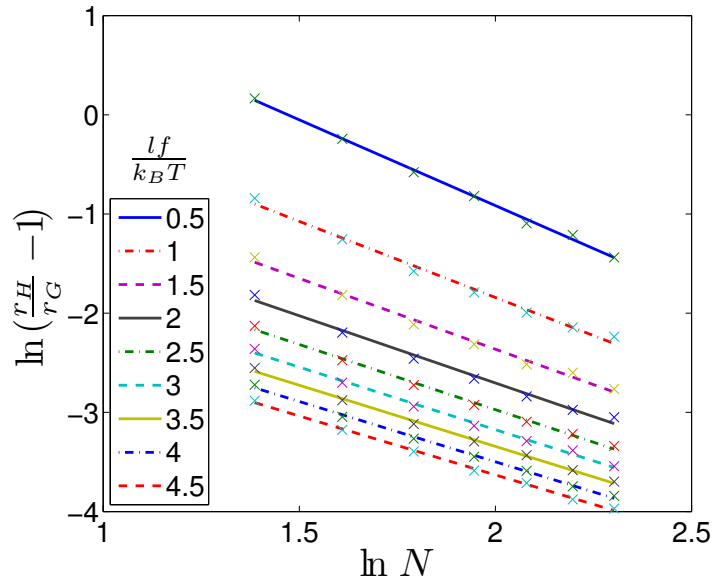


Figure 6.9: Comparison between the elongations  $r_H$  and  $r_G$  for the pure WLC model. The elongations are calculated, respectively, in the Helmholtz and Gibbs ensembles as a function of the polymer length (given by the number  $N$  of monomers in the chain). All sets of data are nicely fitted by Eq. (6.46) with the same scaling exponent  $\alpha = 1.30 \pm 0.05$ .

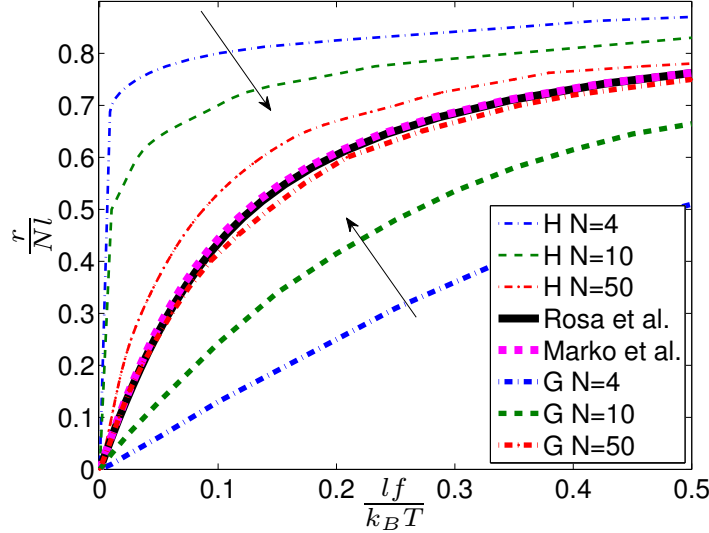


Figure 6.10: Same as Fig. 6.8 where the approximated solutions by Marko and Siggia (see Eq.(6.44) and by Rosa et al. (see Eq.(6.45) are reported for the sake of comparison.

These results can be compared with the approximations published in literature for the WLC model. A first interpolation formula was given by the classical Marko and Siggia result [21]

$$\frac{fl}{k_B T} = \frac{l}{L_p} \left[ \frac{1}{4(1-\zeta)^2} - \frac{1}{4} + \zeta \right], \quad (6.44)$$

where  $\zeta = r/(Nl)$  is the polymer extension normalized to the contour length and  $L_p = l\kappa/(k_B T)$  is the persistence length.

This result is asymptotically exact both in the large- and small-force limits of the continuous WLC model. Another, more recent result was derived for the discrete version of the WLC model, where the finite size of the equilibrium length  $l$  is also accounted for [22, 23]

$$\begin{aligned} \frac{fl}{k_B T} = & \frac{2L_p}{l} \left[ \sqrt{1 + \left(\frac{l}{2L_p}\right)^2 \frac{1}{(1-\zeta)^2}} - \sqrt{1 + \left(\frac{l}{2L_p}\right)^2} \right] \\ & + \left[ \frac{1 - \mathcal{L}\left(\frac{L_p}{l}\right)}{1 + \mathcal{L}\left(\frac{L_p}{l}\right)} - \frac{\frac{l}{2L_p}}{\sqrt{1 + \left(\frac{l}{2L_p}\right)^2}} \right] \zeta, \end{aligned} \quad (6.45)$$

$\mathcal{L}(x) = \coth x - 1/x$  being the Langevin function. It is easy to verify that in the continuum limit  $l \rightarrow 0$  one recovers Eq.(6.44),

*Marko  
and  
Siggia  
formula*

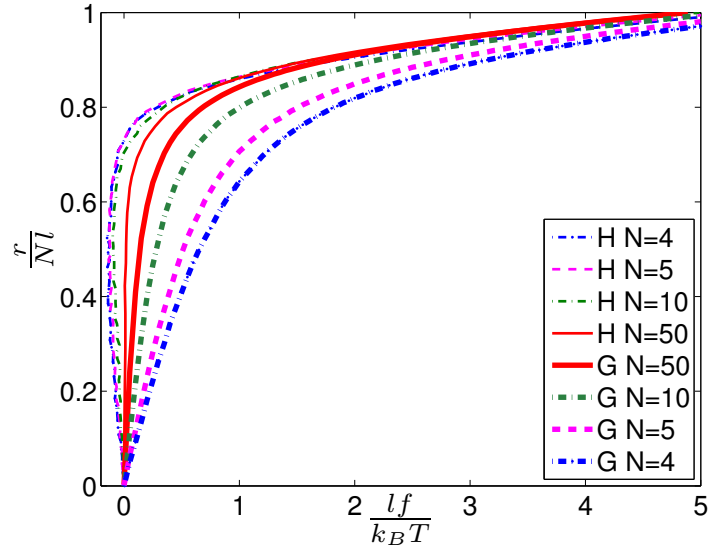


Figure 6.11: Constitutive relation provided by Monte Carlo simulations for the WLC model with elastic bonds between the monomers, both under Helmholtz (H) and Gibbs (G) boundary conditions. The elongation  $r$  and the traction  $f$  are reported, respectively, on the vertical and horizontal axis in dimensionless units (see text). The Helmholtz constitutive relation is reported for different polymer lengths, given by the number  $N$  of monomers in the chain.

as expected. Other interesting expressions for the force-extension curves can be found in Ref.[178]. In Fig. 6.10 we report an enlarged detail of Fig. 6.8 together with the constitutive equations given in Eqs.(6.44) and (6.45): plots corresponding to both analytical approximations are contained between the Gibbs and Helmholtz Monte Carlo solutions for the larger value of  $N$  considered. Therefore, the interpolation formulas in Eqs.(6.44) and (6.45) are in very good agreement with the behaviour of the WLC model when the thermodynamic limit is reached ( $N > 50$  in this case).

We can next analyse the convergence toward the thermodynamic limit. To this aim, we consider again the data in Fig. 6.8 and the ratio  $\frac{r_H(N)}{r_G(N)}$  at a given fixed value of the normalized force. As before, it is found that Monte Carlo simulations are nicely fitted by the power law

$$\frac{r_H(N)}{r_G(N)} = 1 + \frac{\alpha}{N^\alpha} \quad (6.46)$$

where  $\alpha$  and  $\alpha$  are fitting parameters. All sets of data have been interpolated by linear regression in Fig. 6.9 and they provided the

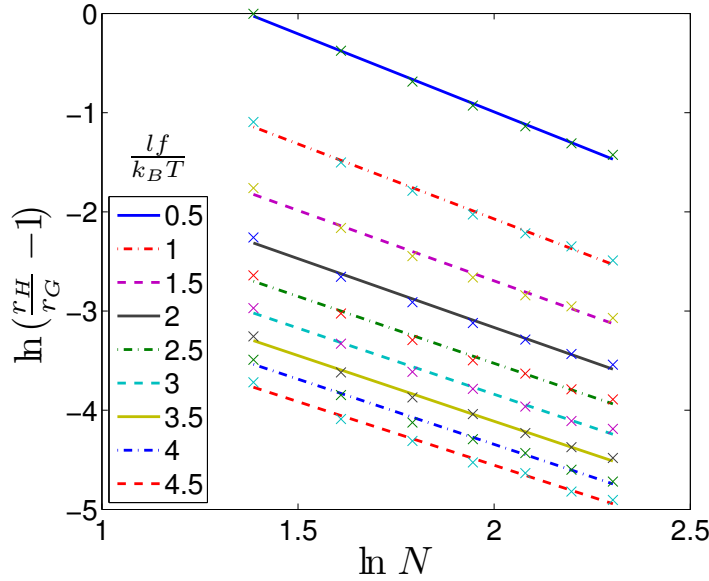


Figure 6.12: Comparison between the elongations  $r_H$  and  $r_G$  for the WLC model with elastic bonds between the monomers. The elongations are calculated, respectively in the Helmholtz and Gibbs ensembles as a function of the polymer length (given by the number  $N$  of monomers in the chain). All sets of data are nicely fitted by Eq. (6.46) with the same scaling exponent  $\alpha = 1.40 \pm 0.05$ .

same scaling exponent  $\alpha = 1.30 \pm 0.05$ . We finally consider the semiflexible discrete WLC model with extensible bonds. We set the parameters  $\kappa = 10k_B T$  (for the bending) and  $k = 10k_B T / (\text{nm})^2$  (for the stretching). In Fig. 6.11 we report the Monte Carlo results for both ensembles: the two families of curves are converging (from the top for the Helmholtz case and from the bottom for the Gibbs one) to the same constitutive relation for an increasing contour length, or number of monomers  $N$ .

*WLC  
extensible  
bonds*

As before, the curves in Fig. 6.11 can be used to analyze the convergence toward the thermodynamic limit through Eq.(6.46). Fig. 6.12 shows that in this case the linear regression leads to a scaling exponent  $\alpha = 1.40 \pm 0.05$  for any value of the normalized force.

## 6.6 OUTLINE OF THE RESULTS

We discussed here the notion of thermodynamic limit showing that different experimental strategies used for stretching the polymer lead to the same results when the number of monomers is

large enough. The development of ad-hoc MMC simulations has been necessary for investigate the convergence to the thermodynamic limit, which we found to be well described by suitable power laws with well defined scaling exponents. The results of this work and the demonstration of different scaling laws, may help to discriminate the response of polymers with different internal chemical structure, in the short-length limit. A similar treatment can be followed also for different deformation modes. For example the twisting experiments can be performed by means of magnetic tweezers [179]: the equivalent of the present fixed-ends versus fixed-force scheme would be substituted with the fixed-twist versus fixed-torque scheme.

## TWO-STATE THEORY OF SINGLE POLYMER STRETCHING

---

### Contents

---

7.1	General framework	123
7.2	Theoretical model and calculations	124
7.2.1	Gibbs ensemble: cooperative response	126
7.2.2	Helmholtz ensemble: non-cooperative response	130
7.3	Outline of the results	134

---

So far, we discussed how the direct probing of the elasticity of individual molecules is obtained by means of the atomic-force microscope (AFM), laser- or magnetic-tweezers apparatus, or the biomembrane force probe [1, 2, 12, 70]. These mechanical devices are quite different from one another. One prominent difference is their equivalent stiffness, in the range of  $10^{-4} - 1$  pN/nm for tweezers, versus  $10 - 10^2$  pN/nm for the AFM [70] (see Table 2). The typical experiment is a mechanically-induced unfolding of a biological polymer made of N domains, e.g. a polysaccharide such as dextran [10], a protein such as titin [62], a DNA or RNA strand [180], and so on. As a function of increasing force levels different mechanical response regimes are observed, beginning with the entropic unfolding of the polymer chain (now well understood in terms of simple worm-like chain (WLC) or freely-jointed chain (FJC) models [21]); to the linear-elastic extension of the straightened chain; to the so-called *overstretching*, typically interpreted as a conformational transformation of the domain geometry; up to the eventual fracturing of the polymer [181, 182, 183, 184].

In spite of the richness of experimental results and the large number of models devoted to explain specific situations, a universal theoretical approach able to describe the different observed responses is not yet available. Typically the experimental results can be subdivided in two separated classes showing cooperative

and non-cooperative mechanically induced unfolding. Any of the above discussed polymer model is able to explain only one of these two observed responses.

Several theoretical models have been introduced to shed light on the force-induced transformations, notably in DNA. For example, a macroscopic thermodynamics analysis led to a *melting* interpretation of the overstretching transition [185], with *double-strained* DNA (*dsDNA*) separating into non-interacting *single-strained* DNA (*ssDNA*) strands. This model was subsequently extended in order to consider different conditions of temperature, pH and ionic strength [186]. However, a more recent thermodynamics analysis [187] compared DNA melting (the process by which *dsDNA* unwinds and separates into single-stranded strands through the breaking of hydrophobic stacking attractions between the bases) with the conformational transformation from *dsDNA* to a supposed *stretched-DNA*, or *S-DNA* form, and found the latter to be in much better agreement with available experimental data. On the other hand, recent experimental results show that when the content of Adenine-Thymine (AT) pairs is high, a force induced denaturation (melting) is observed; by contrast, sequences with a prevalence of Guanine-Cytosine (GC) pairs are found to undergo an overstretch transition into a distinct base-paired form [188]. Comparisons of experimental results with *ad-hoc* models have been also drawn for analysing structural transitions of simultaneously twisted and stretched DNA molecules [189]. Some other general properties of bi-stable systems have been studied through the Fermi-Pasta-Ulam chain model [190, 191], by a two-state FJC polymer [192, 193], and by the so-called discrete persistent chain that borrows features from both the FJC and the WLC chain models [194]. Also atomic-scale computer simulations based on molecular dynamics have been used to analyze physicochemical details of different polymers and biomolecules [195, 196]. As an example, concerning the DNA mechanics, it has been shown that the double helix can be extended to twice its normal length before its base pairs break [197]. Moreover, the force needed to completely separate the two strands has been numerically determined [198], and some non-canonical forms generated by DNA stretching and compression have been predicted [199].

We propose here a statistical mechanics analysis of the finite-size elasticity of model polymers, consisting of domains that can

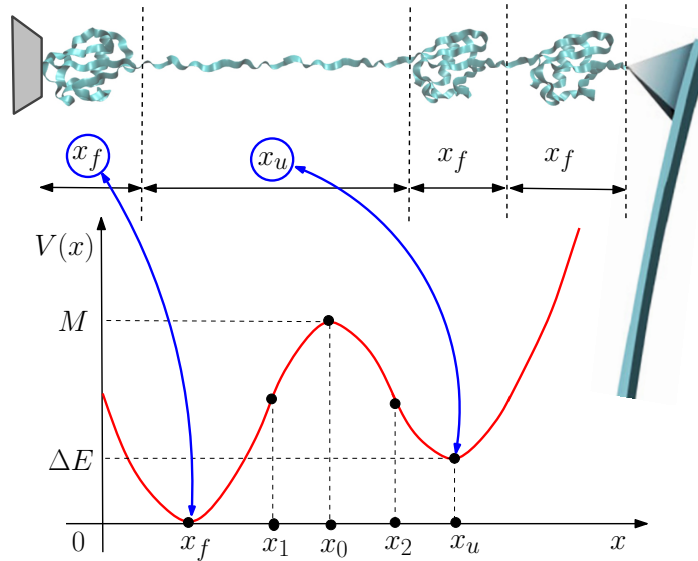


Figure 7.1: Potential energy function with an energy barrier. Folded and unfolded configurations of the domains are schematically represented.

exhibit transitions between more than one stable state at large applied force. A unifying model capturing at the same time the main features of both cooperative and non-cooperative behaviors is presented. Also in this case, the constant-force (Gibbs) and constant-displacement (Helmholtz) formulations of single molecule stretching experiments are shown to converge in the thermodynamic limit. Monte Carlo simulations of continuous three dimensional polymers of variable length are carried out, based on this formulation. We demonstrate that the experimental force-extension curves for short and long polymers are described by a unique universal model, despite the differences in chemistry and rate-dependence of transition forces.

## 7.1 GENERAL FRAMEWORK

We deal here with the problem of the interpretation of the overstretching regime (or conformational transitions regime), which we describe in terms of the internal dynamics of a chain of two-state systems undergoing a conformational transformation, as described by the double-well potential in Fig. 7.1.

For the sake of argument we call “folded” and “unfolded” the two conformations; however the transformation occurs, more generally, between two principal local minima of the domain free-

*folded and  
unfolded  
conformations*

energy hypersurface (e.g., for DNA it could as well represent the melting transition [105]). Then, we firstly develop a theoretical model describing experiments at constant applied force (a realization of Gibbs ensemble statistics) and we show that the conformational change must occur simultaneously for all the domains at a given threshold force. On the other hand, experiments performed at constant-displacement are a realization of the Helmholtz ensemble of statistical mechanics. In Chapter 6, we showed that the outcome of the two types of experiment converge in the thermodynamic limit of infinite chain length,  $N \rightarrow \infty$ . Moreover, the equivalence of the different statistical ensembles in the thermodynamic limit (for Gaussian polymers and chains of rigid rods) is largely discussed in Ref. [171]. On the contrary, if the thermodynamic limit is not reached, it has been shown that different boundary conditions (Helmholtz and Gibbs ensembles) imposed for stretching the polymer lead to different force-extension curves [114, 123, 124, 171, 200]. In practice, real experiments always fall inbetween these two ideal extremes. Therefore, here we focus on the intermediate cases described by finite values of the  $k_c/k$  ratio,  $k$  and  $k_c$  being the equivalent spring constant (i.e., stiffness) of the domain and of the pulling device, respectively. We demonstrate by means of Monte Carlo simulations that the typical “sawtooth” pattern [62], observed for the unfolding of large protein domains (such as the Ig units in titin), and the “plateau” or kink [10, 180], observed in the overstretching of DNA and polysaccharides (e.g. dextran), have a common origin in the size-dependence of the polymer response to the external force, the plateau shape being attained in the limit of large  $N$ . On the same grounds, at a fixed number  $N$  of domains, the transition from the “plateau” (cooperative) to the “sawtooth” (non-cooperative) response is recovered for increasing values of  $k_c/k$ . Notably, such a behavior of the force-extension curves is universal with respect to the specification of any additional parameters, such as chemical, structural or mechanical constants of the domains.

*real  
experiments  
always fall  
inbetween  
the two  
ideal extremes*

*plateau and  
sawtooth  
patterns*

## 7.2 THEORETICAL MODEL AND CALCULATIONS

We work out a simple model containing the minimal ingredients fully describing the overall complex behavior of a polymer chain.

It consists of an N-domain, non-branched chain clamped at one end, able to describe conformational transitions across an energy barrier. The internal state of each domain is described by a potential energy  $V(x)$  that exhibits two minima corresponding to the lengths  $x = x_f$  (folded conformation) and  $x = x_u$  (unfolded conformation), connected via an energy barrier  $M$  at  $x = x_0$  (see Fig. 7.1). The energy is written as a  $\mathcal{C}^2$  piecewise function, constructed by imposing continuity and differentiability at the joining points  $x_1$  and  $x_2$

*bistable  
potential*

$$V(x) = \begin{cases} \frac{1}{2}k(x - x_f)^2 & 0 < x < x_1 \\ -\frac{1}{2}k(x - x_0)^2 + M & x_1 < x < x_2 \\ \frac{1}{2}k(x - x_u)^2 + \Delta E & x > x_2. \end{cases} \quad (7.1)$$

For chosen values of the lengths  $x_f$  and  $x_u$ , the domain spring constant  $k$ , and the energy difference  $\Delta E$  between the two conformations, the other parameters are simply given by:

$$\delta = x_u - x_f, \quad (7.2)$$

which represents the length rise per base-pair generated by the force-induced conformational transition,

$$x_0 = \frac{x_u + x_f}{2} + 2\frac{\Delta E}{k\delta}, \quad (7.3)$$

the energy barrier  $M$

$$M = \frac{k}{4} \left[ \frac{\delta}{2} + 2\frac{\Delta E}{k\delta} \right]^2, \quad (7.4)$$

and the extremes of the domains  $x_1$  and  $x_2$ , namely

$$x_1 = x_f + \frac{\delta}{4} + \frac{\Delta E}{k\delta}, \quad (7.5)$$

and

$$x_2 = x_u - \frac{\delta}{4} + \frac{\Delta E}{k\delta}. \quad (7.6)$$

Therefore, this model properly gives a barrier with

$$x_f < x_0 < x_u \quad (7.7)$$

only for

$$|\Delta E| \leq k \frac{\delta^2}{4}. \quad (7.8)$$

The model is based on the equilibrium statistical mechanics and therefore it should be applied to the case of very slow stretching cycles or for all transitions occurring much faster than the characteristic velocity of the experiment. Then, we will investigate and obtain the mechanical equation of state and all other thermodynamic properties under equilibrium conditions. Important enough, we underline that the model represents a multi-domain polymer chain as a sequence of domains connected each other (see Fig. 7.1). Each domain is intended to represent a series of monomers that can exhibit a conformational transition. Actually, to modelize the bistability, instead of really consider a series of monomers composing each domain, each former is represented by the short-ranged bond potential  $V(x)$  in Eq.(7.1). Under the influence of an external force, the multi-domain polymer extends according to the WLC model. In addition, because each domain in the modular polymer can undergo a transition, the total contour length of the polymer changes during a transition; this change is modulated by the external force applied to the end of the last domain.

### 7.2.1 Gibbs ensemble: cooperative response

Upon application of a constant force  $f$  to the end of the polymer identified by the position vector  $\mathbf{r}_N = (x_N, y_N, z_N)$  (the other end being fixed in the origin), the statistics of the fluctuating chain is a realization of the Gibbs ensemble [124]. The partition function in thermodynamic equilibrium is given by

$$Z_f(f, T) = \iint_{\Gamma_N} e^{-\tilde{h}/k_B T} dq^N dp^N, \quad (7.9)$$

with  $\Gamma_N = \mathfrak{R}^{6N}$ . The augmented Hamiltonian  $\tilde{h}$  includes the classical kinetic energy of the domains with mass  $m$ , their total potential energy, and a term,  $-fz_N$ , describing the applied force along the  $z$ -axis [124]. In the framework of the present minimal model, the

*Gibbs  
partition  
function*

partition function can be explicitly calculated as

$$\begin{aligned}
 Z_f(f, T) &= \left( \frac{2\pi m}{\beta} \right)^{3N/2} \left( \frac{2\pi}{\beta f} \right)^N \\
 &\times \left[ \Pi(\beta k, \beta f, x_f, 0, x_1) \right. \\
 &+ e^{-\beta M} \Pi(-\beta k, \beta f, x_0, x_1, x_2) \\
 &\left. + e^{-\beta \Delta E} \Pi(\beta k, \beta f, x_u, x_2, +\infty) \right]^N,
 \end{aligned} \tag{7.10}$$

with  $\beta = (k_B T)^{-1}$  and

$$\Pi(\alpha, \gamma, x_0, a, b) = 2 \int_a^b x e^{-\frac{\alpha}{2}(x-x_0)^2} \sinh(\gamma x) dx. \tag{7.11}$$

The function  $\Pi$  can be written as

$$\Pi(\alpha, \gamma, x_0, a, b) = I(\alpha, \gamma, x_0, a, b) - I(\alpha, -\gamma, x_0, a, b), \tag{7.12}$$

where the integral  $I$  can be calculated in closed form

$$\begin{aligned}
 I(\alpha, \gamma, x_0, a, b) &= \int_a^b x e^{-\alpha(x-x_0)^2} e^{\gamma x} dx \\
 &= e^{\gamma x_0} e^{\frac{\gamma^2}{4\alpha}} \left\{ \frac{1}{2\alpha} \left( e^{-\mathcal{A}^2} - e^{-\mathcal{B}^2} \right) \right. \\
 &\left. + \sqrt{\frac{\pi}{\alpha}} \frac{\gamma + 2\alpha x_0}{4\alpha} \left[ \text{Erf}(\mathcal{B}) - \text{Erf}(\mathcal{A}) \right] \right\},
 \end{aligned} \tag{7.13}$$

with

$$\mathcal{A} = \sqrt{\alpha} \left( a - x_0 - \frac{\gamma}{2\alpha} \right), \tag{7.14}$$

and

$$\mathcal{B} = \sqrt{\alpha} \left( b - x_0 - \frac{\gamma}{2\alpha} \right). \tag{7.15}$$

The extension  $r$  at a given force is obtained from the partition function as

$$r = k_B T (\partial \log Z_f / \partial f). \tag{7.16}$$

Since the extension is linearly dependent on  $N$ , the data for chains of different lengths can be scaled to a single curve upon dividing by  $N$ .

Figure 7.2 shows the results of the normalized force-extension

*theoretical  
results*

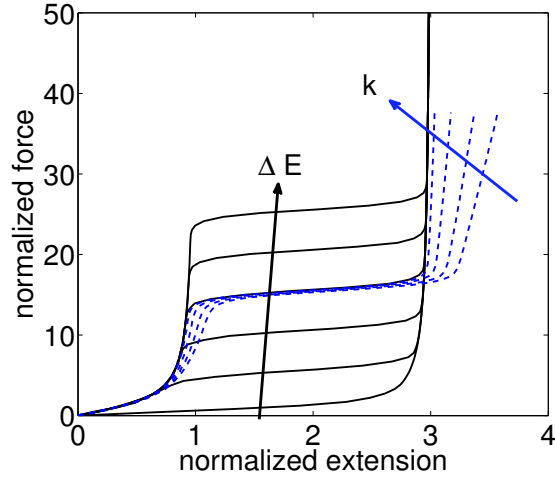


Figure 7.2: Force-extension curves for the Gibbs ensemble: normalized force  $f/f_\beta$  vs normalized extension  $r/(N\chi_f)$ . The black solid lines correspond to different values of the energy  $\Delta E=0, 10, 20, 30, 40, 50 k_B T$  (increasing values from the bottom up) for a fixed spring constant  $k = 2000 k_B T/(nm)^2$ . The blue dashed lines correspond to different values of the spring constant  $k=10, 15, 30, 100 k_B T/(nm)^2$  (increasing values from the right to the left) for a fixed value of the energy barrier  $\Delta E = 30 k_B T$ .

curves,  $f/f_\beta$  (where  $f_\beta^{-1} = \beta\chi_f$ ) in terms of  $r/(N\chi_f)$  for different values of the energy barrier  $\Delta E=0, 10, 20, 30, 40, 50 k_B T$  (black solid lines) at a fixed value of  $k=2000 k_B T/(nm)^2$ , and for different values of the spring constant  $k$  (blue dashed lines) at a fixed value of  $\Delta E=30 k_B T$ . As an example, we also adopted  $\chi_u = 3\chi_f$  or, equivalently,  $\delta = 2\chi_f$ . Both sets of curves display a force plateau at  $f \simeq \Delta E/\delta$ , for any  $\Delta E > 0$ , with a normalized width equal to  $\delta$ . In our model, the plateau indicates a transition in the polymer conformation, meaning that for  $f < \Delta E/\delta$  each domain is found in the folded conformation at  $\chi=\chi_f$ , while for  $f > \Delta E/\delta$  domains are in the unfolded conformation at  $\chi=\chi_u$ ; i.e., the ensemble of domains respond *cooperatively* to the external force. Important enough, we stress the fact that for the Gibbs ensemble the pattern of the force extension curve shows always a “plateau”, independently of the number of monomers composing the chain (see Fig. 7.2): this is the reflection of the linear dependence on  $N$  in the constitutive equation Eq.(7.16). Furthermore, we notice that also the value of the plateau force inducing the conformation transition does not depend on the spring constant,  $k$ , nor on the temperature. Such a result is readily interpreted in the framework of the Bell expres-

sion [201], as the threshold value of force necessary to make the unfolding rate equal to the (reverse) folding one, i.e. lowering the difference  $\Delta E$  to zero.

As an example of application, in the case of dsDNA, which displays a plateau at  $f=65$  pN with a  $\delta \approx 2.4$  Å, our criterion gives an energy estimate  $\Delta E=3.8$   $k_B T$ . Here, the value of  $f$  is the observed transition force and the parameter  $\delta$  represents the measured length rise per base pair in the transition from dsDNA to its stretched version (experimentally estimated [105, 180] to be a factor of  $\sim 1.7$  larger than the normal value of  $3.4$  Å [6, 202]). It turns out that the above theoretical  $\Delta E=3.8$   $k_B T$  fits quite well with the available experimental data [105, 203]. On the other hand, the difference of extension between dsDNA and ssDNA is characterized by a smaller factor of  $\sim 1.5$  [180] and the energetic difference  $\Delta E$  is about  $2.5 k_B T$  (per base pair) [204, 205]. Since  $2.5 k_B T < 3.8 k_B T$  the process should be interpreted as a melting transition (at lower energy and therefore preferred). As a matter of fact, there is a wide debate on the interpretation of the dsDNA transition by means of a melting process or through the emerging of a stretched (S-DNA) structure; the problem is still awaiting conclusive experimental evidences. In our context we have simply used the experimental data ( $f, \Delta E, \delta$ ) of the transition, which are valid independently of the real nature of the process.

*biophysical  
examples*

To further show the complexity of this problem, we also note that it has been recently approached by analyzing the behavior of DNA sequences with controlled base content [188]. It has been proved that when the AT content is around 70% the application of a force of about 62 pN generates a denaturation (melting) with an extension factor of  $\sim 1.7$ . Conversely, sequences with GC content of 60%, under the same force, show a reversible transition into a new stable structure extent by a factor  $\sim 1.5$  [188]. Unfortunately no energetic data are available to make a comparison with our theory. A similar plateau was observed for other long chain polymers, such as dextran with  $N=275$ ,  $x_f=0.5$  nm,  $x_u=0.56$  nm,  $\Delta E = 13.2$   $k_B T$  [10], for which the simple criterion  $f \approx \Delta E/\delta$  gives plateau forces in the range of  $\approx 900$  pN, as indeed observed [206]. From the theoretical point of view, another description of the cooperative response can be found in Refs. [192, 193, 194]. Nevertheless, our formulation is appropriate to obtain the force-extension curves also under Helmholtz conditions, as described below.

## 7.2.2 Helmholtz ensemble: non-cooperative response

While Gibbs ensemble statistics are sampled with a constant applied force, a dual situation can be realized by imposing the extension. The statistics of the fluctuating polymer in this latter scheme is a realization of the Helmholtz ensemble. As shown in Ref. [124], the corresponding partition function  $Z_r$  cannot be written in closed form and, as opposed to the Gibbs case, the corresponding extension  $r$  is non-linearly dependent on  $N$ . However, we showed that the partition functions in the two ensembles are formally related via a Laplace transform, and we demonstrated [124] that they lead to a common force-extension curve in the thermodynamic limit. It should be noted that any AFM or tweezers

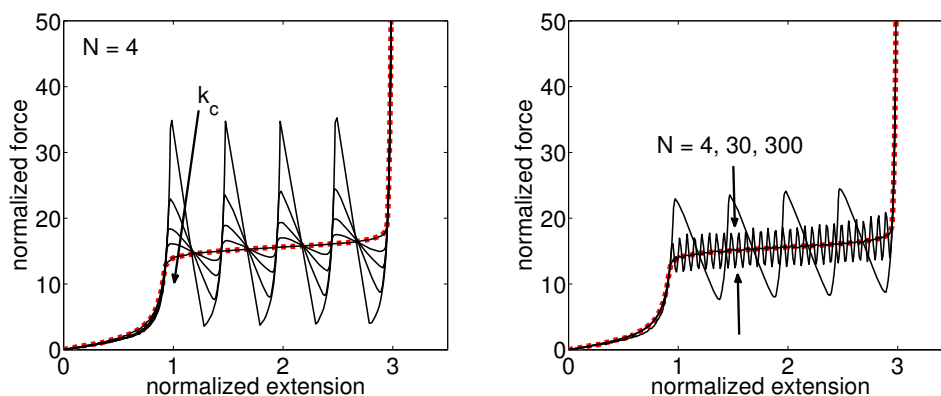


Figure 7.3: Monte Carlo force-extension curves at  $T=293$  K, for: (right panel) different decreasing values of the device spring constant  $k_c = 5, 2, 1, 0.5, 0.01$   $k_B T / (\text{nm})^2$  (from the top down) and  $N=4$ ; (left panel) increasing number of domains  $N = 4, 30, 300$  with  $k_c = 2$   $k_B T / (\text{nm})^2$ . The red dashed line corresponds to the Gibbs ensemble. The remaining parameters are  $\Delta E = 30$   $k_B T$ ,  $x_f = 2.5$  nm,  $x_u = 3x_f$  and  $k = 100$   $k_B T / (\text{nm})^2$ .

experiment falls in an intermediate regime between the two ideal extremes, of purely constant-force or constant-extension, since either constraint on the terminal domain of the chain is mediated by a mechanical device (such as the AFM cantilever, or the laser-bound microsphere, plus a molecular spacer providing adhesion). The device is characterized by its own effective elastic constant  $k_c$ , which is coupled in series to the chain of domain springs  $k$ . In

the limit of a soft device,  $k_c/k \rightarrow 0$ , the statistics of the coupled system reduces to the Gibbs ensemble for the isolated molecule fluctuating under a constant force. On the other hand, for a very stiff device,  $k_c/k \rightarrow \infty$ , one recovers the Helmholtz ensemble for the isolated molecule held at a fixed extension by the fluctuating force [168].

To describe such a situation, we adopt a Monte Carlo (MC) numerical approach, simulating the stretching of the chain produced by a device with a proper adjustable elastic stiffness. Compared to previous MC simulations of the polymer stretching [207, 208, 209, 210], we adopted a scheme ensuring a very efficient exploration of the bimodal configuration space [211, 212]. While in the Metropolis method one usually adopts a single step size for each MC move [124], in the present simulations we added a second step size, equal to  $\delta = x_f - x_u$  [211]. The first step size is used for most moves, while the second one is sampled for a small fraction of the moves, ensuring the overcoming of the barrier at any temperature, while still preserving the detailed balance [212]. In Figure 7.3, left panel, we report the results of the MC simulations at  $T=293$  K, for decreasing values of the  $k_c/k$  ratio, from 0.05, that is well within the Helmholtz statistics regime, down to  $1 \times 10^{-4}$ , i.e., approaching Gibbs ensemble statistics. The remaining parameters are set to  $N=4$ ,  $\Delta E=30 k_B T$ ,  $x_f=2.5$  nm,  $x_u=3x_f$  and  $k=100 k_B T/\text{nm}^2$ , which can be considered representative of a medium-sized, multi-domain chain protein. At large values of  $k_c/k$ , the domains exhibit a sequence of *independent* conformational transitions to the unfolded configuration, generating a series of  $N$  peaks (sawtooth pattern) that closely resemble the experimental results obtained for short chains (e.g., a titin fragment with  $N=8$ ,  $x_f=4$  nm,  $x_u=32$  nm,  $\Delta E=11.1 k_B T$  [206]). For  $k_c/k \rightarrow 0$  the peak-to-valley width,  $\Delta f$ , of the sawtooth shrinks and the curve approaches the  $k_c=0$  cooperative plateau of Gibbs statistics. In substantial agreement with this finding, pulling experiments on native titin by means of optical tweezers [213], having a very small equivalent  $k_c$  compared to the AFM one, do not reveal the sawtooth pattern, but rather a smooth, monotonic branch reminiscent of the horizontal plateau.

On the other hand, a similar asymptotic trend is observed (Fig. 7.3, right panel) when the chain length, i.e. the number of domains, is increased, at a fixed value of  $k_c/k$ . As  $N$  increases, the width  $\Delta f$  is decreased until, at a large enough  $N$ , the force-extension

*Monte Carlo  
approach*

*sawtooth  
pattern*

*plateau  
pattern*

*asymptotic  
trend*

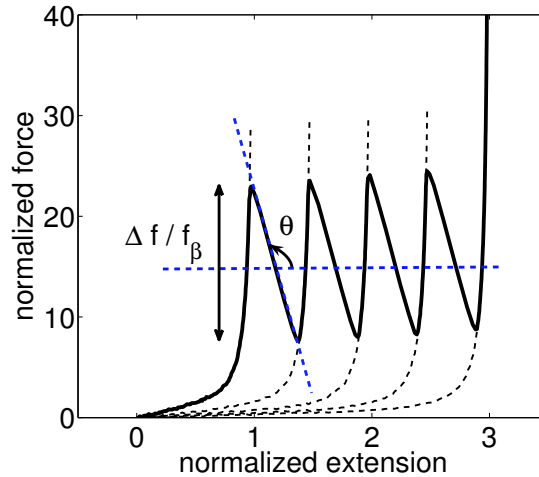


Figure 7.4: Definition of  $\Delta f$  and  $\theta$  for a typical force-extension curve with  $N = 4$ . Dashed lines for the growing branches fitted to FJC with increasing contour length.

curves approach again the plateau curve of the Gibbs ensemble. It is worth noting that a similar trend was observed in experiments performed on native titin, comprising several hundreds of Ig domains, for which the width  $\Delta f$  was of the order of 80 pN [62], compared to the much shorter 8-monomer titin, for which  $\Delta f > 200$  pN. The experiments performed on dextran, a long polysaccharide with  $N = 275$ , [10, 206] whose response to the applied force shows a plateau closer to the typical DNA-like behavior, can also be rationalized on this basis.

In summary, we proved that the macroscopically different behavior of small- $N$  polymers (such as titin) vs. long polymers (such as dextran, DNA), as well as experiments done on a same polymer but with devices having widely different stiffness, can be interpreted with the very same unifying model, interpolating between the two extremes of pure Gibbs or Helmholtz statistics. A similar dependence of the results on the type of loading devices has been found in recent literature for a one-dimensional chain of bi-stable elements [190, 191]: the authors prove that the system “snaps” for a soft device, while it “pops” for a hard device. Our results extend these previous ones by considering thermal fluctuations in the whole three-dimensional space.

*interpretation  
of the  
sawtooth  
pattern*

As observed by several authors, each branch of the sawtooth pattern can be nicely fitted by a sequence of FJC, or WLC curves (see Fig. 7.4, dashed lines) with a proper value of the persistence

length, up to the unfolding of each domain (see e.g. titin [62], spectrin [214], fibronectin [215], synaptotagmin [183]). Beyond this point, the force relaxes to a smaller value, until the next curve is met and the force can start rising again upon increasing displacement. By considering Fig. 7.4, we determine the position  $r_n$  of the peaks as follows: in correspondence of the  $n$ -th peak we have  $n - 1$  domains in the unfolded configuration (extension  $x_u$ ) and  $N - n + 1$  domains in the folded configuration (extension  $x_f$ ). Therefore

$$\frac{r_n}{Nx_f} = 1 + \frac{(n-1)(x_u - x_f)}{Nx_f} \quad (7.17)$$

for  $n = 1, \dots, N$  ( $n = N + 1$  corresponding to the final asymptote). We also note that the increasing parts of the force-extension curve (dashed lines in Fig. 7.4) can be represented by polymers with  $N$  domains described by simple harmonic potentials  $V(x) = (1/2)k(x - r_n/N)^2$ . Since the physical origin of the growing branch of the curves is well understood on the basis of FJC or WLC models, we analyzed the decreasing branch, as identified by the common width  $\Delta f$  and angle  $\theta$  in Fig. 7.4 which were extracted from our MC simulations as a function of  $N$  and  $k_c/k$ .

By looking at Fig. 7.5 (left panel), the peak-to-valley width shows a power-law decrease with the chain length,  $\Delta f \sim N^{-\alpha}$ , the exponent  $\alpha = 1.3$  being remarkably independent on the  $k_c/k$  ratio. This finding indicates that attainment of the thermodynamic limit is mainly dictated by the thermal force scale,  $f_\beta$ , and to a much lesser extent by other structural and chemical details of the polymer. It is worth noting that the value of the exponent is in agreement with previous results on mono-stable FJC and WLC models with extensible bonds [124].

*thermodynamic  
limit*

The plot on the right of Fig. 7.5 reports the behavior of  $\tan(\theta)$  as a function of the device stiffness,  $k_c$ . The observed linear dependence is another remarkable result, completely describing the transition between the two extremes (Gibbs and Helmholtz ensembles), while taking into account all the intermediate cases. For  $k_c/k \rightarrow \infty$  we have  $\tan(\theta) \rightarrow -\infty$  or, equivalently,  $\theta \rightarrow \pi/2$ . In other words, the decreasing branches of the force-extension curve must be exactly vertical in the case of the Helmholtz ensemble. Interestingly enough, as can be observed from Fig. 7.4, once the values of  $\Delta f$  and  $\theta$  are determined, it is possible to uniquely define the entire shape of the force-extension curve via a graphic

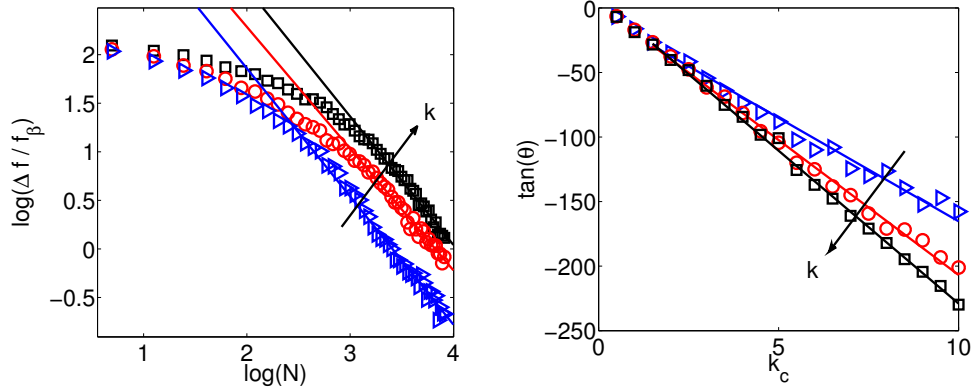


Figure 7.5: Left panel: plot of  $\log(\Delta f / f_\beta)$  vs.  $\log(N)$  for  $k_c=1 k_B T / (\text{nm})^2$  and  $k/k_c=20, 30, 100$  (blue, red and black line, respectively). Right panel: plot of  $\tan(\theta)$  vs.  $k_c$  for  $N=4$ , and the same  $k$  values. Remaining parameters  $\Delta E = 30 k_B T$ ,  $x_f = 2.5 \text{ nm}$ ,  $x_u = 3x_f$  and  $T=293 \text{ K}$ .

procedure, connecting each others the growing branches fitted to FJC (or WLC) with increasing contour length (dashed lines in Fig. 7.4).

### 7.3 OUTLINE OF THE RESULTS

Starting from experimental results on forced unfolding of multi-domain polymers, we developed a theory that explains these experiments by a unique universal model. As a matter of fact, various efforts have been made in this topic: experimental [10, 62, 180] and computational [195, 196] results showed the different behaviour of the force-extension curve for specific type of polymers, as proteins, polysaccharides, and nucleic acids. The majority of the results points out a number of difficulties in their interpretation [181], and makes suggestions for further experiments [182], even though, it appears clear the lack of universality in the presented models, which are often circumscribed to a specific type of molecules [183, 184]. One advantage of our approach is that it shows that the force-extension curves is universal with respect to the specification of any multi-domain polymer. This is due to the original interpretation of the two different mechanical behaviour discussed for the exactly same polymer chain. In fact, while experiments showed a different behaviour for different polymer chains, here we observed two different behaviours for the same polymer chain. A primary cause of the different elasticity is found on the

finite values of the ratio, between the stiffness of the domain and the one of the pulling device. On the other ground, considering the same type of polymer chain, but with different size, we observed as well the “sawtooth” and “plateau” response being recovered for different contour length. Apart from providing a unified picture for such apparently contrasting experimental situations, this framework and the presented results stress some important factors to take into account for a more accurate interpretation of a single molecule stretching experiment.



Part V

POLYMER CHAINS LOADED BY  
EXTERNAL FIELDS



## EFFECT OF A SEQUENCE OF FORCES ON MONOMERS CHAINS

---

### Contents

---

8.1	General theoretical framework	141
8.2	Freely-jointed chain under external field	146
8.2.1	Average values of positions	146
8.2.2	Covariances and variances of positions	152
8.3	Freely-jointed chain with elastic bonds	158
8.4	Worm-like chain under external field	161
8.5	Action of a pulling force not aligned with the external field	167
8.6	Outline of the results	171

---

We profusely discussed how modern methods for stretching single molecules provide a valuable insight about the response of polymers to external forces. Typically, mechanical methods allow the manipulation of a polymer molecule in two ways: the stretching of the chain by the direct action of an external force or by the application of an external field. If we consider homogeneous polymers (with all monomers described by the same effective elastic stiffness), then we obtain a uniform strain with the external force and a non-uniform strain with the applied field.

To exert an external force on a polymer fixed at one end, laser optical tweezers (LOTs) [3], magnetic tweezers (MTs) [4] or atomic force microscope (AFM) [5] can be used. Many experiments have been performed over a wide class of polymers with biological relevance, such as the nucleic acids (DNA, RNA) [6], allowing the stretching of the entire molecule and providing the reading and the mapping of genetic information along the chain [60, 61]. Furthermore, it has been possible to describe the elastic behaviour of single polymers consisting of domains which may exhibit transitions between different stable states [10, 62, 216].

Alternatively, it is possible to manipulate single molecules by an external field (see Sections 1.3 and 1.3.5). The flow field tech-

nique was extensively applied in single-molecule study of DNA elasticity [20] as well as to characterize the rheological properties of individual DNA molecules [90, 91, 92].

In order to understand the response of polymers to external fields and to study their statistics, some theoretical models have been proposed. As for the case of external applied forces, these models are typically based on the FJC and WLC schemes, generalized with the inclusion of the given applied field. Some studies have shown that in a weak external field the persistence length along the field direction is increased, while it is decreased in the perpendicular direction; moreover, as the external field becomes stronger, the effective persistence length grows exponentially with the field strength [14, 217, 218]. The behavior of a Gaussian chain in an elongational flow has been studied through the dumbbell model [219]. Other investigations under a constant velocity flow have shown that a flexible polymer displays three types of conformation: unperturbed at low velocity; “trumpet” shaped when partially stretched; “stem and flowers” shaped, with a completely stretched portion (the stem) and a series of blobs (the flowers), at larger loading [220, 221, 222]. Polymer models have been studied in elongational flows to analyze the coil stretching and chain retraction as a function of polymer and flow parameters, finding good agreement with experimental data [223, 224]. Conformational properties of semiflexible polymer chains in uniform force field were also studied for two-dimensional models [225]. Some important results have been obtained for the dynamic behavior of polymers containing positive and negative charges in the presence of external electrical fields [226, 227, 228, 229]. In spite of all these relevant efforts, it is yet a challenge to base on one same unified theoretical framework and understanding of all aspects of polymer mechanics in an external field.

In this Chapter we study the conformational and mechanical properties of flexible and semi-flexible non-branched polymer model chains tethered at one end and immersed in an external force field. This situation is useful to describe at least two physical conditions of interest: a polymer chain immersed in a fluid in a uniform motion (our model is valid only when the action of the fluid motion can be described by a distribution of given forces applied to all monomers) and an arbitrarily charged chain inserted in a uniform electric field.

We adopt both analytical (statistical mechanics [57, 96]) and numerical techniques (Monte Carlo simulations [177, 209]). While the analytical approach is useful to obtain the explicit partition function in some specific cases, Monte Carlo simulations are crucial to study more generic cases, inaccessible to analytical treatments. In particular, while we develop our theoretical framework starting from the more tractable FJC model, we take full profit from our MC simulations to extend our study also to the WLC model.

We first introduce the mathematical formalism adopted and we derive a generic form of the partition function in  $\mathfrak{R}^d$  for a generalized FJC model where the extensibility of the bonds is taken into account. Next, we find the two specific forms of the partition function for the 2D- and the 3D-case for the pure FJC polymer with non extensible bonds. Moreover, we obtain in both cases the variance and the covariance among the positions of the monomers. Generalization of previous results to the semi-flexible WLC model are then discussed. We present two closed-forms approximations for the 2D- and the 3D-case and the comparisons with MC simulations. Finally, we analyze the behavior of a polymer in an external field taking into account also an external force applied at the end of the chain. The case with the force not aligned with the field is particularly interesting and shows the power of the MC method.

## 8.1 GENERAL THEORETICAL FRAMEWORK

As argued in Ref.[230], for weak tension and weak external field, it is acceptable to model the polymer as a FJC model. This model breaks down only when the curvature of the conformation is very large because it ignores the consequent great bending energy. Since we will look upon this problem in the end of this Chapter, we now give way to the case of a FJC. In particular we consider a FJC with two additional hypothesis. Firstly we consider the possible extensibility of the bonds of the chain through a standard quadratic potential characterized by a given equilibrium length: such an extension mimics the possible stretching of the chemical bond between two adjacent monomers. If necessary, the extensibility of the bonds, here described by linear springs, can be easily extended to more complex, nonlinear springs [231]. Moreover, we take into account a series of arbitrary forces applied to

*series of  
arbitrary  
forces*

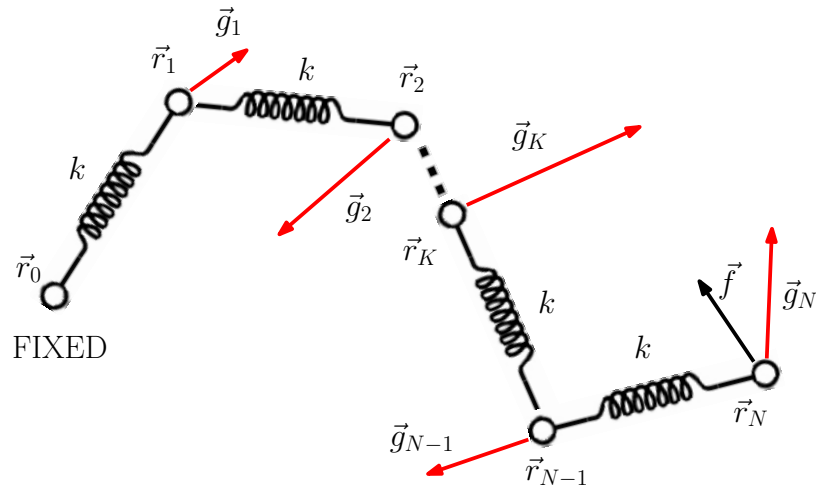


Figure 8.1: A polymer chain in an external field. The first monomer is clamped at position  $\vec{r}_0$  while the others are free to fluctuate. Each monomer is subjected to an external force  $\vec{g}_K$  (different in strength and direction for any  $K$ ): all these forces mimic an external field. Another external force, playing the role of a main pulling load,  $\vec{f}$ , is applied to the last monomer at the position  $\vec{r}_N$ .

each monomer: these actions mimic the effects of an external physical field applied to the system. In addition, we contemplate the presence of an arbitrary force applied to the terminal monomer of the chain. All calculations will be performed in  $\mathfrak{R}^d$  and we will specialize the results both in the 2D-case and in the 3D-case when needed. The idea is to write the complete form of the Hamiltonian of the system and to build up the corresponding statistical mechanics [124]. The starting point is therefore the calculation of the classical partition function. In fact, when this quantity is determined, it is possible to obtain the force-extension curve (the equation of state) through simple derivations.

*our model*

Let us consider a non-branched linear polymer with  $N$  monomers (see Fig. 8.1) at positions defined by  $\vec{r}_1, \dots, \vec{r}_N \in \mathfrak{R}^d$  (for considering  $d = 2$  or  $d = 3$  according to the specific problem of interest). To each monomer a given external force is applied and named  $\vec{g}_1, \dots, \vec{g}_N$ . Another external force, playing the role of main pulling load,  $\vec{f}$ , is applied to the last monomer at the position  $\vec{r}_N$ .

While the chain is clamped at position  $\mathbf{r}_0$ , the monomers are free to fluctuate. The Hamiltonian of the system is therefore given by

$$\begin{aligned} h = & \sum_{i=1}^N \frac{\mathbf{p}_i \cdot \mathbf{p}_i}{2m} + \frac{1}{2}k \sum_{K=1}^N (|\mathbf{r}_K - \mathbf{r}_{K-1}| - l)^2 \\ & - \sum_{K=1}^N \mathbf{g}_K \cdot \mathbf{r}_K - \mathbf{f} \cdot \mathbf{r}_N \end{aligned} \quad (8.1)$$

where  $\mathbf{p}_i$  are the linear momenta,  $m$  the mass of the monomers,  $k$  the spring constant of the inter-monomer interaction, and  $l$  the equilibrium length of the monomer-monomer bond. We search for the partition function of the system defined as:

$$Z_d = c \underbrace{\int_{\mathcal{R}^d} \dots \int_{\mathcal{R}^d}}_{2N\text{-times}} \exp\left(-\frac{h}{k_B T}\right) d\mathbf{r}_1 \dots d\mathbf{r}_N d\mathbf{p}_1 \dots d\mathbf{p}_N \quad (8.2)$$

*the  
generalized  
Gibbs  
partition  
function*

where  $c$  is a multiplicative constant which takes into account the number of microstates. As well known, the kinetic part can be straightforwardly integrated and it yields a further non-influencing multiplicative constant; then we can write the partition function as an integral over the positional space only. This integral can be easily handled through the standard change of variable

$$\begin{cases} \xi_1 = \mathbf{r}_1 - \mathbf{r}_0 \\ \xi_2 = \mathbf{r}_2 - \mathbf{r}_1 \\ \vdots \\ \xi_N = \mathbf{r}_N - \mathbf{r}_{N-1} \end{cases} \quad (8.3)$$

having the Jacobian determinant  $J = \left| \frac{\partial(\mathbf{r}_1 \dots \mathbf{r}_N)}{\partial(\xi_1 \dots \xi_N)} \right| = 1$ . We consider the terminal  $\mathbf{r}_0$  of the chain fixed in the origin of axes, i.e.  $\mathbf{r}_0 = \mathbf{0}$ . So, we cast the positions  $\mathbf{r}_i$  in terms of the variables  $\xi_J$  as follows

$$\begin{cases} \mathbf{r}_1 = \xi_1 + \mathbf{r}_0 = \xi_1 \\ \mathbf{r}_2 = \xi_2 + \mathbf{r}_1 = \xi_2 + \xi_1 \\ \vdots \\ \mathbf{r}_N = \xi_N + \xi_{N-1} + \dots + \xi_1 \end{cases} \quad (8.4)$$

By setting the general solution as  $\mathbf{r}_i = \sum_{k=1}^i \xi_k$ , the partition function becomes

$$\begin{aligned} Z_d &= c \underbrace{\int_{\mathfrak{R}^d} \dots \int_{\mathfrak{R}^d}}_{N\text{-times}} \exp \left[ -\frac{k}{2k_B T} \sum_{K=1}^N (|\xi_K| - l)^2 \right] \\ &\quad \times \exp \left[ \frac{1}{k_B T} \sum_{K=1}^N \mathbf{g}_K \cdot \sum_{J=1}^K \xi_J \right] \\ &\quad \times \exp \left[ \frac{1}{k_B T} \mathbf{f} \cdot \sum_{K=1}^N \xi_K \right] d\xi_1 \dots d\xi_N \end{aligned} \quad (8.5)$$

Inverting the two summation symbols

$$\sum_{K=1}^N \mathbf{g}_K \cdot \sum_{J=1}^K \xi_J = \sum_{K=1}^N \xi_K \cdot \sum_{i=K}^N \mathbf{g}_i \quad (8.6)$$

we obtain

$$\begin{aligned} Z_d &= c \underbrace{\int_{\mathfrak{R}^d} \dots \int_{\mathfrak{R}^d}}_{N\text{-times}} \exp \left[ -\frac{k}{2k_B T} \sum_{K=1}^N (|\xi_K| - l)^2 \right] \\ &\quad \times \exp \left[ \frac{1}{k_B T} \sum_{K=1}^N \xi_K \cdot \sum_{i=K}^N \mathbf{g}_i \right] \exp \left[ \frac{1}{k_B T} \mathbf{f} \cdot \sum_{K=1}^N \xi_K \right] d\xi_1 \dots d\xi_N \\ &= c \prod_{K=1}^N \int_{\mathfrak{R}^d} \exp \left[ -\frac{k}{2k_B T} (|\xi_K| - l)^2 \right] \exp \left[ \frac{1}{k_B T} \left( \mathbf{f} + \sum_{i=K}^N \mathbf{g}_i \right) \cdot \xi_K \right] d\xi_K \\ &= c \prod_{K=1}^N \int_{\mathfrak{R}^d} e^{-a(|\xi|-l)^2} e^{\mathbf{v}_K \cdot \xi} d\xi \end{aligned} \quad (8.7)$$

where

$$a = \frac{k}{2k_B T} > 0 \quad (8.8)$$

$$\mathbf{v}_K = \frac{1}{k_B T} \left( \mathbf{f} + \sum_{i=K}^N \mathbf{g}_i \right) \quad (8.9)$$

It exists a deep conceptual connection between the last integral for the partition function and the theory of the  $d$ -dimensional Fourier

transforms. The Fourier integral of an arbitrary function  $f(\xi)$  is defined as

$$F(\omega) = \int_{\mathfrak{R}^d} f(\xi) e^{-i\omega \cdot \xi} d\xi \quad (8.10)$$

with inverse transform given by

$$f(\xi) = \frac{1}{(2\pi)^d} \int_{\mathfrak{R}^d} F(\omega) e^{i\omega \cdot \xi} d\omega \quad (8.11)$$

If we consider

$$f(\xi) = e^{-a(|\xi|-1)^2} \quad (8.12)$$

*connection  
with the  
Fourier  
transform*

it is easy to realize that the integral in Eq. (8.7) is the Fourier transform of  $f(\xi)$  calculated for  $\omega = i\mathbf{V}_K$ , i.e.

$$Z_d = c \prod_{K=1}^N F(i\mathbf{V}_K) \quad (8.13)$$

with  $a$  e  $\mathbf{V}_K$  defined respectively in Eq. (8.8) and Eq. (8.9). It is important to remark that the function in Eq. (8.12) has a spherical symmetry (i.e. it depends only on the length of the vector  $\xi$ ) and, therefore, also its Fourier transform  $F(\omega)$  exhibits the spherical symmetry, depending only on the quantity  $|\omega|$  in the transformed domain. In fact, for such spherically-symmetric functions it holds that: if  $f(\xi) = f(|\xi|)$  then  $F(\omega) = F(|\omega|)$ . Furthermore, we have that

*Fourier  
transform  
for spherically  
symmetric  
functions*

$$F(\Omega) = \int_0^{+\infty} 2\pi\rho f(\rho) \left(\frac{2\pi\rho}{\Omega}\right)^{\frac{d}{2}-1} J_{\frac{d}{2}-1}(\rho\Omega) d\rho \quad (8.14)$$

for  $d = 2n$  (even), and

$$F(\Omega) = \int_0^{+\infty} 4\pi\rho^2 f(\rho) \left(\frac{2\pi\rho}{\Omega}\right)^{\frac{d-3}{2}} j_{\frac{d-3}{2}}(\rho\Omega) d\rho \quad (8.15)$$

for  $d = 2n + 1$  (odd), where  $\rho = |\xi|$  and  $\Omega = |\omega|$  [232] (see Appendix A.2 for a complete proof). Here  $J_\nu(z)$  and  $j_\nu(z)$  are the cylindrical and spherical Bessel functions of the first kind respectively, correlated by the standard relation  $j_\nu(z) = \sqrt{\frac{\pi}{2z}} J_{\nu+\frac{1}{2}}(z)$  [175, 233]. In our calculations we have to set  $\omega = i\mathbf{V}_K$  and, therefore, we obtain  $\Omega = i|\mathbf{V}_K|$ . Moreover, when the argument of  $J_\nu(z)$  and  $j_\nu(z)$

is supposed imaginary we obtain the modified Bessel functions of the first kind [175, 233]

$$\begin{aligned} I_\nu(z) &= (i)^{-\nu} J_\nu(iz) \\ i_\nu(z) &= (i)^{-\nu} j_\nu(iz) \end{aligned} \quad (8.16)$$

For example we have the explicit expression  $j_0(z) = \frac{\sin z}{z}$  and  $i_0(z) = \frac{\sinh z}{z}$  while, on the contrary,  $I_0(z)$  and  $J_0(z)$  cannot be written in closed form. So, for  $d$  even we eventually obtain

$$\frac{F(i\mathbf{V}_K)}{2\pi} = \int_0^{+\infty} \rho e^{-a(\rho-1)^2} \left( \frac{2\pi\rho}{|\mathbf{V}_K|} \right)^{\frac{d-2}{2}} I_{\frac{d-2}{2}}(\rho|\mathbf{V}_K|) d\rho \quad (8.17)$$

and, on the other hand, for  $d$  odd we have

$$\frac{F(i\mathbf{V}_K)}{4\pi} = \int_0^{+\infty} \rho^2 e^{-a(\rho-1)^2} \left( \frac{2\pi\rho}{|\mathbf{V}_K|} \right)^{\frac{d-3}{2}} i_{\frac{d-3}{2}}(\rho|\mathbf{V}_K|) d\rho \quad (8.18)$$

*partition  
functions  
in terms of  
Bessel  
functions*

Finally, by using Eq. (8.13), the partition function is given by

$$Z_d = c \prod_{K=1}^N \int_0^{+\infty} \rho e^{-a(\rho-1)^2} \left( \frac{\rho}{|\mathbf{V}_K|} \right)^{\frac{d-2}{2}} I_{\frac{d-2}{2}}(\rho|\mathbf{V}_K|) d\rho \quad (8.19)$$

for  $d$  even, and

$$Z_d = c \prod_{K=1}^N \int_0^{+\infty} \rho^2 e^{-a(\rho-1)^2} \left( \frac{\rho}{|\mathbf{V}_K|} \right)^{\frac{d-3}{2}} i_{\frac{d-3}{2}}(\rho|\mathbf{V}_K|) d\rho \quad (8.20)$$

for  $d$  odd, where  $a$  and  $\mathbf{V}_K$  are given in Eqs.(8.8) and (8.9). In the framework of statistical mechanics, the knowledge of the partition function allows to determine all needed expected values describing the statistics of the chain (i.e., average values of the positions, variances of the positions and so on).

## 8.2 FREELY-JOINTED CHAIN UNDER EXTERNAL FIELD

### 8.2.1 Average values of positions

In the previous section we obtained the general expression of the partition function for the case where the extensibility of the bonds is taken into account. This is described by the parameter  $k$ ,

which characterizes the elastic bond between adjacent monomers. In the present Section we want to study the effects of an arbitrary distribution of forces on a pure freely jointed chain model (FJC). Therefore we need to obtain the specific form of the partition function in the case of rigid bonds of fixed length  $l$ . From the mathematical point of view it means that we will consider  $k \rightarrow \infty$ , a condition representing a inextensible spring. Because of the relation  $\sqrt{\frac{\alpha}{\pi}} e^{-\alpha x^2} = \delta(x)$  when  $\alpha \rightarrow \infty$  we may determine the limit of Eq. (8.19) and Eq. (8.20) for  $a \rightarrow \infty$  (i.e. for  $k \rightarrow \infty$ , FJC limit). Since the arbitrariness of the constant  $c$ , we may consider in Eqs. (8.19) and (8.20) a multiplicative constant term  $(\sqrt{\frac{a}{\pi}})^N$ . Then, by using the translated property  $\sqrt{\frac{a}{\pi}} e^{-a(\rho-l)^2} \rightarrow \delta(\rho-l)$  for  $a \rightarrow \infty$  we perform all the integrals thereby obtaining

$$Z_d = c \prod_{k=1}^N \frac{1}{|\mathbf{V}_k|^{\frac{d-2}{2}}} I_{\frac{d-2}{2}}(l|\mathbf{V}_k|) \quad d \text{ even} \quad (8.21)$$

$$Z_d = c \prod_{k=1}^N \frac{1}{|\mathbf{V}_k|^{\frac{d-3}{2}}} i_{\frac{d-3}{2}}(l|\mathbf{V}_k|) \quad d \text{ odd} \quad (8.22)$$

Similar forms for the partition function can be found in Ref. [44] where, however, the external field was not taken into account. A different important analysis concerning the determination of the partition function for the FJC model can be found in literature [234, 235, 236]. In these investigations all holonomic constraints have been explicitly considered. In particular, for  $d = 2$  we have

$$Z_2 = c \prod_{k=1}^N I_0 \left( \frac{l}{k_B T} \left| \mathbf{f} + \sum_{i=K}^N \mathbf{g}_i \right| \right) \quad (8.23)$$

while for  $d = 3$  we obtain

$$Z_3 = c \prod_{k=1}^N \frac{\sinh \left( \frac{l}{k_B T} \left| \mathbf{f} + \sum_{i=K}^N \mathbf{g}_i \right| \right)}{\frac{l}{k_B T} \left| \mathbf{f} + \sum_{i=K}^N \mathbf{g}_i \right|} \quad (8.24)$$

All the expressions given in Eqs.(8.21), (8.22), (8.23), (8.24) can be summarized in the general form

$$Z_d = c \prod_{k=1}^N f(|\mathbf{V}_k|) \quad (8.25)$$

*FJC inextensible model*

*d-dimensional FJC partition function*

*2D and 3D partition functions*

with a suitable function  $f(x)$ . By using this expression of the partition function we can find the average position of the  $i$ -th monomer of the chain; indeed, from the definition of the Hamiltonian in Eq. (8.1) we state that  $\mathbf{r}_i = -\frac{\partial h}{\partial \mathbf{g}_i}$  and, therefore, we get

$$\langle \mathbf{r}_i \rangle = k_B T \frac{\partial}{\partial \mathbf{g}_i} \ln Z_d \quad (8.26)$$

*shape of  
the polymer*

which represents the shape of the polymer chain under the effects of the external field  $\mathbf{g}_i$  and the applied force  $\mathbf{f}$ . Now we can substitute Eq. (8.25) into Eq. (8.26), obtaining

$$\begin{aligned} \langle \mathbf{r}_i \rangle &= k_B T \frac{\partial}{\partial \mathbf{g}_i} \ln \left[ c \prod_{K=1}^N f(|\mathbf{V}_K|) \right] \quad (8.27) \\ &= k_B T \frac{\partial}{\partial \mathbf{g}_i} \left[ \ln c + \sum_{K=1}^N \ln f(|\mathbf{V}_K|) \right] \\ &= k_B T \sum_{K=1}^N \frac{\partial}{\partial \mathbf{g}_i} \ln f(|\mathbf{V}_K|) \\ &= k_B T \sum_{K=1}^N \frac{1}{f(x)} \frac{\partial f(x)}{\partial x} \frac{\partial x}{\partial \mathbf{g}_i} \end{aligned}$$

where we have defined  $x = |\mathbf{V}_K|$ ; we calculate  $\frac{\partial x}{\partial \mathbf{g}_i}$  as follows:

$$\begin{aligned} \frac{\partial x}{\partial \mathbf{g}_i} &= \frac{\partial}{\partial \mathbf{g}_i} \sqrt{\mathbf{V}_K \cdot \mathbf{V}_K} = \frac{2\mathbf{V}_K}{2\sqrt{\mathbf{V}_K \cdot \mathbf{V}_K}} \frac{\partial \mathbf{V}_K}{\partial \mathbf{g}_i} \quad (8.28) \\ &= \frac{\mathbf{V}_K}{\sqrt{\mathbf{V}_K \cdot \mathbf{V}_K}} \frac{\partial}{\partial \mathbf{g}_i} \left[ \frac{1}{k_B T} \left( \mathbf{f} + \sum_{J=K}^N \mathbf{g}_J \right) \right] \\ &= \frac{1}{k_B T} \frac{\mathbf{V}_K}{|\mathbf{V}_K|} \sum_{J=K}^N \delta_{iJ} \end{aligned}$$

we observe that  $\sum_{J=K}^N \delta_{iJ} = \delta_{iK} + \delta_{iK+1} + \dots + \delta_{iN}$  is equal to 1 if  $k \leq i$  and equal to 0 elsewhere. Therefore, by substituting Eq. (8.28) in Eq. (8.27) we obtain

$$\langle \mathbf{r}_i \rangle = \sum_{K=1}^i \frac{\mathbf{V}_K}{|\mathbf{V}_K|} \left[ \frac{1}{f(x)} \frac{\partial f(x)}{\partial x} \right]_{x=|\mathbf{V}_K|} \quad (8.29)$$

In the 2D-case we have  $f(x) = I_0(lx)$  and therefore

$$\frac{1}{f(x)} \frac{\partial f(x)}{\partial x} = l \frac{I_1(lx)}{I_0(lx)} \quad (8.30)$$

where  $\mathbf{V}_K = \frac{1}{k_B T} \left( \mathbf{f} + \sum_{J=K}^N \mathbf{g}_J \right)$  and  $x = |\mathbf{V}_K|$ .

In the end we obtain

$$\langle \mathbf{r}_i \rangle = l \sum_{K=1}^i \frac{I_1 \left( \frac{l}{k_B T} \left| \mathbf{f} + \sum_{J=K}^N \mathbf{g}_J \right| \right)}{I_0 \left( \frac{l}{k_B T} \left| \mathbf{f} + \sum_{J=K}^N \mathbf{g}_J \right| \right)} \frac{\mathbf{f} + \sum_{J=K}^N \mathbf{g}_J}{\left| \mathbf{f} + \sum_{J=K}^N \mathbf{g}_J \right|} \quad (8.31)$$

*2D average  
value of  
positions*

For such a 2D case, by applying Eq. (8.31), the average values of the longitudinal component of the positions have been calculated and are plotted in Fig. 8.2 as a function of the chain length  $N$  and the field strength  $g$ . We have considered only the action of an external uniform field with  $\mathbf{g}_J = \mathbf{g}$  and amplitude  $g$ .

Although this case lends itself to a full analytical solution, numerical simulations were also performed by using a conventional implementation of the Metropolis version of the Monte Carlo algorithm [177]. The initial state of the chain is defined by a set of randomly chosen positions. The displacement extent of each step governs the efficiency of the configurational space sampling. Therefore, we analysed several runs in order to optimize its value [125, 126]. The perfect agreement between the theory and the MC simulations provides a strict check of the numerical procedure, to be used in the foregoing.

*Monte Carlo  
method*

On the other hand, in 3D we have  $f(x) = \frac{\sinh(lx)}{lx}$ , and deriving

$$\begin{aligned} \frac{1}{f(x)} \frac{\partial f(x)}{\partial x} &= \frac{\partial}{\partial x} \ln f(x) = \frac{\partial}{\partial x} \ln \left( \frac{\sinh(lx)}{lx} \right) \\ &= \frac{\partial}{\partial x} [\ln \sinh(lx) - \ln(lx)] = l \frac{\cosh(lx)}{\sinh(lx)} - \frac{1}{lx} = l \mathcal{L}(lx) \end{aligned} \quad (8.32)$$

In the end we obtain

$$\langle \mathbf{r}_i \rangle = l \sum_{K=1}^i \mathcal{L} \left( \frac{l}{k_B T} \left| \mathbf{f} + \sum_{J=K}^N \mathbf{g}_J \right| \right) \frac{\mathbf{f} + \sum_{J=K}^N \mathbf{g}_J}{\left| \mathbf{f} + \sum_{J=K}^N \mathbf{g}_J \right|} \quad (8.33)$$

*3D average  
value of  
positions*

where  $\mathcal{L}(x) = \coth x - \frac{1}{x}$  is the Langevin function. By using Eq. (8.33), as before, it is possible to plot the average values of the

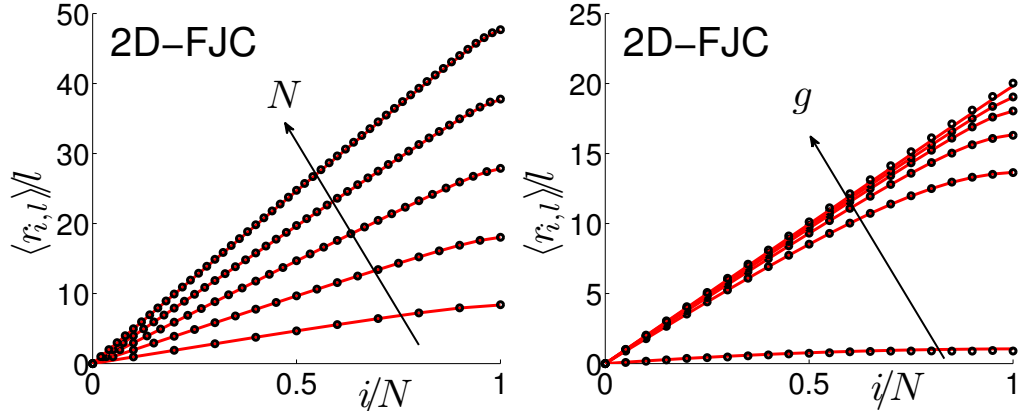


Figure 8.2: Average values of the longitudinal component of the positions induced by the external field for the 2D FJC case. The red solid lines correspond to the analytical results Eqs.(8.31) and (8.36), MC results are superimposed in black circles. Left panel: each curve corresponds to different chain lengths  $N = 10, 20, 30, 40, 50$  for a fixed value  $gl/(k_B T) = 1$  (e.g., corresponding to  $l = 1\text{nm}$ ,  $g = 4\text{pN}$  at  $T = 293\text{K}$ ). Right panel: each curve corresponds to the different values  $gl/(k_B T) = 0.1, 0.25, 0.5, 1, 2, 10$  for a fixed chain length  $N = 20$ .

longitudinal component of the positions for the 3D case (Fig. 8.3). Also in this case we adopted a uniform field  $g$  and the good agreement with the MC simulations is evident. As particular case, if there is only the force  $f$  applied to the system we obtain the standard scalar force-extension curves linking  $r = |\langle \mathbf{r}_N \rangle|$  with  $f = |f|$ . In 2D we have

*2D and 3D  
single external  
force equations*

$$\frac{r}{lN} = \frac{I_1\left(\frac{lf}{k_B T}\right)}{I_0\left(\frac{lf}{k_B T}\right)} \quad (8.34)$$

in agreement with recent results, [178] while in 3D we obtain

$$\frac{r}{lN} = \mathcal{L}\left(\frac{lf}{k_B T}\right) \quad (8.35)$$

which is a classical result [16, 124]. The simple results in Eqs.(8.34) and (8.35) have been used to obtain the limiting behaviors under low ( $f \rightarrow 0$ ) and high ( $f \rightarrow \infty$ ) values of the applied force, as shown in Table 3.

Building on such first results we now focus on some particular interesting approximations. More specifically, it can be interesting to find approximate results for the case of a homogeneous field

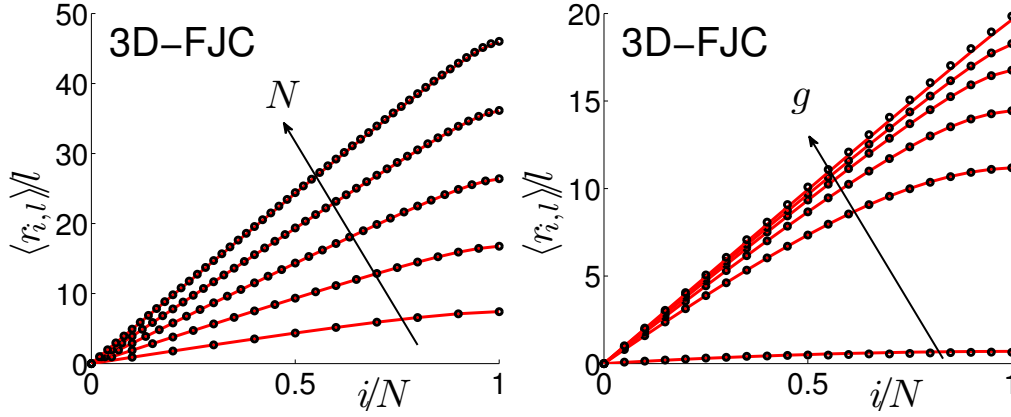


Figure 8.3: Average values of the longitudinal component of the positions induced by the external field for the 3D FJC case. The red solid lines correspond to the analytical results Eqs.(8.33) and (8.37), MC results are superimposed in black circles. Left panel: each curve corresponds to different chain lengths  $N = 10, 20, 30, 40, 50$  for a fixed value  $gl/(k_B T) = 1$ . Right panel: each curve corresponds to the different values  $gl/(k_B T) = 0.1, 0.25, 0.5, 1, 2, 10$  for a fixed chain length  $N = 20$ .

and no end-force,  $\mathbf{f} = 0$  and  $\mathbf{g}_J = \mathbf{g}$  for any  $J$ . In this case we search for the scalar relation between  $r = |\langle \mathbf{r}_N \rangle|$  and  $g = |\mathbf{g}|$ . In the 2D case, from Eq. (8.31), we have

$$\begin{aligned}
 \frac{r}{lN} &= \frac{1}{N} \sum_{k=1}^N \frac{I_1\left(\frac{lg}{k_B T}(N-k+1)\right)}{I_0\left(\frac{lg}{k_B T}(N-k+1)\right)} \\
 &\simeq \frac{1}{N} \int_0^N \frac{I_1\left(\frac{lg}{k_B T}(N-x+1)\right)}{I_0\left(\frac{lg}{k_B T}(N-x+1)\right)} dx \\
 &= \frac{1}{N} \frac{1}{\frac{lg}{k_B T}} \log \frac{I_0\left(\frac{lg}{k_B T}(N+1)\right)}{I_0\left(\frac{lg}{k_B T}\right)} \quad (8.36)
 \end{aligned}$$

On the other hand, for the 3D case we obtain

*2D -FJC  
force-extension  
curve  
interpolation*

*3D -FJC  
force-extension  
curve  
interpolation*

$$\begin{aligned}
\frac{r}{lN} &= \frac{1}{N} \sum_{k=1}^N \mathcal{L} \left( \frac{l}{k_B T} (N - k + 1) \right) \\
&\simeq \frac{1}{N} \int_0^N \mathcal{L} \left( \frac{l}{k_B T} (N - x + 1) \right) dx \\
&= \frac{1}{N} \frac{1}{\frac{lg}{k_B T}} \log \frac{e^{2 \frac{lg}{k_B T} (N+1)} - 1}{(N+1) \left( e^{2 \frac{lg}{k_B T}} - 1 \right)} - 1 \tag{8.37}
\end{aligned}$$

We have usefully exploited the fact that, for large  $N$ , the sums can be approximately substituted with the corresponding integrals, which are easier to be handled. The closed-form expressions given in Eqs.(8.36) and (8.37) are very useful to obtain the limiting behaviors of the polymer under low ( $g \rightarrow 0$ ) and high ( $g \rightarrow \infty$ ) values of the applied field, as shown in Table 3. Moreover, we have verified the validity of Eqs.(8.36) and (8.37) through a series of comparisons with MC results (see Fig. 8.6 in the next Section for details).

### 8.2.2 Covariances and variances of positions

In this Section, we search for the covariance among the positions of the monomers. It is important to evaluate such a quantity in order to estimate the variance of a given position (measuring the width of the probability density around its average value) and the correlation among different monomer positions (measuring the persistence of some geometrical features along the chain). In order to do this, we identify the  $\alpha$ -th component of the  $i$ -th monomer as  $r_{i\alpha}$ . The covariance of the generic monomer simply defined as (it represent the expectation value of the second order):

$$\begin{aligned}
\text{Cov}(r_{i\alpha}, r_{j\beta}) &= \langle (r_{i\alpha} - \langle r_{i\alpha} \rangle)(r_{j\beta} - \langle r_{j\beta} \rangle) \rangle \tag{8.38} \\
&= \langle r_{i\alpha} r_{j\beta} - \langle r_{i\alpha} \rangle r_{j\beta} - r_{i\alpha} \langle r_{j\beta} \rangle + \langle r_{i\alpha} \rangle \langle r_{j\beta} \rangle \rangle \\
&= \langle r_{i\alpha} r_{j\beta} \rangle - \langle r_{i\alpha} \rangle \langle r_{j\beta} \rangle.
\end{aligned}$$

It is important to evaluate such a quantity in order to estimate the variance of a given position (measuring the width of the probability density around its average value) and the correlation among different monomer positions (measuring the persistence of some geometrical features along the chain). Taking the derivative of the

partition function with respect to the  $\alpha$  and the  $\beta$  components of the force vectors  $\mathbf{g}_i$  and  $\mathbf{g}_j$  we can solve the problem as follows. We consider the standard expression for the partition function

$$Z = c \iint e^{-\frac{\mathbf{h}}{k_B T}} d\mathbf{q} d\mathbf{p}, \quad (8.39)$$

and we obtain the successive derivatives

$$\begin{aligned} \frac{\partial Z}{\partial g_{i\alpha}} &= c \iint -\frac{1}{k_B T} \frac{\partial \mathbf{h}}{\partial g_{i\alpha}} e^{-\frac{\mathbf{h}}{k_B T}} d\mathbf{q} d\mathbf{p} \\ &= \frac{c}{k_B T} \iint r_{i\alpha} e^{-\frac{\mathbf{h}}{k_B T}} d\mathbf{q} d\mathbf{p}, \end{aligned} \quad (8.40)$$

$$\begin{aligned} \frac{\partial^2 Z}{\partial g_{i\alpha} \partial g_{j\beta}} &= c \iint -\frac{r_{i\alpha}}{(k_B T)^2} \frac{\partial \mathbf{h}}{\partial g_{j\beta}} e^{-\frac{\mathbf{h}}{k_B T}} d\mathbf{q} d\mathbf{p} \\ &= \frac{c}{(k_B T)^2} \iint r_{i\alpha} r_{j\beta} e^{-\frac{\mathbf{h}}{k_B T}} d\mathbf{q} d\mathbf{p}. \end{aligned} \quad (8.41)$$

Noting that the probability density can be written as

$$\rho = c \frac{e^{-\frac{\mathbf{h}}{k_B T}}}{Z}, \quad (8.42)$$

we can obtain the following expression

$$\begin{aligned} \langle r_{i\alpha} r_{j\beta} \rangle &= \iint r_{i\alpha} r_{j\beta} \rho d\mathbf{q} d\mathbf{p} \\ &= c \iint r_{i\alpha} r_{j\beta} \frac{e^{-\frac{\mathbf{h}}{k_B T}}}{Z} d\mathbf{q} d\mathbf{p} \\ &= \frac{(k_B T)^2}{Z} \frac{\partial^2 Z}{\partial g_{i\alpha} \partial g_{j\beta}} \\ &= \frac{(k_B T)^2}{Z} \frac{\partial}{\partial g_{i\alpha}} \frac{\partial Z}{\partial g_{j\beta}} \\ &= \frac{(k_B T)^2}{Z} \frac{\partial}{\partial g_{i\alpha}} \left( Z \frac{\partial}{\partial g_{j\beta}} \ln Z \right) \\ &= \frac{(k_B T)^2}{Z} \left( \frac{\partial Z}{\partial g_{i\alpha}} \frac{\partial}{\partial g_{j\beta}} \ln Z + Z \frac{\partial^2}{\partial g_{i\alpha} \partial g_{j\beta}} \ln Z \right) \\ &= (k_B T)^2 \left( \frac{\partial \ln Z}{\partial g_{i\alpha}} \frac{\partial \ln Z}{\partial g_{j\beta}} + \frac{\partial^2 \ln Z}{\partial g_{i\alpha} \partial g_{j\beta}} \right). \end{aligned} \quad (8.43)$$

Now substituting Eq. (8.25) in Eq. (8.43) we have

$$\begin{aligned}
\langle r_{i\alpha} r_{j\beta} \rangle &= (k_B T)^2 \left[ \left( \frac{\partial}{\partial g_{i\alpha}} \sum_{k=1}^N \ln f(|\mathbf{V}_k|) \right) \left( \frac{\partial}{\partial g_{j\beta}} \sum_{h=1}^N \ln f(|\mathbf{V}_h|) \right) \right. \\
&\quad \left. + \frac{\partial^2}{\partial g_{i\alpha} \partial g_{j\beta}} \sum_{k=1}^N \ln f(|\mathbf{V}_k|) \right] \\
&= (k_B T)^2 \left( \frac{\langle r_{i\alpha} \rangle \langle r_{j\beta} \rangle}{k_B T} + \frac{\partial}{\partial g_{j\beta}} \left\langle \frac{r_{i\alpha}}{k_B T} \right\rangle \right) \\
&= \langle r_{i\alpha} \rangle \langle r_{j\beta} \rangle + k_B T \frac{\partial}{\partial g_{j\beta}} \langle r_{i\alpha} \rangle,
\end{aligned}$$

but we can simply determine that

$$\frac{\partial}{\partial g_{j\beta}} \langle r_{i\alpha} \rangle = \frac{\partial}{\partial g_{j\beta}} \sum_{k=1}^i \frac{\mathbf{V}_k \cdot \mathbf{e}_\alpha}{|\mathbf{V}_k|} \left[ \frac{1}{f(x)} \frac{\partial f(x)}{\partial x} \right]_{x=|\mathbf{V}_k|}, \quad (8.44)$$

where we have defined the unit vector  $\mathbf{e}_\alpha$  as the basis of the orthonormal reference frame. Being

$$\mathbf{V}_k \cdot \mathbf{e}_\alpha = \frac{1}{k_B T} \left( f_\alpha + \sum_{i=k}^N g_{i\alpha} \right), \quad (8.45)$$

we simply obtain

$$\begin{aligned}
\frac{\partial}{\partial g_{j\beta}} \langle r_{i\alpha} \rangle &= \frac{\partial}{\partial g_{j\beta}} \sum_{k=1}^i \frac{\frac{1}{k_B T} \left( f_\alpha + \sum_{l=k}^N g_{l\alpha} \right) f'(|\mathbf{V}_k|)}{|\mathbf{V}_k| f(|\mathbf{V}_k|)} \\
&= \frac{1}{k_B T} \sum_{k=1}^i \frac{1}{|\mathbf{V}_k| f(|\mathbf{V}_k|)} \\
&\quad \times \left\{ \sum_{l=k}^N \frac{\partial g_{l\alpha}}{\partial g_{j\beta}} f'(|\mathbf{V}_k|) + f''(|\mathbf{V}_k|) \frac{\partial |\mathbf{V}_k|}{\partial g_{j\beta}} \left( f_\alpha + \sum_{l=k}^N g_{l\alpha} \right) \right. \\
&\quad \left. - \left( f_\alpha + \sum_{l=k}^N g_{l\alpha} \right) f'(|\mathbf{V}_k|) \left[ \frac{\partial |\mathbf{V}_k|}{\partial g_{j\beta}} \frac{1}{|\mathbf{V}_k|} + \frac{f'(|\mathbf{V}_k|)}{f(|\mathbf{V}_k|)} \frac{\partial |\mathbf{V}_k|}{\partial g_{j\beta}} \right] \right\}, \quad (8.46)
\end{aligned}$$

and noting that

$$\frac{\partial |\mathbf{V}_k|}{\partial g_{j\beta}} = \frac{1}{k_B T} \frac{\mathbf{V}_k \cdot \mathbf{e}_\beta}{|\mathbf{V}_k|} \sum_{q=k}^N \delta_{jq}, \quad (8.47)$$

we also have

$$\begin{aligned}
k_B T \frac{\partial}{\partial g_{J\beta}} \langle r_{i\alpha} \rangle &= \sum_{K=1}^{\min\{i,J\}} \frac{1}{|\mathbf{V}_K| f(|\mathbf{V}_K|)} \\
&\times \left\{ \delta_{\alpha\beta} f'(|\mathbf{V}_K|) + f''(|\mathbf{V}_K|) \frac{V_{K\alpha} V_{K\beta}}{|\mathbf{V}_K|} \right. \\
&\left. - V_{K\alpha} f'(|\mathbf{V}_K|) \frac{V_{K\beta}}{|\mathbf{V}_K|^2} - V_{K\alpha} \frac{f'(|\mathbf{V}_K|)^2 V_{K\beta}}{f(|\mathbf{V}_K|) |\mathbf{V}_K|} \right\}.
\end{aligned} \tag{8.48}$$

Ordering the terms we finally obtain

$$\begin{aligned}
\langle r_{i\alpha} r_{J\beta} \rangle - \langle r_{i\alpha} \rangle \langle r_{J\beta} \rangle &= k_B T \frac{\partial}{\partial g_{J\beta}} \langle r_{i\alpha} \rangle \\
&= \sum_{K=1}^{\min\{i,J\}} \frac{\delta_{\alpha\beta} f'(|\mathbf{V}_K|)}{|\mathbf{V}_K| f(|\mathbf{V}_K|)} + \sum_{K=1}^{\min\{i,J\}} \frac{V_{K\alpha} V_{K\beta}}{|\mathbf{V}_K|^2 f(|\mathbf{V}_K|)} \\
&\times \left\{ f''(|\mathbf{V}_K|) - \frac{f'(|\mathbf{V}_K|)}{|\mathbf{V}_K|} - \frac{f'(|\mathbf{V}_K|)^2}{f(|\mathbf{V}_K|)} \right\}.
\end{aligned} \tag{8.49}$$

So the important result is

*covariances*

$$\begin{aligned}
\text{Cov}(r_{i\alpha}, r_{J\beta}) &= \sum_{K=1}^{\min\{i,J\}} \frac{\delta_{\alpha\beta} f'(|\mathbf{V}_K|)}{|\mathbf{V}_K| f(|\mathbf{V}_K|)} + \sum_{K=1}^{\min\{i,J\}} \frac{V_{K\alpha} V_{K\beta}}{|\mathbf{V}_K|^2 f(|\mathbf{V}_K|)} \\
&\times \left\{ f''(|\mathbf{V}_K|) - \frac{f'(|\mathbf{V}_K|)}{|\mathbf{V}_K|} - \frac{f'(|\mathbf{V}_K|)^2}{f(|\mathbf{V}_K|)} \right\}.
\end{aligned}$$

If we look at the variance of a single component of a single position ( $i = J$ ,  $\alpha = \beta$ ) we have the simpler result

*variances*

$$\begin{aligned}
\sigma_{i\alpha}^2 &= \sum_{K=1}^i \frac{f'(|\mathbf{V}_K|)}{|\mathbf{V}_K| f(|\mathbf{V}_K|)} + \sum_{K=1}^i \frac{V_{K\alpha}^2}{|\mathbf{V}_K|^2 f(|\mathbf{V}_K|)} \\
&\times \left\{ f''(|\mathbf{V}_K|) - \frac{f'(|\mathbf{V}_K|)}{|\mathbf{V}_K|} - \frac{f'(|\mathbf{V}_K|)^2}{f(|\mathbf{V}_K|)} \right\}.
\end{aligned} \tag{8.50}$$

It could be interesting to consider the sum of the variances for the  $d$ -components (in  $d$ -dimension) of a given monomer position; we have

$$\sum_{\alpha=1}^d \sigma_{i\alpha}^2 = \sum_{\alpha=1}^d \langle (r_{i\alpha} - \langle r_{i\alpha} \rangle)^2 \rangle \quad (8.51)$$

$$\begin{aligned} &= \sum_{k=1}^i \frac{d}{|\mathbf{V}_k| f(|\mathbf{V}_k|)} f'(|\mathbf{V}_k|) + \sum_{k=1}^i \frac{1}{f(|\mathbf{V}_k|)} \\ &\quad \times \left\{ f''(|\mathbf{V}_k|) - \frac{f'(|\mathbf{V}_k|)}{|\mathbf{V}_k|} - \frac{f'(|\mathbf{V}_k|)^2}{f(|\mathbf{V}_k|)} \right\} \\ &= \sum_{k=1}^i \frac{1}{f(|\mathbf{V}_k|)} \left\{ f''(|\mathbf{V}_k|) + \frac{(d-1)}{|\mathbf{V}_k|} f'(|\mathbf{V}_k|) - \frac{f'(|\mathbf{V}_k|)^2}{f(|\mathbf{V}_k|)} \right\}. \end{aligned} \quad (8.52)$$

This quantity is a measure of the incertitude on the knowledge of the position of the monomer around its average value. In order to use the previous expressions we have to specify the function  $f$  and its derivatives for the two-dimensional and the three-dimensional case. In the 2D case we have

$$f(x) = I_0(lx) \rightarrow f'(x) = lI_1(lx) \rightarrow f''(x) = \frac{l^2}{2} [I_0(lx) + I_2(lx)].$$

On the other hand, for the 3D case we have  $f(x) = \frac{\sinh(lx)}{lx}$ ,

$$f'(x) = \mathcal{L}(lx) \rightarrow f''(x) = \frac{1}{lx} \left( l^2 + \frac{2}{x^2} \right) \sinh(lx) - \frac{2}{x^2} \cosh(lx),$$

then  $f'(x)/f(x) = \mathcal{L}(lx)$  and  $f''(x)/f(x) = l^2 - 2\mathcal{L}(lx)/x$ .

This completes the determination of the covariance.

We report in Fig. 8.4 and Fig. 8.5 the longitudinal and transversal component of the variance as a function of the chain length and the field strength for the 3D case (with  $f = 0$ ). The 2D case is very similar and it has not been reported here for sake of brevity. We can observe some interesting trends: the longitudinal variance of the position is a decreasing function of the number of polymers  $N$  while the transversal one is a increasing function (with a fixed amplitude of the external field  $g$ ). Moreover, both variances are rapidly increasing along the chain, assuming the largest value in the last free monomer, which is more subject to strong fluctuations. It interesting to observe that the variance (both longitudinal and

*trends  
of the  
variances*

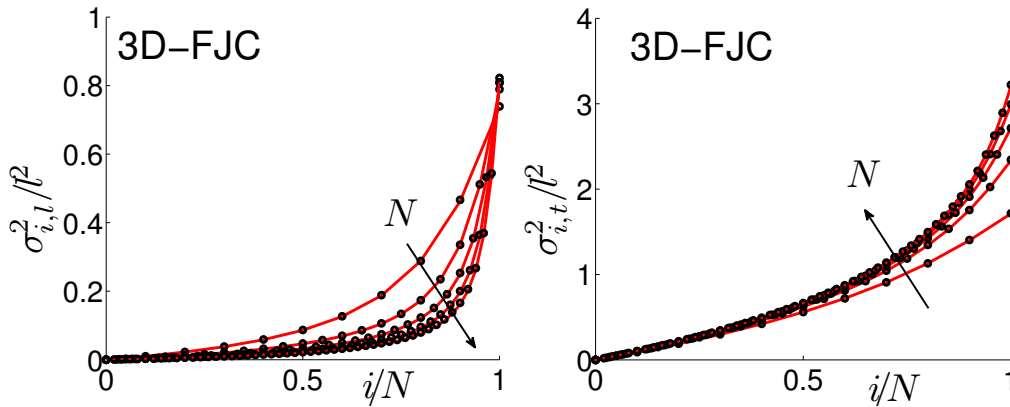


Figure 8.4: Longitudinal (left panel) and transversal (right panel) component of the variance of positions for the 3D FJC case. The red solid lines correspond to the analytical result Eq. (8.50), MC results are superimposed in black circles. Each curve corresponds to different chain lengths  $N = 10, 20, 30, 40, 50$  for a fixed value of the external field defined by  $gl/(k_B T) = 1$ .

transversal components) is a linear function of the position  $i$  along the chain (it linearly intensifies along the chain itself) with a simple force  $f$  applied at the free end: conversely, with a uniform field  $g$ , the distribution of forces generates a strongly non-linear intensification of the variances moving towards the free end-terminal. So, from the point of view of the variances, the application of a field or the application of a single force generates completely different responses. In Fig. 8.5 we can also observe that the variances are decreasing functions of the strength of the field (both for the longitudinal and transversal components); in fact, the intensity of the fields tends to reduce the fluctuations of the chain, increasing, at the same time, the tension within the bonds.

*different  
responses*

These trends are in qualitative agreement with results reported in Refs. [220, 221, 222]. In fact, the behavior of the variances reflect the fluctuations of the chain shape. As already discussed the polymer assumes different shapes for different external field amplitudes. For moderate field the trumpet regime was observed, while for larger values of the field the stem and flower shape was predicted.

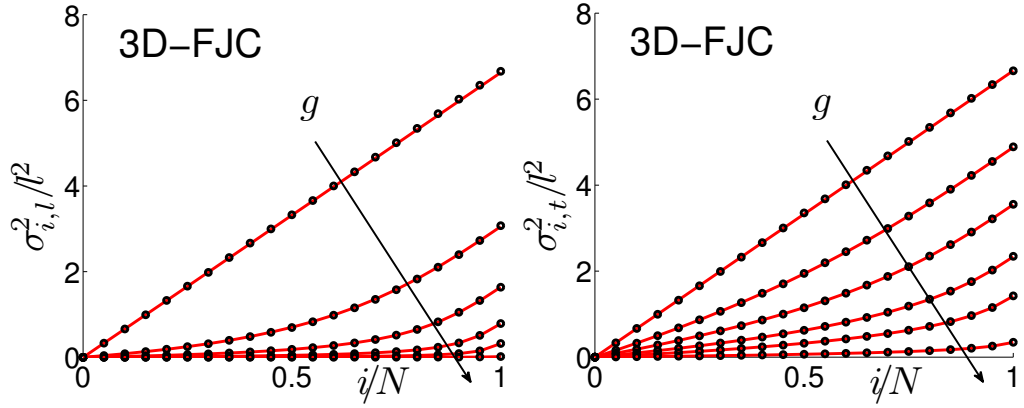


Figure 8.5: Longitudinal (left panel) and transversal (right panel) component of the variance of positions for the 3D FJC case. The red solid lines correspond to the analytical result Eq. (8.50), MC results are superimposed in black circles. Each curve corresponds to different values of the external field amplitude defined by  $gl/(k_B T) = 0.1, 0.25, 0.5, 1, 2, 10$  for a fixed chain length  $N = 20$ .

### 8.3 FREELY-JOINTED CHAIN WITH ELASTIC BONDS

In the general case Eq. (8.29) remains still valid and the function  $f(x)$  assumes the form given below for even or odd dimensionality

$$f(x) = \int_0^{+\infty} \rho e^{-a(\rho-1)^2} \left(\frac{\rho}{x}\right)^{\frac{d-2}{2}} I_{\frac{d-2}{2}}(\rho x) d\rho \quad d \text{ even, (8.53)}$$

$$f(x) = \int_0^{+\infty} \rho^2 e^{-a(\rho-1)^2} \left(\frac{\rho}{x}\right)^{\frac{d-3}{2}} i_{\frac{d-3}{2}}(\rho x) d\rho \quad d \text{ odd. (8.54)}$$

We can also write the simplified versions

$$f(x) = \frac{1}{x^{\frac{d-2}{2}}} \int_0^{+\infty} \rho^{\frac{d}{2}} e^{-a(\rho-1)^2} I_{\frac{d-2}{2}}(\rho x) d\rho \quad d \text{ even, (8.55)}$$

$$f(x) = \frac{1}{x^{\frac{d-3}{2}}} \int_0^{+\infty} \rho^{\frac{d+1}{2}} e^{-a(\rho-1)^2} i_{\frac{d-3}{2}}(\rho x) d\rho \quad d \text{ odd. (8.56)}$$

We develop now a method to calculate  $f(x)$  when  $a$  (or  $k$ ) is large enough. Indeed, when  $a$  is very large, we are in the FJC case and the exponential term converges to a Dirac delta function centered

in  $\rho = l$ . When  $a$  is lower, the integral is dominated by the interval around  $\rho = l$ . So we can develop the Bessel functions around  $\rho = l$  as follows. We use a generic development (Taylor series) of a function centered in a given point:

$$g(x) = \sum_{K=0}^{\infty} \frac{f^K(x_0)}{K!} (x - x_0)^K. \quad (8.57)$$

So, we have

$$I_{\frac{d-2}{2}}(\rho x) = \sum_{K=0}^{+\infty} \frac{1}{K!} \frac{\partial^K}{\partial \rho^K} \left[ I_{\frac{d-2}{2}}(\rho x) \right]_{\rho=l} (\rho - l)^K, \quad (8.58)$$

where

$$\begin{aligned} \frac{\partial^K}{\partial \rho^K} I_{\frac{d-2}{2}}(\rho x) &= \frac{\partial^{K-1}}{\partial \rho^{K-1}} \left[ x I_{\frac{d-2}{2}}^{(1)}(\rho x) \right] \\ &= \frac{\partial^{K-2}}{\partial \rho^{K-2}} \left[ x^2 I_{\frac{d-2}{2}}^{(2)}(\rho x) \right] \\ &= \dots \\ &= x^K I_{\frac{d-2}{2}}^{(K)}(\rho x), \end{aligned} \quad (8.59)$$

and therefore we obtain:

$$I_{\frac{d-2}{2}}(\rho x) = \sum_{K=0}^{+\infty} \frac{x^K}{K!} \left[ I_{\frac{d-2}{2}}^{(K)}(lx) \right] (\rho - l)^K. \quad (8.60)$$

Similarly, we have:

$$i_{\frac{d-3}{2}}(\rho x) = \sum_{K=0}^{+\infty} \frac{x^K}{K!} \left[ i_{\frac{d-3}{2}}^{(K)}(lx) \right] (\rho - l)^K. \quad (8.61)$$

We remark that the  $K$ -th derivatives of the Bessel functions  $I_n$  and  $i_m$  can be evaluated through the standard recursive formulas (see Abramowitz-Stegun).

By using Eq. (8.60) in Eq. (8.55) we get for  $d$  even:

$$f(x) = \sum_{K=0}^{\infty} \frac{1}{x^{(\frac{d-2}{2}-K)}} \frac{1}{K!} I_{\frac{d-2}{2}}^{(K)}(lx) \int_0^{+\infty} \rho^{\frac{d}{2}} (\rho - l)^K e^{-a(\rho-l)^2} d\rho, \quad (8.62)$$

and for  $d$  odd:

$$f(x) = \sum_{K=0}^{\infty} \frac{1}{x^{(\frac{d-3}{2}-K)}} \frac{1}{K!} i_{\frac{d-3}{2}}^{(K)}(lx) \int_0^{+\infty} \rho^{\frac{d+1}{2}} (\rho - l)^K e^{-a(\rho-l)^2} d\rho.$$

(8.63)

We have therefore to calculate the integral

$$E_{nK} = \int_0^{\infty} \rho^n (\rho - l)^K e^{-a(\rho-l)^2} d\rho. \quad (8.64)$$

In order to do so, we define  $\eta = \rho - l$  from which  $d\rho = d\eta$  and we get

$$E_{nK} = \int_{-l}^{\infty} \eta^K (\eta + l)^n e^{-a\eta^2} d\eta. \quad (8.65)$$

By means of the binomial Newton formula we obtain

$$\begin{aligned} E_{nK} &= \int_{-l}^{\infty} e^{-a\eta^2} \sum_{i=0}^n \binom{n}{i} \eta^i l^{n-i} \eta^K d\eta \\ &= \sum_{i=0}^n \binom{n}{i} l^{n-i} \int_{-l}^{\infty} e^{-a\eta^2} \eta^{(i+K)} d\eta, \end{aligned} \quad (8.66)$$

where we use the integral

$$S_m = \int_{-l}^{\infty} e^{-a\eta^2} \eta^m d\eta, \quad (8.67)$$

which can be solved by the following recursive relations

$$\left\{ \begin{array}{l} S_0 = \frac{1}{2} \sqrt{\frac{\pi}{a}} [1 + \operatorname{erf}(l\sqrt{a})] \\ S_1 = \frac{1}{2a} e^{-al^2} \\ S_2 = -\frac{\partial}{\partial a} S_0 \\ S_3 = -\frac{\partial}{\partial a} S_1 \\ \vdots \\ S_{K+2} = -\frac{\partial}{\partial a} S_K. \end{array} \right. \quad (8.68)$$

So we have

$$E_{nK} = \sum_{i=0}^n \binom{n}{i} l^{n-i} S_{i+K}, \quad (8.69)$$

and therefore we get:

$$f(x) = \sum_{K=0}^{\infty} \frac{1}{K!} \frac{E_{\frac{d}{2},K}}{x^{(\frac{d-2}{2}-K)}} I_{\frac{d-2}{2}}^{(K)}(lx), \quad (8.70)$$

for  $d$  even, and

$$f(x) = \sum_{K=0}^{\infty} \frac{1}{K!} \frac{E_{\frac{d+1}{2},K}}{x^{(\frac{d-3}{2}-K)}} i_{\frac{d-3}{2}}^{(K)}(lx) \quad (8.71)$$

for  $d$  odd. It is important to remark that for high values of the parameter  $\alpha$ , a small number of terms in the series is necessary. In the extreme case with  $\alpha \rightarrow \infty$  we obtain the FJC results. For a smaller value of  $\alpha$  a larger number of terms in the series is necessary.

#### 8.4 WORM-LIKE CHAIN UNDER EXTERNAL FIELD

In previous Sections we treated systems described by the FJC model, characterized by the complete flexibility of the chain and, therefore, by the absence of any bending contribution to the total energy. Nevertheless, in many polymer chains, especially of biological origin, the specific flexibility (described by the so-called persistence length [237]) has a relevant role in several bio-mechanical processes. In order to take into consideration these important features, with relevant applications to bio-molecules and bio-structures, in this Section we introduce the semi-flexible polymer chain characterized by a given bending energy added to the previous Hamiltonian

$$h = \sum_{i=1}^N \frac{\mathbf{p}_i \cdot \mathbf{p}_i}{2m} + \frac{1}{2}k \sum_{K=1}^N (\|\mathbf{r}_K - \mathbf{r}_{K-1}\| - l)^2 \quad (8.72)$$

$$+ \frac{1}{2}\kappa \sum_{i=1}^{N-1} (\mathbf{t}_{i+1} - \mathbf{t}_i)^2 - \sum_{K=1}^N \mathbf{g}_K \cdot \mathbf{r}_K - \mathbf{f} \cdot \mathbf{r}_N$$

where  $\kappa$  is the bending stiffness,  $k$  is the stretching modulus and  $\mathbf{t}_i = (\mathbf{r}_{i+1} - \mathbf{r}_i)/\|\mathbf{r}_{i+1} - \mathbf{r}_i\|$  is the unit vector collinear with the  $i$ -th bond.

In particular we take into consideration the classical WLC model, describing an inextensible semi-flexible chain: it means

WLC  
Hamiltonian

inextensible  
WLC model

that the spring constant  $k$  is set to a very large value (ideally  $k \rightarrow \infty$ ) so that the bond lengths remain fixed at the value  $l$ . It is well known that it is not possible to calculate the partition functions in closed form for the WLC polymers. Nevertheless, some standard approximations exist for such cases leading to simple expressions for the force-extension curves when a single force  $f$  is applied to one end of the chain. In the following, starting from these results, we search for the force-extension curves when the polymers is stretched through a constant field  $g$ .

We start with the result for the 2D-WLC with an applied force  $f$ : the approximated force extension curve is given by [238]

$$\frac{fl}{k_B T} = \frac{l}{L_p} \left[ \frac{1}{16(1-\zeta)^2} - \frac{1}{16} + \frac{7}{8}\zeta \right], \quad (8.73)$$

where  $\zeta = r/(lN)$  is the dimensionless elongation and  $L_p = l\kappa/(k_B T)$  is the persistence length. We suppose that such a constitutive equation is invertible through the function  $\mathcal{F}$ , leading to the expression  $\zeta = r/(lN) = \mathcal{F}(fl/(k_B T))$ . When  $f = 0$  and  $\mathbf{g}_J = \mathbf{g}$  for any  $J$  we search for the 2D scalar relation between  $r$  and  $g = |\mathbf{g}|$ . As discussed in a previous section (see Eqs.(8.36) and (8.37)), we can write

$$\begin{aligned} \frac{r}{lN} &= \frac{1}{N} \sum_{k=1}^N \mathcal{F} \left( \frac{lg}{k_B T} (N - k + 1) \right) \\ &\simeq \frac{1}{N} \int_{k=0}^N \mathcal{F} \left( \frac{lg}{k_B T} (N - x + 1) \right) dx \\ &= \frac{1}{N} \frac{1}{\frac{lg}{k_B T}} \int_{\frac{lg}{k_B T}}^{\frac{lg}{k_B T} (N+1)} \mathcal{F}(y) dy, \end{aligned} \quad (8.74)$$

where we have defined the change of variable  $y = \frac{lg}{k_B T} (N - x + 1)$ . We adopt now a second change of variable through the relation  $z = \mathcal{F}(y)$  or  $y = \mathcal{F}^{-1}(z)$ ; it leads to

$$\begin{aligned} \frac{r}{lN} &= \frac{1}{N} \frac{1}{\frac{lg}{k_B T}} \int_{\mathcal{F}(\frac{lg}{k_B T})}^{\mathcal{F}(\frac{lg}{k_B T} (N+1))} z \frac{\mathcal{F}^{-1}(z)}{dz} dz \\ &= \frac{1}{N} \frac{1}{\frac{lg}{k_B T}} \frac{l}{L_p} \\ &\times \left[ \frac{7}{16} z^2 - \frac{1}{8(1-z)} + \frac{1}{16(1-z)^2} \right]_{\mathcal{F}(\frac{lg}{k_B T})}^{\mathcal{F}(\frac{lg}{k_B T} (N+1))} \end{aligned} \quad (8.75)$$

where we used the notation  $[h(z)]_a^b = h(b) - h(a)$ . This result represents (although in implicit form) the approximated force-extension curve for the 2D-WLC under external fields. To evaluate Eq. (8.75) we need to know the inverse function  $\mathcal{F}(\cdot)$ , a task that can be performed numerically. Similarly, we may consider the standard 3D-WLC model with an applied force  $f$ ; the classical Marko-Siggia result [21] is

$$\frac{fl}{k_B T} = \frac{l}{L_p} \left[ \frac{1}{4(1-\zeta)^2} - \frac{1}{4} + \zeta \right], \quad (8.76)$$

where as before,  $\zeta = r/(lN)$  is the dimensionless elongation and  $L_p = l\kappa/(k_B T)$  is the persistence length. We suppose again that such constitutive equation is invertible through the function  $\mathcal{G}$ , leading to the expression  $\zeta = r/(lN) = \mathcal{G}(fl/(k_B T))$ . When  $f = 0$  and  $\mathbf{g}_j = \mathbf{g}$  for any  $j$  we search for the 3D scalar relation between  $r$  and  $g = |\mathbf{g}|$ . By repeating the previous procedure, we can write

$$\begin{aligned} \frac{r}{lN} &= \frac{1}{N} \frac{1}{\frac{lg}{k_B T}} \int_{\mathcal{G}\left(\frac{lg}{k_B T}\right)}^{\mathcal{G}\left(\frac{lg}{k_B T}(N+1)\right)} z \frac{\mathcal{G}^{-1}(z)}{dz} dz \\ &= \frac{1}{N} \frac{1}{\frac{lg}{k_B T}} \frac{l}{L_p} \\ &\quad \times \left[ \frac{1}{2} z^2 - \frac{1}{2(1-z)} + \frac{1}{4(1-z)^2} \right]_{\mathcal{G}\left(\frac{lg}{k_B T}\right)}^{\mathcal{G}\left(\frac{lg}{k_B T}(N+1)\right)} \end{aligned} \quad (8.77)$$

which represents the implicit form of the approximated force-extension curve for the 3D-WLC under external fields.

It is interesting to compare the very different force-extension curves for a single molecule in the two cases of a uniform (only  $f$  applied) and non-uniform (only  $g$  applied) stretch. In particular, taking advantage of our approximated formulas, we can analyse the case of a FJC and a WLC polymer. The 2D and 3D FJC results are plotted in Fig. 8.6; on the other hand, the 2D and 3D WLC curves have been shown in Fig. 8.7. For the WLC case we assumed  $\kappa = 10k_B T$  for the bending modulus at  $T = 293\text{K}$ . This value is comparable to that of polymer chains of biological interest (e.g., for DNA  $\kappa = 15k_B T$ ) [21]. In all cases three curves have been reported for drawing all the possible comparisons: the response under the field  $g$ , the response under the force  $f = g$  and, finally, the response to an external force  $f = Ng$ . Interesting enough we

*force-extension  
curves  
comparison*

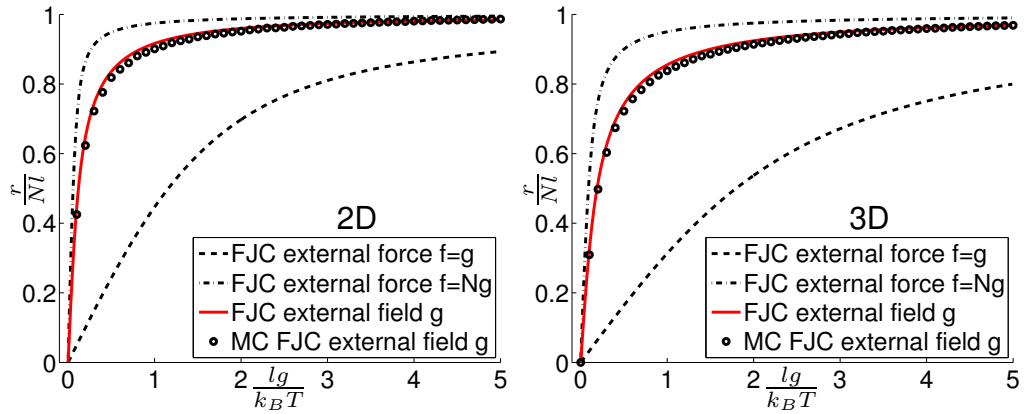


Figure 8.6: Force-extension curves of a FJC polymer in an external field (or external force) with  $N=20$ . The red line corresponds to the approximated expressions given in Eqs.(8.36) and Eqs.(8.37) while the black circles have been obtained through MC simulations. The 2D (Eq. (8.34)) and 3D (Eq. (8.35)) FJC expressions (without an external field) are plotted for comparison with  $f = g$  and  $f = Ng$ .

note that the curve corresponding to the field  $g$  is always comprised between the cases with only the force  $f = g$  and  $f = Ng$ . The response with the field  $g$  is clearly larger than that with the single force  $f = g$  since the field corresponds to a distribution of  $N$  forces (of intensity  $f$ ) applied to all monomers; therefore, the total force applied is larger, generating a more intense effect. However, the case with a single force  $f = Ng$  shows a response larger than that of the field  $g$ . In this case the total force applied in the two cases is the same but the single force  $Nf$  is applied entirely to the last terminal monomer, generating an overall stronger effect compared to the same force evenly distributed on the monomers. In fact, a force generates a stronger effect if it is placed in the region near the free polymer end (its effect is redistributed also to all preceding bonds). The curves in Fig. 8.6 and Fig. 8.7 have been obtained with the theoretical formulations presented in this Section and confirmed by a series of MC simulations. In all case we obtained a quite perfect agreement between the two formulations. The knowledge of the closed-form expressions allowed us to analytically analyze the behavior of the chains for very low and very high applied forces (or fields). The results are shown in Table 3: interestingly, we note that the extension is always a linear function of the small applied perturbation. Nevertheless, the corresponding constant of proportionality depends on  $N$  only when a field

*comparison  
of the  
closed-form  
expressions*

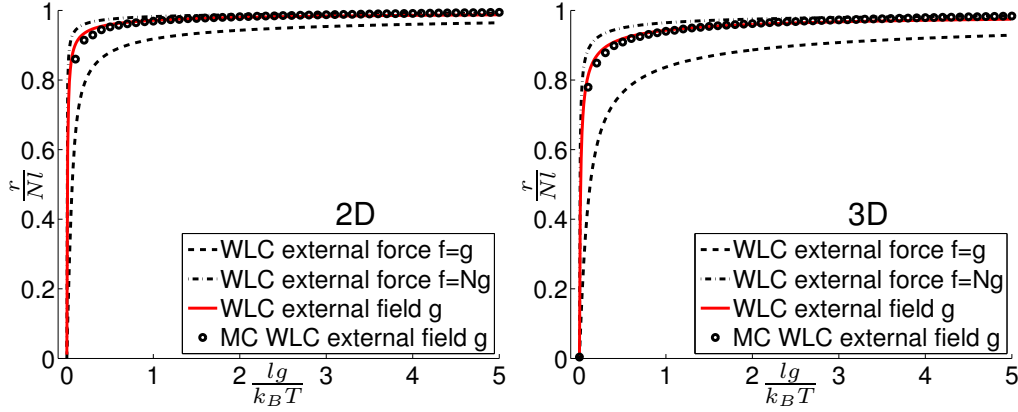


Figure 8.7: Force-extension curves of a WLC polymer in an external field (or external force) with  $N=20$ . The red line corresponds to the approximated expressions given in Eqs.(8.75) and Eqs.(8.77) while the black circles have been obtained through MC simulations. The 2D (Eq. (8.73)) and 3D (Eq. (8.76)) WLC expressions (without an external field) are plotted for comparison with  $f = g$  and  $f = Ng$ . The value of the bending spring constant is  $\kappa = 0.4 \cdot 10^{-19} \text{ Nm} \simeq 10k_B T$  at  $T = 293\text{K}$ .

is applied to the chain; conversely, it is independent of  $N$  with a single force applied at one end. On the other hand, with a large perturbation applied to the molecule, we observe a  $1/x$  behavior for the FJC models and a  $1/\sqrt{x}$  behavior for the WLC models.

To conclude we also remark that the order of the curves observed in Fig. 8.6 and Fig. 8.7 is confirmed also in the low and high force (or field) regime by the following inequalities:  $1 < 1 + N/2 < N$  (low force regime) and  $1 < \log(N + 1) < N$  (high force regime) for the FJC model and  $1 < 1 + N/2 < N$  (low force regime) and  $\sqrt{N} < 2(\sqrt{N} + 1) < N$  (high force regime) for the WLC model (always for  $N \geq 2$ ). Interesting enough, we can write two explicit approximate expressions for the WLC polymer under an applied field, which represent a generalization of the classical Marko-Siggia results. Starting from the asymptotic forms shown in the last two lines of Tab. 3, we can derive the interpolations with the same technique adopted in Ref. [21]. To perform this calculation we assume a very large number  $N$  of monomers. For the 2D case we obtain

$$N \frac{gl}{k_B T} = \frac{l}{L_p} \left[ \frac{1}{4(1-\zeta)^2} - \frac{1}{4} + \frac{3}{2}\zeta \right], \quad (8.78)$$

2D and 3D  
WLC  
interpolation

Table 3: Asymptotic forms of the force-extension curves for all cases described in this Chapter: FJC and WLC models in 2D and 3D geometry with force applied  $f$  or field applied  $g$ .

Polymer chain Equation	Asymptotic form of $\frac{r}{lN}$ for $f, g \rightarrow 0$ $\left(x = \frac{lf}{k_B T} \text{ or } \frac{lg}{k_B T}\right)$	Asymptotic form of $\frac{r}{lN}$ for $f, g \rightarrow \infty$ $\left(x = \frac{lf}{k_B T} \text{ or } \frac{lg}{k_B T}\right)$
$\underbrace{\text{FJC (2D) } f}_{\text{Eq.(8.34)}}$	$\frac{1}{2}x$	$1 - \frac{1}{2x}$
$\underbrace{\text{FJC (3D) } f}_{\text{Eq.(8.35)}}$	$\frac{1}{3}x$	$1 - \frac{1}{x}$
$\underbrace{\text{FJC (2D) } g}_{\text{Eq.(8.36)}}$	$\frac{1}{2} \left(1 + \frac{N}{2}\right) x$	$1 - \frac{\log(N+1)}{2N} \frac{1}{x}$
$\underbrace{\text{FJC (3D) } g}_{\text{Eq.(8.37)}}$	$\frac{1}{3} \left(1 + \frac{N}{2}\right) x$	$1 - \frac{\log(N+1)}{N} \frac{1}{x}$
$\underbrace{\text{WLC (2D) } f}_{\text{Eq.(8.73)}}$	$\frac{L_p}{l} x$	$1 - \frac{1}{4} \frac{1}{\sqrt{\frac{L_p}{l} x}}$
$\underbrace{\text{WLC (3D) } f}_{\text{Eq.(8.76)}}$	$\frac{2}{3} \frac{L_p}{l} x$	$1 - \frac{1}{2} \frac{1}{\sqrt{\frac{L_p}{l} x}}$
$\underbrace{\text{WLC (2D) } g}_{\text{Eq.(8.75)}}$	$\frac{L_p}{l} \left(1 + \frac{N}{2}\right) x$	$1 - \frac{1}{\sqrt{\frac{L_p}{l} x}} \frac{\sqrt{N+1}-1}{2N}$
$\underbrace{\text{WLC (3D) } g}_{\text{Eq.(8.77)}}$	$\frac{2}{3} \frac{L_p}{l} \left(1 + \frac{N}{2}\right) x$	$1 - \frac{1}{\sqrt{\frac{L_p}{l} x}} \frac{\sqrt{N+1}-1}{N}$

and for the 3D one we have

$$N \frac{gl}{k_B T} = \frac{l}{L_p} \left[ \frac{1}{(1-\zeta)^2} - 1 + \zeta \right]. \quad (8.79)$$

These relationships represent the approximation of the results given in Eqs.(8.75) and (8.77). They can be compared with the classical results concerning the system with the applied force (see Eqs.(8.73) and (8.76)) [21, 238]. First of all we note that in place of the force  $f$  we find the total force  $Ng$  applied to the polymer (by means of the field action). Moreover, the coefficients of  $1/(1-\zeta)^2$ ,  $\zeta$  and the constant term are different because of the different distribution of forces.

A brief comparison with previously published limiting values follows. Our asymptotic forms for the WLC model with applied force ( $f \rightarrow \infty$ ) are perfectly coincident with those obtained in Ref. [47] by means of the small-fluctuation assumption leading to the fluctuating rod limit of a semiflexible polymer (see Eq.(22) of Ref. [47]). Moreover, the limiting value for three-dimensional case is the well-known result at the base of the Marko-Siggia relation [21]. Also the asymptotic results for the WLC model under an applied field ( $g \rightarrow \infty$ ) are in agreement with Eq.(42) of Ref. [47] where, however, a large number of monomers  $N$  was considered. Our results for the WLC under field ( $g \rightarrow \infty$ ) lead for large  $N$  to the expressions:  $r/(Nl) = 1 - 1/\sqrt{4L_p N x/l}$  for the 2D geometry and  $r/(Nl) = 1 - 1/\sqrt{L_p N x/l}$  for the 3D case, actually coinciding with Eq.(42) of Ref. [47]. It should be noted that the limiting value for the 2D geometry has been also derived with different phenomenological arguments [229].

*comparisons  
with  
recent  
investigations*

## 8.5 ACTION OF A PULLING FORCE NOT ALIGNED WITH THE EXTERNAL FIELD

In previous Sections we considered the polymer chain immersed in an external field with an external force equal to zero at its end. However, since we developed a form of the partition function also taking into account an external force applied at the end of the chain (at least for the FJC model), we can directly study the important case with a non zero force superimposed to an external field, in general having different orientation. To do this, we keep fixed the origin of the chain and apply a constant force at the end

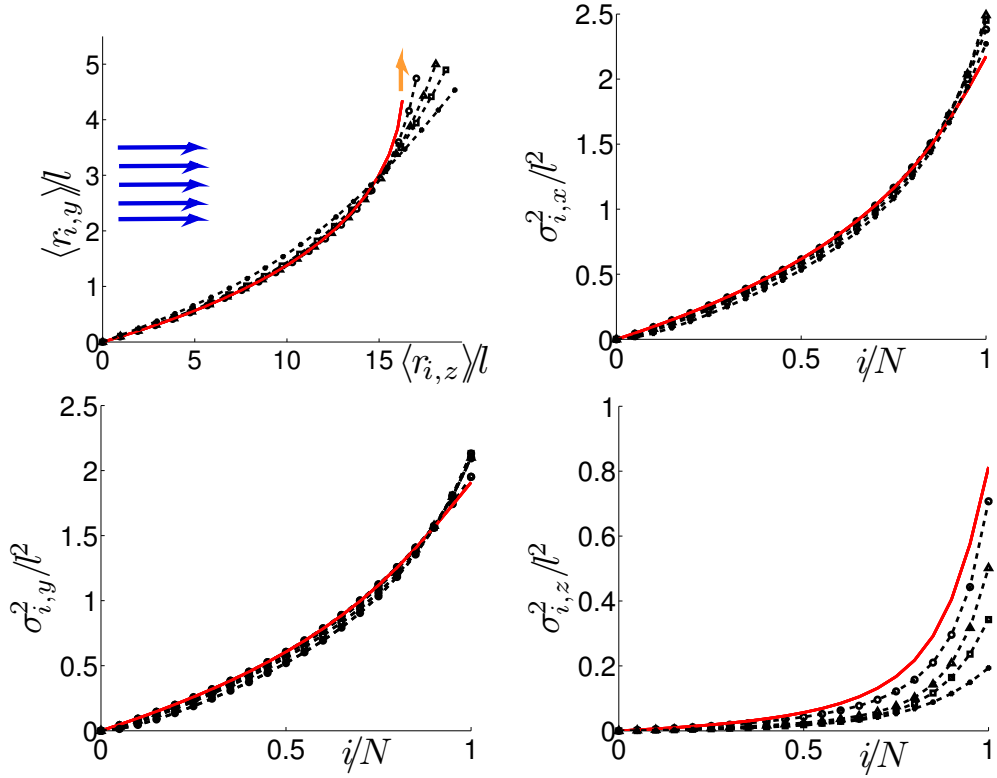


Figure 8.8: Action of a pulling force  $f$  (along the  $y$ -axis) perpendicular to the applied field  $g$  (along the  $z$ -axis). We adopted different values of the bending spring constant:  $\kappa = 0.08, 0.6, 2, 8 \cdot 10^{-19}$  Nm. The chain length is fixed ( $N = 20$ ), the external field amplitude is  $g = 4$  pN and the force applied to the last monomer of the chain corresponds to  $f = 8$  pN. The red solid lines correspond to the analytical results for the FJC case (see Eqs.(8.33) and (8.50)). Black circles correspond to the MC simulations with the different bending spring constants. In the left panel we reported the average positions, while in the others the three variances of the  $x$ ,  $y$  and  $z$  components.

*pulling force  
perpendicular  
to the  
direction of  
the field*

of the polymer with different angles with respect to the direction of the applied field. We will analyse such a problem for both the FJC and WLC cases. To begin, we consider a pulling force perpendicular to the direction of the applied field, respectively the  $y$  and  $z$  axis of our reference frame. For increasing values of the bending spring constant  $\kappa$  going from nearly zero (FJC model) to  $8 \cdot 10^{-19}$  Nm (WLC model, including the bending constant of the DNA given by  $\kappa = 0.6 \cdot 10^{-19}$  Nm  $\simeq 15k_B T$ ). In Fig. 8.8 we reported the results for the average monomers positions and their variances. The red solid lines correspond to the analytical results for the FJC case, while the black symbols correspond to the MC

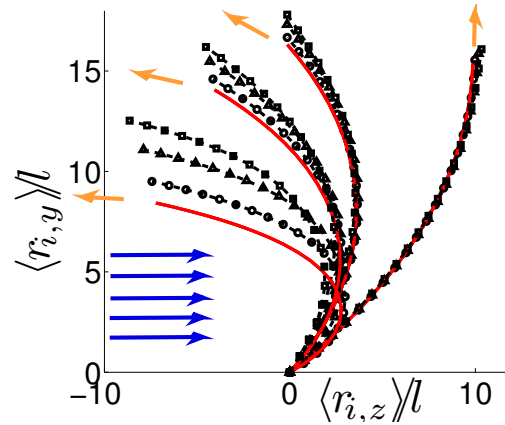


Figure 8.9: Average positions of the chain for different angles between the external traction force  $f$  and the direction of the applied field  $g$ . We adopted  $N = 20$ ,  $g = 4$  pN and  $f = 60$  pN. The red solid lines correspond to the FJC analytical result, Eq. (8.33). The symbols represent the MC results for the WLC model with  $\kappa = 0.08, 0.6, 2 \cdot 10^{-19}$  Nm (circles, triangles and squares, respectively). For both FJC and WLC models we used different values of the angle between the applied field and the traction force  $\theta = \pi/2, 3\pi/4, 5\pi/6, 15\pi/16$  from the right left.

simulations. It is interesting to observe the effect of the persistence length (or, equivalently of the bending stiffness): in fact, in the left panel of Fig. 8.8 we note that the chains with an higher bending spring constant tend to remain more straight under the same applied load. At the same time, in the fourth panel of Fig. 8.8 we observe a decreasing variance along the  $z$ -axis (direction of the applied field) with an increasing bending spring constant; this fact can be easily interpreted observing that an higher rigidity of the chain reduces the statistical fluctuations in the direction of the applied field. The situation is more complicated for the variances along the  $x$  and  $y$  directions: in fact, along the chain, there are some monomers with variances larger than the corresponding FJC case and others with smaller values. In Fig. 8.9 the average positions of the monomers for different directions of the external force are reported. The figure shows how the average monomer positions depend on the bending rigidity  $\kappa$  and on the external force angle  $\theta$ . As expected, we observe that the persistence length of the chain tends to maintain a low curvature in the shape of the chain. This phenomenon is more evident with an increasing angle between the force and the field. In fact, in Fig. 8.9, the deviation between the FJC results and the WLC ones is higher for the an-

*pulling force  
with different  
directions*

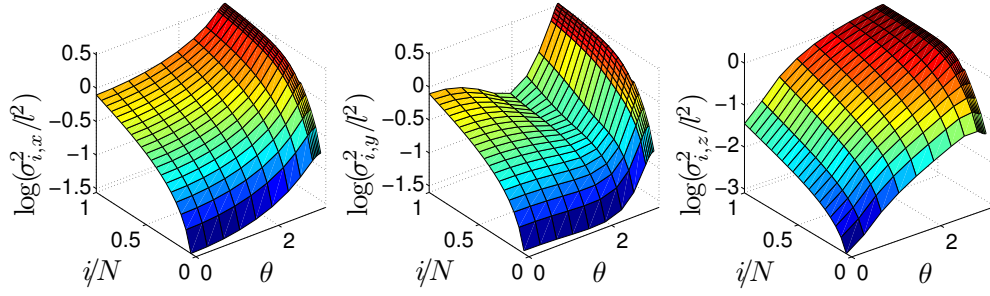


Figure 8.10: Monomer variances versus the position along the chain ( $i$ ) and the angle between force and field ( $0 < \theta < \pi$ ) for the FJC model. As before we used  $N = 20$ ,  $g = 4$  pN and  $f = 60$  pN.

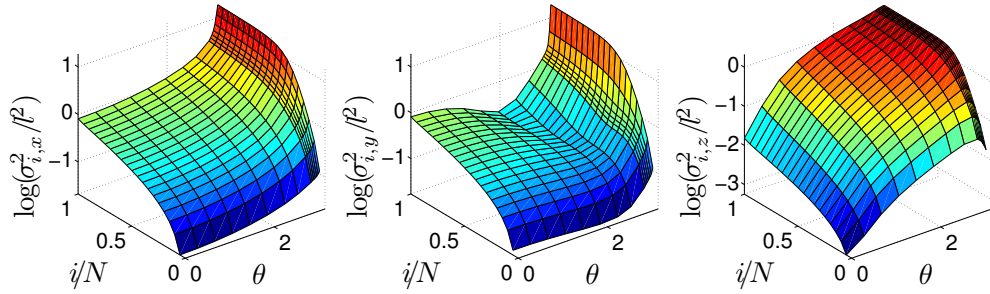


Figure 8.11: Monomer variances versus the position along the chain ( $i$ ) and the angle between force and field ( $0 < \theta < \pi$ ) for the WLC model. As before we used  $N = 20$ ,  $g = 4$  pN and  $f = 60$  pN. We also adopted a bending stiffness  $\kappa = 0.6 \cdot 10^{-19}$  Nm.

gles approaching  $\pi$ , where the force and the field are applied in opposite directions.

*a very complex scenario for the variances*

In Figs. 8.10 and 8.11 the three components of the variance are reported versus the position of the monomer along the chain and the angle between the field and the force directions, for the FJC and WLC case, respectively. We can extract some general rules about this very complex scenario: as for the variance along the  $x$  direction we observe it to be an increasing function both of the position  $i$  along the chain and of the angle  $\theta$  between  $f$  and  $g$ . Both behaviors can be interpreted with the concept of persistence length, as discussed above. Conversely, the description of the variance along the  $y$  direction is more complicated. In fact, while the increasing trend of the variance with the position  $i$  along the chain is maintained, we observe a non monotonic behavior in terms of the angle  $\theta$ , with a minimum of the variance at about  $\theta = 2\pi/3$ . Finally, the variance along the  $z$  direction is always increasing along the chain,

but it shows a maximum near  $\theta = \pi$  (at least in the first part of the polymer chain).

## 8.6 OUTLINE OF THE RESULTS

Here we investigated the mechanical and conformational properties of flexible and semi-flexible polymer chains immersed in external fields. Some examples in literature testify the interest on investigate the elasticity of a polymer chains subjected to external fields, analyzing the average configurational properties of the polymer [14, 217, 218], and reporting the behavior of the variances [220, 221, 222]. However, there is a prominent lacking of investigations presenting closed analytical forms. In this context, our contribution has been focused in developing a statistical theory based on the exact analytical determination of the partition function. We obtained expressions in closed form for both the average conformation of the chain and its covariance distribution. This theoretical formula can be used as a reference for interpreting experimental results on single polymers for some physical conditions as a polymer chain immersed in a fluid in a uniform motion or an arbitrarily charged chain inserted in a uniform electric field. Moreover, we derived new approximate expressions describing the force-extension curve under the effect of an external field that can be considered as the extensions of the classical Marko-Siggia relationships [21] describing the polymer pulled by a single external force applied at the free end of the chain.



## CONCLUSIONS AND PERSPECTIVES

---

In this thesis we investigated the thermo-elastic behaviour of single polymer chains under stretching.

As a first analysis, we studied how the force-extension curve of a model polymer chain is affected by the loading protocol which can be typically fixed-ends or fixed-force. We showed how such macroscopic boundary conditions can be formulated within the Helmholtz and the Gibbs ensembles of the statistical mechanics. We adopted flexible and semiflexible polymer models, with and without extensible bonds. Extensible bonds were described by linear springs for simply comparing analytical and Metropolis Monte Carlo (MMC) results.

After a theoretical introduction on different boundary conditions, we discussed the notion of thermodynamic limit. In particular, we proved that different experimental strategies used for stretching the polymer lead to the same results when the number of monomers is large enough. On the other hand, by MMC simulations we showed that for short chains the two ensembles are characterized by very different elastic behaviors. In all cases here investigated (FJC, WLC and their extensible versions) we found that the convergence to the thermodynamic limit is well described by suitable power laws with well defined scaling exponents. More specifically, we proved that such power laws can fit the MMC results with high accuracy and that different polymer models have different scaling exponents. The presented results and the demonstration of different scaling laws, may help to discriminate the response of polymers with different internal chemical structure, in the short-length limit.

Moreover, we described the statistical mechanics of chain polymers composed by domains with two stable states, subjected to a pulling force by a molecular-scale mechanical device. We showed that for short chain length, or large stiffness of the device, the domain response is uncorrelated and originates the typical sawtooth force-extension curve observed in many experiments. On the other hand, upon increasing chain length, or vanishing device stiffness,

the response is cooperative and results in the plateau-like curve, also observed in other experiments. Despite the simplicity of the model, such a framework provides a unified picture for such apparently contrasting experimental situations.

After having considered the elasticity effects on single polymer chains loaded by external forces, we investigated the mechanical and conformational properties of flexible and semi-flexible polymer chains immersed in external fields. As for the FJC model we developed a statistical theory, based on the exact analytical determination of the partition function, which generalizes previous results to the case where an external field is applied to the system. In particular we obtained closed form expression for both the average conformation of the chain and its covariance distribution. For sake of completeness, all calculations have been performed both in two-dimensional and three-dimensional geometry. On the other hand, as for the WLC model we derived new approximate expressions describing the force-extension curve under the effect of an external field. They can be considered as the extensions of the classical Marko-Siggia relationships describing the polymer pulled by a single external force applied at the free end of the chain. All our analytical results, for both FJC and WLC models, have been confirmed by a series of Monte Carlo simulations, always found in very good agreement with the theory. The overall effects generated on the tethered polymer by the application of an external field can be summarized as follows. As for the average configuration of a chain, it is well known that a single pulling force generates a uniform deformation along the chain (for a homogeneous polymer with all monomers described by the same effective elastic stiffness). On the contrary, the application of an external field produces a non uniform deformation along the chain, showing a larger deformation in the portion of the chain closest to the fixed end. Moreover, the variances of the positions increase linearly along the chain with a single force applied to the polymer. Conversely, the polymer subjected to an external field exhibits a non-linearly increasing behavior of the variances along the chain. More specifically the variances assume the largest values nearby the last free monomers, where we can measure the highest fluctuations. The use of the MMC method, once validated against known analytical solutions, has been crucial for analyzing models conditions which are beyond reach of a full analytical calculation. We

took full profit of this approach for analyzing the effects of the combination of an applied force at the free end together with an external field, especially when the two are not aligned. We have analyzed the average configurational properties of the polymer, observing a very complex scenario concerning the behavior of the variances.

In conclusion, it is useful to look at the whole work to gain some perspectives for future studies.

In a biophysical context, the understanding of the rheological properties of bundle of polymers is important to investigate the assembly of bio-molecules as filaments of DNA, actin, or microtubules. Starting from our theoretical approach, would be intriguing to extend our models for investigating bundles of polymers winded together and interacting with each others, giving particular attention to the *viscosity* of the system. The description of the polymer viscosity requires the formalism of the statistical mechanics of *non-equilibrium*. Furthermore, the implementation of non-equilibrium molecular simulations would be mandatory in order to better correlate the theoretical and experimental results with the complex living-cell DNA.

The mechanical behaviour of bundle of polymers is taking increasing interest also in the medical context. In clinical radiotherapy recent experimental methods have been proposed to establish a direct correlation between the ionizing radiation and its damaging effects on DNA. For example, a silicon Nanotweezers (SNT) has been employed, to directly measure the rate of breaking of DNA placed under a radiation beam [239]. The real-time DNA bundle degradation was observed in terms of biomechanical stiffness and viscosity reduction. The obtained results trace the way for both fundamental and clinical studies of DNA degradation mechanisms under ionizing radiation. This can allow the improving of tumor treatments. In this context, a first theoretical investigation of interest would be consider the behaviour of the elasticity of DNA bundles subjected to a degradation in time trapped and held straight in parallel strands between the tips of a cantilever (mimiking, for instance, the loading by the SNT device).



Part VI

APPENDIX



## APPENDIX

---

**Contents**


---

- A.1 Beta Euler function **179**  
 A.2 Fourier integral for functions with spherical symmetry **181**
- 

## A.1 BETA EULER FUNCTION

We introduce here some properties of the Beta Euler function which will be used in Appendix [A.2](#). The convolution theorem affirms that the Laplace transform of the convolution integral

$$u(t) = \int_0^t x(\xi)h(t - \xi)d\xi \quad (\text{A.1})$$

is given by the product of the Laplace transform of the functions  $x$  and  $h$ , namely

$$U(s) = H(s)X(s). \quad (\text{A.2})$$

We consider here only causal function which are different from zero only for a positive argument (so, the second limit of integration can be considered as  $t$  or  $\infty$  without changing the result). We can firstly prove this property as follows. Considering the convolution integral

$$u(t) = \int_0^\infty x(\xi)h(t - \xi)d\xi \quad (\text{A.3})$$

and its Laplace transform calculated through the standard definition

$$\begin{aligned} U(s) &= \int_0^\infty u(t)e^{-st}dt \\ &= \int_0^\infty \left[ \int_0^\infty x(\xi)h(t - \xi)d\xi \right] e^{-st}dt \\ &= \int_0^\infty x(\xi) \left[ \int_0^\infty h(t - \xi)e^{-st}dt \right] d\xi. \end{aligned} \quad (\text{A.4})$$

Now, performing the change of variable

$$t - \xi = \eta \rightarrow dt = d\eta, \quad (\text{A.5})$$

leading to

$$t = (0, \infty) \rightarrow \eta = (-\xi, \infty), \quad (\text{A.6})$$

we simply obtain the result

$$\begin{aligned} U(s) &= \int_0^\infty x(\xi) \left[ \int_{-\eta}^\infty h(\eta) e^{-s(\xi+\eta)} d\eta \right] d\xi \\ &= \int_0^\infty x(\xi) e^{-s\xi} d\xi \int_0^\infty h(\eta) e^{-s\eta} d\eta \\ &= X(s)H(s), \end{aligned} \quad (\text{A.7})$$

which represents the requested convolution theorem.

We take into account now two functions  $x$  and  $t$  as follows:

$$x = t^\alpha \rightarrow X(s) = \frac{\Gamma(\alpha + 1)}{s^{\alpha+1}}, \quad (\text{A.8})$$

$$h = t^\beta \rightarrow H(s) = \frac{\Gamma(\beta + 1)}{s^{\beta+1}}. \quad (\text{A.9})$$

The two Laplace transforms have been simply calculated making use of the well known Euler Gamma function. Now we can consider the convolution of the previously defined functions:

$$u(t) = \int_0^t \xi^\alpha (t - \xi)^\beta d\xi, \quad (\text{A.10})$$

and, by the convolution theorem, the Laplace transform of  $u$  is directly written as

$$U(s) = \frac{\Gamma(\alpha + 1)\Gamma(\beta + 1)}{s^{\alpha+\beta+2}}. \quad (\text{A.11})$$

But, it is evident that such a function has the same form of the transforms of  $h$  and  $x$ . So, the inverse Laplace transform is easily obtained as

$$u(t) = \int_0^t \xi^\alpha (t - \xi)^\beta d\xi = \frac{\Gamma(\alpha + 1)\Gamma(\beta + 1)}{\Gamma(\alpha + \beta + 2)} t^{\alpha+\beta+1}. \quad (\text{A.12})$$

If we let  $t = 1$  we obtain the definition of the Beta function  $B$

$$u(1) = \int_0^1 \xi^\alpha (1 - \xi)^\beta d\xi = \frac{\Gamma(\alpha + 1)\Gamma(\beta + 1)}{\Gamma(\alpha + \beta + 2)} = B(\alpha + 1, \beta + 1). \tag{A.13}$$

So, we have finally proved the important relationship

$$\frac{\Gamma(\alpha + 1)\Gamma(\beta + 1)}{\Gamma(\alpha + \beta + 2)} = B(\alpha + 1, \beta + 1), \tag{A.14}$$

which will be used in Appendix [A.2](#).

A.2 FOURIER INTEGRAL FOR FUNCTIONS WITH SPHERICAL SYMMETRY

We consider the definition

$$F(\boldsymbol{\omega}) = \int_{\mathfrak{R}^d} f(\mathbf{x}) e^{-i\boldsymbol{\omega} \cdot \mathbf{x}} d\mathbf{x} \tag{A.15}$$

of the Fourier transform  $F(\boldsymbol{\omega})$  of the original function  $f(\mathbf{x})$ . We suppose that  $f(\mathbf{x})$  is a function with spherical symmetry and, therefore,  $f$  is a function of the norm of  $\mathbf{x}$  only, i.e.  $f(\mathbf{x}) = f(\rho)$  with  $\rho = |\mathbf{x}|$ . Throughout all the discussion we adopt the standard euclidean norm  $|\mathbf{x}| = |\mathbf{x}|_2$  in  $\mathfrak{R}^d$ .

We consider  $\mathbf{x} = \rho\mathbf{V}$  and  $\boldsymbol{\omega} = \Omega\mathbf{W}$  with  $|\mathbf{V}| = |\mathbf{W}| = 1$ . Then

$$F(\Omega\mathbf{W}) = \int_{\mathfrak{R}^d} f(\rho) e^{-i\rho\Omega\mathbf{V} \cdot \mathbf{W}} d(\rho\mathbf{V}). \tag{A.16}$$

We use the  $d$ -dimensional spherical coordinates defined as

$$\begin{cases} x_1 = \rho \cos \theta_1 \\ x_2 = \rho \sin \theta_1 \cos \theta_2 \\ x_3 = \rho \sin \theta_1 \sin \theta_2 \cos \theta_3 \\ x_4 = \rho \sin \theta_1 \sin \theta_2 \sin \theta_3 \cos \theta_4 \\ \vdots \\ x_{d-1} = \rho \sin \theta_1 \dots \sin \theta_{d-2} \cos \theta_{d-1} \\ x_d = \rho \sin \theta_1 \dots \sin \theta_{d-2} \sin \theta_{d-1} \end{cases} \tag{A.17}$$

with Jacobian determinant

$$J = \rho^{d-1} \underbrace{\sin^{d-2} \theta_1 \sin^{d-3} \theta_2 \sin^{d-4} \theta_3 \dots \sin \theta_{d-2}}_{d-2 \text{ terms}} \tag{A.18}$$

and with limitations

$$\begin{cases} 0 \leq \theta_1, \theta_2, \dots, \theta_{d-2} \leq \pi \\ 0 \leq \theta_{d-1} \leq 2\pi \\ 0 \leq \rho < \infty. \end{cases} \quad (\text{A.19})$$

Eq.(A.16) becomes (letting  $\mathbf{W} = \hat{e}_1$ )

$$\begin{aligned} F(\Omega) &= \int_0^\infty f(\rho) \int_{[0,\pi]^{d-2}} \rho^{d-1} \sin^{d-2} \theta_1 \sin^{d-3} \theta_2 \dots \sin \theta_{d-2} \\ &\quad \times \int_0^{2\pi} e^{-i\rho\Omega \cos \theta_1} d\theta_{d-1} d\theta_{d-2} \dots d\theta_1 d\rho. \end{aligned} \quad (\text{A.20})$$

In fact, from Eq.(A.16) we observe that  $F$  does not depend on  $\mathbf{W}$  and therefore we may fix an arbitrary direction for  $\mathbf{W}$ . In particular, if we fix  $\mathbf{W} = \hat{e}_1$  the result is indicated in Eq.(A.20). It can be arranged as follows

$$\begin{aligned} F(\Omega) &= \int_0^\infty 2\pi\rho^{d-1} f(\rho) d\rho \int_0^\pi \sin^{d-2} \theta_1 e^{-i\rho\Omega \cos \theta_1} d\theta_1 \quad (\text{A.21}) \\ &\quad \times \underbrace{\int_0^\pi \sin \theta_{d-2} d\theta_{d-2} \int_0^\pi \sin^2 \theta_{d-3} d\theta_{d-3} \dots \int_0^\pi \sin^{d-3} \theta_2 d\theta_2}_{d-3 \text{ integrals}}. \end{aligned}$$

We use the integral

$$\int_0^\pi \sin^K \theta d\theta = \sqrt{\pi} \frac{\Gamma(\frac{K+1}{2})}{\Gamma(\frac{K}{2} + 1)}, \quad (\text{A.22})$$

which can be obtained as follows

$$\int_0^\pi \sin^K \theta d\theta = 2 \int_0^{\frac{\pi}{2}} \sin^K \theta d\theta. \quad (\text{A.23})$$

Performing the change of variable

$$\sin^2 \theta = x \Rightarrow \cos \theta = \sqrt{1-x}, \quad (\text{A.24})$$

which means that

$$\sin x = \sqrt{x}, \quad (\text{A.25})$$

we simply obtain

$$\int_0^\pi \sin^K \theta d\theta = 2 \int_0^1 (\sqrt{x})^K \frac{dx}{2\sqrt{x}\sqrt{1-x}} = \int_0^1 x^{\frac{K-1}{2}} (1-x)^{-\frac{1}{2}} dx. \quad (\text{A.26})$$

Through the Beta (Euler) function (see Appendix A.2), we obtain

$$B(x, y) = \int_0^1 t^{x-1} (1-t)^{y-1} dt = \frac{\Gamma(x)\Gamma(y)}{\Gamma(x+y)} = B(y, x) \quad x > 0, y > 0, \tag{A.27}$$

and therefore

$$\int_0^\pi \sin^K \theta d\theta = B\left(\frac{K+1}{2}, \frac{1}{2}\right) = \frac{\Gamma(\frac{K+1}{2})\Gamma(\frac{1}{2})}{\Gamma(\frac{K}{2}+1)}. \tag{A.28}$$

Finally, using the standard property

$$\Gamma\left(\frac{1}{2}\right) = \sqrt{\pi}, \tag{A.29}$$

we have the result in Eq.(A.22).

From Eq.(A.21), we have

$$F(\Omega) = (\sqrt{\pi})^{d-3} \frac{\Gamma(1)}{\Gamma(\frac{1}{2}+1)} \frac{\Gamma(\frac{3}{2})}{\Gamma(2)} \frac{\Gamma(2)}{\Gamma(\frac{3}{2}+1)} \dots \frac{\Gamma(\frac{d-3}{2}+1)}{\Gamma(\frac{d-3}{2}+1)} \tag{A.30}$$

$$\times \int_0^\infty 2\pi\rho^{d-1} f(\rho) d\rho \int_0^\pi \sin^{d-2} \theta_1 e^{-i\rho\Omega \cos \theta_1} d\theta_1.$$

Consequently, we get

$$F(\Omega) = \frac{2\pi^{\frac{d-1}{2}}}{\Gamma(\frac{d-1}{2})} \int_0^\infty \rho^{d-1} f(\rho) d\rho \int_0^\pi \sin^{d-2} \theta_1 e^{-i\rho\Omega \cos \theta_1} d\theta_1$$

$$= \frac{2\pi^{\frac{d-1}{2}}}{\Gamma(\frac{d-1}{2})} \int_0^\infty \rho^{d-1} f(\rho) d\rho \int_0^\pi \sin^{d-2} \theta_1 \cos(\rho\Omega \cos \theta_1) d\theta_1. \tag{A.31}$$

Recalling the integral representation of the cylindrical and spherical Bessel functions of the first kind,

$$J_n(z) = \frac{(\frac{1}{2}z)^n}{\pi^{\frac{1}{2}}\Gamma(n+\frac{1}{2})} \int_0^\pi \cos(z \cos \theta) \sin^{2n} \theta d\theta \tag{A.32}$$

$$j_n(z) = \frac{z^n}{2^{n+1}n!} \int_0^\pi \cos(z \cos \theta) \sin^{2n+1} \theta d\theta, \tag{A.33}$$

(see Ref. [175]), we note that Eqs.(A.32) and (A.33) are simply related by the cylindrical-spherical connection, namely

$$j_n(z) = \sqrt{\frac{\pi}{2z}} J_{n+\frac{1}{2}}(z), \quad (\text{A.34})$$

as well known in standard Bessel function theory.

By using Eqs.(A.32) and (A.33) in Eq.(A.31), we obtain the two important final results

$$F(\Omega) = \int_0^\infty 2\pi\rho f(\rho) \left(\frac{2\pi\rho}{\Omega}\right)^{\frac{d}{2}-1} J_{\frac{d}{2}-1}(\rho\Omega) d\rho \quad d = 2K \text{ (even)}, \quad (\text{A.35})$$

$$F(\Omega) = \int_0^\infty 4\pi\rho^2 f(\rho) \left(\frac{2\pi\rho}{\Omega}\right)^{\frac{d-3}{2}} j_{\frac{d-3}{2}}(\rho\Omega) d\rho \quad d = 2K + 1 \text{ (odd)}. \quad (\text{A.36})$$

## ACKNOWLEDGMENTS

---

Working on the Ph.D. has been a marvelous and overwhelming experience. It is difficult to enumerate the motivations of my satisfaction on this adventure. For as long as I can remember, I have been accompanied by a combination of chance, hard work and passion. In any case, I am indebted to many people that have been definitely the most important driving force for this experience.

First, I am grateful to my advisor, Prof. **Luciano Colombo**, for his guidance, support and encouragement and for having oriented and supported me with promptness and care. Further, for providing me the opportunity to work in two different stimulating research environment, first in Sardinia, secondly in Lille. Your guidance has been fundamental for my Ph.D. experience.

I would like to extend my warm thanks to my tutor **Stefano Giordano**. Your ability to select and to approach compelling research problems, your mathematical and physical insight, and your way to work set an example. Your guidance and scientific collaboration have been crucial for improving my scientific skills. As well, it is admirable your modesty, from which I tried to learn something as long as I could. Above all, you made me feel a friend, which I appreciate from my heart. I have been very privileged to get to know and to collaborate with you.

I'm also indebted and grateful to **Pier Luca Palla**, of the University of Lille I (France), for his assistance in writing code and for his encouragement during my whole Ph.D. work. Your support has been really important for me.

I would like to thank Prof. **Fabrizio Cleri**, of the University of Lille I (France), for providing me the opportunity to work in a foreign research environment, as well as the opportunity to start a collaboration with his group in a new and very stimulating investigation topic.

I would like to extend my thanks to **Philippe Pernod** and all the International Associated Laboratory LEMAC/LICS, ECLille, for their friendliness, as much as their manifested interest on my works. I really appreciated it.

I further want to thank **Marc Goueygou** and **Ilyesse Bihi** for their kindness on helping me on the present thesis French abstract.

I acknowledge also the **Department of Physics of the University of Cagliari** for the extended visiting grant offered for this work, the **IEMN** (UMR CNRS 8520), and the **University of Lille I** for the kind hospitality offered during part of this work.

Continuing a fine tradition, I want to thank some people who have been crucial for my staying in Lille. I am thinking to my aunt **Zia Giovanna**, and others outstanding friends as **Alessandra Pesce**, **Batista Sirigu**, **Thomas Lucky**, who have made the last part of my Ph.D. in Lille worthy of memory. As well, I would like to express my gratefulness to all my other friends.

A special thanks to my **dad**, **mom** and **sister** for their infinite support throughout everything.

*Villeneuve d'Ascq, Lille (France), March 2013*

*Fabio Manca*

## BIBLIOGRAPHY

---

- [1] F. Ritort. *J. Phys.: Condens. Matter*, **18**: R531, 2006.
- [2] K. R. Chaurasiya et al. *Phys. Life Rev.*, **7**: 299, 2010.
- [3] A. Ashkin. *Proc. Natl Acad. Sci.*, **94**: 4853, 1997.
- [4] C. Gosse and V. Croquette. *Biophys. J.*, **82**: 3314, 2002.
- [5] D. M. Czajkowsky and Z. Shao. *FEBS Lett.*, **430**: 51, 1998.
- [6] C. R. Calladine, H. R. Drew, B. F. Luisi, and A. A. Travers. *Understanding DNA: the molecule and how it works*. Elsevier Academic Press, Amsterdam, 1992.
- [7] H. Yang et al. *Science*, **302**: 262, 2003.
- [8] E. A. Lipman, B. Schuler, O. Bakajin, and W. A. Eaton. *Science*, **301**: 1233, 2003.
- [9] F. Jülicher, A. Adjari, and J. Prost. *Rev. Mod. Phys.*, **69**: 1269, 1997.
- [10] M. Rief et al. *Science*, **275**: 28, 1997.
- [11] J. Liphardt et al. *Science*, **296**: 1832, 2002.
- [12] F. Cleri. *Sci. Model. Simul.*, **15**: 369, 2008.
- [13] A. Alemany and F. Ritort. *Europhys. News*, **41**: 27, 2010.
- [14] R. D. Kamien. *Rev. Mod. Phys.*, **74**: 953, 2002.
- [15] C. Anselmi, P. DeSantis, and A. Scipioni. *Biophys. Chem.*, **113**: 209, 2005.
- [16] M. Rubinstein and R. H. Colby. *Polymer Physics*. Oxford University Press, New York, 2003.
- [17] P. Nelson. *Biological Physics: Energy, Information, Life*. W H Freeman and Company, 2003.

- [18] H. Berg. *Random Walks in Biology*. Princeton University Press, New York, 1993.
- [19] J. M. Huguet et al. *Proc. Nat. Ac. Sci. (PNAS)*, **107**: 15341, 2010.
- [20] S. B. Smith, L. Finzi, and C. Bustamante. *Science*, **258**: 1122, 1992.
- [21] J. F. Marko and E. D. Siggia. *Macromolecules*, **28**: 8759, 1995.
- [22] A. Rosa, T. X. Hoang, D. Marenduzzo, and A. Maritan. *Macromolecules*, **36**: 10095, 2003.
- [23] A. Rosa, T. X. Hoang, D. Marenduzzo, and A. Maritan. *Biophys. Chem.*, **115**: 251, 2005.
- [24] P. K. Purohit et al. *Int. J. Non-Linear Mech.*, **43**: 1056, 2008.
- [25] R. Cotterill. *Biophysics: an introduction*. Chichester, New York, 2002.
- [26] D. Boal. *Mechanics of the Cell*. Cambridge University Press, 2002.
- [27] A. L. Lehninger, D. L. Nelson, and M. M. Cox. *Principles of Biochemistry*. Worth Publishers, 2000.
- [28] H. Lodish, Arnold Berk, and Paul Matsudaira. *Molecular Cell Biology*. W.H. Freeman and Company, 2004.
- [29] T. R. Strick et al. *Rep. Prog. Phys.*, **66**: 1, 2003.
- [30] Rodin et al. *Biology Direct*, **6**: 14, 2011.
- [31] F.H.C. Crick et al. *Orig Life*, **7**: 389, 1976.
- [32] A.A. Turanov et al. *Science*, **323**: 259, 2009.
- [33] E. Szathmárya. *Proc. Natl. Acad. Sci.*, **90**: 9916, 1993.
- [34] E. Szathmárya. *Trends Genet.*, **15**: 223, 1999.
- [35] L. E. Hunter and J. Lederberg. *Artificial intelligence and molecular biology*. The MIT press, Menlo Park, CA, 1993.

- [36] M. Daune. *Molecular biophysics: structures in motion*. Oxford University Press, New York, 1999.
- [37] R. Glaser. *Biophysics*. Springer, New York, 2001.
- [38] G. S. Grest and K. Kremer. *Phys. Rev. A*, **33**: 3628, 1986.
- [39] M. V. Volkenstein. *Configurational Statistics of Polymer Chains*. Interscience, New York, 1963.
- [40] G. W. Slater et al. *Soft Materials*, **2**: 155, 2004.
- [41] A. V. Dobrynin, J. M. Y. Carrillo, and M. Rubinstein. *Macromolecules*, **43**: 9181, 2010.
- [42] L. Livadaru, R. R. Netz, and H. J. Kreuzer. *Macromolecules*, **36**: 3732, 2003.
- [43] R. G. Winkler. *J. Chem. Phys.*, **118**: 2919, 2003.
- [44] H. Kleinert. *Path Integrals in Quantum Mechanics, Statistics and Polymer Physics*. World Scientific, Singapore, 1990.
- [45] T. A. Vilgis. *Physics Reports*, **336**: 167, 2000.
- [46] B.-Y. Ha and D. Thirumalai. *J. Chem. Phys.*, **106**: 4243, 1997.
- [47] Y. Hori, A. Prasad, and J. Kondev. *Phys. Rev. E*, **75**: 041904, 2007.
- [48] R. P. Feynman and A. R. Hibbs. *Quantum Mechanics and Path Integrals*. McGraw-Hill, New York, 1965.
- [49] E. Jarkova, T. J. Vlught, and N.-K. Lee. *J. Chem. Phys.*, **122**: 114904, 2005.
- [50] T. Su and P. K. Purohit. *J. Mech. Phys. Solids*, **58**: 164, 2010.
- [51] C. Bustamante, S. Smith, J. Liphardt, and D. Smith. *Curr. Opin. Struct. Biol.*, **10**: 279, 2000.
- [52] K. Svoboda and S. M. Block. *Annu. Rev. Biophys. Biomol. Struct.*, **23**: 247, 1994.
- [53] M. Ludwig et al. *Appl. Phys. Mater. Sci. Process.*, **68**: 173, 1999.

- [54] A. D. Mehta, M. Rief, and J. A. Spudich. *J. Biol. Chem.*, **274**: 14517, 1999.
- [55] M. Doi. *Introduction to Polymer Physics*. Clarendon Press, Oxford, 1996.
- [56] R. H. Boyd and P. J. Phillips. *The Science of Polymer Molecules*. Cambridge University Press, Cambridge, 1993.
- [57] J. H. Weiner. *Statistical mechanics of elasticity*. Dover Publication Inc., New York, 2002.
- [58] L. R. G. Treloar. *The Physics of Rubber Elasticity*. Oxford University Press, Oxford, 1975.
- [59] G. V. Semisotnov. *Biopolymers*, **31**: 119, 1991.
- [60] A. Bensimon et al. *Science*, **265**: 2096, 1994.
- [61] E. Y. Chan et al. *Genome Res.*, **14**: 1137, 2004.
- [62] M. Rief et al. *Science*, **276**: 1109, 1997.
- [63] C. Bustamante, J.C. Macosko, and G.J. Wuite. *Nat. Rev. Mol. Cell. Biol.*, **1**: 130, 2000.
- [64] D. W. Trahan and P. S. Doyle. *Biomicrofluidics*, **3**: 012803, 2009.
- [65] S. G. Wang and Y. G. Zhu. *Biomicrofluidics*, **6**: 024116, 2012.
- [66] C.-C. Hsieh and T.-H. Lin. *Biomicrofluidics*, **5**: 044106, 2011.
- [67] D. C. Schwartz et al. *Science*, **262**: 110, 1993.
- [68] T. R. Strick et al. *Science*, **271**: 1835, 1996.
- [69] T. R. Strick, V. Croquette, and D. Bensimon. *Nature*, **404**: 901, 2000.
- [70] K. C. Neuman and A. Nagy. *Nature Meth.*, **5**: 491, 2008.
- [71] P. Dai et al. *Phys. Rev. B Condens. Matter*, **47**: 7401, 1993.
- [72] G. Binnig, N. Garcia, and H. Rohrer. *Phys. Rev. B Condens. Matter*, **32**: 1336, 1985.

- [73] O. Marti et al. *J. Microsc.*, **152**: 803, 1988.
- [74] A. Engel. *Annu. Rev. Biophys. Biophys. Chem.*, **20**: 79, 1991.
- [75] S. M. Lindsay. *Biophys. J.*, **67**: 2134, 1994.
- [76] J. O. Bustamante et al. *J. Membr. Biol.*, **263**: 146, 1995.
- [77] Z. Shao, J. Yang, and A. P. Somlyo. *Annu. Rev. Cell Dev. Biol.*, **11**: 241, 1995.
- [78] B. Drake et al. *Science*, **243**: 1586, 1989.
- [79] C. Bustamante, C. Rivetti, and D. J. Keller. *Curr. Opin. Struct. Biol.*, **7**: 709, 1997.
- [80] S. Chu. *Science*, **861**: 253, 1991.
- [81] A. Ashkin, J.M. Dziedzic, J.E. Bjorkholm, and S. Chu. *Optics Letters*, **11**: 288, 1986.
- [82] M.D. Wang et al. *Biophys. J.*, **72**: 1335, 1997.
- [83] J. Liphardt et al. *Science*, **292**: 733, 2001.
- [84] J.D. Wen et al. *Biophys. J.*, **92**: 2996, 2007.
- [85] R. Jeffrey et al. *Annual Review of Biochemistry*, **77**: 205, 2008.
- [86] T. Strick, J.-F. Allemand, V. Croquette, and D. Bensimon. *Progr. Biophys. Mol. Biol.*, **74**: 115, 2000.
- [87] G. Charvin, T.R. Strick, D. Bensimon, and V. Croquette. *Annu. Rev. Biophys. Biomol. Struct.*, **34**: 201, 2005.
- [88] Gore and J. et al. *Nature*, **439**: 100, 2006.
- [89] H. Itoh et al. *Nature*, **427**: 465, 2004.
- [90] D. E. Smith, H. P. Babcock, and S. Chu. *Science*, **283**: 1724, 1999.
- [91] T. T. Perkins, D. E. Smith, R. G. Larson, and S. Chu. *Science*, **268**: 83, 1995.
- [92] T. T. Perkins, S. R. Quake, D. E. Smith, and S. Chu. *Science*, **264**: 822, 1994.

- [93] D. T. Greenwood. *Principles of Dynamics*. Prentice-Hall, New Jersey, 1988.
- [94] H. Goldstein, C. Poole, and J. Safko. *Classical Mechanics*. Addison Wesley, New Jersey, 3rd edition, 2002.
- [95] N.C. Rana and P.S. Joag. *Classical Mechanics*. Tata McGraw-Hill, New Delhi, 1991.
- [96] J. W. Gibbs. *Elementary principles in statistical mechanics*. Charles Scribner's Sons, New York, 1902.
- [97] S. R. S. Varadhan. *Probability Theory*. New York University, 2000.
- [98] R. Abraham and J. E. Marsden. *Foundations of Mechanics*. Benjamin-Cummings, London, 1978.
- [99] D. Chandler. *Introduction to Modern Statistical Mechanics*. Oxford University Press, 1987.
- [100] C. W. Gardiner. *Handbook of stochastic methods for physics, chemistry, and the natural sciences*. Springer, 2nd edition edition, 1985.
- [101] L. Boltzmann. *Theorie des gase alft einatomigen moiekqien, deren dimensionen gegen die mittlere weglänge verschwinden*. J. A. Barth, London, 1923.
- [102] R. C. Tolman. *The Principles of Statistical Mechanics*. Courier Dover, 1938.
- [103] M. Plischke and B. Bergersen. *Equilibrium Satistical Physics*. World Scientific, 3rd edition, 2006.
- [104] R. Reif. *Fundamentals of statistical and thermal physics*. McGraw-Hill, 1965.
- [105] P. Cluzel et al. *Science*, **271**: 792, 1997.
- [106] T. Hugel et al. *Macromolecules*, **34**: 1039, 2001.
- [107] X. Liu and G. H. Pollack. *Biophys. J.*, **83**: 2705, 2002.
- [108] C. Bouchiat et al. *Biophys. J.*, **76**: 409, 1999.

- [109] P. T. Underhill and P. S. Doyle. *J. Rheol.*, **49**: 963, 2005.
- [110] R. B. Bird. *Dynamics of polymeric liquids*. Elsevier Academic Press, New York, 2nd ed. edition, 1987.
- [111] J.M. Wiest. *J. Rheol.*, **33**: 281, 1989.
- [112] J. G. Kirkwood. *J. Chem. Phys.*, **3**: 300, 1935.
- [113] D. L. Goodstein. *States of matter*. Dover publications, New York, 3rd edition, 1975.
- [114] J. H. Weiner and M. R. Pear. *Macromolecules*, **10**: 317, 1977.
- [115] R. M. Neumann. *Phys. Rev. A*, **31**: 3516, 1985.
- [116] D. Keller, D. Swigon, and C. Bustamante. *Biophys. J.*, **84**: 733, 2003.
- [117] J. T. Titantah, C. Pierleoni, and J. P. Ryckaert. *Phys. Rev. E.*, **60**: 7010, 1999.
- [118] J. H. Weiner and D. Berman. *J. Chem. Phys.*, **82**: 548, 1985.
- [119] D. Berman and J. H. Weiner. *J. Chem. Phys.*, **83**: 1311, 1985.
- [120] R. A. Guyer and J. A. Y. Johnson. *Phys. Rev. A*, **32**: 3661, 1985.
- [121] M. Süzen, M. Sega, and C. Holm. *Phys. Rev. E*, **79**: 051118, 2009.
- [122] G. Glatting, R. G. Winkler, and P. Reineker. *J. Chem. Phys.*, **26**: 6085, 1993.
- [123] S. Sinha and J. Samuel. *Phys. Rev. E*, **71**: 021104, 2005.
- [124] F. Manca et al. *J. Chem. Phys.*, **136**: 154906, 2012.
- [125] D. Frenkel and B. Smit. *Understanding Molecular Simulation*. Academic Press, San Diego, 1996.
- [126] M. P. Allen and D. J. Tildesley. *Computer Simulations of Liquids*. Clarendon Press, Oxford, 1987.
- [127] J. M. Hammersley and D. C. Handscomb. *Monte Carlo Methods*. Methuen, London, 1964.

- [128] F. James. *Rep. Prog. Phys.*, **43**: 73, 1980.
- [129] K. Binder. *Monte Carlo and Molecular Dynamics Simulations in Polymer Science*. Oxford University Press, New York, 1995.
- [130] N. Bakhvalov. *Methodes Numériques*. Moscou, 1976.
- [131] D. J. Earl and M. W. Deem. *Methods Mol Biol.*, **25**: 443, 2008.
- [132] S. Rajasekaran and J. Reif. *Handbook of Parallel Computing: Models, Algorithms and Applications*. CRC Press, New York, 2007.
- [133] W. L. Jorgensen and J. T. Rives. *J. Phys. Chem.*, **100**: 14508, 1996.
- [134] J. P. Ulmschneider, M. B. Ulmschneider, and A. Di Nola. *J. Phys. Chem. B*, **110**: 16733, 2006.
- [135] S. A. Northrup and J. A. McCammon. *Biopolymers*, **19**: 1001, 1980.
- [136] R. Q. Topper et al. *Review in Computational Chemistry*. John Wiley and Sons, New York, 2003.
- [137] N. Metropolis et al. *J. Chem. Phys.*, **21**: 1087, 1953.
- [138] R. Q. Topper. *Adv. Chem. Phys.*, **105**: 117, 1999.
- [139] U. Grenander. *Ark. Matemat.*, **1**: 195, 1950.
- [140] W. K. Hastings. *Biometrika*, **5**: 97, 1970.
- [141] R. L. Rowley. *Statistical Mechanics for Thermophysical Property Calculations*. PTR Prentice-Hall, Englewood Cliffs, 1994.
- [142] M. H. Kalos and P. A. Whitlock. *Monte Carlo Methods*. Wiley, New York, 1986.
- [143] M. A. Miller, L. M. Amon, and W. P. Reinhardt. *Chem. Phys. Lett.*, **331**: 278, 2000.
- [144] J. E. Gentle. *Random Number Generation and Monte Carlo Methods*. Springer, USA, 2003.

- [145] S. K. Park and W. K. Miller. *Communications of the ACM*, **31**: 1192, 1988.
- [146] L.Y. Deng and K. J. L. Dennis. *The American Statistician*, **54**: 145, 2000.
- [147] D. H. Lehmer. *Ann. Comp. Lab. Harvard Univ.*, **26**: 141, 1951.
- [148] J.F. Traub et al. *Math. Comp.*, **58**: 323, 1989.
- [149] S. Hoops et al. *Bioinformatics*, **22**: 3067, 2006.
- [150] Q. Fang and A. B. David. *Optics Express*, **17**: 20178, 2009.
- [151] N. Singla. *Workshop High Perf. Comp. Finance*, **99**: 1, 2008.
- [152] M. Matsumoto and T. Nishimura. *ACM Trans. Mod. Comp. Simulation*, **8**: 3, 1998.
- [153] J.P. Valleau and S.G. Whittington. *Statistical Mechanics*. Plenum Press, New York, 1977.
- [154] M. Iwamatsu and Y. Okabe. *Physica A*, **278**: 414, 2000.
- [155] R. W. Wilde and S. Singh. *Statistical Mechanics: Fundamentals and Modern Applications*. Wiley, New York, 1998.
- [156] D.D. Frantz, D.L. Freeman, and J.D. Doll. *J. Chem. Phys.*, **93**: 2769, 1990.
- [157] D. L. Freeman and J. D. Doll. *Ann. Rev. Phys. Chem.*, **47**: 43, 1996.
- [158] J. I. Siepmann and I. R. McDonald. *Molec. Phys.*, **75**: 255, 1992.
- [159] Jérôme Hénin and Christophe Chipot. *J. Chem. Phys.*, **121**: 2904, 2004.
- [160] C.-Y. Shew and P. Mills. *J. Phys. Chem.*, **97**: 13824, 1993.
- [161] I. Andricioaei and J.E. Straub. *Physica A*, **247**: 553, 1997.
- [162] C. Tsallis. *J. Stat. Phys.*, **52**: 479, 1998.
- [163] R.H. Swendsen and J.S. Wang. *Physical Review Letters*, **57**: 2607, 1986.

- [164] J. D. Earl and M. W. Deem. *Phys. Chem. Chem. Phys.*, **7**: 3910, 2005.
- [165] A. M. Ferrenberg and R. H. Swendsen. *Phys. Rev. Lett.*, **61**: 2635, 1988.
- [166] A. Erdelyi. *Asymptotic Expansions*. Dover Publication Inc., New York, 1956.
- [167] R. M. Neumann. *Biophys. J.*, **85**: 3418, 2003.
- [168] H. J. Kreuzer and S. H. Payne. *Phys. Rev. E*, **63**: 021906, 2001.
- [169] R. G. Winkler and P. Reineker. *Macromolecules*, **25**: 6891, 1992.
- [170] D. Perchak and J. H. Weiner. *Macromolecules*, **15**: 545, 1982.
- [171] R. G. Winkler. *Soft Matter*, **6**: 6183, 2010.
- [172] J. Schröter and R. Wegener. *Math. Methods Appl. Sci.*, **14**: 319, 1991.
- [173] S. Li and G. Wang. *Introduction To Micromechanics And Nanomechanics*. World Scientific Publishing, New Jersey, 2008.
- [174] R. R. Netz. *Macromolecules*, **34**: 7522, 2001.
- [175] M. Abramowitz and I. A. Stegun. *Handbook of Mathematical Functions*. Dover Publication Inc., New York, 1970.
- [176] A. Dhar and D. Chaudhuri. *Phys. Rev. Lett.*, **89**: 065502, 2002.
- [177] K. Binder. *Rep. Progr. Phys.*, **60**: 487, 1997.
- [178] J. Kierfeld, O. Niamploy, V. Sa-yakanit, and R. Lipowsky. *Eur. Phys. J. E*, **14**: 17, 2004.
- [179] M. Tanase, N. Biais, and M. Sheetz. *Methods Cell Biol.*, **83**: 473, 2007.
- [180] S. M. Smith, Y. Cui, and C. Bustamante. *Science*, **271**: 795, 1996.
- [181] L. Tskhovrebova et al. *Nature*, **387**: 308, 1997.

- [182] H. Lu et al. *Biophys. J.*, **75**: 662, 1998.
- [183] M. Carrion-Vazquez et al. *Prog. Biophys. Mol. Biol.*, **74**: 63, 2000.
- [184] M. Carrion-Vazquez et al. *Proc. Natl Acad. Sci.*, **96**: 3694, 1999.
- [185] I. Rouzina and V. A. Bloomfield. *Biophys. J.*, **80**: 882, 2001.
- [186] I. Rouzina and V. A. Bloomfield. *Biophys. J.*, **80**: 894, 2001.
- [187] S. Cocco et al. *Phys. Rev. E*, **70**: 011910, 2004.
- [188] N. Bosaeus et al. *Proc. Natl. Acad. Sci. USA*, **109**: 15179, 2012.
- [189] J. F. Léger et al. *Phys. Rev. Lett.*, **83**: 1066, 1999.
- [190] G. Puglisi and L. Truskinovsky. *J. Mech. Phys. Sol.*, **48**: 1, 2000.
- [191] Y. R. Efendiev and L. Truskinovsky. *Continuum Mech. Thermodyn.*, **22**: 679, 2010.
- [192] H. J. Kreuzer and M. Grunze. *Europhys. Lett.*, **55**: 640, 2001.
- [193] F. Hanke and H. J. Kreuzer. *Eur. Phys. J. E*, **22**: 163, 2007.
- [194] C. Storm and P. C. Nelson. *Phys. Rev. E*, **67**: 051906, 2003.
- [195] D. E. Makarov, P. K. Hansma, and H. Metiu. *J. Chem. Phys.*, **114**: 9663, 2001.
- [196] M. Gao, H. Lu, and K. Schulten. *J. Muscle Res. Cell Motil.*, **23**: 513, 2002.
- [197] A. Lebrun and R. Lavery. *Nucleic Acid Res.*, **24**: 2260, 1996.
- [198] M. W. Konrad and J. T. Bolonick. *J. Am. Chem. Soc.*, **118**: 10989, 1996.
- [199] K. M. Kosikov et al. *J. Mol. Biol.*, **289**: 1301, 1999.
- [200] D. Keller, D. Swigon, and C. Bustamante. *Biophys. J.*, **84**: 733, 2003.
- [201] G. I. Bell. *Science*, **200**: 618, 1978.

- [202] W. Saenger. *Principles of Nucleic Acid Structure*. Springer-Verlag, New York, 1984.
- [203] A. Ahsan, J. Rudnick, and R. Bruinsma. *Biophys. J.*, **74**: 132, 1998.
- [204] J. J. SantaLucia. *Proc. Natl. Acad. Sci. USA*, **95**: 1460, 1998.
- [205] J. J. SantaLucia and D. Hicks. *Annu. Rev. Biophys. Biomol. Struct.*, **33**: 415, 2004.
- [206] M. Rief, J. M. Fernandez, and H. E. Gaub. *Phys. Rev. Lett.*, **81**: 4764, 1998.
- [207] W. T. King et al. *Int. J. Biol. Macromol.*, **46**: 159, 2010.
- [208] A. R. Singh, D. Giri, and S. Kumar. *J. Stat. Mech.*, page P05019, 2011.
- [209] F. Manca et al. *J. Phys.: Conf. Ser.*, **383**: 012016, 2012.
- [210] F. Manca et al. *J. Chem. Phys.*, **137**: 244907, 2012.
- [211] R. Q. Topper et al. *Rev. Comp. Chem.*, **19**: 1, 2003.
- [212] D. D. Frantz, D. L. Freeman, and J. D. Doll. *J. Chem. Phys.*, **93**: 2769, 1990.
- [213] M. S. Kellermayer et al. *Science*, **276**: 1112, 1997.
- [214] M. Rief, J. Pascual, and M. Saraste. *J. Mol. Biol.*, **286**: 553, 1999.
- [215] A. F. Oberhauser et al. *J. Mol. Biol.*, **319**: 433, 2002.
- [216] F. Manca et al. *Phys. Rev. E*, **87**: 032705, 2013.
- [217] M. Warner, J. M. F. Gunn, and A. B. Baumgartner. *J. Phys. A: Math. Gen.*, **19**: 2215, 1986.
- [218] G. J. Vroege and T. Odijk. *Macromolecules*, **21**: 2848, 1988.
- [219] R. M. Neumann. *J. Chem. Phys.*, **110**: 15, 1999.
- [220] F. Brochard-Wyart. *Europhys. Lett.*, **23**: 105, 1993.

- [221] F. Brochard-Wyart, H. Hervet, and P. Pincus. *Europhys. Lett.*, **26**: 511, 1994.
- [222] F. Brochard-Wyart. *Europhys. Lett.*, **30**: 387, 1995.
- [223] F. S. Henyey and Y. Rabin. *J. Chem. Phys.*, **82**: 4362, 1985.
- [224] Y. Rabin, F. S. Henyey, and D. B. Creamer. *J. Chem. Phys.*, **85**: 4696, 1986.
- [225] A. Lamura, T. W. Burkhardt, and G. Gompper. *Phys. Rev. E*, **64**: 061801, 2001.
- [226] R. Podgornik. *J. Chem. Phys.*, **99**: 7221, 1993.
- [227] H. Schiessel, G. Oshanin, and A. Blumen. *J. Chem. Phys.*, **103**: 5070, 1995.
- [228] H. Schiessel and A. Blumen. *J. Chem. Phys.*, **104**: 6036, 1996.
- [229] B. Maier, U. Seifert, and J. O. Rädler. *Europhys. Lett.*, **60**: 622, 2002.
- [230] A. E. Cohen. *Phys. Rev. Lett.*, **91**: 235506, 2003.
- [231] J. R. Blundell and E. M. Terentjev. *Soft Matter*, **7**: 3967, 2011.
- [232] L. Schwartz. *Mathematics for Physical Sciences*. Addison-Wesley, Reading and MA, 1966.
- [233] I. S. Gradshteyn and I. M. Ryzhik. *Table of Integrals, Series and Products*. Academic Press, San Diego, 1965.
- [234] M. Mazars. *Phys. Rev. E*, **53**: 6297, 1996.
- [235] M. Mazars. *J. Phys. A: Math. Gen.*, **31**: 1949, 1998.
- [236] M. Mazars. *J. Phys. A: Math. Gen.*, **32**: 1841, 1999.
- [237] K. D. Kamien, P. L. Doussal, and D. R. Nelson. *Phys. Rev. A*, **45**: 8727, 1992.
- [238] N. J. Woo, E. S. G. Shaqfeh, and B. Khomami. *J. Rheol.*, **48**: 281, 2004.
- [239] C. Yamahata et al. *J. Microelectromech. S.*, **17**: 623, 2008.